

The Gold Standard; Enhancing Antibiotic Effectiveness through Gold Nanoparticles

by

Melanie Fuller

*Thesis
Submitted to Flinders University
for the degree of*

Doctor of Philosophy
College of Science and Engineering
31st January 2020

SUMMARY

Antibiotic resistance is predicted to become one of the greatest threats to humanity and we need to start acting now to find alternative treatment methods. As a short-term solution, this research has explored the use of gold nanoparticles to enhance antibiotic effectiveness whilst also lowering the dosage of the antibiotic.

Gold nanoparticles were chosen as the main component in this work due to their biocompatibility as well as their favourable optical and physical properties. In this thesis, the polyelectrolyte coating parameters of gold nanoparticles were optimised to ensure stability of the nanoparticles, which is vital in medical applications. The stabilised nanoparticles were then used to pre-treat Gram-negative membrane models before addition of the membrane active antibiotic, Colistin. Pre-treatment with nanoparticles prior to the addition of Colistin showed increased defect formation after the Colistin was removed compared to using Colistin alone. It was also found that high concentrations of gold nanoparticles caused defects on the membrane's surface, likely through binding to the outer membrane.

In addition to the pre-treatment, the use of Colistin coated gold nanoparticles were evaluated to reduce the amount of Colistin required to kill bacteria. It was found that the gold nanoparticles were more stable when coated with Colistin and cationic polyelectrolyte, compared to coating with Colistin only. The anionic Colistin coated nanoparticles had a 6.8-fold decrease in the amount of Colistin required to achieve the minimum inhibitory concentration, compared to Colistin alone. This study also determined that the addition of either cationic or anionic gold nanoparticles to bacteria do not inhibit bacterial growth, indicating they are not inherently antimicrobial.

Following the successes of utilising polyelectrolyte coated gold nanoparticles in antibiotic treatment, a wound dressing application was considered and a proof-of-concept antibiotic loaded bandage was produced. The nanomesh bandage was fabricated through electrospinning, incorporating Colistin into the mesh. The drug release profile could be modified through addition of gold nanoparticles during mesh formation. Although this research is only in its infancy, it has shown promising

results, with the addition of anionic gold nanoparticles into the mesh leading to sufficient release of Colistin over 14 days to kill *E. coli*.

In summary, this thesis explores a wide range of disciplines and brings together new knowledge of increasing susceptibility to Colistin with the use of gold nanoparticles. Although the problem of antibiotic resistance is significant, this work will further the knowledge base to help us move toward an eventual solution.

TABLE OF CONTENTS

SUMMARY	I
TABLE OF CONTENTS	III
LIST OF FIGURES	VII
LIST OF SUPPLEMENTARY FIGURES	XI
LIST OF TABLES	XII
LIST OF SUPPLEMENTARY TABLES	XIII
ABBREVIATIONS	XIV
ACKNOWLEDGEMENTS	XVII
DETAILS OF PUBLICATIONS	XIX
CONFERENCE PRESENTATIONS	XX
DECLARATION	XXII
CHAPTER 1: INTRODUCTION	1
1.0 Background:.....	1
1.1 Research Aims:.....	3
1.2 Research Methods:.....	3
1.3 Structure of the thesis:	4
References:.....	6
CHAPTER 2: BIOMEDICAL APPLICATIONS OF POLYELECTROLYTE COATED SPHERICAL GOLD NANOPARTICLES	8
Abstract:.....	9
1. Introduction:	9
2. Synthesis of polyelectrolyte coated nanoparticles:.....	12
3. Characterising the attachment of polyelectrolytes onto gold nanoparticles:	13
3.1 Surface Plasmon Resonance:	13
3.2 Zeta Potential:.....	15
4. Uptake and Interaction with Cells:.....	16
5. Applications:.....	19
5.1 Drug Delivery:.....	20
5.2 Gene Therapy:.....	22
5.3 Photothermal Therapy:	23
5.4 Imaging:.....	24
6. Toxicity:.....	25
7. Conclusions and future outlook:.....	26
Acknowledgements:.....	28

References:.....	28
CHAPTER 3: POLYELECTROLYTE-COATED GOLD NANOPARTICLES	42
Abstract:.....	44
1. Introduction	44
2. Materials and Methods.....	47
2.1. Polyelectrolyte (PE) Concentration	47
2.2. Salt Concentration	48
2.3. Solvent Stability	48
3. Results and Discussion.....	48
3.1. Effect of PE Concentration	49
3.2. Effect of Salt Concentration	52
3.3. Effect of Solvent.....	54
4. Conclusions	54
Acknowledgements:.....	55
References:.....	55
CHAPTER 4: INCREASING ANTIBIOTIC SUSCEPTIBILITY - THE USE OF CATIONIC GOLD NANOPARTICLES IN GRAM-NEGATIVE BACTERIAL MEMBRANE MODELS.....	59
Abstract:.....	61
1.0 Introduction:	61
2.0 Materials and Methods:.....	64
2.1 Membrane chemicals:.....	64
2.2 Cationic gold nanoparticles:.....	65
2.3 Electrochemical Impedance Spectroscopy (EIS):	65
2.4 Neutron scattering experimental method:	66
3.0 Results and Discussion.....	67
3.1 Addition of Gold Nanoparticles to the Membrane	67
3.2 Simultaneous addition of Colistin and Gold Nanoparticles	69
3.3 Pre-treating with gold nanoparticles before Colistin addition	73
4.0 Conclusion:	79
Acknowledgement:	80
References:.....	80
CHAPTER 5: DELIVERY OF COLISTIN USING GOLD NANOPARTICLES	82
Abstract:.....	84
1.0 Introduction:	84
2.0 Materials and Methods:.....	87
2.1 Fabrication of Colistin and PDADMAC coated gold nanoparticles:.....	87

2.2 Fabrication of Colistin coated gold nanoparticles:.....	87
2.3 Characterisation of Col-PDADMAC-AuNP and Col-AuNP:.....	87
2.4 Minimum inhibitory concentration:	87
2.5 Effect on <i>E. coli</i> growth curve:	88
2.6 Effect on <i>E. coli</i> viability:	89
3.0 Results and Discussion:.....	89
3.1 Confirming the attachment of Colistin:	89
3.2 Stability of the nanoparticles after attachment:	90
3.3 Antimicrobial efficacy of ColAuNPs:.....	91
4.0 Conclusion:	94
Acknowledgements:.....	95
References:.....	95
CHAPTER 6: NANOPARTICLES IN AN ANTIBIOTIC-LOADED NANOMESH FOR DRUG DELIVERY	98
Abstract:.....	100
1.0 Introduction:	100
2.0 Materials and Methods:.....	103
2.1 Mesh Formation:.....	103
2.2 Mesh imaging:	104
2.3 Antibiotic Addition to Nanomesh:	104
2.4 Characterisation of antibiotic addition into the mesh:.....	104
2.5 <i>In vitro</i> antibiotic release:	105
2.6 Broth Dilution Assay:	105
2.7 Zone of Inhibition (ZOI) Assay:	106
3.0 Results and Discussion:.....	106
3.1 Optimisation of Parameters for Mesh Formation:	106
3.2 Addition of Antibiotics into the Nanomesh:	108
3.3 Zone of Inhibition Assay:	110
3.4 Drug Release Studies:.....	110
4.0 Conclusion:	115
Acknowledgements:.....	115
References:.....	116
CHAPTER 7: CONCLUSIONS AND FUTURE DIRECTIONS	122
References:.....	129
APPENDICES	134
Appendix A:	136
Appendix B:	137

Appendix C:	147
Appendix D:	150

LIST OF FIGURES

- Figure 1: Schematic of the mechanism of action of Colistin sulfate showing Lipid A binding, displacement of Mg^{2+} and Ca^{2+} and disruption of the outer membrane. 2
- Figure 2: Graphical abstract of this thesis, with each part of the figure representing a different chapter. 5
- Figure 3: Diagram of the overall thesis, indicating Chapter 2 and how it fits into the larger body of work..... 8
- Figure 4: Graphical abstract from the publication 'Biomedical applications of polyelectrolyte coated spherical gold nanoparticles'..... 9
- Figure 5: Method for self-assembly of polyelectrolyte-coated citrate capped gold nanoparticles using the LbL method..... 11
- Figure 6: Schematic representation of the conduction electrons oscillating across the gold nanoparticle in the electromagnetic field of incident light..... 14
- Figure 7: (A) UV-Vis spectra of mercaptoundecanoic acid coated AuNPs (dashed line) subsequently coated in (a) Polydiallyldimethylammonium chloride (PDADMAC) and (b) PDADMAC/polystyrenesulfonate (PSS). Reproduced from Ref ⁶¹ with permission from Wiley. (B) Surface plasmon band shifts compared to the number of polyelectrolyte coatings on the AuNPs. Reproduced from Ref ⁵² with permission from Wiley. (C) Zeta potential of uncoated citrate capped AuNPs (0) then subsequent addition of positively charged polyallylamine (PAA) and negatively charged polystyrenesulfonate (PSS). Reproduced and adapted from Ref ⁵² with permission from Wiley, 15
- Figure 8: Citrate stabilized gold nanoparticles coated with PSS and PAA in a LbL method with the addition of IgG antibody through amide linkages. Reproduced from Ref ⁵² with permission from Wiley. 21
- Figure 9: A schematic of the cancer drug, Imatinib Mesylate being encapsulated in the multilayer coated PEI/PSS/PEI AuNPs, showing the use of iontophoresis for topical delivery into the layers of the skin. Reprinted from Ref ⁴⁸ with permission from the American Chemical Society. 22
- Figure 10: Diagram of the overall thesis, indicating Chapter 3 and how it fits into the larger body of work..... 43

Figure 11: Graphical abstract from the publication 'Polyelectrolyte-coated gold nanoparticles: the effect of salt and polyelectrolyte concentration on colloidal stability'.....	43
Figure 12: Layer-by-layer (LbL) attachment of polydiallyldimethylammonium chloride (PDADMAC) onto citrate-capped gold nanoparticles.	45
Figure 13: (A) UV–vis spectra of PDADMAC coated AuNP at concentrations of 0–30 mg/mL PDADMAC in 1 mM NaCl. (B) Zeta potential measurements as a function of PDADMAC concentration at pH 6.0.	51
Figure 14: UV–vis spectra of varying salt concentrations of 5 mg/mL PDADMAC on 5 nm AuNPs.	53
Figure 15: Diagram of the overall thesis, indicating Chapter 4 and how it fits into the larger body of work.....	60
Figure 16: Graphical abstract for the chapter entitled 'Increasing Antibiotic Susceptibility – The Use of Cationic Gold Nanoparticles in Gram-Negative Bacterial Membrane Models'.....	60
Figure 17: Schematic of the eight layers of a sparsely tethered tBLM.	64
Figure 18: (A) Bode plot showing 80% DPhyTI, 94% RcLPS tBLMs prior to (bilayer) (black) and after the exposure of 200 μ L cationic AuNPs for 18 h (red). The lines represent the fitted data with the filled shapes representing impedance and the un-filled representing the phase angle. (B) Schematic of the equivalent circuit, which the EIS data is fitted to.	68
Figure 19. (A) Bode plot showing 80% DPhyTI, 94% RcLPS tBLMs prior to (bilayer) (black) and after the exposure of 200 μ L cationic AuNPs with 100 mg/mL Colistin for 17 h (red). The lines represent the fitted data with the filled shapes representing impedance and the un-filled representing the phase angle.....	71
Figure 20: Bode plot showing 80% DPhyTI, 94% RcLPS tBLMs after pre-treating the membrane with 200 μ L cationic AuNPs (black) and after exposing the membrane to 10 mg/mL Colistin for 17 h (red). The lines represent the fitted data with the filled shapes representing impedance and the un-filled representing the phase angle.....	75
Figure 21: Diagram of the overall thesis, indicating Chapter 5 and how it fits into the larger body of work.....	83

Figure 22: Graphical abstract from the submitted publication 'Delivery of Colistin using Gold Nanoparticles'.	83
Figure 23: Schematic of the electrostatic attachment of Colistin onto the AuNP surface.	86
Figure 24: Effect of ColAu(+), ColAu(-) and Colistin on the growth curve of <i>E. coli</i> (ATCC 700891) in nutrient broth measured by changes in turbidity (OD600). *Indicates <i>E. coli</i> was present in the sample.	92
Figure 25: Concentration of <i>E. coli</i> (CFU/mL) after 4 and 8 hrs of growth (at 37oC) in nutrient broth containing ColAu(+), ColAu(-) and Colistin compared to the positive control (<i>E. coli</i> and nutrient broth). *P<0.05, ***P<0.0005, ns P>0.05 using one way ANOVA.	93
Figure 26: Diagram of the overall thesis, indicating Chapter 6 and how it fits into the larger body of work.	99
Figure 27: Graphical abstract from the publication 'Nanoparticles in an Antibiotic-Loaded Nanomesh for Drug Delivery'.	99
Figure 28: Schematic of the electrospinning instrument showing the Taylor cone and mesh formation.	102
Figure 29: The chemical structure of (A) Vancomycin and (B) Colistin.	103
Figure 30: SEM images of different %w/w of PCL in HFIP showing the changes in morphology at a flow rate of 0.5 mL/hr and 1 mL/hr. All scale bars are 10 μ m.	108
Figure 31: (Top) ^1H NMR of 10 mg PCL in 95% DMSO, 5% D ₂ O. (Bottom) ^1H NMR of 10 mg PCL with Colistin in 95% DMSO, 5% D ₂ O.	109
Figure 32: ATR-FTIR of PCL, PCL + Colistin and PCL + Vancomycin nanomesh confirming the addition of the antibiotics with an ether peak for Vancomycin at $\sim 1030\text{ cm}^{-1}$ (see inset) and amine groups at 3300 cm^{-1} for both antibiotics.	109
Figure 33: Zone of Inhibition assays after 48 h for meshes tested on <i>E. coli</i> lawns with 8 mm mesh disks.	110
Figure 34: Top: Colistin cumulative release, Bottom: Vancomycin cumulative release. Both show Korsmeyer-Peppas fitting models.	111

Figure 35: Absorbance at OD600 monitoring increased turbidity representing *E. coli* growth in aliquots removed during the Colistin release study of Van, Col, and ColAu(-) nanomesh samples in DPBS over various time points..... 114

Figure 36: Schematic of mechanisms for release of the additives Colistin and gold nanoparticles from a PCL nanomesh. 124

Figure 37: Mean roughness of a PCL/gelatin electrospun nanomesh with increasing degradation time in either phosphate buffered saline (PBS) or simulated culture medium (SCM) measured using quantitative AFM analysis.¹² 126

Figure 38: Example of degradation of PCL fibres before (A) and after (B) implantation for 18 months. as a vascular implant in rats.¹⁴ Scale bar is 20 μm . Reprinted with permission from John Wiley and Sons. 127

LIST OF SUPPLEMENTARY FIGURES

- Figure S1: Reflectivity plot of LPS bilayer (A), bilayer after exposure to 100 μ L cationic gold nanoparticles (B) and bilayer after exposure to 10 mg/mL Colistin sulfate (C)..... 141
- Figure S2: SLD plot of LPS bilayer (A), bilayer after exposure to 100 μ L cationic gold nanoparticles (B) and bilayer after exposure to 10 mg/mL Colistin sulfate (C)..... 142
- Figure S3: Reflectivity plot of LPS bilayer (A), bilayer after exposure to 100 μ L cationic gold nanoparticles and 10 mg/mL Colistin sulfate simultaneously (B)..... 143
- Figure S4: SLD plot of LPS bilayer (A), bilayer after exposure to 100 μ L cationic gold nanoparticles and 10 mg/mL Colistin sulfate simultaneously (B). 144
- Figure S5: Reflectivity plot of LPS bilayer (A), bilayer after exposure to 1 mL cationic gold nanoparticles (B) and bilayer after exposure to 10 mg/mL Colistin sulfate (C) 145
- Figure S6: SLD plot of LPS bilayer (A), bilayer after exposure to 1 mL cationic gold nanoparticles (B) and bilayer after exposure to 10 mg/mL Colistin sulfate (C)..... 146
- Figure S7: A: UV-Vis spectra of the ColAu(-) with three washes. The solid line shows the maximum peak of Colistin at 219 nm and the dotted line is the surface plasmon resonance peak of the gold nanoparticles at 555 nm. 148
- Figure S8: Calibration curve of Colistin Sulfate at a wavelength of 219 nm. 148
- Figure S9: The concentration of Colistin present in ColAu(+) compared to the ColAu(-)..... 149
- Figure S10: Calibration curves of (A) Colistin and (B) Vancomycin in DPBS using UV-Vis Spectroscopy at 214 nm and 290 nm respectively. 151

LIST OF TABLES

Table 1: Commonly used polyelectrolytes showing their charge at pH 7 and their current applications.	13
Table 2: Concentrations of PDADMAC showing polyelectrolyte chains to nanoparticles (PC/NP) ratio, compared to their average surface plasmon resonance (SPR) peak position and zeta potentials at pH 6.0 ± 0.3	50
Table 3: The average SPR peak and absorbance as determined by UV-vis spectroscopy for 5 mg/mL PDADAMAC-coated AuNP.....	53
Table 4: The changes in electrical properties of two different LPS-tBLMs from the addition of gold nanoparticles exposed for 18-20 h.....	69
Table 5: Electrochemical measurements of the simultaneous addition of gold nanoparticles with 10 mg/mL Colistin with various rinse times.....	70
Table 6: Neutron reflectivity results for sparsely tethered tBLMS when exposed to 100 μ L AuNP and 10 mg/mL Colistin sulfate simultaneously. Units for thickness and roughness are in \AA , SLD is 10^{-6}\AA^{-2} and hydration is volume %. The parameters for the additional layers can be found in the supporting information.....	72
Table 7: Electrochemical measurements with pre-treatment of the membrane with gold nanoparticles for various concentrations of gold nanoparticles with the addition post treatment of 10 mg/mL Colistin.....	74
Table 8: Sparsely tethered tBLMS and their parameter changes when exposed to 100 μ L AuNP for 18 h and then and 10 mg/mL Colistin sulfate for 18 h. Units for thickness and roughness are in \AA , SLD is 10^{-6}\AA^{-2} and hydration is volume %. The parameters for the additional layers can be found in the supporting information.	76
Table 9: Sparsely tethered tBLMS and their parameter changes when exposed to 1 mL AuNP for 18 h and then and 10 mg/mL Colistin sulfate for 18 h. Units for thickness and roughness are in \AA , SLD is 10^{-6}\AA^{-2} and hydration is volume %. The parameters for the additional layers can be found in the supporting information.	78
Table 10: Comparison of the amount of Colistin concentration, zeta potential and AuNP absorbance peak of ColAu(+) and ColAu(+).	90
Table 11: Minimum Inhibitory Concentration of Colistin, ColAu(+) and ColAu(-) against <i>E. coli</i> (ATCC 700891).....	91

LIST OF SUPPLEMENTARY TABLES

Table S1: Difference in SPR peak and absorbance for citrate capped AuNP and PDADMAC coated AuNP in Ethanol, Tween20 and PBS..... 136

Table S2: Sparsely tethered bilayer with the addition of 100 μL cationic AuNP and the addition of 10 mg.mL Colistin sulfate. The thickness and roughness are given in \AA , hydration is given in volume % and SLD is given in 10^{-6}\AA^{-2} 138

Table S3: Sparsely tethered bilayer compared to the same bilayer with 100 μL cationic AuNP added simultaneously with 10 mg/mL Colistin sulfate. The thickness and roughness are given in \AA , hydration is given in volume-% and SLD is given in 10^{-6}\AA^{-2} 139

Table S4: Sparsely tethered bilayer compared to the same bilayer with 1 mL cationic AuNP added and then addition of 10 mg/mL Colistin sulfate. The thickness and roughness are given in \AA , hydration is given in volume-% and SLD is given in 10^{-6}\AA^{-2} 140

Table S5: MIC experimental set-up showing constituents in well 1. Broth and bacteria indicate 50 μL nutrient broth and 50 μL of 10^3 CFU *E. coli* respectively. Concentrations of ColAuNP and Colistin are halved for each subsequent well prior to the addition of *E. coli*. 147

Table S6: ImageJ analysis of fibre diameters for various PCL% w/w at 0.5 mg/mL and 1 mg/mL flow rates. 150

Table S7: Drug release kinetics of Colistin from various electrospun mesh samples. 150

ABBREVIATIONS

AFM	Atomic force microscopy
ATR-FTIR	Attenuated Total Reflection Fourier Transform Infrared
AuNPs	Gold nanoparticles
AuNRs	Gold nanorods
Col	Colistin sulfate
ColAu(+)	Colistin sulfate coated cationic gold nanoparticles
ColAu(-)	Colistin sulfate coated anionic gold nanoparticles
ColAuNPs	Colistin sulfate coated gold nanoparticles
CFU	Cell forming units
CMS	Colistimethate sodium
CT	Computed tomography
CTAB	Cetyl Trimethyl Ammonium Bromide
CV	Crystal violet
Dap	Daptomycin
DLS	Dynamic light scattering
DLVO	Derjaguin, Landau, Verwey and Overbeek
D-PBS	Dulbecco's Phosphate Buffered Saline
EGFP	Enhanced green fluorescent protein
EIS	Electrochemical Impedance Spectroscopy
EPS	Extracellular polymeric substances

FTIR	Fourier Transform Infrared
HFIP	1,1,1,3,3,3-hexafluoroisopropanol
IM	Imatinib Mesylate
LB	Lysogeny Broth
LbL	Layer-by-layer
Lin	Linezolid
LPS	Lipopolysaccharides
MIC	Minimum inhibitory concentration
MRSA	Methicillin-Resistant Staphylococcus Aureus
NIR	Near infrared
NMR	Nuclear magnetic resonance
NR	Neutron Reflectivity
PAA	Polyallylamine
PAA	Poly(acrylic) acid
PAH	Polyallylamine hydrochloride
PBS	Phosphate Buffered Saline
PDADMAC	Polydiallyldimethylammonium chloride
PE	Polyelectrolytes
PEI	Polyethylenimine
PLA	poly(LD-lactide)
PSS	Polystyrenesulfonate

Rif	Rifampin
SCM	Simulated culture medium
SERS	Surface enhanced raman spectroscopy
SEM	Scanning electron microscope
SiRNA	Small interfering ribonucleic acid
SPR	Surface plasmon resonance
TEM	Transmission electron microscope
TOAB	Tetraoctylammonium bromide
UV-Vis	Ultraviolet-visible spectroscopy
Van	Vancomycin
XRD	X-ray diffraction
ZOI	Zone of Inhibition

ACKNOWLEDGEMENTS

There are a number of people who have made this research and my PhD journey possible. Firstly I want to thank my Supervisor, Associate Professor Ingo Köper for guiding me through my PhD journey. His knowledge and support have pushed me to achieve more and to take on other projects during my PhD to further develop my skills. He has assisted me to create a solid grounding for my career and for that I am immensely thankful.

I would also like to thank my ANSTO Co-supervisor Dr Kathleen Wood. She introduced me to the world of neutron scattering and has offered me so much support throughout my time at Lucas Heights.

Similarly, a big thank you needs to be extended to Dr Harriet Whiley and her students for taking the time to teach me microbiology techniques and for answering all my questions.

To Dr Stephen Holt and Dr Jakob Andersson, thank you for your assistance and guidance in neutron reflectivity, your expertise was greatly appreciated.

A significant part of this research was also possible due to an internship at the National Institute for Materials Science. I would like to extend a special thank you to Dr Mitsuhiro Ebara and Rio Kurimoto for making me feel so welcome and assisting me to carry out research in Japan.

To the members of the Köper group past and present who worked alongside me - thank you for your encouragement and friendship. I would like to extend a special mention to Ashley Carey - thank you for volunteering your time to assist me in my research. I hope you continue with the same enthusiasm and wish you all the best for your future in science.

I am extremely grateful to have received a Research Training Scholarship from the Australian Government and a top-up scholarship from the Australian Institute of Neutron Science and Engineering.

To my family and friends who have reminded me constantly that 'I am still a university student' I appreciate all the encouragement and support. To Debra and Brenton my loving parents I thank you for believing in me and guiding me for all these years. To my sisters, Alannah and Elise – your friendship is so important to me and I thank you for always being there for me. Finally, to my fiancé who has supported me, motivated me and helped me work through times when I didn't think I could do it – you have been my rock and I love and admire you.

DETAILS OF PUBLICATIONS

1. **Fuller, M.** & Köper, I. Biomedical Applications of Polyelectrolyte Coated Spherical Gold Nanoparticles, Nano Convergence, 2019. DOI: 10.1186/s40580-019-0183-4
2. **Fuller, M.** & Köper, I. Polyelectrolyte-coated Gold Nanoparticles: the Effect of Salt and Polyelectrolyte Concentration on colloidal stability, Polymers, 2018. DOI: 10.3390/polym10121336.
3. **Fuller, M.**, Carey, A., Whiley, H., Kurimoto, R., Ebara, M. & Köper, I. Nanoparticles in an Antibiotic-Loaded Nanomesh for Drug Delivery, 2019. DOI: 10.1039/C9RA06398F.
4. Andersson, J., **Fuller, M.**, Wood, K., Holt, S. & Köper, I. A Tethered Bilayer Lipid Membrane that Mimicks Microbial Membranes, ChemPhysChem, 2018. DOI: 10.1039/c8cp01346b

CONFERENCE PRESENTATIONS

Oral presentations:

1. **M. Fuller**, I. Köper, M. Ebara, Gold Nanoparticles in Antibiotic Loaded Wound Dressings, 10th International Nanomedicine Conference, Sydney, New South Wales, 2019.
2. **M. Fuller**, I. Köper, M. Ebara, Gold Nanoparticles in Antibiotic Loaded Wound Dressings, Australian Society for Medical Research Conference, Adelaide, South Australia, 2019.
3. **M. Fuller**, I. Köper, M. Ebara, Preventing Infection of Wounds through Nanomesh, Australian Society for Medical Research Conference, Adelaide, South Australia, 2018.
4. **M. Fuller**, I. Köper, M. Ebara, Preventing Infection through Implantable Nanomesh, Flinders University College of Science and Engineering Higher Research Degree Conference, Adelaide, South Australia, 2018.
5. **M. Fuller**, 3MT Thesis Presentation, Emerging Disruptive Technology Assessment Symposium, Melbourne, Victoria, 2018.

Poster presentations:

1. **M. Fuller**, I. Köper, M. Ebara, The Gold Standard in Wound Dressings, Flinders Institute for Nanoscale Science and Technology Conference, Adelaide, South Australia, 2019.
2. **M. Fuller**, I. Köper, M. Ebara, Nanomesh Loaded with Antibiotics and Nanoparticles for Improved Antibiotic Delivery, 2018 Controlled Release Asia Conference, Biopolis, Singapore, 2018.
3. **M. Fuller**, I. Köper, M. Ebara, Preventing Infection through Implantable Nanomesh, Flinders Institute for Nanoscale Science and Technology Conference, Adelaide, South Australia, 2018.

4. **M. Fuller**, I. Köper, M. Ebara, Preventing Infection through Implantable Nanomesh, Drug Delivery Australia Colloids on the Coast Conference, Wollongong, New South Wales, 2017.
5. **M. Fuller**, Harsha Padmanabhan, David Parsons, Ingo Köper, A Breath of Fresh Air For Cystic Fibrosis, Helmholtz Zentrum Berlin Neutron School, Munich, Germany, 2017.
6. **M. Fuller**, Harsha Padmanabhan, David Parsons, Ingo Köper, A Breath of Fresh Air For Cystic Fibrosis, Biophysics Conference, Adelaide, South Australia, 2016.

DECLARATION

I certify that this thesis does not incorporate without acknowledgment any material previously submitted for a degree or diploma in any university; and that to the best of my knowledge and belief it does not contain any material previously published or written by another person except where due reference is made in the text.

Signed: 

Date: 21/10/19

CHAPTER 1: INTRODUCTION

1.0 Background:

Antimicrobial resistance (AMR) is the ability of a disease-causing microbe to survive exposure to an antimicrobial agent that was previously effective at killing the microbe. Resistance occurs through mutation or gene transfer by the microbe and it is an ever-increasing problem worldwide. Without any advances in current treatment methods, resistant infections are predicted to kill 50 million people by the year 2050.¹ If this prediction is accurate, it means that more people will die of AMR infections than from cancer. To address AMR, my research has focused on using gold nanoparticles in combination with the membrane targeting antibiotic Colistin, to not only increase bacterial susceptibility but also to lower the dosage required to treat an infection. Gold nanoparticles were used in this research as recent studies have demonstrated that resistance develops less frequently against gold nanoparticles compared to the more commonly used silver nanoparticles.²

Colistin is considered a last-line antibiotic as it has serious dose-dependent side effects including neurotoxicity and nephrotoxicity.³ Increasing bacterial susceptibility means less Colistin is required to achieve the same therapeutic effect. By reducing the amount of Colistin required, the severity of side effects will also be reduced. Colistin is a restricted antibiotic, only prescribed when other antibiotics fail at treating an infection. As Colistin is used less frequently, less resistance for Colistin has developed compared to commonly used antibiotics such as penicillin.

Colistin is a cationic polypeptide made up of two major components, Colistin A (Polymyxin E1) and Colistin B (Polymyxin E2).⁴ Depending on the manufacturer, the ratio of the two polymyxins may differ. Commercially, there are two variations of Colistin; Colistin sulfate which is used both orally and topically and Colistimethate sodium (CMS) which is used intravenously or intramuscularly.⁵ Both variations can also be used via inhalation.⁵ CMS is the less potent prodrug of Colistin, and therefore it has fewer undesirable side effects and is less toxic.^{6,7} In order to ensure potency, Colistin has been used exclusively in this research rather than exploring both Colistin and CMS.

Colistin's mechanism of action involves interacting with the fatty acids and the phosphates in the lipopolysaccharides (LPS) which make up the outer membrane of Gram-negative bacteria.⁸ Colistin is electrostatically attracted to the anionic phosphate groups on the lipid A portion of the LPS membrane of Gram-negative bacteria through its cationic α,γ -diaminobutyric acid residue.^{9,10} This attraction leads to displacement of the membrane stabilisers calcium (Ca^{2+}) and magnesium (Mg^{2+}), which causes significant defects in the outer membrane (Fig. 1).¹¹ These defects increase the permeability of the bacterial cell, causing leakage of cytoplasmic contents, cell lysis and subsequently cell death.

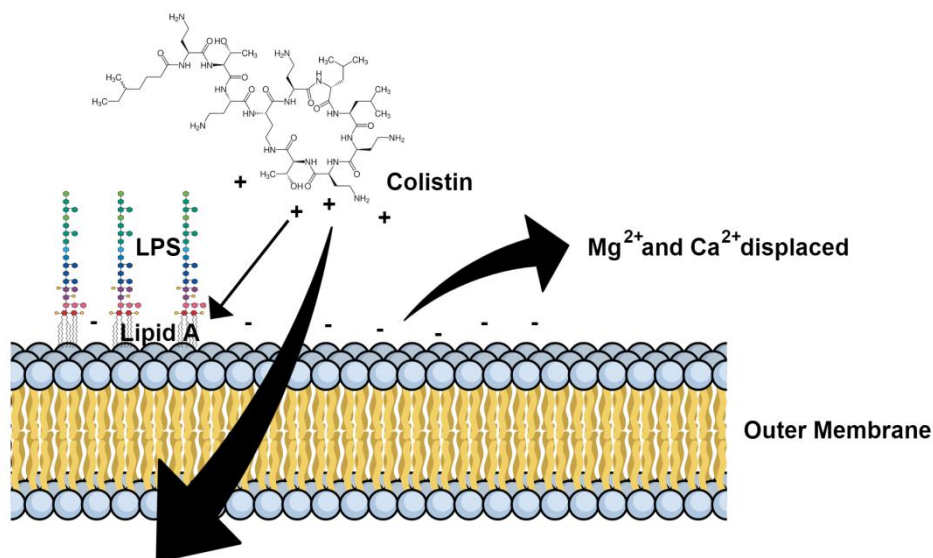


Figure 1: Schematic of the mechanism of action of Colistin sulfate showing Lipid A binding, displacement of Mg^{2+} and Ca^{2+} and disruption of the outer membrane.

The electrostatic interaction forms the basis of the reasoning behind utilising gold nanoparticles in this research. Positively charged nanoparticles can attach to the bacterial cell surface causing defects. When the bacterial cell is then attacked by Colistin, the dosage required to kill the cell is reduced as the defects offer an easier pathway into the cell. Gold nanoparticles were also chosen as they have some unique properties such as their ease of functionality and their Surface Plasmon Resonance (SPR) effect which have been further explained in Chapter 2.

1.1 Research Aims:

The primary aim of this research was to enhance the antibiotic effectiveness of Colistin through the use of gold nanoparticles. This required a multidisciplinary approach that included aspects of nanotechnology, chemistry, microbiology and materials science to determine an effective delivery mechanism that would increase an organism's susceptibility to Colistin. To achieve this overall aim, the secondary aims were as follows:

1. To assess the current understanding of the use of polyelectrolyte (PE) coated nanoparticles in biomedical applications.
2. To fabricate stable cationic polyelectrolyte coated gold nanoparticles.
3. To determine if these polyelectrolyte coated gold nanoparticles could increase bacterial susceptibility to Colistin.
4. To fabricate and assess the activity of Colistin coated anionic and cationic gold nanoparticles.
5. To develop a scaffold that can deliver Colistin over an extended period at a reduced dosage through the use of gold nanoparticles.

1.2 Research Methods:

In order to achieve these aims, a range of experiments were undertaken. The first aim was achieved through the use of a literature review to determine the current outlook for PE coated gold nanoparticles (Chapter 2). This included applications in medicine, their toxicity profile as well as the future outlook for PE based nanoparticles. The second aim was achieved through electrostatic attachment of PEs onto the surface of gold nanoparticles. The specific experimental methods as well as the characterisation techniques can be found in Chapter 3. The third aim used a combination of electrical impedance spectroscopy (EIS) and neutron reflectivity (NR) to assess how cationic polyelectrolyte charged gold nanoparticles interact with a Gram-negative bacterial model membrane (Chapter 4). This interaction was then monitored with the addition of Colistin either simultaneously with the PE coated gold nanoparticles or after the

nanoparticles had been removed. Differences in the membrane resistance as well as the outer membrane parameters were used to determine the effects that Colistin and the polyelectrolyte gold nanoparticles have on the bacterial model membrane. The fourth aim was achieved through fabrication and characterisation of Colistin coated gold nanoparticles using methods described in Chapter 5. The coated nanoparticles were then tested against *E. coli* to assess differences in susceptibility to Colistin. Finally, the last aim was accomplished through development of an optimised electrospun polymer nanomesh which contained the antibiotics Colistin and Vancomycin (Chapter 6). The release kinetics, cumulative release percentage and drug diffusion capability of the mesh was investigated with promising initial results. The full experimental methods are discussed in the individual chapters to allow ease of reading.

1.3 Structure of the thesis:

This thesis is primarily publication based. It is organised into 7 chapters, with each chapter exploring a different step in understanding how to increase bacterial susceptibility to Colistin. The various steps, which are presented as chapters, are shown in Figure 2.

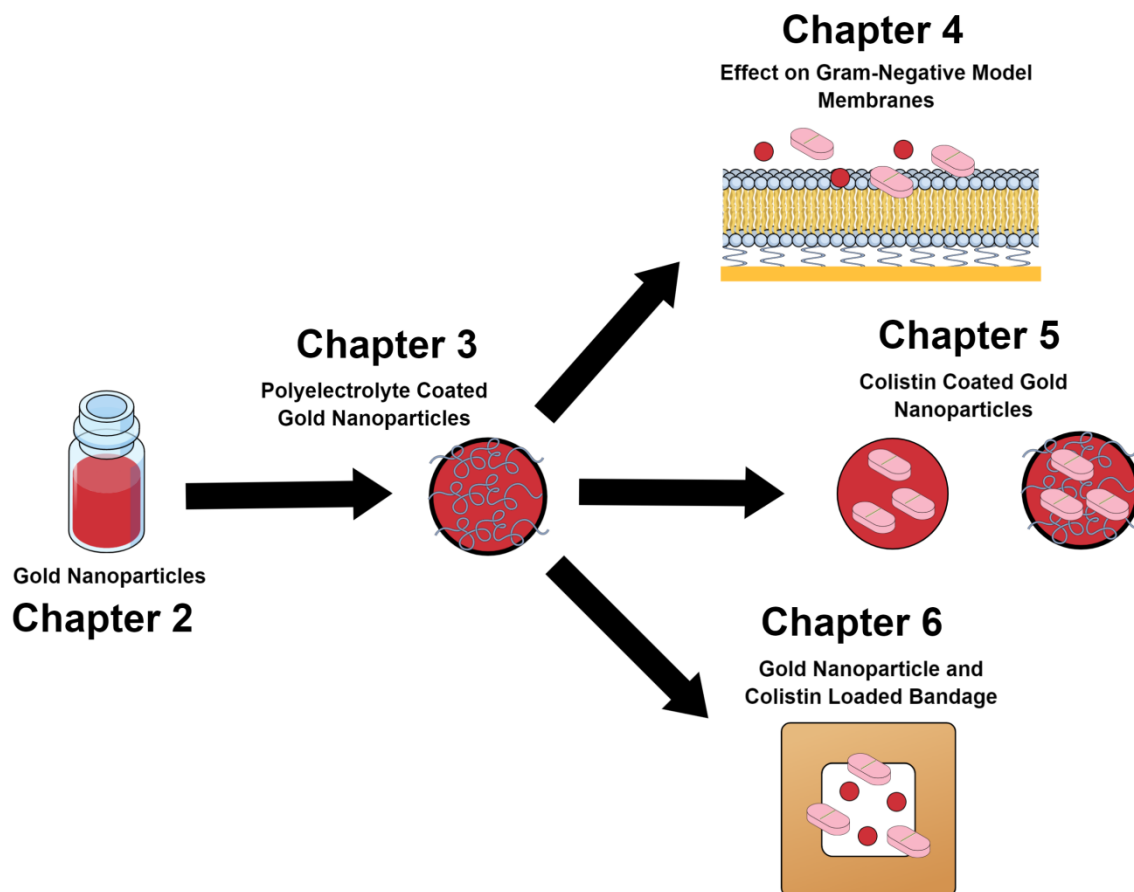


Figure 2: Graphical abstract of this thesis, with each part of the figure representing a different chapter.

Chapter 1 provides a brief background into the reasoning for the thesis topic and covers the methods and structure. Chapter 2 is a literature review of current biomedical applications of polyelectrolyte coated gold nanoparticles, taking into account synthesis, characterisation, uptake, applications and toxicity. Chapter 3 is a publication which describes how to achieve stable polyelectrolyte coated gold nanoparticles for future biomedical use. Chapter 4 explores the extent of defect formation caused by gold nanoparticles on a Gram-negative bacterial model membrane. It also provides evidence of increasing Colistin susceptibility by pre-treating the membrane with nanoparticles. Chapter 5 describes the formation of Colistin coated gold nanoparticles and assesses their ability to inhibit bacterial growth compared to Colistin on its own. Chapter 6 is a publication which discusses and assesses the use of an electrospun nanomesh as a

Colistin delivery system. It delves into the release kinetics and is a proof-of-concept study for effective antibiotic release. Finally, Chapter 7 looks into the conclusions of this work and suggests future directions for continuation of this research.

References:

1. O'Neill, J. Antimicrobial Resistance: Tackling a crisis for the health and wealth of nations; **2014**.
2. Elbehiry, A.; Al-Dubaib, M.; Marzouk, E.; Moussa, I., Antibacterial effects and resistance induction of silver and gold nanoparticles against *Staphylococcus aureus*-induced mastitis and the potential toxicity in rats. *MicrobiologyOpen* **2019**, 8 (4), e00698.
3. Edrees, N. E.; Galal, A. A. A.; Abdel Monaem, A. R.; Beheiry, R. R.; Metwally, M. M., Curcumin alleviates colistin-induced nephrotoxicity and neurotoxicity in rats via attenuation of oxidative stress, inflammation and apoptosis. *Chemico-Biological Interactions* **2018**, 294, 56-64.
4. Nation, R. L.; Velkov, T.; Li, J., Colistin and polymyxin B: peas in a pod, or chalk and cheese? *Clin Infect Dis* **2014**, 59 (1), 88-94.
5. Conly, J.; Johnston, B., Colistin: the phoenix arises. *Can J Infect Dis Med Microbiol* **2006**, 17 (5), 267-269.
6. Mendes, C. A.; Burdmann, E. A., [Polymyxins - review with emphasis on nephrotoxicity]. *Revista da Associacao Medica Brasileira (1992)* **2009**, 55 (6), 752-9.
7. Li, J.; Milne, R. W.; Nation, R. L.; Turnidge, J. D.; Smeaton, T. C.; Coulthard, K., Pharmacokinetics of colistin methanesulphonate and colistin in rats following an intravenous dose of colistin methanesulphonate. *Journal of Antimicrobial Chemotherapy* **2004**, 53 (5), 837-840.

8. Tran, T. B.; Velkov, T.; Nation, R. L.; Forrest, A.; Tsuji, B. T.; Bergen, P. J.; Li, J., Pharmacokinetics/pharmacodynamics of colistin and polymyxin B: are we there yet? *Int J Antimicrob Agents* **2016**, 48 (6), 592-597.
9. Velkov, T.; Thompson, P. E.; Nation, R. L.; Li, J., Structure--activity relationships of polymyxin antibiotics. *Journal of medicinal chemistry* **2010**, 53 (5), 1898-916.
10. Melo, M. N.; Ferre, R.; Castanho, M. A., Antimicrobial peptides: linking partition, activity and high membrane-bound concentrations. *Nature reviews. Microbiology* **2009**, 7 (3), 245-50.
11. Velkov, T.; Roberts, K. D.; Nation, R. L.; Thompson, P. E.; Li, J., Pharmacology of polymyxins: new insights into an 'old' class of antibiotics. *Future microbiology* **2013**, 8 (6), 711-24.

CHAPTER 2: BIOMEDICAL APPLICATIONS OF POLYELECTROLYTE COATED SPHERICAL GOLD NANOPARTICLES

This chapter has been published in Nano convergence and is entitled 'Biomedical applications of polyelectrolyte coated spherical gold nanoparticles'. It is a literature review which addresses the use of polyelectrolyte coated nanoparticles and discusses their current use in biomedical applications. It is authored by **Melanie Fuller** and Ingo Köper.

This review introduces and provides background information on polyelectrolyte coated gold nanoparticles, which has been used throughout this thesis (Fig. 3). It discusses different types of polyelectrolyte coatings and their current uses in biomedicine as well as summarises what is currently understood in literature.

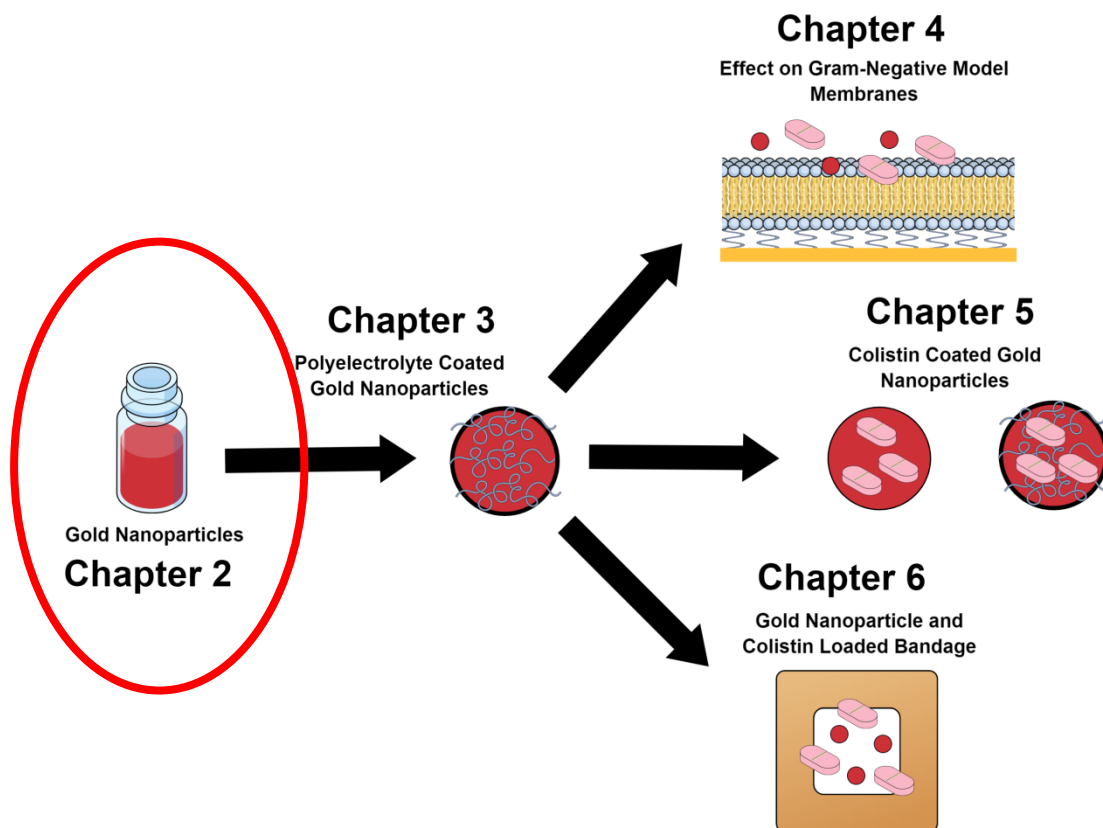


Figure 3: Diagram of the overall thesis, indicating Chapter 2 and how it fits into the larger body of work.

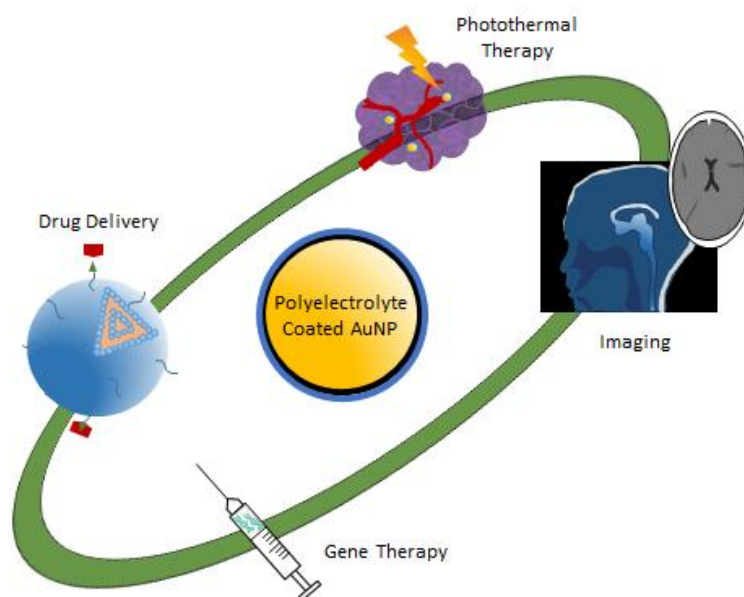


Figure 4: Graphical abstract from the publication 'Biomedical applications of polyelectrolyte coated spherical gold nanoparticles'.

Abstract:

Surface modified gold nanoparticles are becoming more and more popular for use in biomaterials due to the possibility for specific targeting and increased biocompatibility. This review provides a summary of the recent literature surrounding polyelectrolyte coatings on spherical gold nanoparticles and their potential biomedical applications. The synthesis and layer-by-layer coating approach are briefly discussed together with common characterisation methods. The potential applications and recent developments in drug delivery, gene therapy, photothermal therapy and imaging are summarized as well as the effects on cellular uptake and toxicity. Finally, the future outlook for polyelectrolyte coated gold nanoparticles is explored, focusing on their use in biomedicine.

1. Introduction:

Gold nanoparticles (AuNPs) which can be described as solid gold particles with a diameter between 1 and 100 nm, have the potential to be used in a range of biomedical applications due to their unique physical and optical properties.¹⁻⁴.

Examples of these unique properties include the surface plasmon resonance (SPR) effect, which can give information about the local environment including the size and physical dimensions of the particles, as well as Surface Enhanced Raman Scattering (SERS) where AuNPs can be used as probes to enhance Raman scattering.⁵⁻⁸ After a typical synthesis, AuNPs are coated with an organic material or capping agent to provide stability to the particles. One of the advantages of AuNPs is that they can be easily functionalized with a range of different materials including antibodies, proteins, ligands, DNA, polymers and polyelectrolytes.⁹⁻¹¹ This ease of functionality is useful in many of the biomedical applications which are discussed here.

Polyelectrolytes (PEs) are polymers of repeating units which bear an ionizable group.¹² These charged polymers can be used to coat surfaces and particles in a number of ways including covalent attachment, hydrogen bonding and electrostatic interactions between layers.^{13,14} Although there are many ways PEs can be attached to NPs, this review will focus on electrostatic attachment of PE coatings as they are easy to produce and have a range of applications from microfluidics to water membrane filtration systems.^{14,15} Specifically, the layer-by-layer (LbL) approach will be reviewed, where PEs can be attached to surface in a single or multilayer deposition. Essentially the LbL electrostatic approach uses two solutions of opposite charge. A substrate can be dipped into a solution or a particle solution can be mixed with PEs to coat a surface (Fig. 5).^{16,17} Once a coating of the polyelectrolyte has been added, the charge on the substrate or particle is inverted, and hence a subsequent polymer layer of opposite charge can be applied (Fig. 5). The number of layers applied determines the total thickness of the polymer coating.¹³ Due to the ease of deposition, LbL polyelectrolyte coatings have been initially investigated mainly on flat substrates for a wide range of applications, but now coating of 3-dimensional objects is also being explored.^{15,18,19} These objects, such as spherical nanoparticles, offer larger surface area to volume ratios and larger reactive surface areas, which is essential in drug delivery and catalysis.^{20,21}

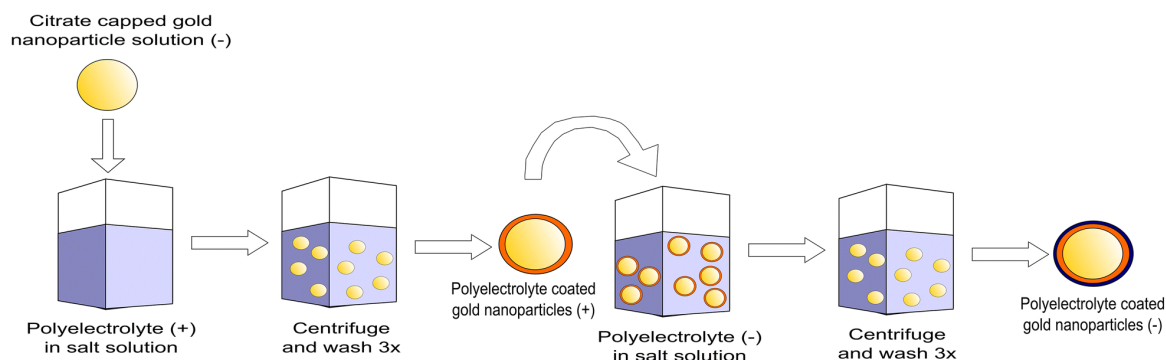


Figure 5: Method for self-assembly of polyelectrolyte-coated citrate capped gold nanoparticles using the LbL method.

The coating efficiency of the PEs on NPs is influenced by the shape of the nanoparticle, the type, length and concentration of the polymer, as well as the total salt concentration in the solution used.^{22,23} Gold nanorods (GNRs) have been the most widely studied 3D particle shape for PE coatings, as their structure allows for relatively homogeneous coatings. Additionally, they have been extensively used for sensing applications, as their surface plasmon is particularly sensitive to changes in the local environment.^{20,24-27} This review however is focused on exploring spherical AuNPs, and comprehensive reviews of AuNRs can be found elsewhere.^{28,29} The curved surface of small (<50 nm) NPs makes it difficult to form complete and homogeneous coatings, in part due to the lack of flexibility of the polymer chains, resulting in poor coverage on the nanoparticle surface and a decrease in stability of the coating.³⁰ In general, incomplete coatings can cause particle aggregation.^{23,31,32} To avoid incomplete coatings, the polymer which is coating the NP needs to be in excess to ensure complete coverage on the surface.²³ Similarly the addition of salt in the coating solution typically allows for more flexibility in the PE chains, which can lead to an improved coverage of the particles.^{22,33-35}

2. Synthesis of polyelectrolyte coated nanoparticles:

There are many different approaches to synthesizing AuNPs, each aiming to control nanoparticle size, shape and surface functionality.³⁶⁻³⁸ In the Turkevich method, hydrogen tetrachloroaurate (HAuCl_4) is treated with citric acid in boiling water, with the citrate acting both as a reducing and stabilizing agent.^{39,40} This method produces NPs with diameters in the range of 10-20 nm, with the particle size being controlled by the gold to citrate ratio.⁴¹ Alkanethiol-stabilized AuNPs, which are soluble in organic solvents, can be formed using tetraoctylammonium bromide (TOAB) as the capping and sodium borohydrate (NaBH_4) as the reducing agent.⁴² Depending on the gold-to-thiol ratio, temperature and reduction rate, NPs between 1.5 and 5 nm in diameter can be produced.⁴² Other synthesis methods resulting in size and particle uniformity distributions use different reducing agents such as sucrose, ethylenediaminetetraacetic acid, fruit extracts and amines.⁴³⁻⁴⁷

The capping agent used in the NP synthesis influences which PE can be used for the initial coating. The LbL technique is based on the attraction of oppositely charged layers and is the main interaction employed in coating AuNPs with PEs. Commonly used PE polymers are shown in Table 1. The charge of the PE is important as the polymer will electrostatically attach to a particle only if the capping agent is of the opposite charge.¹⁴ For example, in the Turkevich method which caps the particles in negatively charged citrate, only positively charged PEs will attach.

Table 1: Commonly used polyelectrolytes showing their charge at pH 7 and their current applications.

Abbreviation	Name	Charge at neutral pH	Application	References
PEI	Polyethyleneimine	Positive	Gene therapy, Drug delivery	48,49
PAH	Polyallylamine hydrochloride	Positive	Drug delivery, Gene therapy.	50,51
PSS	Polystyrene sulfonate	Negative	Drug delivery	52,53
PLL	Poly-L-lysine	Positive	Gene therapy	54

3. Characterising the attachment of polyelectrolytes onto gold nanoparticles:

Typically, the attachment of PE coatings on AuNPs is characterized using Surface Plasmon Resonance (SPR), Dynamic Light Scattering (DLS) and zeta potential. Other methods such as Transmission Electron Microscopy (TEM) and Nuclear Magnetic Resonance (NMR) are commonly used but will not be discussed here.

3.1 Surface Plasmon Resonance:

A surface plasmon is a charge-density oscillation phenomenon, which exists at the interface of two media with dielectric constants of opposite signs.⁵⁵ Nobel metals have a negative dielectric constant and are therefore ideal materials for

surface plasmon detection. When light of a specific wavelength interacts with a AuNP, it causes a collective oscillation of the free electrons in the metal.⁵⁶ When the incoming electromagnetic wave has the same wavevector as the oscillating conduction electrons, resonance occurs (Fig. 6) and the incoming energy is absorbed into the plasmon wave. Typically, SPR is observed by measuring the absorbance of the NP-containing solution as a function of wavelength. The resulting signal depends on the shape, size, surface ligand, solvent, temperature and proximity of other NPs in the solution.^{57,58} For example, spherical AuNPs exhibit size dependent absorption peaks (surface plasmon band) from 500-550 nm.^{11,59}

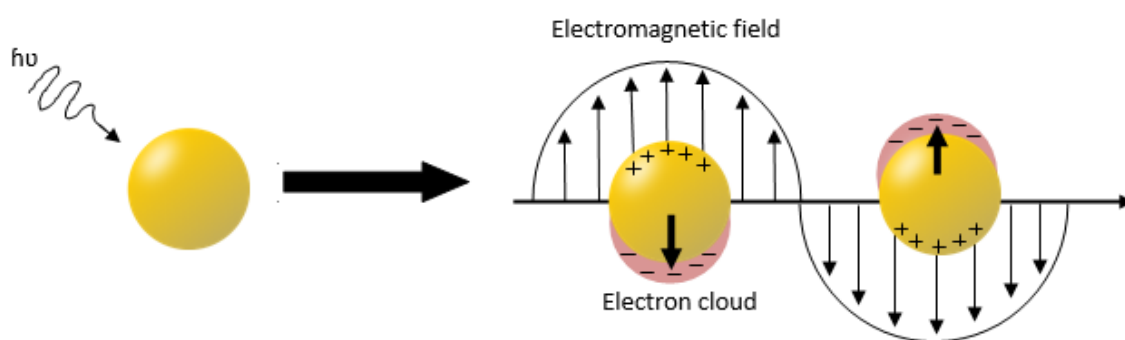


Figure 6: Schematic representation of the conduction electrons oscillating across the gold nanoparticle in the electromagnetic field of incident light.

Aggregation of NPs can be observed by a red-shifting and broadening of the SPR peak, and the colour of NP solution changes from a red to blue due to interparticle plasmon coupling.⁶⁰ The addition of a polymer onto the surface of the AuNP results in a change in the dielectric properties at the nanoparticle surface which shifts the SPR peak (Fig. 7A, B).³⁰ As each polymer layer is added, the peak's wavelength increases as the dielectric property changes. Due to this, the LbL addition of PE multilayer architectures can be monitored through changes in the NPs SPR peak (Fig. 7A).

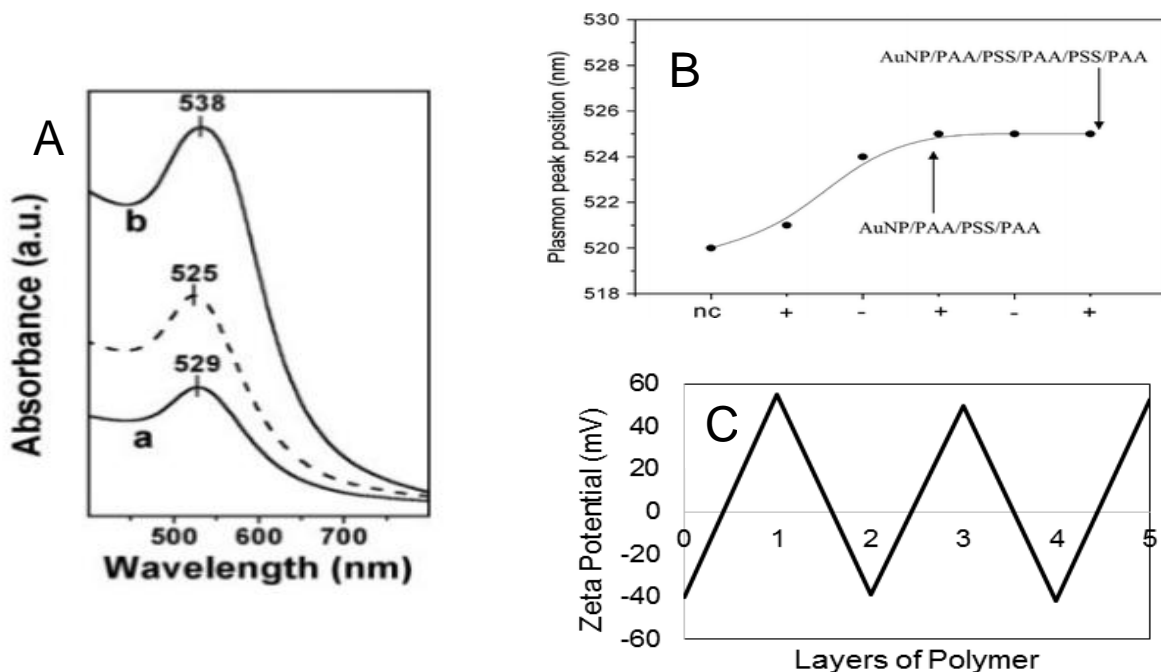


Figure 7: (A) UV-Vis spectra of mercaptoundecanoic acid coated AuNPs (dashed line) subsequently coated in (a) Polydiallyldimethylammonium chloride (PDADMAC) and (b) PDADMAC/polystyrenesulfonate (PSS). Reproduced from Ref ⁶¹ with permission from Wiley. (B) Surface plasmon band shifts compared to the number of polyelectrolyte coatings on the AuNPs. Reproduced from Ref ⁵² with permission from Wiley. (C) Zeta potential of uncoated citrate capped AuNPs (0) then subsequent addition of positively charged polyallylamine (PAA) and negatively charged polystyrenesulfonate (PSS). Reproduced and adapted from Ref ⁵² with permission from Wiley,

3.2 Zeta Potential:

Measuring the zeta potential of AuNPs is a quick and efficient way to determine the charge of particles and the stability of the colloidal system.⁶² The zeta potential can be described as the potential at the shear plane of a solid particle moving under an electric field, where the shear plane is the boundary at the solid-liquid interface, between the stationary and diffuse layers.^{63,64} At neutral pH, citrate capped AuNPs have a resulting negative charge, which attracts positively charged electrolyte ions. These ions then form an electrical layer at the surface of the particle, known as the Stern layer. A secondary layer called the diffuse layer also forms, which consists of both positive and negative ions with a high counter-

ion charge. Together these two layers make up an electrical double layer. The zeta potential of the particle corresponds to the amount of energy required to shear a particle and associated double layer from the bulk solution. In order to calculate the zeta potential, the electrophoretic mobility of a particle is measured in a direct current electric field.⁶² Stable colloidal solutions typically have zeta potentials smaller than -30 mV or larger than +30 mV. Values between these potentials indicate unstable solutions, as the particles do not carry enough charge to repel each other, which can lead to aggregation.⁶⁵ In the case of PE-coated NPs, the charge of the coated particles alternates between a positive and negative charge, depending on the polymers used (Fig. 7C). This process is often used to show attachment of the polyelectrolyte layer, as well as to confirm the colloidal stability of the system.

4. Uptake and Interaction with Cells:

Biocompatibility is essential in any biomedical application as well as the ability for the uptake of NPs into cells, especially for applications such as drug delivery. The interactions of the particle with the cell membrane is ultimately what determines cellular uptake, as it is the key to the regulation of the uptake process.⁶⁶ Cellular interactions and cellular uptake is a large and complex topic area and hence this section will only discuss the main considerations with select examples. More in-depth explanations in this area can be found in other review articles.^{67,68} The cellular uptake of AuNPs is dependent on the size, charge and surface properties of the NP.⁶⁹ Other biological factors include the type of cell, cellular recognition and the temperature.⁷⁰ These biological factors also affect the protein corona, which is a protein layer attached to the AuNP, brought about by the proteins found in the body (*in vivo*) and in serum (*in vitro*) which attach to the NPs surface.⁷⁰

There are five ways in which mammalian cells can internalize nanoparticles: phagocytosis, macropinocytosis, clatherin-mediated, caveolin-mediated and clatherin/caveolin-independent endocytosis.⁷¹⁻⁷⁴ Of these pathways, clatherin and

caveolin mediated endocytosis are often widely grouped as receptor mediated endocytosis.⁷⁵⁻⁷⁷ It has been proposed that receptor mediated endocytosis is the primary mechanism for cellular entry of AuNPs less than 100 nm in diameter into mammalian cells.^{67,78} In receptor mediated endocytosis, NPs which have ligands on their surface that target specific receptors, attach to the cells by receptor-ligand binding. The membrane of the cell then wraps around the NP, internalizing it into the cell. The time it takes for the NP to be taken up by the cell depends on the size of the NP, with generally a faster uptake for larger NPs.^{70,78} However, the size and uptake will change depending on the protein corona and its composition when it forms around the particle. The addition of serum to *in vitro* testing provides a more realistic biological environment, as the proteins in the serum can attach to the NP forming the protein corona. The protein corona prevents the NP from having direct contact with the cell membrane, hence altering the uptake. The uptake rate is determined by the receptor diffusion kinetics and the thermodynamic driving force for the membrane wrapping.⁷⁸ This rate was shown to be dependent on the cell type, particle size and the composition of the protein corona.

It has been shown that ~55 nm diameter NPs are taken up by the cell the fastest, as the chemical energy released by the receptor-ligand interaction produces enough free energy (thermodynamic driving force) to drive the NP into the cell.⁷⁸⁻⁸⁰ For NPs less than 40 nm in diameter, the receptor-ligand interactions cannot provide enough energy to 'wrap' the NP on the cell's surface as there are fewer ligands that can interact with receptors, meaning not enough chemical energy is produced to overcome the more unfavorable deformation of the cell membrane.⁸⁰ Therefore in order for smaller NPs to be taken into the cell, a cluster of NPs are required to overcome the energy barrier to internalization.⁷⁸ However, when taking into account the protein corona, for 50 nm diameter AuNP in serum, the presence of the corona decreased the uptake efficiency significantly, with a 70% decrease in RAW 264.7 cells and 40% decrease in Hep G2 cells. For 20 nm and 5 nm AuNP, it was found the inhibitory effect of the corona on cellular uptake becomes negligible for both types of cells.⁷⁰ Even with a considerably lower

uptake efficiency, the uptake was still higher in larger (50 nm) AuNP, suggesting for biomedical applications, ≥ 50 nm AuNPs should be used.⁷⁰

The influence of the surface charge on cellular uptake is relatively well understood, but also dependant on a number of experimental factors. These experimental factors including particle size, surface functionalisation, NP shape and cell type are often observed to interplay with each other, making identifying differences of one variable a complex endeavour. Typically, positively charged NPs are more easily taken up by the cell, probably due to being attracted by the negatively charged cell membrane.⁸¹⁻⁸³ However, proteins from the growth serum of cells can adsorb to both cationic and anionic particles, forming a protein corona which has the potential to alter their charge and thus minimizes attractive forces.^{84,85} The effect of proteins adsorbing onto AuNPs has been observed through numerous studies including on curcumin-functionalized AuNP where the uptake in human prostate cancer cells was decreased when curcumin-AuNP were in the presence of serum containing media compared to serum-free media.⁸⁶

The localization of the NP inside the cells is important for biomedical applications but once again the intracellular distribution of AuNPs depends on a number of factors including size, concentration, and serum/media type. NPs with no specific surface functionalisation and a diameter of less than 6 nm have been shown to enter the nucleus of various cells.⁸⁷⁻⁸⁹ Similarly, other studies have observed that diameters of greater than 6 nm do not enter the nucleus but often enter cells inside vesicles.^{78,90-92} Knowing the size range of NPs which reach the nucleus is important for inducing apoptosis in cells when treating conditions such as cancer and therefore needs to be taken into consideration depending on the application.

The biodistribution of AuNP when injected into mice, was observed to change depending on the charge of a 2 nm core AuNP.⁹³ Although the research did not

use PEs to alter the charge, similar results would be expected when using PEs. It was found that positively charged NPs accumulate in the filtering regions of the spleen and liver, indicating they filter from the bloodstream at a faster rate than anionic or neutral NPs. The neutral NPs were shown to accumulate in the arteries and negatively charged NPs were found homogeneously distributed within the kidney. Another key difference was the neutral NPs which were shown to interact with the immune system. This interaction however may be due to the type of proteins which make up the corona surrounding the particle.⁹³

In terms of PE coated AuNP, there was very little research found surrounding the uptake and cellular interactions. Thus, the majority of uptake and interaction research has come from studies on AuNP with a large variety of coatings. When comparing experiments for AuNP, even being such a large research area, it is difficult to form conclusions for *in vitro* studies, as there are many complex parameters which dictate the cellular response. The cell type, serum used, AuNP size, concentration and charge among others can alter the outcome significantly. Similarly another difficulty is being able to predict the biodistribution as the protein corona which forms when the NPs enter the body, (i.e. blood, lung etc) changes as the NP is transported through different regions such as the bloodstream.⁹³ Overall the uptake and distribution is a complex interplay between different experimental factors which makes drawing direct comparisons difficult.

5. Applications:

The unique optical and physical properties of AuNPs and the increased biocompatibility of PE-coated nanoparticles has led to a range of potential biomedical applications, including drug delivery, gene therapy and cancer therapy (Table 1).^{50,52,53,69,94} The type of PE used has a significant influence on how the particles can be used and how they interact with tissues and cells. A fundamental understanding of the influence of the PEs on interactions with biological material is hence crucial to optimize their use. There are two main delivery methods for drug delivery: targeted and non-targeted. In targeted delivery, a ligand, generally

an antibody or peptide, is attached to the NP and will target a receptor on a specific cell.^{95,96} Non-targeted delivery is the delivery without targeting specific cells, where the drug will be released to both healthy and diseased cells. The type of delivery is extremely important in applications such as gene therapy and photothermal therapy, where treatment needs to be given into a specific area of the body. siRNA delivery for example will target a specific cell's cytoplasm to achieve down-regulation (80-90% decrease) of an overproduced protein.⁹⁷ Similarly in photothermal therapy, ensuring the AuNPs reaches the diseased cells to cause cell death rather than healthy cells is vital to reduce collateral damage.⁹⁸

5.1 Drug Delivery:

Targeted drug delivery allows for an increased concentration of drug to be given to a specific cell type compared to conventional untargeted delivery. In many cases this higher concentration increases the efficacy and decreases unwanted side effects, especially useful for drugs that can have debilitating side effects such those used in chemotherapy. Attaching ligands such as antibodies to the surface of a drug carrier allows drug release into specific cells which have the correct receptors.

For targeted drug delivery, PE coatings can be used as anchoring points for antibodies. This was shown in a proof of concept study, where IgG monoclonal antibodies, which target proteins overexpressed in cancer cells, were anchored to the surface of polyallylamine (PAA) and PSS coated AuNPs (Fig. 8).⁵² Conceptually, this could have great implications for the cancer treatments, as drugs could be loaded inside the AuNP or within the PE layers and then be targeted to cancer cells by the antibody attached on its surface. This would mean a lower dose of chemotherapy could be given with less systemic exposure, lessening the side effects and increasing the survival rate. Issues however with this type of antibody targeting is the administration into the body, where unlike an *in vitro* test there are many proteins which attach themselves to foreign bodies like NPs, making the receptor to antibody attachment problematic.

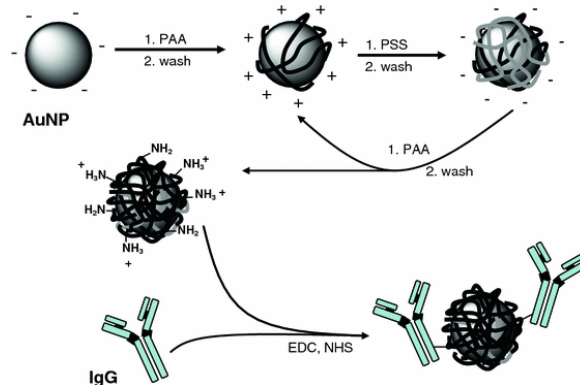


Figure 8: Citrate stabilized gold nanoparticles coated with PSS and PAA in a LbL method with the addition of IgG antibody through amide linkages. Reproduced from Ref ⁵² with permission from Wiley.

One of the advantages of the PE systems is that water insoluble drugs, which previously have been difficult to deliver, now have an easier pathway.⁹⁹ This is shown to be possible through the use of multilayer based drug carrier systems, where a vehicle such as a NPs can have water-insoluble drugs encapsulated within its PE chains. In a proof of concept study, three polymer layers with one containing a water-insoluble drug, were absorbed onto a NP carrier and this carrier was able to increase the drug deposition efficiency by a factor of 100.⁵³ In order to trap the drug, citrate coated AuNPs were used, then subsequently coated with polyallylamine hydrochloride (PAH) before the complexed drug was mixed with PSS and electrostatically attached to the PAH coating.

A more recent proof of concept study has found that the drug, Imatinib Mesylate (IM), used for cancer treatment could be encapsulated into PSS/PEI multilayer functionalized gold nanoparticles. This IM-PSS/PEI-AuNP system was tested in several ways with uptake into B16F10 murine melanoma cells measured as well as an *in vitro* skin penetration study.⁴⁸ At a gold concentration greater than 50 μM and IM concentrations above 31 μM , the IM-PSS/PEI-AuNP had a significantly higher growth inhibition of cancer cells compared to IM alone. The *in vitro* skin penetration studies conducted using pig ear skin, showed the use of iontophoresis (voltage gradient on the skin) enhanced the skin penetration of the IM-PSS/PEI-

AuNPs. Thus a topical treatment of IM-PSS/PEI-AuNPs with iontophoresis shows potential for enhanced melanoma treatment compared to IM alone.

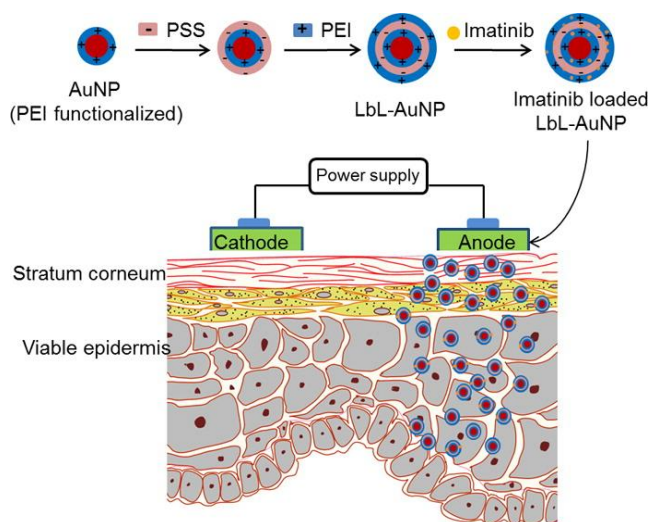


Figure 9: A schematic of the cancer drug, Imatinib Mesylate being encapsulated in the multilayer coated PEI/PSS/PEI AuNPs, showing the use of iontophoresis for topical delivery into the layers of the skin. Reprinted from Ref ⁴⁸ with permission from the American Chemical Society.

5.2 Gene Therapy:

Small interfering RNA (siRNA) delivery has the potential to be used in therapeutics to temporarily silence genes which could have significant effects on genetic diseases, however siRNA are notoriously difficult to deliver due to instability.¹⁰⁰ PE coated AuNPs have been shown to be better delivery vehicles than commonly used polymer vehicles.⁴⁹ Other delivery platforms such as cationic lipids and polymers have shown promise however instability is often the biggest issue, leading to decreases in efficacy.⁶⁹ In a proof of concept study, siRNA has been attached onto a PE coated AuNP system and delivered into CHO-K1 cells which express enhanced green fluorescent protein (EGFP).⁶⁹ The siRNA successfully reduced the EGFP expression and the cells remained viable after the addition of the AuNPs.

The current gold standard for non-viral gene transfection is using PEI or Lipofectamine. PEI is a polyelectrolyte in its own right, however in this case it is used to form a polyplex with DNA, rather than as a coating. This gold standard has been recently challenged in a study which synthesized PEI (25kDa) coated AuNP as DNA nanocarriers which found that these nanoparticles were more efficient gene vectors than both Lipofectamine and un-modified PEI.⁴⁹ PEI coated nanoparticles also showed low cell cytotoxicity and were fabricated in a simple one-pot method. Thus PE coated gold nanoparticles show great promise for gene transfection in the future, as they can out-perform the current gold standard.

One of the challenges with using PEs is that the strong interaction of oppositely charged polymers often leads to retardation of the payload release. One way this has been overcome is by changing the pH of the PE system, allowing for a charge reversal on the PE in acidic conditions, leading to release of the siRNA. Using the charge reversal method, a study which used PEI/PAH-Cit/PEI/MUA-AuNPs to release siRNA into cancer cells was able to knock-down 80% of Lamin A/C protein expression in acidic conditions, whereas the siRNA remained attached at a neutral or basic pH.⁹⁴ Interestingly, the siRNA was released with 14% more efficiency than what is commercially available for this knockdown.

5.3 Photothermal Therapy:

Hyperthermia is a cancer treatment that has been used since the early 1990s.¹⁰¹ When heat, typically just above the physiological temperature, is generated in a region of the body, it can lead to damage and destruction of cells.¹⁰¹ In Photothermal therapy, the heating is more intense and is applied to a specific area through the use of NPs, resulting in fewer unwanted side effects compared to the hyperthermic treatment.¹⁰² AuNPs can be targeted to a site in the body (i.e. a tumor) by manual injection or through targeted delivery. An external laser with a wavelength between 650-1350 nm is then aimed at the specific site where the NPs absorb or scatter that light.¹⁰³ This wavelength range is important as it can

deeply penetrate through healthy tissue to reach the AuNPs. The absorbed light causes resonance and is converted into heat, which is released to the surrounding tissue causing cellular death. Although this concept has been shown in several examples, so far PE coated AuNPs have not been used. However, PE-coated GNRs have been shown to be effective in killing cancer cells in mice and cell lines through photothermal therapy.¹⁰⁴⁻¹⁰⁷ Compared to GNR, there is little research surrounding spherical AuNPs for use in Photothermal therapy, likely due to the potentially limited applications, as this therapy seeks to penetrate and heat the deeper tissue with near infrared (NIR) light. As spherical nanoparticles tend to have absorbance between 500-550 nm, this does not target the NIR region and thus will not penetrate deep tissue in the same way as other shapes such as nanorods would.¹⁰⁸ Recent studies using AuNP have overcome this by using aggregated or clustered nanoparticles, as this shifts the absorbance peak to higher wavelengths, allowing the wavelength of absorption to be within the therapeutic window.^{109,110}

5.4 Imaging:

Imaging in medicine is an important tool for a number of procedures including the localization and diagnosis of cancers. The optical properties of gold make it very attractive for use as a contrast agent in imaging. So far, PE coated GNRs have been used for imaging applications rather than spherical AuNPs. A comprehensive review on PE GNRs and their imaging capabilities can be found by Pissuwan and Niidome and is not within the scope of this review.²⁹

Photoacoustic (PA) imaging and computed tomography (CT) are also useful tools in clinical practice for imaging. PA imaging is based on the PA effect, where pulsed laser light is utilized as probing energy which produces acoustic waves by thermal expansion. These waves are then detected at the surface of the tissue by ultrasound and are re-constructed to form an image.¹¹¹ A study in which PEG-b-poly(ϵ -caprolactone) was tethered to AuNPs showed a strong plasmon coupling effect where NIR absorption induced plasmon coupling causing an increase in PA

signal with high conversion efficiency.¹¹² Similarly AuNP have also shown promise as CT contrast agents due to their favourable properties. CT images are produced by a combination of x-ray images taken at different angles by rotation around an object, to form a cross-sectional 3D image known as a CT scan. Depending on what is being imaged, contrast agents can be used to highlight specific areas such as blood vessels or the tissue structure of organs by attenuating the x-rays to improve image quality.¹¹³ Gold nanoparticles are being explored for their use as a contrast agent in CT due to gold having a high atomic number and electron density, meaning it has good X-ray attenuation ability. In an experiment using a range of sizes of PEGylated AuNP as a contrast agent for CT scans, it was found NPs with a size of 13.2 nm and sizes greater than 34.8 nm performed ~20% better in attenuation intensity than Iohexal, a common CT contrast agent.¹¹⁴ Thus the area of imaging is extremely promising for PE coated AuNP and AuNPs in general.

6. Toxicity:

The cytotoxicity of AuNPs is extremely important, especially if they are being used in the biomedical field. The cytotoxicity is dependent on the size, shape, functionalisation, surface charge and aggregation of the NPs as well as biological factors including the type of cell and the uptake mechanisms into the cell.¹¹⁵⁻¹¹⁹ PE coatings on AuNPs appear to be relatively non-toxic to cells, however other factors including the type of coating and the NP size need to be considered. For example, PAH coated 18 nm diameter AuNP were compared with CTAB, citrate and poly(acrylic acid) (PAA) coated AuNPs. They were exposed to SH-SY5Y (human neuroblastoma) cells for 24 hours and after incubation all coatings except the CTAB coating showed >95% cell viability. Interestingly, when 40 nm PAA coated AuNP were used, cell viability dropped considerably to only 10% using the same gold concentration.¹²⁰ Another study has a similar result, where 10 nm diameter PEI coated AuNP showed to be biocompatible through *in vitro* cytotoxicity studies, where in gold concentrations of up to 400 μ M they were shown to be non-toxic to three different cancer cell lines (HCT116 colorectal carcinoma, MCF7 breast adenocarcinoma and PC3 prostate adenocarcinoma).¹²¹

Whereas, the 23 nm diameter PEI coated AuNP showed a moderate level of cytotoxicity to the same three cancer cell lines, with IC₅₀ results below 80 μM.¹²¹ In both experiments the larger nanoparticles proved to be more cytotoxic than their smaller counterparts. In contrast to this, a recent study has found that *in vitro* toxicity of PEG coated AuNPs is dependent upon size of the particles and the dose, with smaller size and higher concentration leading to increased cytotoxicity.² Similarly in another study, 1.4 nm AuNPs were 100 times more toxic than 15 nm AuNPs using the same coating.¹²² Thus there are discrepancies found about size and toxicity throughout the literature which further emphasizes the complexity of experimental design, especially when testing *in vitro*.

With many discrepancies found, drawing conclusions from the collective body of evidence is difficult as results vary depending on a number of experimental factors. The toxicity seems to be dependent on the size, surface functionalisation, concentration and surface charge of the AuNP as well as cell type, serum used, incubation time etc. Although there are many studies on AuNP toxicity, there are very few studies on the toxicity of PE coated AuNP. In order to understand the role PEs play in the toxicity space, standardized protocols for both *in vivo* and *in vitro* studies including appropriate cell types, assays and dosages would be beneficial to directly compare different coatings to determine the toxicity in a range of cell types.

7. Conclusions and future outlook:

The available literature on PE coated spherical AuNPs is limited compared to AuNP with other coatings or its PE coated GNR counterpart. The interaction of AuNP with cells in the body as well as uptake is dictated by a range of parameters and despite a large body of research, drawing conclusions is difficult as there are many inconsistencies and complexities to consider. Variables such as the cell type, the medium used, AuNP size, concentration and charge among others can alter the outcome significantly and hence care needs to be taken when comparing results from literature. Conclusions that can be drawn from the presented work are:

- PE coated AuNPs have shown to be very effective as siRNA carriers – even more so than the current gold standard of gene transfection. In addition, proof-of-concept studies have indicated they can be used as effective drug delivery vehicles.
- The use of AuNP in imaging techniques such as photoacoustic imaging and computed tomography have shown great promise in initial studies, with PEGylated AuNPs out-performing Iohexal, a common CT contrast agent.
- Typically, ~50 nm diameter AuNP have the highest uptake efficiency compared to smaller AuNPs.

There is however, a large gap of knowledge and more research is required to determine how the variables (size of the PE, salt concentration of PE mixture, strength of the attached anion on the AuNPs surface and pH) play a role in the deposition of PEs onto the AuNPs. Other challenges include how the addition of the PE coatings on AuNPs affect the cellular uptake and interaction both *in vitro* and *in vivo*. The future outlook for the use of PE coated AuNPs is positive, and this review has shown several of the possible uses in biomedicine. There is still much research to be conducted to better understand these systems and how each individual parameter impacts how they interact with cells but the initial literature in this area shows promise that PE coated AuNPs could reach their potential in the biomedical field.

Acknowledgements:

The authors would like to thank the Australian Institute of Nuclear Science and Engineering (AINSE Ltd) (Award –PGRA) for the top-up scholarship and the Australian Government Research Training Program for providing financial assistance.

References:

1. Elahi, N.; Kamali, M.; Baghersad, M.H. Recent biomedical applications of gold nanoparticles: A review, *Talanta* **2018**, *184*, 537-556.
2. Li, X.; Hu, Z.; Ma, J.; Wang, X.; Zhang, Y.; Wang, W.; Yuan, Z. The systematic evaluation of size-dependent toxicity and multi-time biodistribution of gold nanoparticles, *Colloids and Surfaces B: Biointerfaces* 2018, *167*, 260-266.
3. Nanjwade, B.K.; Sarkar, A.B.; Srichana, T. Chapter 12 - Design and Characterization of Nanoparticulate Drug Delivery. In *Characterization and Biology of Nanomaterials for Drug Delivery*, Mohapatra, S.S., Ranjan, S., Dasgupta, N., Mishra, R.K., Thomas, S., Eds. Elsevier: 2019; pp. 337-350.
4. Piella, J.; Bastús, N.G.; Puentes, V. Size-Dependent Protein–Nanoparticle Interactions in Citrate-Stabilized Gold Nanoparticles: The Emergence of the Protein Corona, *Bioconjugate Chemistry* 2017, *28*, 88-97.
5. Kerr, M.A.; Yan, F. Bromide-Assisted Anisotropic Growth of Gold Nanoparticles as Substrates for Surface-Enhanced Raman Scattering, *Journal of Spectroscopy* 2016, *2016*, 8.
6. Cao, Y.C.; Jin, R.; Mirkin, C.A. Nanoparticles with Raman spectroscopic fingerprints for DNA and RNA detection, *Science (New York, N.Y.)* 2002, *297*, 1536-1540.
7. Ashley, M.J.; Bourgeois, M.R.; Murthy, R.R.; Laramy, C.R.; Ross, M.B.; Naik, R.R.; Schatz, G.C.; Mirkin, C.A. Shape and Size Control of Substrate-Grown Gold Nanoparticles for Surface-Enhanced Raman Spectroscopy Detection

of Chemical Analytes, *The Journal of Physical Chemistry C* 2018, 122, 2307-2314.

8. Lane, L.A.; Qian, X.; Nie, S. SERS Nanoparticles in Medicine: From Label-Free Detection to Spectroscopic Tagging, *Chemical Reviews* 2015, 115, 10489-10529.

9. Fratoddi, I.; Venditti, I.; Cametti, C.; Russo, M.V. How toxic are gold nanoparticles? The state-of-the-art, *Nano Research* 2015, 8, 1771-1799.

10. Kong, F.-Y.; Zhang, J.-W.; Li, R.-F.; Wang, Z.-X.; Wang, W.-J.; Wang, W. Unique Roles of Gold Nanoparticles in Drug Delivery, Targeting and Imaging Applications, *Molecules* 2017, 22, 1445.

11. Yeh, Y.-C.; Creran, B.; Rotello, V.M. Gold nanoparticles: preparation, properties, and applications in bionanotechnology, *Nanoscale* **2012**, 4, 1871-1880.

12. Qu, C.; Jing, B.; Wang, S.; Zhu, Y. Distinct Effects of Multivalent Macroion and Simple Ion on the Structure and Local Electric Environment of a Weak Polyelectrolyte in Aqueous Solution, *The Journal of Physical Chemistry B* **2017**, 121, 8829-8837.

13. Decher, G. Fuzzy Nanoassemblies: Toward Layered Polymeric Multicomposites, *Science (New York, N.Y.)* **1997**, 277, 1232.

14. Guzmán, E.; Mateos-Maroto, A.; Ruano, M.; Ortega, F.; Rubio, R.G. Layer-by-Layer polyelectrolyte assemblies for encapsulation and release of active compounds, *Advances in Colloid and Interface Science* **2017**, 249, 290-307.

15. Figoli, A.; Hoinkis, J.; Altinkaya, S.A.; Bundschuh, J. *Application of Nanotechnology in Membranes for Water Treatment*; CRC Press: 2017.

16. Caruso, F. Nanoengineering of Particle Surfaces, *Advanced Materials* **2001**, 13, 11-22.

17. Brown, P.S.; Bhushan, B. Mechanically durable, superoleophobic coatings prepared by layer-by-layer technique for anti-smudge and oil-water separation, *Scientific Reports* **2015**, *5*, 8701.
18. Elosua, C.; Lopez-Torres, D.; Hernaez, M.; Matias, I.R.; Arregui, F.J. Comparative study of layer-by-layer deposition techniques for poly(sodium phosphate) and poly(allylamine hydrochloride), *Nanoscale Research Letters* **2013**, *8*, 539-539.
19. Costa, R.R.; Alatorre-Meda, M.; Mano, J.F. Drug nano-reservoirs synthesized using layer-by-layer technologies, *Biotechnology Advances* **2015**, *33*, 1310-1326.
20. Yu, A.; Liang, Z.; Cho, J.; Caruso, F. Nanostructured Electrochemical Sensor Based on Dense Gold Nanoparticle Films, *Nano Letters* **2003**, *3*, 1203-1207.
21. Shah, V.; Malardier-Jugroot, C.; Jugroot, M. Mediating gold nanoparticle growth in nanoreactors: Role of template-metal interactions and external energy, *Materials Chemistry and Physics* **2017**, *196*, 92-102.
22. Gittins, D.I.; Caruso, F. Tailoring the Polyelectrolyte Coating of Metal Nanoparticles, *The Journal of Physical Chemistry B* **2001**, *105*, 6846-6852.
23. Fuller, M.; Köper, I. Polyelectrolyte-Coated Gold Nanoparticles: The Effect of Salt and Polyelectrolyte Concentration on Colloidal Stability, *Polymers (Basel)* **2018**, *10*, 1336.
24. Thi Nhat Hang, N.; Thi Le Trinh, N.; Thi Thanh Tuyen, L.; Canh Minh Thang, N.; Thi Phuong Phong, N. Synthesis of gold nanorods with a longitudinal surface plasmon resonance peak of around 1250 nm, *Advances in Natural Sciences: Nanoscience and Nanotechnology* **2016**, *7*, 015006.
25. Lee, K.S.; El-Sayed, M.A. Gold and silver nanoparticles in sensing and imaging: sensitivity of plasmon response to size, shape, and metal composition, *The journal of physical chemistry. B* **2006**, *110*, 19220-19225.

26. Yu, C.; Irudayaraj, J. Multiplex biosensor using gold nanorods, *Analytical chemistry* **2007**, *79*, 572-579.
27. Matthews, J.R.; Payne, C.M.; Hafner, J.H. Analysis of Phospholipid Bilayers on Gold Nanorods by Plasmon Resonance Sensing and Surface-Enhanced Raman Scattering, *Langmuir* **2015**, *31*, 9893-9900.
28. An, L.; Wang, Y.; Tian, Q.; Yang, S. Small Gold Nanorods: Recent Advances in Synthesis, Biological Imaging, and Cancer Therapy, *Materials* **2017**, *10*, 1372.
29. Pissuwan, D.; Niidome, T. Polyelectrolyte-coated gold nanorods and their biomedical applications, *Nanoscale* **2015**, *7*, 59-65.
30. Dorris, A.; Rucareanu, S.; Reven, L.; Barrett, C.J.; Lennox, R.B. Preparation and Characterization of Polyelectrolyte-Coated Gold Nanoparticles, *Langmuir* **2008**, *24*, 2532-2538.
31. Nayef, L.; Castiello, R.; Tabrizian, M. Washless Method Enables Multilayer Coating of an Aggregation-Prone Nanoparticulate Drug Delivery System with Enhanced Yields, Colloidal Stability, and Scalability, *Macromolecular Bioscience* **2017**, *17*, 1600535.
32. Pugh, T.L.; Heller, W. Coagulation and stabilization of colloidal solutions with polyelectrolytes, *Journal of Polymer Science* **1960**, *47*, 219-227.
33. Ahmed, S.; Sheraz, M.A.; Rehman, I.U. Studies on tolfenamic acid-chitosan intermolecular interactions: effect of pH, polymer concentration and molecular weight, *AAPS PharmSciTech* **2013**, *14*, 870-879.
34. Maiti, S.; Jana, S.; Laha, B. Chapter 6 - Cationic polyelectrolyte-biopolymer complex hydrogel particles for drug delivery A2 - Grumezescu, Alexandru Mihai. In *Design and Development of New Nanocarriers*, William Andrew Publishing: 2018; pp. 223-256.

35. Netz, R.R.; Joanny, J.-F. Adsorption of Semiflexible Polyelectrolytes on Charged Planar Surfaces: Charge Compensation, Charge Reversal, and Multilayer Formation, *Macromolecules* **1999**, *32*, 9013-9025.
36. Sardar, R.; Shumaker-Parry, J.S. Spectroscopic and microscopic investigation of gold nanoparticle formation: ligand and temperature effects on rate and particle size, *Journal of the American Chemical Society* **2011**, *133*, 8179-8190.
37. Piella, J.; Bastús, N.G.; Puentes, V. Size-Controlled Synthesis of Sub-10-nanometer Citrate-Stabilized Gold Nanoparticles and Related Optical Properties, *Chemistry of Materials* **2016**, *28*, 1066-1075.
38. Xia, H.; Xiahou, Y.; Zhang, P.; Ding, W.; Wang, D. Revitalizing the Frens Method To Synthesize Uniform, Quasi-Spherical Gold Nanoparticles with Deliberately Regulated Sizes from 2 to 330 nm, *Langmuir* **2016**, *32*, 5870-5880.
39. Turkevich, J.; Stevenson, P.C.; Hillier, J. A study of the nucleation and growth processes in the synthesis of colloidal gold, *Discussions of the Faraday Society* **1951**, *11*, 55-75.
40. Xiang, Z.; Wang, K.; Zhang, W.; Teh, S.W.; Peli, A.; Mok, P.L.; Higuchi, A.; Suresh Kumar, S. Gold Nanoparticles Inducing Osteogenic Differentiation of Stem Cells: A Review, *Journal of Cluster Science* **2018**, *29*, 1-7.
41. Frens, G. Controlled Nucleation for the Regulation of the Particle Size in Monodisperse Gold Suspensions, *Nature Phys Sci* **1973**, *241*, 20-22.
42. Brust, M.; Walker, M.; Bethell, D.; Schiffrin, D.J.; Whyman, R. Synthesis of thiol-derivatised gold nanoparticles in a two-phase Liquid-Liquid system, *Journal of the Chemical Society, Chemical Communications* **1994**, 801-802.
43. Newman, J.D.S.; Blanchard, G.J. Formation of Gold Nanoparticles Using Amine Reducing Agents, *Langmuir* **2006**, *22*, 5882-5887.

44. Dozol, H.; Mériguet, G.; Ancian, B.; Cabuil, V.; Xu, H.; Wang, D.; Abou-Hassan, A. On the Synthesis of Au Nanoparticles Using EDTA as a Reducing Agent, *The Journal of Physical Chemistry C* **2013**, *117*, 20958-20966.
45. Arghya, S.; Manoj, G.; Pragya, S.; Manab, D.; Utpal, B. Green synthesis of gold nanoparticles using aqueous extract of *Dillenia indica*, *Advances in Natural Sciences: Nanoscience and Nanotechnology* **2016**, *7*, 025005.
46. Jang, Y.; Lee, N.; Kim, J.; Park, Y.; Piao, Y. Shape-Controlled Synthesis of Au Nanostructures Using EDTA Tetrasodium Salt and Their Photothermal Therapy Applications, *Nanomaterials* **2018**, *8*, 252.
47. Gopinath, V.; Priyadarshini, S.; MubarakAli, D.; Loke, M.F.; Thajuddin, N.; Alharbi, N.S.; Yadavalli, T.; Alagiri, M.; Vadivelu, J. Anti-Helicobacter pylori, cytotoxicity and catalytic activity of biosynthesized gold nanoparticles: Multifaceted application, *Arabian Journal of Chemistry* **2016**.
48. Labala, S.; Mandapalli, P.K.; Kurumaddali, A.; Venuganti, V.V.K. Layer-by-Layer Polymer Coated Gold Nanoparticles for Topical Delivery of Imatinib Mesylate To Treat Melanoma, *Molecular Pharmaceutics* **2015**, *12*, 878-888.
49. Ortega-Munoz, M.; Giron-Gonzalez, M.D.; Salto-Gonzalez, R.; Jodar-Reyes, A.B.; De Jesus, S.E.; Lopez-Jaramillo, F.J.; Hernandez-Mateo, F.; Santoyo-Gonzalez, F. Polyethyleneimine-Coated Gold Nanoparticles: Straightforward Preparation of Efficient DNA Delivery Nanocarriers, *Chemistry, an Asian journal* **2016**, *11*, 3365-3375.
50. Dreaden, E.C.; Alkilany, A.M.; Huang, X.; Murphy, C.J.; El-Sayed, M.A. The golden age: gold nanoparticles for biomedicine, *Chemical Society Reviews* **2012**, *41*, 2740-2779.
51. Xie, X.; Xu, S.; Pi, P.; Cheng, J.; Wen, X.; Liu, X.; Wang, S. Dissipative particle dynamic simulation on the assembly and release of siRNA/polymer/gold nanoparticles based polyplex, *AIChE Journal* **2018**, *64*, 810-821.
52. Masereel, B.; Dinguizli, M.; Bouzin, C.; Moniotte, N.; Feron, O.; Gallez, B.; Vander Borght, T.; Michiels, C.; Lucas, S. Antibody immobilization on gold

nanoparticles coated layer-by-layer with polyelectrolytes, *Journal of Nanoparticle Research* **2011**, *13*, 1573-1580.

53. Reum, N.; Fink-Straube, C.; Klein, T.; Hartmann, R.W.; Lehr, C.-M.; Schneider, M. Multilayer Coating of Gold Nanoparticles with Drug-Polymer Coadsorbates, *Langmuir* **2010**, *26*, 16901-16908.

54. Lee, Y.; Lee, S.H.; Kim, J.S.; Maruyama, A.; Chen, X.; Park, T.G. Controlled synthesis of PEI-coated gold nanoparticles using reductive catechol chemistry for siRNA delivery, *Journal of Controlled Release* **2011**, *155*, 3-10.

55. Homola, J.; Yee, S.S.; Gauglitz, G. Surface plasmon resonance sensors: review, *Sensors and Actuators B: Chemical* **1999**, *54*, 3-15.

56. Vincenzo, A.; Roberto, P.; Marco, F.; Onofrio, M.M.; Maria Antonia, I. Surface plasmon resonance in gold nanoparticles: a review, *Journal of Physics: Condensed Matter* **2017**, *29*, 203002.

57. Felicia, T.; Monica, B.; Lucian, B.; Simion, A. Controlling gold nanoparticle assemblies for efficient surface-enhanced Raman scattering and localized surface plasmon resonance sensors, *Nanotechnology* **2007**, *18*, 255702.

58. Chang, H.-H.; Murphy, C.J. Mini Gold Nanorods with Tunable Plasmonic Peaks beyond 1000 nm, *Chemistry of Materials* **2018**, *30*, 1427-1435.

59. Mie, G. Beiträge zur Optik trüber Medien, speziell kolloidaler Metallösungen, *Annalen der Physik* **1908**, *330*, 377-445.

60. Aldewachi, H.; Chalati, T.; Woodroffe, M.N.; Bricklebank, N.; Sharrack, B.; Gardiner, P. Gold nanoparticle-based colorimetric biosensors, *Nanoscale* **2018**, *10*, 18-33.

61. Mayya, K.S.; Schoeler, B.; Caruso, F. Preparation and Organization of Nanoscale Polyelectrolyte-Coated Gold Nanoparticles, *Advanced Functional Materials* **2003**, *13*, 183-188.

62. Pollastri, S.; Gualtieri, A.F.; Gualtieri, M.L.; Hanuskova, M.; Cavallo, A.; Gaudino, G. The zeta potential of mineral fibres, *Journal of hazardous materials* **2014**, *276*, 469-479.
63. Spriano, S.; Sarath Chandra, V.; Cochis, A.; Uberti, F.; Rimondini, L.; Bertone, E.; Vitale, A.; Scolaro, C.; Ferrari, M.; Cirisano, F., et al. How do wettability, zeta potential and hydroxylation degree affect the biological response of biomaterials?, *Materials Science and Engineering: C* **2017**, *74*, 542-555.
64. Luxbacher, T. The ZETA guide: principles of the streaming potential technique. Paar, A., Ed. 2014.
65. Junior, J.A.A.; Baldo, J.B. The Behavior of Zeta Potential of Silica Suspensions, *New Journal of Glass and Ceramics* **2014**, *Vol.04No.02*, 9.
66. Behzadi, S.; Serpooshan, V.; Tao, W.; Hamaly, M.A.; Alkawareek, M.Y.; Dreaden, E.C.; Brown, D.; Alkilany, A.M.; Farokhzad, O.C.; Mahmoudi, M. Cellular uptake of nanoparticles: journey inside the cell, *Chem Soc Rev* **2017**, *46*, 4218-4244.
67. Cheng, X.; Tian, X.; Wu, A.; Li, J.; Tian, J.; Chong, Y.; Chai, Z.; Zhao, Y.; Chen, C.; Ge, C. Protein Corona Influences Cellular Uptake of Gold Nanoparticles by Phagocytic and Nonphagocytic Cells in a Size-Dependent Manner, *ACS Applied Materials & Interfaces* **2015**, *7*, 20568-20575.
68. Corbo, C.; Molinaro, R.; Parodi, A.; Furman, N.E.T.; Salvatore, F.; Tasciotti, E. The impact of nanoparticle protein corona on cytotoxicity, immunotoxicity and target drug delivery, *Nanomedicine* **2016**, *11*, 81-100.
69. Elbakry, A.; Zaky, A.; Liebl, R.; Rachel, R.; Goepferich, A.; Breunig, M. Layer-by-Layer Assembled Gold Nanoparticles for siRNA Delivery, *Nano Letters* **2009**, *9*, 2059-2064.
70. Charbgoon, F.; Nejabat, M.; Abnous, K.; Soltani, F.; Taghdisi, S.M.; Alibolandi, M.; Thomas Shier, W.; Steele, T.W.J.; Ramezani, M. Gold nanoparticle should understand protein corona for being a clinical nanomaterial, *Journal of Controlled Release* **2018**, *272*, 39-53.

71. Blander, J.M.; Medzhitov, R. On regulation of phagosome maturation and antigen presentation, *Nat Immunol* **2006**, *7*, 1029-1035.
72. Dobrovolskaia, M.A.; McNeil, S.E. Immunological properties of engineered nanomaterials, *Nat Nano* **2007**, *2*, 469-478.
73. Conner, S.D.; Schmid, S.L. Regulated portals of entry into the cell, *Nature* **2003**, *422*, 37-44.
74. Aderem, A.U., D. Mechanisms of Phagocytosis in Macrophages, *Annual Review of Immunology* **1999**, *17*, 593-623.
75. Oh, N.; Park, J.-H. Endocytosis and exocytosis of nanoparticles in mammalian cells, *International Journal of Nanomedicine* **2014**, *9*, 51-63.
76. Xiang, S.D.; Scholzen, A.; Minigo, G.; David, C.; Apostolopoulos, V.; Mottram, P.L.; Plebanski, M. Pathogen recognition and development of particulate vaccines: Does size matter?, *Methods* **2006**, *40*, 1-9.
77. Fekri, F.; Delos Santos, R.C.; Karshafian, R.; Antonescu, C.N. Ultrasound Microbubble Treatment Enhances Clathrin-Mediated Endocytosis and Fluid-Phase Uptake through Distinct Mechanisms, *PLOS ONE* **2016**, *11*, e0156754.
78. Chithrani, B.D.; Chan, W.C.W. Elucidating the Mechanism of Cellular Uptake and Removal of Protein-Coated Gold Nanoparticles of Different Sizes and Shapes, *Nano Letters* **2007**, *7*, 1542-1550.
79. Gao, H.; Shi, W.; Freund, L.B. Mechanics of receptor-mediated endocytosis, *Proceedings of the National Academy of Sciences of the United States of America* **2005**, *102*, 9469-9474.
80. Torchilin, V.P. *Smart Pharmaceutical Nanocarriers*; Imperial College Press: 2015.
81. Shang, L.; Nienhaus, K.; Nienhaus, G.U. Engineered nanoparticles interacting with cells: size matters, *Journal of Nanobiotechnology* **2014**, *12*, 5.

82. Wong, A.C.; Wright, D.W. Size-Dependent Cellular Uptake of DNA Functionalized Gold Nanoparticles, *Small* **2016**, *12*, 5592-5600.
83. Fleischer, C.C.; Payne, C.K. Nanoparticle–Cell Interactions: Molecular Structure of the Protein Corona and Cellular Outcomes, *Accounts of Chemical Research* **2014**, *47*, 2651-2659.
84. Alkilany, A.M.; Nagaria, P.K.; Hexel, C.R.; Shaw, T.J.; Murphy, C.J.; Wyatt, M.D. Cellular Uptake and Cytotoxicity of Gold Nanorods: Molecular Origin of Cytotoxicity and Surface Effects, *Small* **2009**, *5*, 701-708.
85. Goodman, C.M.; McCusker, C.D.; Yilmaz, T.; Rotello, V.M. Toxicity of Gold Nanoparticles Functionalized with Cationic and Anionic Side Chains, *Bioconjugate Chemistry* **2004**, *15*, 897-900.
86. Nambiar, S.; Osei, E.; Fleck, A.; Darko, J.; Mutsaers, A.J.; Wettig, S. Synthesis of curcumin-functionalized gold nanoparticles and cytotoxicity studies in human prostate cancer cell line, *Applied Nanoscience* **2018**, *8*, 347-357.
87. Huo, S.; Jin, S.; Ma, X.; Xue, X.; Yang, K.; Kumar, A.; Wang, P.C.; Zhang, J.; Hu, Z.; Liang, X.-J. Ultrasmall Gold Nanoparticles as Carriers for Nucleus-Based Gene Therapy Due to Size-Dependent Nuclear Entry, *ACS Nano* **2014**, *8*, 5852-5862.
88. Ryan, J.A.; Overton, K.W.; Speight, M.E.; Oldenburg, C.N.; Loo, L.; Robarge, W.; Franzen, S.; Feldheim, D.L. Cellular uptake of gold nanoparticles passivated with BSA-SV40 large T antigen conjugates, *Analytical chemistry* **2007**, *79*, 9150-9159.
89. Kodiha, M.; Wang, Y.M.; Hutter, E.; Maysinger, D.; Stochaj, U. Off to the organelles - killing cancer cells with targeted gold nanoparticles, *Theranostics* **2015**, *5*, 357-370.
90. Shukla, R.; Bansal, V.; Chaudhary, M.; Basu, A.; Bhonde, R.R.; Sastry, M. Biocompatibility of gold nanoparticles and their endocytotic fate inside the cellular compartment: a microscopic overview, *Langmuir* **2005**, *21*, 10644-10654.

91. Pernodet, N.; Fang, X.; Sun, Y.; Bakhtina, A.; Ramakrishnan, A.; Sokolov, J.; Ulman, A.; Rafailovich, M. Adverse effects of citrate/gold nanoparticles on human dermal fibroblasts, *Small* **2006**, *2*, 766-773.
92. Han, G.; Ghosh, P.; Rotello, V.M. Functionalized gold nanoparticles for drug delivery, *Nanomedicine (London, England)* **2007**, *2*, 113-123.
93. Elci, S.G.; Jiang, Y.; Yan, B.; Kim, S.T.; Saha, K.; Moyano, D.F.; Yesilbag Tonga, G.; Jackson, L.C.; Rotello, V.M.; Vachet, R.W. Surface Charge Controls the Suborgan Biodistributions of Gold Nanoparticles, *ACS Nano* **2016**, *10*, 5536-5542.
94. Guo, S.; Huang, Y.; Jiang, Q.; Sun, Y.; Deng, L.; Liang, Z.; Du, Q.; Xing, J.; Zhao, Y.; Wang, P.C., et al. Enhanced Gene Delivery and siRNA Silencing by Gold Nanoparticles Coated with Charge-Reversal Polyelectrolyte, *ACS Nano* **2010**, *4*, 5505-5511.
95. Lamprecht, A.; Ubrich, N.; Yamamoto, H.; Schafer, U.; Takeuchi, H.; Maincent, P.; Kawashima, Y.; Lehr, C.M. Biodegradable nanoparticles for targeted drug delivery in treatment of inflammatory bowel disease, *The Journal of pharmacology and experimental therapeutics* **2001**, *299*, 775-781.
96. Singh, R.; Lillard, J.W. Nanoparticle-based targeted drug delivery, *Experimental and molecular pathology* **2009**, *86*, 215-223.
97. Zatspein, T.S.; Kotelevtsev, Y.V.; Koteliansky, V. Lipid nanoparticles for targeted siRNA delivery – going from bench to bedside, *International Journal of Nanomedicine* **2016**, *11*, 3077-3086.
98. Singh, M.; Harris-Birtill, D.C.C.; Markar, S.R.; Hanna, G.B.; Elson, D.S. Application of gold nanoparticles for gastrointestinal cancer theranostics: A systematic review, *Nanomedicine: Nanotechnology, Biology and Medicine* **2015**, *11*, 2083-2098.
99. Konan, Y.N.; Gurny, R.; Allemann, E. State of the art in the delivery of photosensitizers for photodynamic therapy, *Journal of photochemistry and photobiology. B, Biology* **2002**, *66*, 89-106.

100. Kanasty, R.; Dorkin, J.R.; Vegas, A.; Anderson, D. Delivery materials for siRNA therapeutics, *Nat Mater* **2013**, *12*, 967-977.
101. Abadeer, N.S.; Murphy, C.J. Recent Progress in Cancer Thermal Therapy Using Gold Nanoparticles, *The Journal of Physical Chemistry C* **2016**, *120*, 4691-4716.
102. Day, E.S.; Morton, J.G.; West, J.L. Nanoparticles for thermal cancer therapy, *Journal of biomechanical engineering* **2009**, *131*, 074001.
103. Rache S. Riley, E.S.D. Gold nanoparticle-mediated photothermal therapy: applications and opportunities for multimodal cancer therapy, *Wiley Interdisciplinary Reviews: Nanomedicine and Nanobiotechnology* **2017**, *9*.
104. Huang, X.; El-Sayed, I.H.; Qian, W.; El-Sayed, M.A. Cancer Cell Imaging and Photothermal Therapy in the Near-Infrared Region by Using Gold Nanorods, *Journal of the American Chemical Society* **2006**, *128*, 2115-2120.
105. Kirui, D.K.; Krishnan, S.; Strickland, A.D.; Batt, C.A. PAA-Derived Gold Nanorods for Cellular Targeting and Photothermal Therapy, *Macromolecular Bioscience* **2011**, *11*, 779-788.
106. Wang, B.; Wang, J.-H.; Liu, Q.; Huang, H.; Chen, M.; Li, K.; Li, C.; Yu, X.-F.; Chu, P.K. Rose-bengal-conjugated gold nanorods for in vivo photodynamic and photothermal oral cancer therapies, *Biomaterials* **2014**, *35*, 1954-1966.
107. Wang, J.; Dong, B.; Chen, B.; Jiang, Z.; Song, H. Selective photothermal therapy for breast cancer with targeting peptide modified gold nanorods, *Dalton Transactions* **2012**, *41*, 11134-11144.
108. Bao, Z.; Liu, X.; Liu, Y.; Liu, H.; Zhao, K. Near-infrared light-responsive inorganic nanomaterials for photothermal therapy, *Asian Journal of Pharmaceutical Sciences* **2016**, *11*, 349-364.
109. Cheng, X.; Sun, R.; Yin, L.; Chai, Z.; Shi, H.; Gao, M. Light-Triggered Assembly of Gold Nanoparticles for Photothermal Therapy and Photoacoustic Imaging of Tumors In Vivo, *Advanced Materials* **2017**, *29*, 1604894.

110. Curry, T.; Kopelman, R.; Shilo, M.; Popovtzer, R. Multifunctional theranostic gold nanoparticles for targeted CT imaging and photothermal therapy, *Contrast media & molecular imaging* **2014**, *9*, 53-61.
111. Mallidi, S.; Kim, S.; Karpiouk, A.; Joshi, P.P.; Sokolov, K.; Emelianov, S. Visualization of molecular composition and functionality of cancer cells using nanoparticle-augmented ultrasound-guided photoacoustics, *Photoacoustics* **2015**, *3*, 26-34.
112. Huang, P.; Lin, J.; Li, W.; Rong, P.; Wang, Z.; Wang, S.; Wang, X.; Sun, X.; Aronova, M.; Niu, G., et al. Biodegradable Gold Nanovesicles with an Ultrastrong Plasmonic Coupling Effect for Photoacoustic Imaging and Photothermal Therapy, *Angewandte Chemie International Edition* **2013**, *52*, 13958-13964.
113. Lusic, H.; Grinstaff, M.W. X-Ray Computed Tomography Contrast Agents, *Chemical reviews* **2013**, *113*, 10.1021/cr200358s.
114. Dou, Y.; Guo, Y.; Li, X.; Li, X.; Wang, S.; Wang, L.; Lv, G.; Zhang, X.; Wang, H.; Gong, X., et al. Size-Tuning Ionization To Optimize Gold Nanoparticles for Simultaneous Enhanced CT Imaging and Radiotherapy, *ACS Nano* **2016**, *10*, 2536-2548.
115. Alkilany, A.M.; Murphy, C.J. Toxicity and cellular uptake of gold nanoparticles: what we have learned so far?, *Journal of Nanoparticle Research* **2010**, *12*, 2313-2333.
116. Sathishkumar, M.; Pavagadhi, S.; Mahadevan, A.; Balasubramanian, R. Biosynthesis of gold nanoparticles and related cytotoxicity evaluation using A549 cells, *Ecotoxicology and Environmental Safety* **2015**, *114*, 232-240.
117. Zhang, Y.; Xu, D.; Li, W.; Yu, J.; Chen, Y. Effect of Size, Shape, and Surface Modification on Cytotoxicity of Gold Nanoparticles to Human HEP-2 and Canine MDCK Cells, *Journal of Nanomaterials* **2012**, *2012*, 7.
118. Vial, S.; Reis, R.L.; Oliveira, J.M. Recent advances using gold nanoparticles as a promising multimodal tool for tissue engineering and

regenerative medicine, *Current Opinion in Solid State and Materials Science* **2017**, *21*, 92-112.

119. Woźniak, A.; Malankowska, A.; Nowaczyk, G.; Grześkowiak, B.F.; Tuśnio, K.; Słomski, R.; Zaleska-Medynska, A.; Jurga, S. Size and shape-dependent cytotoxicity profile of gold nanoparticles for biomedical applications, *Journal of Materials Science: Materials in Medicine* **2017**, *28*, 92.

120. Moore, K.A.; Pate, K.M.; Soto-Ortega, D.D.; Lohse, S.; van der Munnik, N.; Lim, M.; Jackson, K.S.; Lyles, V.D.; Jones, L.; Glassgow, N., et al. Influence of gold nanoparticle surface chemistry and diameter upon Alzheimer's disease amyloid- β protein aggregation, *Journal of Biological Engineering* **2017**, *11*, 5.

121. Bouché, M.; Fournel, S.; Kichler, A.; Selvam, T.; Gallani, J.-L.; Bellemin-Lapponnaz, S. Straightforward Synthesis of L-PEI-Coated Gold Nanoparticles and Their Biological Evaluation, *European Journal of Inorganic Chemistry* **2018**, *2018*, 2972-2975.

122. Pan, Y.; Leifert, A.; Ruau, D.; Neuss, S.; Bornemann, J.; Schmid, G.; Brandau, W.; Simon, U.; Jahnen-Dechent, W. Gold Nanoparticles of Diameter 1.4 nm Trigger Necrosis by Oxidative Stress and Mitochondrial Damage, *Small* **2009**, *5*, 2067-2076.

CHAPTER 3: POLYELECTROLYTE-COATED GOLD NANOPARTICLES

This chapter has been published under the title 'Polyelectrolyte-coated gold nanoparticles: the effect of salt and polyelectrolyte concentration on colloidal stability' in *Polymers* and is authored by **Melanie Fuller** and Ingo Köper. It is a research article which determines the most stable salt and polyelectrolyte concentration to use during the process of polyelectrolyte coating on gold nanoparticles.

Understanding what generates the most stable cationic nanoparticle is important for the subsequent research within this thesis as unstable aggregates may alter the effectiveness of delivering Colistin into a cell membrane. By ensuring nanoparticle stability, any differences observed in membrane stability due to nanoparticle addition are caused by the 5 nm particles and not larger aggregates. This chapter is integral in explaining the most effective way to form stable polyelectrolyte coatings and the method for stable coatings is referenced throughout the thesis.

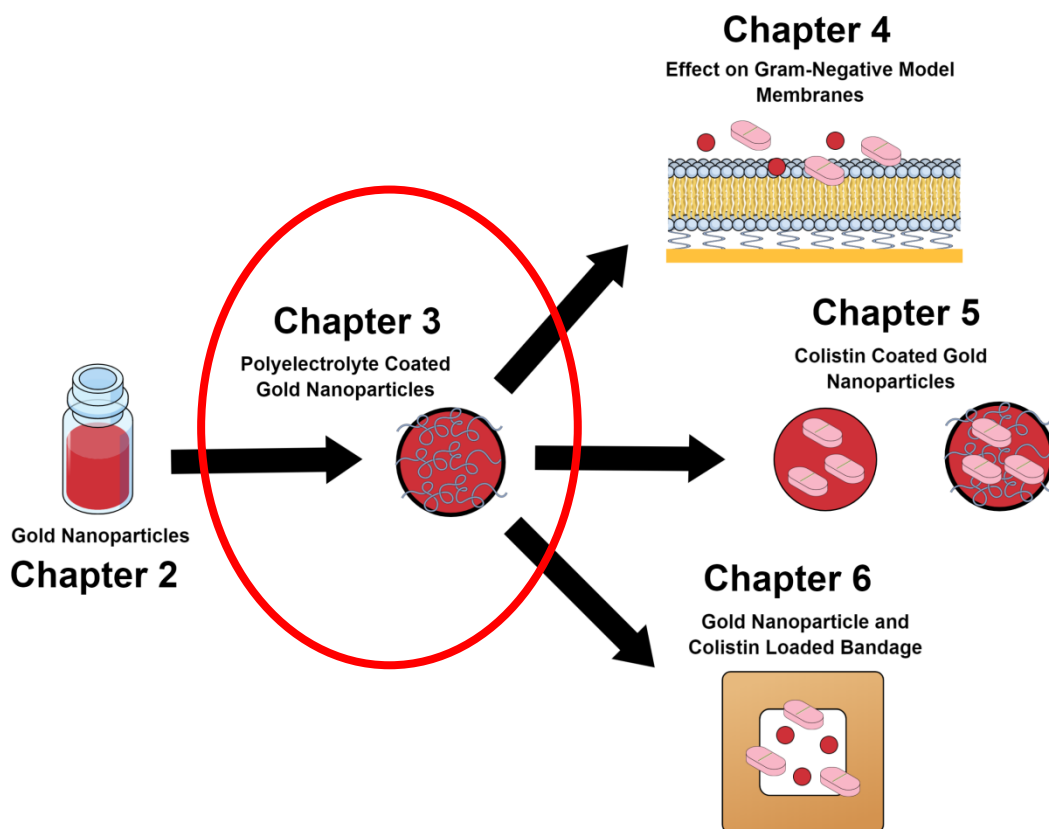


Figure 10: Diagram of the overall thesis, indicating Chapter 3 and how it fits into the larger body of work.

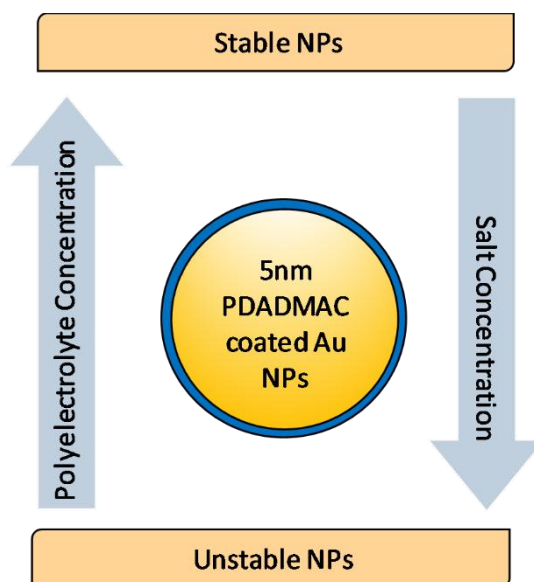


Figure 11: Graphical abstract from the publication 'Polyelectrolyte-coated gold nanoparticles: the effect of salt and polyelectrolyte concentration on colloidal stability'.

Abstract:

Gold nanoparticles are widely used in biomedical applications. Their ease of surface modification, biocompatibility and the presence of surface plasmons makes them ideal tools for a variety of investigations. Polyelectrolyte-coated gold nanoparticles are employed in areas such as imaging, drug delivery and gene therapy; however, it is not well understood how different factors such as the polyelectrolyte and salt concentration affect the coating on the nanoparticles and hence their performance. Here, these parameters were systematically varied and their effect on the stability of the colloidal nanoparticle suspension was monitored. An increase in the polyelectrolyte concentration from 0 to 30 mg/mL led to a red shift of the surface plasmon peak and an increase in the zeta potential. Concentrations between 5 mg/mL and 30 mg/mL resulted in the most stable systems, with 1 mg/mL being the most unstable. Stable nanoparticle suspensions were formed in salt concentrations below 50 mM, while higher concentrations caused colloidal instability and irreversible aggregation.

1. Introduction

Surface modified gold nanoparticles (AuNPs) are becoming more frequently used in biomedical applications and thus being able to understand the effects various surface coatings have on these NPs is becoming more important.^{1,2} AuNPs are being utilised because they are biocompatible and their optical and physical properties make them suitable for sensing purposes. The presence of surface plasmons allows changes in the local environment of the particle to be determined, and the ability to functionalise the surface easily with a range of moieties including polymers, proteins, DNA and polyelectrolytes makes AuNPs suitable for various applications.

The layer-by-layer (LbL) method of coating NPs and planar substrates using polyelectrolytes (PEs) is well established.³⁻⁵ LbL coatings with PEs have distinct advantages over other surface modification methods, specifically the ease of assembly on a wide range of substrates. The LbL method allows the sequential addition of oppositely charged PEs onto a substrate through primarily

electrostatic interactions (Fig. 12).⁶ Polyanions and polycations can be used alternatively to build up multilayer systems which can be used in applications ranging from water treatment to protein immobilisation.^{7,8} The ease of deposition of PEs onto NP surfaces is a result of the simple electrostatic interactions that govern the LbL attachment process. These interactions depend on the type, length and concentration of the PE, as well as the concentration and type of salt used during the assembly process.⁹ These variables need to be optimised, especially when depositing PEs onto NPs, as the colloidal stability of the system can be easily affected. According to the DLVO theory, a colloidal solution requires repulsive forces such as electrostatic or steric stabilisation to prevent aggregation from occurring.¹⁰ Electrostatically stabilised systems have an electric double layer, which is due to the surface charge and solvated ions in solution. This double layer results in inter-particle Coulomb repulsion forces which decay exponentially with the particle to particle distance.¹¹ The thickness of the double layer (Debye length) can be affected by the salt concentration. Increasing salt concentration leads to an increase in the effective screening of these charges, which causes a decrease in the Debye length and hence in the effective distance of the Coulombic interactions.¹² Steric stabilisation can also occur from the absorption of larger molecules such as PEs onto the particle's surface.¹¹ These larger molecules can provide a protective layer around the particle, which can also prevent aggregation. As PE-coated NPs can potentially be used in biomedical applications, the colloidal stability is extremely important, as aggregation can alter their *in vitro* behaviour such as NP uptake and cytotoxicity as well as *in vivo* fate including biodistribution.¹³

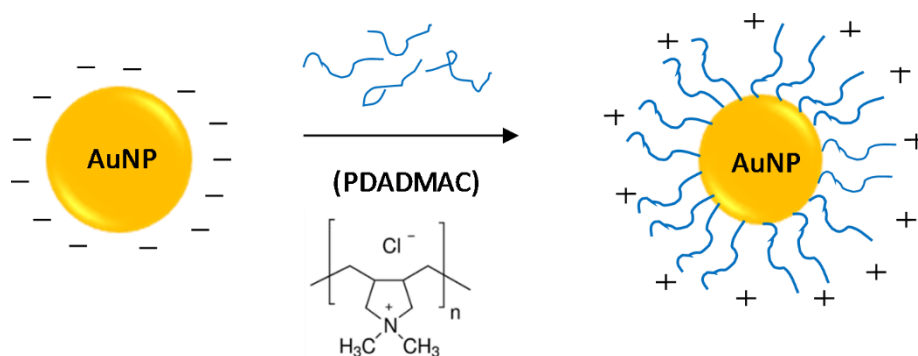


Figure 12: Layer-by-layer (LbL) attachment of polydiallyldimethylammonium chloride (PDADMAC) onto citrate-capped gold nanoparticles.

The assembly mechanisms as well as the effect of salt, PE concentration and temperature on the formation of planar PE-films are well understood.¹⁴ However, the coating of highly curved surfaces such as the surface of small NPs has not been as thoroughly researched. This is partially due to the added difficulty of coating a highly curved surface and potential aggregation issues with altering the surface coating of NPs. Nevertheless, understanding how salt and concentration affects PE coatings on NP could allow for their use in a wider range of applications.

Here, the effects of both PE concentration and the salt concentration during layer formation has been explored to determine how they affect the formation of a PE-coating on AuNPs. PE concentrations which are too low can lead to incomplete particle coverage and subsequent aggregation. Concentrations that are too high will lead to particle bridging, especially when higher molecular weight polymers are used. Bridging occurs when the polymers adsorb simultaneously on more than one particle, 'grouping' the particles together causing aggregation.¹⁵ When salt concentrations are too high, it can lead to screening of interparticle electrostatic repulsions, which are needed to prevent aggregation.^{16,17} However, it has been proposed that concentrations that are too low can lead to inflexibility of the PE chains, which wrap around the NP resulting in an inadequate or incomplete coating, similar to low PE concentrations.⁹

The coating of nanoparticles with PEs can be described by three different scenarios¹⁶: (1) an excess of particles leads to partial and 'patchy' coatings on the nanoparticles, which often results in an increase in particle-particle attractions and subsequent aggregation; (2) equal charge proportions of colloids and PEs yields coated NPs with an overall charge near the isoelectric point of the PE. This in effect neutralises the charge causing the particles to move closer together and aggregate; (3) an excess of PE results in stable solutions of NPs that are saturated by the PE. This final scenario can be expressed as a ratio of polyelectrolyte chains to nanoparticles (PC/NP) and can be calculated by taking the mass of polymer used and dividing by the polymer mass per chain (polymer M_w /Avogadro's number).¹⁸ That number is then divided the number of

nanoparticles to give PC/NP. Previously, ratios of 200–4000 PC/NP provided the most stability, with the least aggregation.¹⁶

Here, the adsorption of polydiallyldimethylammonium chloride (PDADMAC) of differing concentrations onto AuNPs has been explored using ultraviolet-visible (UV–vis) spectroscopy and zeta-potential measurements. The PE concentration in which the NPs are most stable has then been used to investigate how the salt concentration affects the electrostatic attachment and colloidal stability. By determining the optimum concentrations for the PE and salt, the PE–AuNP system could be better adapted for use in biomedical applications. The optimised salt and PE concentrations were then used to determine if PDADMAC-coated AuNP are more stable than citrate capped AuNP. This was tested through a variety of solvents including ethanol, 10% Tween20 and PBS.

2. Materials and Methods

2.1. Polyelectrolyte (PE) Concentration

5 nm diameter AuNPs at a concentration of 8.4×10^{13} particles/mL were purchased from NanoComposix (California, United States). 2 mL of this particle solution were then mixed with 3 mL of PDADMAC (Sigma Aldrich, Castle Hill, Australia), average Mw < 100,000) solution with concentrations of 0, 0.1, 1, 5, 10 or 30 mg/mL. The AuNP/PDADMAC mixtures were stirred overnight before centrifuging at 14500 rpm for 40 min. The supernatant was removed and the pellet resuspended in 1 mL of 1 mM NaCl. This washing was repeated three times to remove any excess PDADMAC. The pH of the nanoparticle solution was adjusted to pH = 6 using 1 M HCl and measured using the Mettler Toledo pH Meter. The attachment of the PEs onto the NPs and the subsequent stability of the NPs was determined through the use of UV–vis spectroscopy (Cary 50) in 1 mM NaCl with the wavelength range of 400–800 nm. Zeta potential (Malvern Zetasizer Nano, Malvern Instruments Ltd, Malvern UK) was measured using flow cells with 1 mM NaCl. All experiments were conducted in triplicate.

2.2. Salt Concentration

PDADMAC (average Mw < 100,000) in solution, was diluted to a concentration of 5 mg/mL using differing NaCl concentrations of 0, 0.1, 1, 5, 10 and 30 mg/mL. 3 mL of the PDADMAC solution was added to 2 mL of AuNPs and the AuNP/PDADMAC mixture was stirred overnight before centrifuging at 14,500 rpm for 40 min. The supernatant was removed and the pellet resuspended in 1 mL of the same salt concentration. This washing was repeated three times to remove any excess PDADMAC. The pH was adjusted to pH = 6 as per the polyelectrolyte concentration method above. The attachment and stability was also measured as per the PDADMAC concentration protocol; however, during the zeta potential measurements, the samples were measured in their respective salt concentrations. All experiments were conducted in triplicate.

2.3. Solvent Stability

Three mL of 5 mg/mL PDADMAC (average Mw < 100,000) in 1 mM NaCl were stirred for 3 h with 2 mL of 5 nm AuNP solution. After 3 h, the sample was centrifuged at 14,500 rpm for 40 min. The supernatant was removed and the pellet resuspended in 1 mM NaCl. This washing was repeated three times to remove any excess PDADMAC. On the final centrifugation step, 50 μ L of the pellet was resuspended in 1 mL of 100% ethanol, 10% Tween20 or PBS in triplicate. Similarly, 50 μ L of citrate capped 5 nm AuNP (NanoComposix), were added to 1 mL of the same three solvents in triplicate. All solutions were then left for 36 h at ambient temperature before surface plasmon resonance (SPR) peak changes were measured by UV–vis spectroscopy (Cary 50) in their respective solvents. In each case, the UV–vis spectrophotometer was blanked with the solvent being used to ensure the solvent itself did not contribute to changes in the SPR peak.

3. Results and Discussion

PDADMAC was chosen to coat the NP as it is a strong, highly charged polyelectrolyte, with one cationic charge group per monomer.¹⁹ The type and

length of polyelectrolyte remained unchanged for the duration of the experiment and the ionic strength of the medium was controlled to probe the effect of different PE concentrations on the coating of the AuNPs. The specific Mw of PDADMAC was chosen as the longer chains can more effectively wrap around the AuNP, providing better surface coverage.

3.1. Effect of PE Concentration

In order to investigate the effect of PE concentration on the stability of the colloidal solution, five different concentrations of PDADMAC were used to coat the AuNPs, and the SPR absorbance peaks were measured using UV–vis spectroscopy (Fig. 13). Changes in the local nanoparticle environment influence the position of the peak as well as its amplitude. Particle aggregation causes a red-shift in the UV–vis absorption spectrum due to a decrease in interparticle distance.²⁰ Thus the stability can be monitored through the peak position.

At very low PE concentrations (0.1 mg/mL), the AuNPs fully aggregated after 24 h (Table 2). This concentration corresponds to a PC/NP ratio of 21.5, most likely falling into scenario 2 of near equal charges. This was confirmed through zeta potential measurements, where the cationic PE neutralised the negative charge on the AuNP (Fig. 13B). Concentrations below 5 mg/mL have unsaturated layers of PE on the NPs, leading to lower and unstable zeta potentials, as the attractive Van der Waals forces become dominant. Charge neutralisation causes the nanoparticles to move closer together, which results in an unstable suspension and particle aggregation.²¹ This is also likely to be the cause for the near zero zeta potential reading in the 1 mg/mL sample, indicating its instability.

Higher concentrations above 5 mg/mL, corresponding to scenario 3 with an excess of PE, led to stable solutions. The PE coatings resulted in shifts in the SPR peak and significantly positive zeta potentials. Above 5 mg/mL, the zeta potential remained relatively stable and this can be attributed to the complete PE coatings on the NPs (Fig. 13B). Prior to the plateau in zeta potential, the absorption of PE onto the NP is quantitative, where there would be in effect no free PE still in solution.²²

Table 2: Concentrations of PDADMAC showing polyelectrolyte chains to nanoparticles (PC/NP) ratio, compared to their average surface plasmon resonance (SPR) peak position and zeta potentials at pH 6.0 ± 0.3 .

PDADMAC Concentration (mg/mL)	PC/NP Ratio	SPR Maximum Absorbance Peak (nm)	Absorbance (a.u.)	Zeta Potential (mV)
0	0	513 ± 0.3	0.48 ± 0.2	-9.6 ± 8.9
0.1	21.5	- *	- *	0.3 ± 3.7
1.0	215	537 ± 1.5	0.10 ± 0.09	5.7 ± 14
5.0	1075	539 ± 0.47	0.58 ± 0.04	35 ± 8.9
10	2150	540 ± 2.5	0.45 ± 0.07	39 ± 9.1
30	6450	542 ± 0.94	0.51 ± 0.08	48 ± 7.9

* Fully aggregated and was unable to be removed from the centrifuge tubes with a concentration of AuNP suitable for ultraviolet-visible (UV–Vis) spectroscopy.

The absorbance values varied for the different PE concentrations. In principle, the absorbance should be independent of the coating concentration, however particles can be lost through repeated centrifugation wash steps, resulting in lower absorbance values. The lowest absorbance values were observed for 1 mg/mL, where most of the particles aggregated and precipitated out of solution.

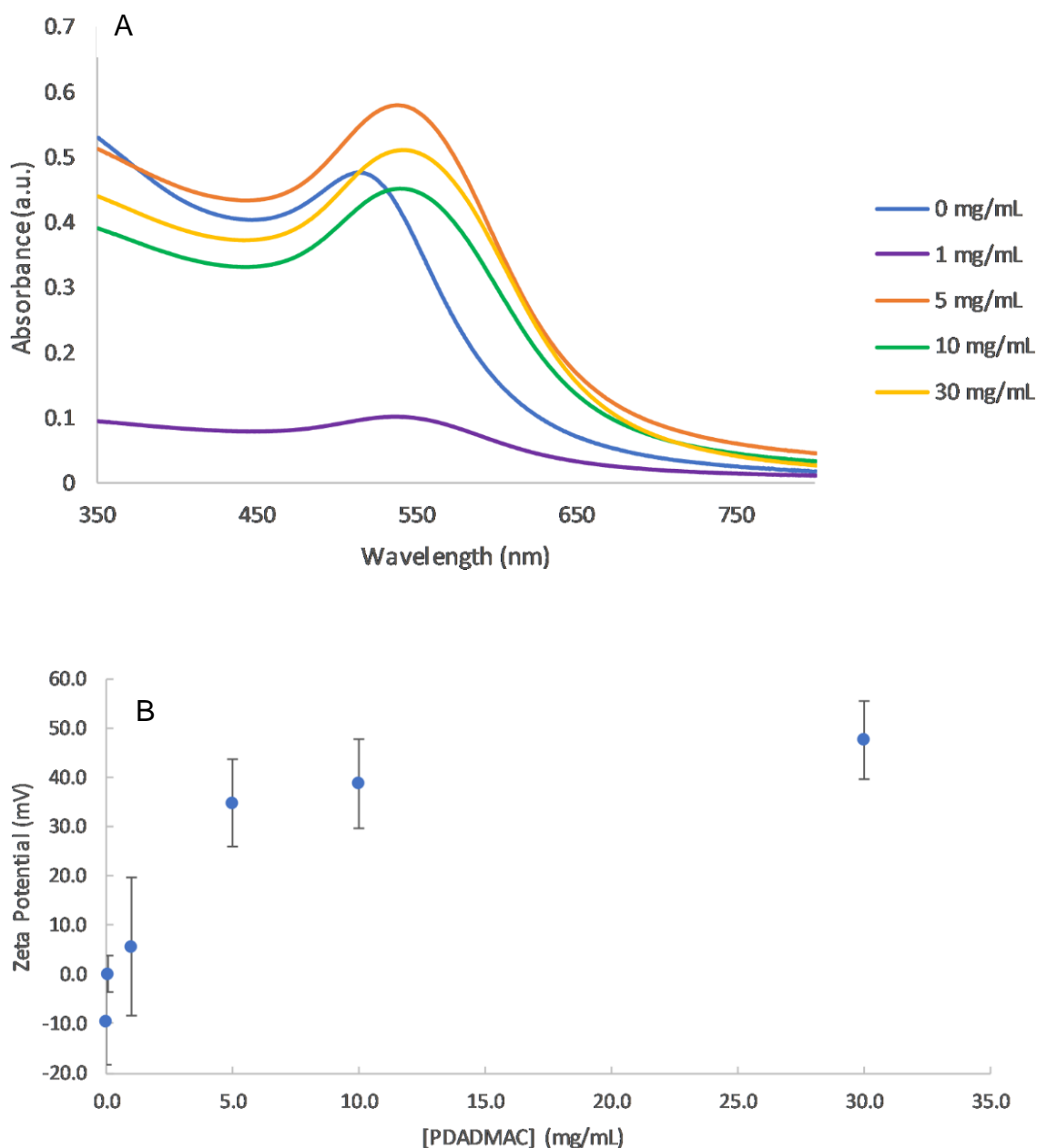


Figure 13: (A) UV–vis spectra of PDADMAC coated AuNP at concentrations of 0–30 mg/mL PDADMAC in 1 mM NaCl. (B) Zeta potential measurements as a function of PDADMAC concentration at pH 6.0.

The addition of a PDADMAC layer to the AuNP changed the overall dielectric constant of the particles, which resulted in a red shift of the SPR peak. A small change in the SPR peak may also be due to the size of NPs increasing with an additional layer, although this will be minor compared to the change in dielectric constant. The shift was dependent on the PE concentration. For 1 mg/mL PDADMAC, the SPR shifted by 24 nm (Fig. 13A). This shift was much larger

than values of 1.5–2 nm reported in other studies.¹⁶ However, both the type and molecular weight of the PE were different in each study which may explain the larger SPR shift. With increasing amounts of the polymer, the SPR peak wavelength increased slowly as not only is the dielectric material surrounding the particle changing, but also the particles are becoming slightly larger with the absorption of the polymer onto the surface.²³

The data collected is in agreement with past studies on PC/NP ratios, where the greatest stability of PE-coated NPs was apparent for PC/NP ratios between 1000–4000.¹⁶ However, is likely dependent on the structure and Mw of the PE.

3.2. Effect of Salt Concentration

As the likelihood of inter-particle bridging and hence aggregation increases with increasing PE concentration, the lowest stable polymer concentration (5 mg/mL) was used for subsequent salt effect studies. On planar substrates, the maximum coverage of PDADMAC typically increases with increasing ionic strength.²⁴ For spherical nanoparticles, the absorbance should, thus, increase with increasing salt concentration. However, colloidal stability becomes a greater issue in coating NPs as increasing the salt concentration can increase the Debye screening length. This increased Debye screening length decreases the repulsive electrostatic interactions and hence Van der Waal's forces dominate causing NP aggregation. Experimentally, an increase in salt concentration caused the NPs to become less stable and at concentrations above 0.05 M, the NPs irreversibly attached to the centrifugation tubes (Table 3). For 0.1 M and 0.5 M NaCl, samples fully aggregated and precipitated. For concentrations of 0.05 M and below, there was no significant difference in peak wavelength (Fig. 14) however; the peak absorbance was much lower indicating the nanoparticles have likely started to attach to the centrifuge tubes.

Table 3: The average SPR peak and absorbance as determined by UV–vis spectroscopy for 5 mg/mL PDADAMAC-coated AuNP.

Salt Concentration (M)	Average SPR Peak (nm)	Average Absorbance (a.u.)
0	543 ± 1.2	0.69 ± 0.04
0.001	539 ± 0.5	0.58 ± 0.04
0.05	540 ± 3.7	0.17 ± 0.05
0.1	*	*
0.5	*	*

* At 0.1 M and 0.5 M, the sample irreversibly aggregated and was unable to be removed from the centrifuge tubes with a concentration of AuNP suitable for UV–vis spectroscopy.

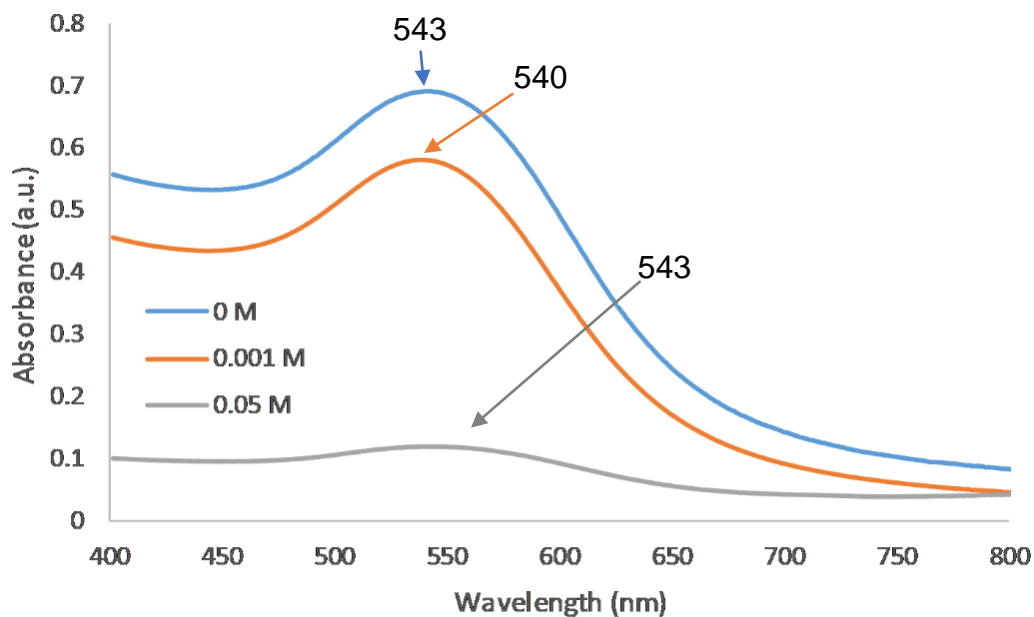


Figure 14: UV–vis spectra of varying salt concentrations of 5 mg/mL PDADMAC on 5 nm AuNPs.

3.3. Effect of Solvent

It has been observed that the addition of a PE layer to Au nanorods can increase the stability of NPs in a range of solvents where they otherwise would aggregate.²⁵ Due to this, the optimised conditions for PDADMAC attachment were used to test the stability of the coated AuNPs in three different solvents: ethanol, Tween20 and phosphate-buffered saline (PBS) to determine if the addition of the PE coating enhanced the NPs stability. The changes were monitored as Δ SPR, which is the difference between the SPR peak in water and the solvent being tested. The larger the shift observed the more likely the NPs are aggregating.

In ethanol, there was a significant shift in the SPR peak, especially for citrate capped AuNPs with Δ SPR = 23 nm, indicating aggregation of the nanoparticles (See supporting information). In comparison, Δ SPR for PDADMAC coated particles was only 6 nm, suggesting a protective effect of the polyelectrolyte coating that reduces the tendency for particle aggregation in ethanol.

Tween 20 had been reported to be a stabilising agent for citrate-capped AuNPs.^{26,27} In good agreement with these results, there was no significant difference observed for both citrate-capped and PDADMAC-coated AuNP when exposed to the surfactant.

Finally, PBS was used as it is often used in cell culture studies.^{28,29} PBS has a relatively high NaCl concentration (~0.1 M). Similar to the results above, both citrate capped and PDADMAC AuNPs aggregated and attached to the centrifugation tubing, hence no peak could be measured using UV-vis spectroscopy.

4. Conclusions

The optimised conditions for polyelectrolyte coatings of 5 nm diameter citrate capped AuNPs were determined to be 5 mg/mL of PDADMAC in 1 mM NaCl. These conditions resulted in the most stable solutions as shown by zeta potential and UV-vis spectroscopy measurements. Additionally, a PC/NP ratio between

1000–4000 resulted in the most stable solutions, in good agreement with the literature. High salt concentrations led to aggregation to the nanoparticles. Finally, when the nanoparticles were suspended in ethanol, the PDADMAC-coated AuNPs showed little aggregation compared to the citrate-coated AuNPs. Further stability testing is required to understand how PDADMAC coatings can prevent aggregation, especially in freeze–thaw experiments. Different polyelectrolytes and nanoparticles will have different influences on the optimised conditions; however, it would be expected that like-sized nanoparticles coated in strong polyelectrolytes would behave in a similar way and, thus, optimisation conditions would be comparable.

Acknowledgements:

The authors would like to thank the Australian Institute of Nuclear Science and Engineering (AINSE Limited) for providing financial assistance (Award – PGRA) and the Australian Government for the Research Training Program Scholarship.

References:

1. Siafaka, P.; Üstündağ Okur, N.; Karavas, E.; Bikiaris, D. Surface Modified Multifunctional and Stimuli Responsive Nanoparticles for Drug Targeting: Current Status and Uses, *International Journal of Molecular Sciences* **2016**, *17*, 1440.
2. Khan, M.S.; Vishakante, G.D.; Siddaramaiah, H. Gold nanoparticles: A paradigm shift in biomedical applications, *Advances in Colloid and Interface Science* **2013**, *199-200*, 44-58.
3. Santos, A.C.; Caldas, M.; Pattekari, P.; Fontes Ribeiro, C.; Ribeiro, A.J.; Lvov, Y.; Veiga, F. Chapter 16 - Layer-by-Layer coated drug-core nanoparticles as versatile delivery platforms A2 - Grumezescu, Alexandru Mihai. In *Design and Development of New Nanocarriers*, William Andrew Publishing: 2018; pp. 595-635.

4. Richardson, J.J.; Björnmalm, M.; Caruso, F. Technology-driven layer-by-layer assembly of nanofilms, *Science (New York, N.Y.)* **2015**, *348*.
5. Harris, C.M.; Miller, S.G.; Andresen, K.; Thompson, L.B. Quantitative measurement of sodium polystyrene sulfonate adsorption onto CTAB capped gold nanoparticles reveals hard and soft coronas, *Journal of Colloid and Interface Science* **2018**, *510*, 39-44.
6. Hirsjärvi, S.; Peltonen, L.; Hirvonen, J. Layer-by-layer polyelectrolyte coating of low molecular weight poly(lactic acid) nanoparticles, *Colloids and Surfaces B: Biointerfaces* **2006**, *49*, 93-99.
7. Wang, S.; Chen, K.; Xu, Y.; Yu, X.; Wang, W.; Li, L.; Guo, X. Protein immobilization and separation using anionic/cationic spherical polyelectrolyte brushes based on charge anisotropy, *Soft Matter* **2013**, *9*, 11276-11287.
8. Wandrey, C.; Hernández-Barajas, J.; Hunkeler, D. Diallyldimethylammonium Chloride and its Polymers. In *Radical Polymerisation Polyelectrolytes*, Capek, I., Hernández-Barajas, J., Hunkeler, D., Reddinger, J.L., Reynolds, J.R., Wandrey, C., Eds. Springer Berlin Heidelberg: Berlin, Heidelberg, 1999; pp. 123-183.
9. Gittins, D.I.; Caruso, F. Tailoring the Polyelectrolyte Coating of Metal Nanoparticles, *The Journal of Physical Chemistry B* **2001**, *105*, 6846-6852.
10. Hierrezuelo, J.; Sadeghpour, A.; Szilagyi, I.; Vaccaro, A.; Borkovec, M. Electrostatic Stabilization of Charged Colloidal Particles with Adsorbed Polyelectrolytes of Opposite Charge, *Langmuir* **2010**, *26*, 15109-15111.
11. Polte, J. Fundamental growth principles of colloidal metal nanoparticles – a new perspective, *CrystEngComm* **2015**, *17*, 6809-6830.
12. Egger, C.C.; Anderson, M.W.; Tiddy, G.J.T.; Casci, J.L. In situ NMR and XRD studies of the growth mechanism of SBA-1, *Physical Chemistry Chemical Physics* **2005**, *7*, 1845-1855.

13. Moore, T.L.; Rodriguez-Lorenzo, L.; Hirsch, V.; Balog, S.; Urban, D.; Jud, C.; Rothen-Rutishauser, B.; Lattuada, M.; Petri-Fink, A. Nanoparticle colloidal stability in cell culture media and impact on cellular interactions, *Chemical Society Reviews* **2015**, *44*, 6287-6305.
14. Tang, K.; Besseling, N.A.M. Formation of polyelectrolyte multilayers: ionic strengths and growth regimes, *Soft Matter* **2016**, *12*, 1032-1040.
15. Huang, H.; Ruckenstein, E. The Bridging Force between Colloidal Particles in a Polyelectrolyte Solution, *Langmuir* **2012**, *28*, 16300-16305.
16. Schneider, G.; Decher, G. Functional Core/Shell Nanoparticles via Layer-by-Layer Assembly. Investigation of the Experimental Parameters for Controlling Particle Aggregation and for Enhancing Dispersion Stability, *Langmuir* **2008**, *24*, 1778-1789.
17. Bizmark, N.; Ioannidis, M.A. Effects of Ionic Strength on the Colloidal Stability and Interfacial Assembly of Hydrophobic Ethyl Cellulose Nanoparticles, *Langmuir* **2015**, *31*, 9282-9289.
18. Benoit, D.N.; Zhu, H.; Lillierose, M.H.; Verm, R.A.; Ali, N.; Morrison, A.N.; Fortner, J.D.; Avendano, C.; Colvin, V.L. Measuring the Grafting Density of Nanoparticles in Solution by Analytical Ultracentrifugation and Total Organic Carbon Analysis, *Analytical chemistry* **2012**, *84*, 9238-9245.
19. Notley, S.M.; Norgren, M. Adsorption of a strong polyelectrolyte to model lignin surfaces, *Biomacromolecules* **2008**, *9*, 2081-2086.
20. Cho, K.; Lee, Y.; Lee, C.-H.; Lee, K.; Kim, Y.; Choi, H.; Ryu, P.-D.; Lee, S.Y.; Joo, S.-W. Selective Aggregation Mechanism of Unmodified Gold Nanoparticles in Detection of Single Nucleotide Polymorphism, *The Journal of Physical Chemistry C* **2008**, *112*, 8629-8633.
21. Mengarelli, V.; Auvray, L.; Pastré, D.; Zeghal, M. Charge inversion, condensation and decondensation of DNA and polystyrene sulfonate by polyethylenimine, *The European Physical Journal E* **2011**, *34*, 127.

22. Kleimann, J.; Gehin-Delval, C.; Auweter, H.; Borkovec, M. Superstoichiometric charge neutralization in particle-polyelectrolyte systems, *Langmuir* **2005**, *21*, 3688-3698.
23. Quinsaat, J.E.Q.; Nuesch, F.A.; Hofmann, H.; Opris, D.M. Dielectric properties of silver nanoparticles coated with silica shells of different thicknesses, *RSC Advances* **2013**, *3*, 6964-6971.
24. Schwarz, S.; Buchhammer, H.M.; Lunkwitz, K.; Jacobasch, H.J. Polyelectrolyte adsorption on charged surfaces: study by electrokinetic measurements, *Colloids and Surfaces A: Physicochemical and Engineering Aspects* **1998**, *140*, 377-384.
25. Alkilany, A.M.; Thompson, L.B.; Murphy, C.J. Polyelectrolyte Coating Provides a Facile Route to Suspend Gold Nanorods in Polar Organic Solvents and Hydrophobic Polymers, *ACS Applied Materials & Interfaces* **2010**, *2*, 3417-3421.
26. Shih, Y.-C., Ke, Chen-Yi., Yu, Chen-Ju., Lu, Chi-Yu., Tseng, Wei-Lung. Combined Tween 20-Stabilized Gold Nanoparticles and Reduced Graphite Oxide-Fe₃O₄ Nanoparticle Composites for Rapid and Efficient Removal of Mercury Species from a Complex Matrix, *ACS Applied Materials & Interfaces* **2014**, *6*, 17437-17445.
27. Lin, C.-Y.; Yu, C.-J.; Lin, Y.-H.; Tseng, W.-L. Colorimetric Sensing of Silver(I) and Mercury(II) Ions Based on an Assembly of Tween 20-Stabilized Gold Nanoparticles, *Analytical chemistry* **2010**, *82*, 6830-6837.
28. McCarthy, K.D.; de Vellis, J. Preparation of separate astroglial and oligodendroglial cell cultures from rat cerebral tissue, *The Journal of Cell Biology* **1980**, *85*, 890-902.
29. Tuomola, E.M.; Salminen, S.J. Adhesion of some probiotic and dairy Lactobacillus strains to Caco-2 cell cultures, *International Journal of Food Microbiology* **1998**, *41*, 45-51.

CHAPTER 4: INCREASING ANTIBIOTIC SUSCEPTIBILITY - THE USE OF CATIONIC GOLD NANOPARTICLES IN GRAM-NEGATIVE BACTERIAL MEMBRANE MODELS

This chapter is an article which will be submitted for publication and is entitled 'Increasing antibiotic susceptibility - the use of cationic gold nanoparticles in Gram-negative bacterial membrane models'. It is authored by **Melanie Fuller**, Alex Ashenden, Jakob Andersson, Stephen Holt and Ingo Köper. This chapter uses the stable, cationic polyelectrolyte coated gold nanoparticles fabricated in Chapter 3 to determine how they affect bacterial cell membranes. Initially it was assessed if the nanoparticles themselves form defects in the membrane. Subsequently, the effect of adding both gold nanoparticles and Colistin simultaneously was determined. Finally, pre-treating the membrane with gold nanoparticles prior to the addition of Colistin was evaluated for defect formation. Both the simultaneous addition and the pre-treatment was compared to using only Colistin.

Understanding the affect nanoparticles have on the membrane as well how increased damage can be caused through combining nanoparticles and Colistin is important in increasing bacterial susceptibility.

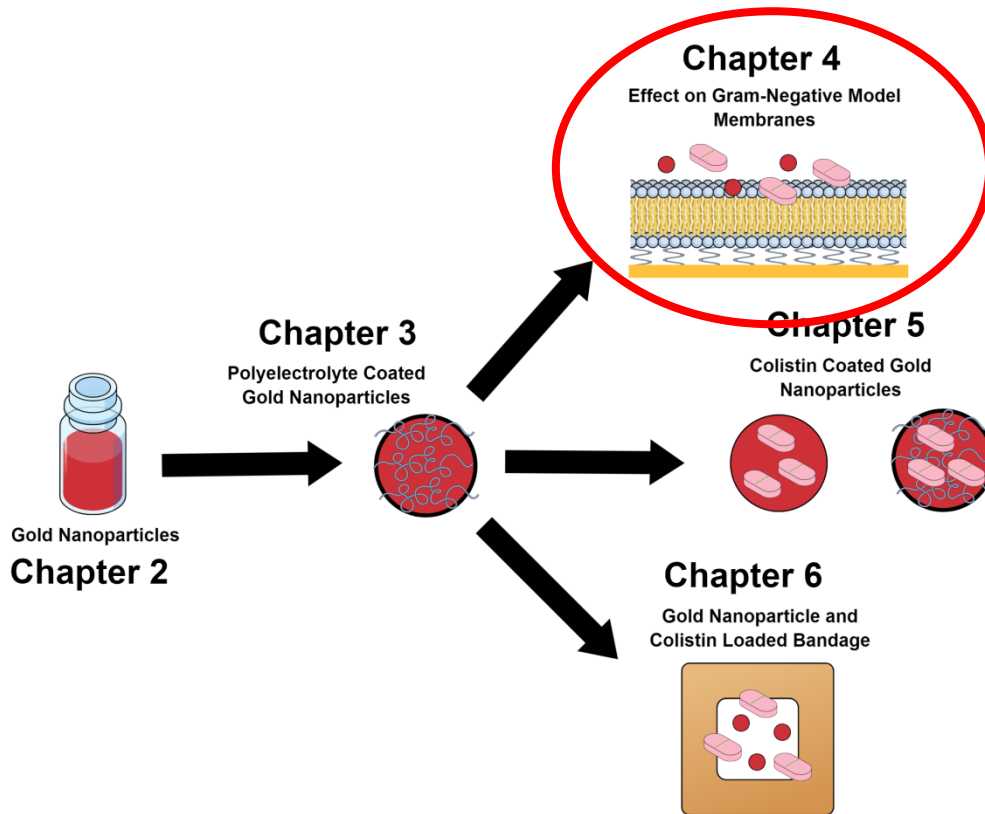


Figure 15: Diagram of the overall thesis, indicating Chapter 4 and how it fits into the larger body of work.

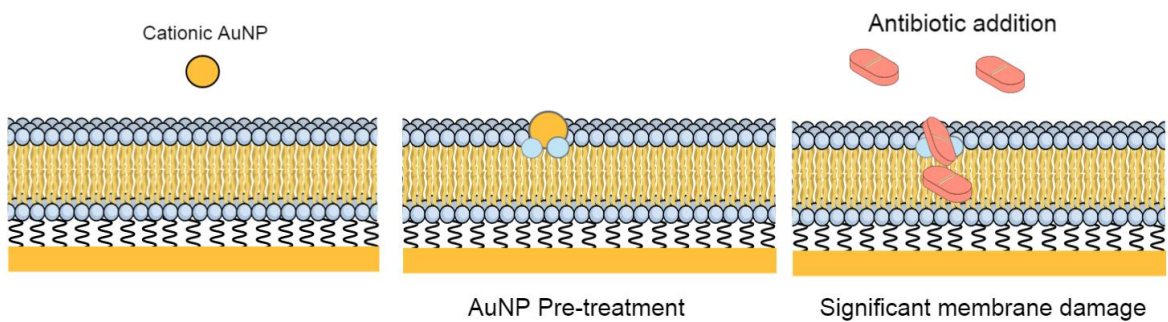


Figure 16: Graphical abstract for the chapter entitled ‘Increasing Antibiotic Susceptibility – The Use of Cationic Gold Nanoparticles in Gram-Negative Bacterial Membrane Models’.

Abstract:

Gram-negative bacterial resistance is predicted to become one of the greatest issues for healthcare systems in the next thirty years. Finding a way to increase bacterial susceptibility towards drugs is an important step in being able to treat resistant infections. Here, the effects of pre-treating a bacterial membrane with cationic gold nanoparticles prior to the addition of the antibiotic, Colistin sulfate was explored. A tethered lipid bilayer membrane was used to mimic a Gram-negative bacterial cell membrane. In comparison to using Colistin sulfate alone, pre-treating the membrane with small amounts of gold nanoparticles showed a significant decrease in outer head group hydration indicating severe defect formation in the membrane structure. Cationic gold nanoparticles could thus be used to increase bacterial susceptibility for antibiotics, leading to a more efficient treatment.

1.0 Introduction:

With the rapid emergence of antibiotic resistance in the last few decades, existing antibiotic treatments have become more and more inefficient. The ramifications of bacterial resistance are substantial, with longer hospital stays, an increase in medical costs and increased mortality.¹⁻³ Treatment of Gram-negative infections are particularly difficult. The cell wall of these bacteria consists of an inner and outer membrane with a layer of peptidoglycans and lipoproteins between the two membrane layers.³ This complex cell wall structure acts as a shield, making it difficult for antibiotics to penetrate the membrane.^{4,5} There are several antibiotics which are currently in circulation that target the bacterial cell membrane, including

the last-line drug Colistin, which is being used in this study. Colistin is a cationic polypeptide antibiotic, which electrostatically interacts with the negatively charged phosphate groups of the lipopolysaccharides (LPS) in the outer membrane.^{6,7} This interaction leads to the formation of defects in the membrane, causing permeability and leakage of cellular contents, which ultimately leads to cell death.⁸

Here, the formation of defects caused by electrostatic binding to the membrane was explored further with the addition of cationic gold nanoparticles. Previous research has shown that 3 nm diameter cationic gold nanoparticles form defects in the outer membrane of both Gram-positive and Gram-negative bacteria.⁹ The defects caused significant increases in cell permeability for *E. coli*, from 5% in untreated control cells compared to 73% for cells treated with gold nanoparticles.⁹ Colistin is a membrane-targeting antibiotic, and should have an increased effect on membranes already damaged from pre-treatment with small nanoparticles. A model lipopolysaccharide tethered bilayer lipid membrane (LPS-tBLM) system has been used (Fig. 17) to explore the effects of nanoparticle pre-treatment. This model membrane system was developed to simplify the bacterial membrane structure and to allow a better understanding of how drugs and nanoparticles interact with the cell membrane. The model consists of a tethered lipid monolayer attached to a gold substrate, which is fused with LPSs to mimic a bacterial membrane. While the model does not contain embedded membrane proteins, transporters or peptides it can mimic the fundamental chemical and physical properties which are essential for cell function.⁴ Electrochemical impedance

spectroscopy (EIS) and neutron reflectometry were used to monitor the interactions of a bacterial cell membrane with antibiotics and nanoparticles. Both of these techniques are sensitive to small changes in the membrane structure and can provide real time insight into the mechanism of drug action. As each membrane is unique, the electrical properties are different for each membrane. To account for this, only high quality membranes were used in the analysis and these were determined as having resistances around 10-100 M Ω .cm² and capacitance around 1 μ F.cm⁻².^{10,11}

While EIS gives information about the electrical properties of the membrane, neutron reflectivity allows determination of structural features at the sub-nanometre level. Thus, small defects or changes in the structure of the membrane to be observed. Neutron reflectivity measures scattered neutron intensity as a function of scattering angle. The membrane structure is probed perpendicularly to the substrate. Experimental data is fitted to a model describing the membrane as a set of 8 layers, with each layer being fitted with a thickness (\AA), scattering length density (SLD) (10^{-6}\AA^{-2}), hydration (volume %) and roughness (\AA). The structural analysis of LPS-tBLMs has been reported previously.⁴

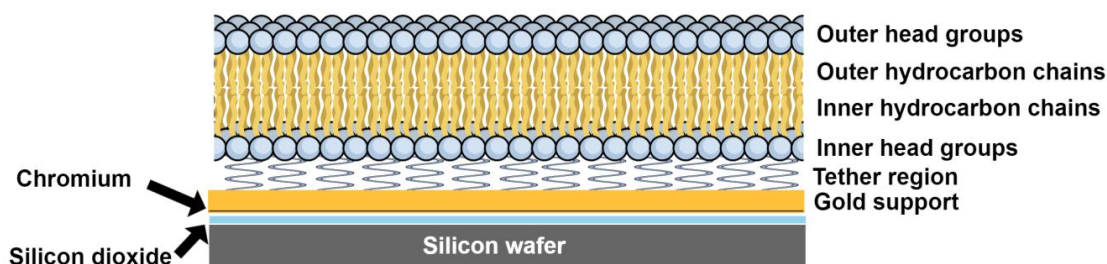


Figure 17: Schematic of the eight layers of a sparsely tethered tBLM.

In previous studies we showed that the addition of Colistin to sparsely tethered LPS membranes causes structural changes on the outer leaflet, observed as an increase in roughness of the outer hydrocarbon chains and a change in hydration of the head groups.⁴ Using this information, we compared the roughness and hydration of the membrane before and after the addition of gold nanoparticles as well as determining if the pre-treatment of the cationic nanoparticles before the addition of Colistin causes a larger disruption to the membrane than the addition of nanoparticles and Colistin together.

2.0 Materials and Methods:

2.1 Membrane chemicals:

Colistin sulfate and Rc-strain Lipopolysaccharides (Rc-LPS) obtained from the J5 mutant of *Escherichia coli* (*E. coli*) (Sigma Aldrich, Australia) were used without further purification. Ultrapure water obtained from WaterPro PS reverse osmosis system (18.2 MΩcm resistance, Labconco) was used for all experiments. D₂O was obtained from the National Deuteration Facility co-located at the Australian Nuclear Science and Technology Organisation (New South Wales, Australia).

2.2 Cationic gold nanoparticles:

5 nm diameter citrate capped gold nanoparticles (AuNPs) at a concentration of 8.4×10^{13} particles/mL was purchased from Nanocomposix (USA). 2 mL of the gold nanoparticle solution were mixed with 3 mL of 5 mg/mL Polydiallyldimethylammonium chloride (PDADMAC) (Sigma-Aldrich, Australia) (average Mw <100,000) in 1 mM NaCl. The AuNP/PDADMAC solution was stirred overnight before centrifuging at 14500 rpm for 40 minutes to remove excess PDADMAC. The supernatant was removed and the pellet resuspended in MilliQ. This washing step was conducted three times to ensure no excess PDADMAC remained. The characterisation of these polyelectrolyte coated gold nanoparticles can be found elsewhere.¹² Prior to using the AuNP for neutron studies they were centrifuged and resuspended in D₂O at a concentration of approximately 3×10^{13} particles/mL.

2.3 Electrochemical Impedance Spectroscopy (EIS):

For all EIS experiments, membranes were assembled as described previously.⁴ Briefly, clean silicon substrates were sputter coated sequentially with layers of 5 nm chromium and 20 nm gold. Once coated, the substrates were rinsed with ethanol before being inserted into 0.1 mM solution of DPhyTL and mercaptoethanol (80/20) for 18 h to allow the formation of the tethered monolayer. After monolayer formation, the substrates were removed from the ethanolic solution and rinsed thoroughly with ethanol before being dried under nitrogen. The bilayers were then formed by vesicle fusion with the already formed monolayer. Vesicles with 6% DPhyPC (Sigma Aldrich, Australia) and 94% R_cLPS at a concentration of 1 mg/mL were used. Vesicles were prepared by mixing

lipids in chloroform, evaporating the solvent and rehydrating the lipids in water. The lipid-water mixture was extruded 31 times through a 200 nm track-etched polycarbonate filter membrane. All vesicle solutions were extruded just prior to use. 10 $\mu\text{L}/\text{mL}$ of the extruded vesicle solution was added to the monolayer in 100 mM CaCl_2 . The bilayers were left to form for 18 h at ambient temperature and the resulting bilayers were rinsed with 5 cell volumes of CaCl_2 .

For the addition of gold nanoparticles to the bilayers, 100 μL of cationic nanoparticles were either added simultaneously with 10 mg/mL Colistin sulfate solution or the nanoparticles were added and left on the membrane for 18 h before being rinsed off and then 10 mg/mL Colistin sulfate solution was added to the membrane.

2.4 Neutron scattering experimental method:

All neutron experiments were performed at the Australian Nuclear Science and Technology Organisation (ANSTO) at the 20 MW OPAL reactor (Lucas Heights, Sydney, Australia). Neutron reflectometry (NR) measurements were conducted using the PLATYPUS time-of-flight neutron reflectometer.¹³ Cold neutrons with wavelengths from 2.5 to 18 \AA were used. The reflected intensity of the neutrons was measured at glancing angles of, 0.5°, 0.9° and 5° under D_2O , H_2O and CM4.5 (mixture of 76% D_2O and 24% H_2O). All measurements were completed in 100 mM CaCl_2 unless otherwise stated for approximately 2 h per contrast. Preparation of the substrates was conducted at the South Australian node of the ANFF. Briefly, 10 cm diameter by 1 cm thickness polished circular crystal silicon

disks were cleaned using a 1 : 1 : 5 mixture of NH₃/H₂O₂/MilliQ for 1 h at 70°C. They were then rinsed with MilliQ and ethanol (Sigma Aldrich, Australia) with Nitrogen used to dry them. They were then coated with 5 nm chromium (100 mA current) and 20 nm gold (10 mA) via sputter coating. Monolayers and bilayers were formed the same as for the EIS experiments.

For neutron scattering, three bilayers were produced. The first bilayer pre-treated with 100 µL of cationic nanoparticles for an exposure of 18 h, before being washed off and then 10 mg/mL Colistin added. The second bilayer had 100 µL of nanoparticles added simultaneously with the 10 mg/mL Colistin sulfate and exposed for 18 h. The final bilayer had 1 mL AuNP added for 18 h, before being washed off and Colistin sulfate added to the membrane for an additional 18 h.

3.0 Results and Discussion

3.1 Addition of Gold Nanoparticles to the Membrane

Initially, the addition of the AuNPs to membranes was explored through EIS measurements. The nanoparticle stock solution used had a concentration of 3.46×10^{12} particles/mL. For convenience, the volume of nanoparticles used will be stated rather than the concentration. The approximate length of time the nanoparticles were exposed to the membrane as well as the concentration of nanoparticles were kept constant. Impedance data was collected over a wide frequency range and fitted to an equivalent circuit describing the membrane as a combination of resistive and capacitive elements, as described elsewhere.⁴ In EIS, a decrease in resistance suggests that the membrane is becoming 'leaky'

allowing charged species to cross the interior of the non-polar membrane. This is indicative of defects forming on the membrane surface. Modelling of the Bode plot indicated that there was no significant change in the membrane resistance upon the addition of 100 μL of nanoparticles. However, upon the addition of 200 μL of gold nanoparticles, there was a decrease in membrane resistance indicating small defects were observed (Fig. 18, Table 4). This was likely caused by the nanoparticles binding to the membrane. After rinsing off the AuNPs, no distinctive changes were observed.

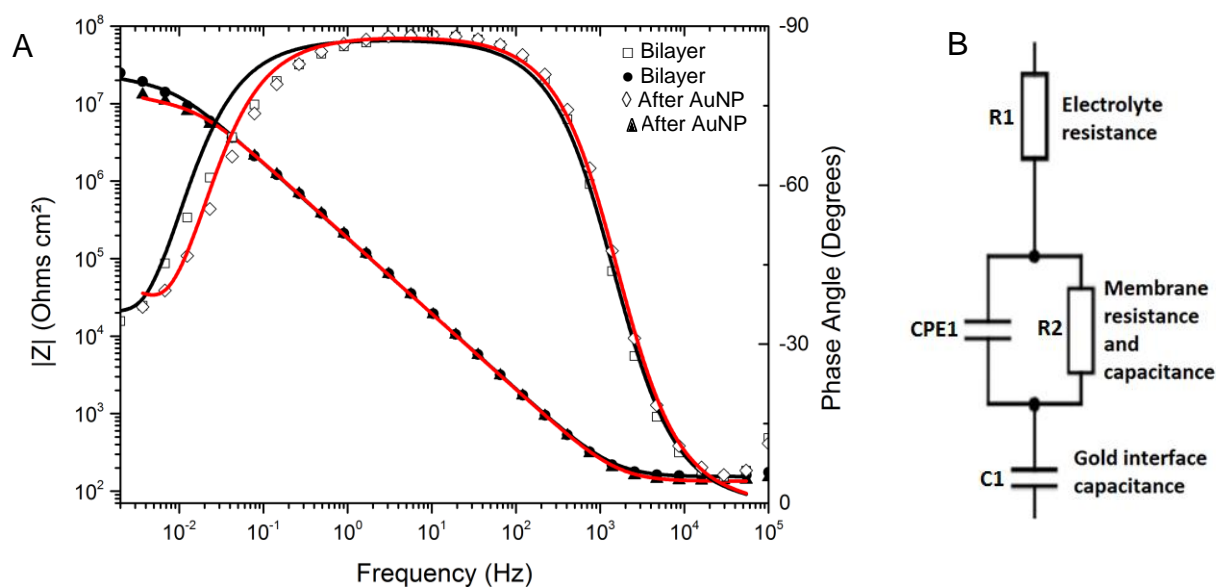


Figure 18: (A) Bode plot showing 80% DPhyTI, 94% R_cLPS tBLMs prior to (bilayer) (black) and after the exposure of 200 μL cationic AuNPs for 18 h (red). The lines represent the fitted data with the filled shapes representing impedance and the un-filled representing the phase angle. (B) Schematic of the equivalent circuit, which the EIS data is fitted to.

Table 4: The changes in electrical properties of two different LPS-tBLMs from the addition of gold nanoparticles exposed for 18-20 h.

	Resistance (MΩcm ²)	Capacitance (μFcm ⁻²)
Bilayer before addition	18.3 ± 0.69	0.91 ± 0.01
Bilayer after exposure to 100 μL AuNP	15.2 ± 1.37	1.42 ± 0.05
After rinse	11.5 ± 1.38	1.62 ± 0.07
Bilayer before addition	18.2 ± 0.96	1.00 ± 0.02
Bilayer after exposure to 200 μL AuNP	8.2 ± 0.49	0.92 ± 0.30
After rinse	9.8 ± 0.35	1.00 ± 0.02

3.2 Simultaneous addition of Colistin and Gold Nanoparticles

The addition of 10 mg/mL Colistin Sulfate in combination with the AuNPs initially did not show any significant damage, regardless of the concentration of nanoparticles (Table 5). In fact, the membrane resistance increase slightly. However, after rinsing, the resistance decreased slightly (Fig. 19). Colistin was likely binding to the defect sites caused by the nanoparticles, blocking the charge

pathways which leads to the lack of change in resistance. It is not until the Colistin and nanoparticles are rinsed off that the damage is observed.

Table 5: Electrochemical measurements of the simultaneous addition of gold nanoparticles with 10 mg/mL Colistin with various rinse times.

	Resistance ($M\Omega\text{cm}^2$)	Capacitance (μFcm^{-2})
Bilayer before addition	12.1 ± 0.46	1.31 ± 0.02
Bilayer after addition of 100 μL AuNP + 10 mg/mL Colistin 19 h	13.8 ± 2.07	0.87 ± 0.06
After rinse	3.5 ± 0.74	0.83 ± 0.07
Bilayer before addition	28.7 ± 1.69	1.07 ± 0.04
Bilayer after addition of 200 μL AuNP + 10 mg/mL Colistin 17 h	28.1 ± 1.04	0.89 ± 0.01
After rinse	21.6 ± 0.95	0.91 ± 0.02

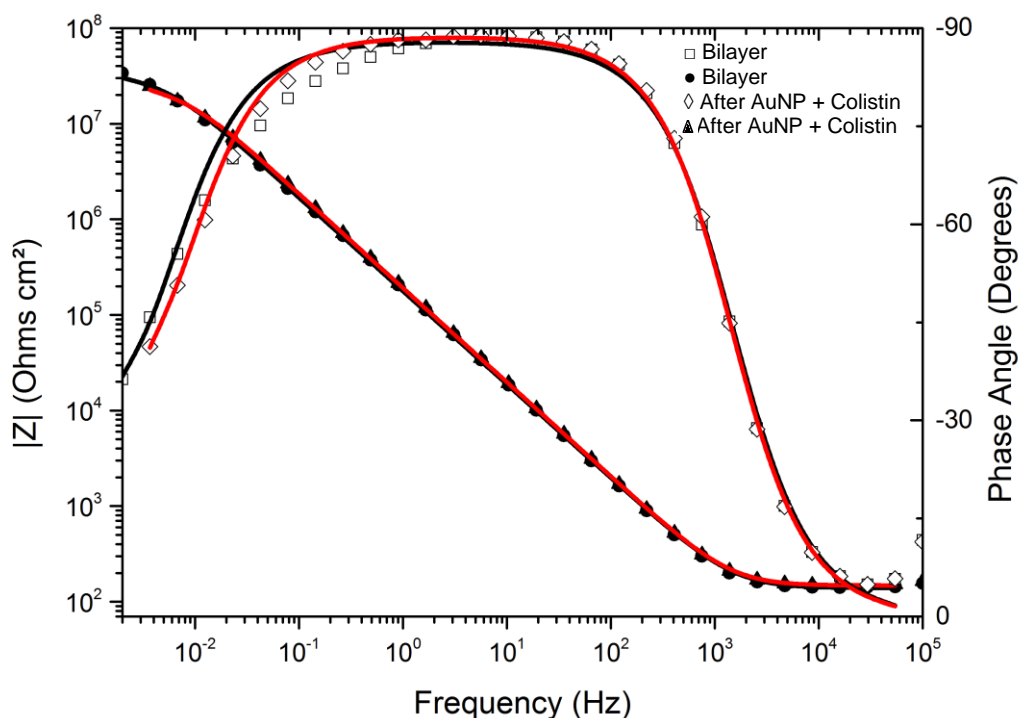


Figure 19. (A) Bode plot showing 80% DPhyTI, 94% RcLPS tBLMs prior to (bilayer) (black) and after the exposure of 200 μ L cationic AuNPs with 10 mg/mL Colistin for 17 h (red). The lines represent the fitted data with the filled shapes representing impedance and the un-filled representing the phase angle.

The disruption of the membrane observed in EIS after rinsing was confirmed through the use of neutron reflectometry. In neutron reflectometry, the effects of AuNP and Colistin to the bilayer can primarily be seen as changes in the outer layers of the membrane. The inner layers such as the inner HG and inner HC are covalently bound to the solid support and thus are unlikely to show any significant changes. During the modelling, the parameters describing the inner layers were kept constant. The simultaneous addition of Colistin and AuNP resulted in a decrease in the outer head group hydration which is indicative of defect formation. This was mirrored in the roughness of the outer hydrocarbon chains,

which increased significantly. The roughness was greater than the thickness of the head group layer suggesting large defects have formed in the outer leaflet of the membrane.

Table 6: Neutron reflectivity results for sparsely tethered tBLMS when exposed to 100 μL AuNP and 10 mg/mL Colistin sulfate simultaneously. Units for thickness and roughness are in \AA , SLD is 10^{-6}\AA^{-2} and hydration is volume %. The parameters for the additional layers can be found in the supporting information.

	Bilayer	AuNP and Colistin Addition
Outer hydrocarbon chain thickness	10.0	10.0
Outer hydrocarbon chain SLD	0.00	-0.03
Outer hydrocarbon chain hydration	5.99	5.80
Outer hydrocarbon chain roughness	5.47	14.8
Outer head group thickness	18.1	17.1
Outer head group SLD	4.23	4.46
Outer head group hydration	64.0	48.2
Outer head group roughness	9.99	8.70

3.3 Pre-treatment with gold nanoparticles prior to Colistin addition

Incubating the membrane with 100 μL AuNPs for 20 h prior to the addition of Colistin resulted in a partially reversible seventeen-fold reduction in membrane resistance (Table 7). When 200 μL of nanoparticles were used to pre-treat the membrane, just under a four-fold reduction was observed in the membrane resistance. However, after rinsing, there was increased damage observed and no recovery indicating complete membrane damage (Fig. 20). The lack of binding competition between the nanoparticles and Colistin on the anionic phosphate groups of the LPS allow more nanoparticles to bind to the membrane causing defects. At an increased concentration of 200 μL of nanoparticles for 18 h, the reduction in resistance was permanently reduced by three orders of magnitude (Table 7). The increased concentration of nanoparticles likely created sufficient defects to allow Colistin to permanently insert into the membrane and solubilise the lipids. This permanent insertion is justified by the inability to increase the resistance after washing with CaCl_2 .

Table 7: Electrochemical measurements with pre-treatment of the membrane with gold nanoparticles for various concentrations of gold nanoparticles with the addition post treatment of 10 mg/mL Colistin.

	Resistance (MΩcm ²)	Capacitance (μFcm ⁻²)
Bilayer before addition	18.3 ± 0.69	0.91 ± 0.01
Bilayer after addition of 100 μL AuNP 20 h + 10 mg/mL Colistin 20 h	1.03 ± 0.49	1.26 ± 0.30
After rinse	6.23 ± 1.49	1.25 ± 0.18
Bilayer before addition	18.2 ± 0.96	1.00 ± 0.02
200 μL AuNP 18 h + 10 mg/mL Colistin 17 h	4.70 ± 0.21	1.09 ± 0.02
After rinse	1.66 ± 0.07	1.12 ± 0.02

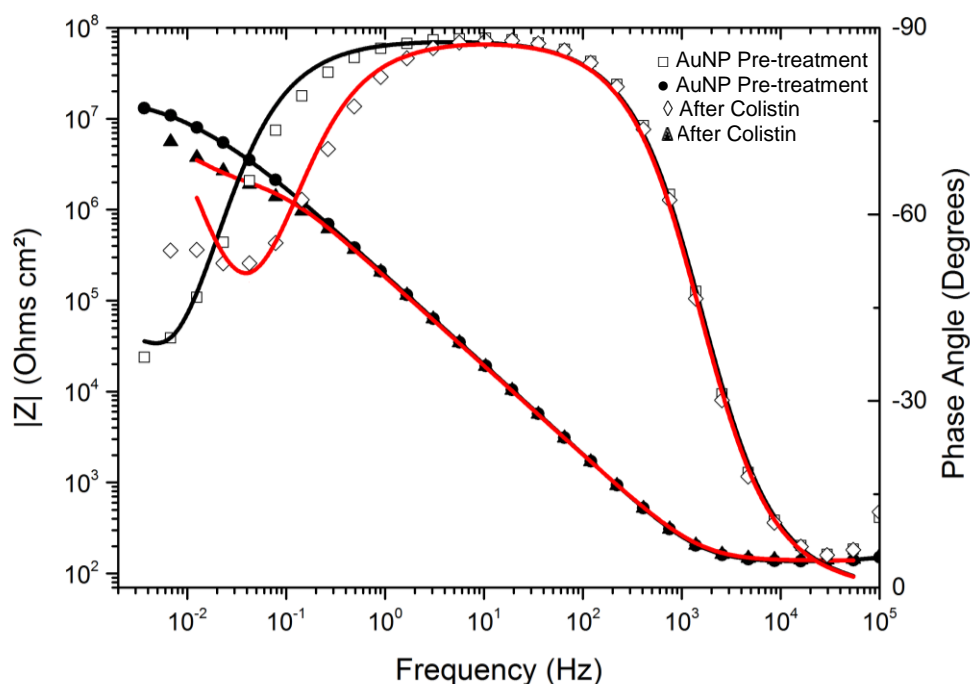


Figure 20: Bode plot showing 80% DPhyTI, 94% RcLPS tBLMs after pre-treating the membrane with 200 μL cationic AuNPs (black) and after exposing the membrane to 10 mg/mL Colistin for 17 h (red). The lines represent the fitted data with the filled shapes representing impedance and the un-filled representing the phase angle.

In the neutron experiments, the addition of 100 μL AuNP prior to 10 mg/mL Colistin addition had a slight decrease in the hydration in the outer HG layer, however the difference is not significant enough to suggest extensive damage to the membrane. Considerable damage was observed once Colistin was added to the membrane. The hydration decreased 5-fold below the initial bilayer hydration (Table 8). This decrease indicates that Colistin is binding to the HG region of the membrane and displaces the water molecules. In addition to the decrease in hydration, there was also an increase in the outer HC roughness with the addition of Colistin. Based on the small differences in the HG hydration and the HC

roughness after the addition of AuNP, it is likely that the AuNP are not causing any significant defects on the membranes surface at that concentration. However, the addition of Colistin after the nanoparticles is where the damage is evident, with a large decrease in the outer HG hydration.

Table 8: Sparsely tethered tBLMS and their parameter changes when exposed to 100 μL AuNP for 18 h then and 10 mg/mL Colistin sulfate for 18 h. Units for thickness and roughness are in \AA , SLD is 10^{-6}\AA^{-2} and hydration is volume %. The parameters for the additional layers can be found in the supporting information.

	Bilayer	AuNP Addition	Colistin Addition
Outer hydrocarbon chain thickness	11.0	11.0	15.2
Outer hydrocarbon chain SLD	-0.39	-0.39	-0.36
Outer hydrocarbon chain hydration	4.96	6.27	1.14
Outer hydrocarbon chain roughness	7.09	8.08	12.06
Outer head group thickness	11.2	12.0	12.0
Outer head group SLD	2.58	2.83	2.78
Outer head group hydration	69.5	64.9	12.1
Outer head group roughness	7.99	7.60	5.04

The concentration of AuNP was increased significantly, to determine if defects could be induced. 1 mL of AuNP in D₂O was added to the tBLM and left exposed to the membrane for 18 h prior to being washed off and 10 mg/mL of Colistin added. At this increased concentration, significant defects were observed in the modelling after the addition of the AuNPs. The hydration of the outer head group decreased four-fold and the roughness of the outer hydrocarbon chain exceeded the thickness of the hydrocarbon chain layer indicating significant membrane disruption (Table 9). Despite this, the membrane recovered slightly after the AuNP addition as observed after exposure to Colistin. Although the outer head group hydration is still significantly lower than that of the bilayer, it is over two fold greater than that after the AuNP addition. Likewise, the roughness is increased compared to the bilayer but not as high as after the AuNP.

Table 9: Sparsely tethered tBLMS and their parameter changes when exposed to 1 mL AuNP for 18 h then and 10 mg/mL Colistin sulfate for 18 h. Units for thickness and roughness are in Å, SLD is 10^{-6}Å^{-2} and hydration is volume %. The parameters for the additional layers can be found in the supporting information.

	Bilayer	AuNP Addition	Colistin Addition
Outer hydrocarbon chain thickness	13.6	13.5	15.0
Outer hydrocarbon chain SLD	-0.13	-0.18	-0.42
Outer hydrocarbon chain hydration	2.26	2.40	3.31
Outer hydrocarbon chain roughness	6.54	14.0	10.5
Outer head group thickness	9.69	9.65	15.0
Outer head group SLD	3.04	2.68	2.51
Outer head group hydration	70.0	15.0	43.7
Outer head group roughness	3.83	6.02	3.02

Previously published work has shown for an equivalent sparsely tBLM, with 94% RcLPS, a 22% decrease in the hydration of the outer head group was observed when the bilayer was exposed to 18 h of Colistin sulfate at the same concentration.⁴ The roughness also increased three-fold after the Colistin addition. In comparison to this, pre-treatment with 100 μL AuNP for 18 h before Colistin was added has a 140% decrease in hydration level and just under two-

fold increase in roughness. Therefore when pre-treated with nanoparticles, the Colistin has a greater effect than if Colistin is used alone. The simultaneous addition of Colistin and AuNP did not differ significantly from the addition of Colistin alone with a 28% decrease in hydration and just under a three-fold increase in roughness.

4.0 Conclusion:

The addition of AuNPs caused concentration dependant defects in the membrane through EIS. In Neutron reflectometry, disruption to the membrane was not observed upon addition of 100 μ L cationic AuNP however the addition of 1 mL AuNP led to significant disruption in the outer membrane. Therefore, the concentration of nanoparticles is important in defect formation. The addition of nanoparticles and Colistin simultaneously to the membrane caused small membrane defects only after washing, however the most significant damage was observed when the membrane was pre-treated with nanoparticles prior to introducing Colistin. The pre-treatment led to permanent damage to the membrane, which could not be recovered after rinsing. The pre-treatment of 100 μ L cationic AuNP led to significantly increased damage compared to both Colistin alone and simultaneous addition of Colistin and AuNP in neutron reflectometry. This finding suggests antibiotic susceptibility could be increased with pre-treatment of cationic gold nanoparticles.

Acknowledgements:

The authors would like to acknowledge the South Australian node of the Australian National Fabrication Facility, a company established under the National Collaborative Research Infrastructure Strategy. Neutron scattering was performed with funding from the Bragg Institute at the Australian Nuclear Science and Technology Organisation under the neutron proposals P7041, P6640 and P6237. M. F acknowledges the support from the Australian Institute of Nuclear Science and Engineering (AINSE) for the top-up scholarship and the Australian Government for the Research Training Scheme Scholarship.

References:

1. Friedman, N.D.; Temkin, E.; Carmeli, Y. The negative impact of antibiotic resistance, *Clinical Microbiology and Infection* **2016**, *22*, 416-422.
2. Eliopoulos, G.M.; Cosgrove, S.E.; Carmeli, Y. The Impact of Antimicrobial Resistance on Health and Economic Outcomes, *Clinical Infectious Diseases* **2003**, *36*, 1433-1437.
3. Exner, M.; Bhattacharya, S.; Christiansen, B.; Gebel, J.; Goroncy-Bermes, P.; Hartemann, P.; Heeg, P.; Ilshner, C.; Kramer, A.; Larson, E., et al. Antibiotic resistance: What is so special about multidrug-resistant Gram-negative bacteria?, *GMS Hyg Infect Control* **2017**, *12*.
4. Andersson, J.; Fuller, M.A.; Wood, K.; Holt, S.A.; Köper, I. A tethered bilayer lipid membrane that mimics microbial membranes, *Physical Chemistry Chemical Physics* **2018**, *20*, 12958-12969.
5. Zgurskaya, H.I.; López, C.A.; Gnanakaran, S. Permeability Barrier of Gram-Negative Cell Envelopes and Approaches To Bypass It, *ACS Infect Dis* **2015**, *1*, 512-522.

6. Fuller, M.A.; Carey, A.; Whiley, H.; Kurimoto, R.; Ebara, M.; Köper, I. Nanoparticles in an antibiotic-loaded nanomesh for drug delivery, *RSC Advances* **2019**, *9*, 30064-30070.
7. Gurjar, M. Colistin for lung infection: an update, *Journal of Intensive Care* **2015**, *3*, 3.
8. Martis, N.; Leroy, S.; Blanc, V. Colistin in multi-drug resistant *Pseudomonas aeruginosa* blood-stream infections: a narrative review for the clinician, *The Journal of infection* **2014**, *69*, 1-12.
9. Zhao, Y.; Tian, Y.; Cui, Y.; Liu, W.; Ma, W.; Jiang, X. Small Molecule-Capped Gold Nanoparticles as Potent Antibacterial Agents That Target Gram-Negative Bacteria, *Journal of the American Chemical Society* **2010**, *132*, 12349-12356.
10. Atanasov, V.; Atanasova, P.P.; Vockenroth, I.K.; Knorr, N.; Köper, I. A Molecular Toolkit for Highly Insulating Tethered Bilayer Lipid Membranes on Various Substrates, *Bioconjugate Chemistry* **2006**, *17*, 631-637.
11. Köper, I. Insulating tethered bilayer lipid membranes to study membrane proteins, *Molecular BioSystems* **2007**, *3*, 651-657.
12. Fuller, M.; Köper, I. Polyelectrolyte-Coated Gold Nanoparticles: The Effect of Salt and Polyelectrolyte Concentration on Colloidal Stability, *Polymers (Basel)* **2018**, *10*, 1336.
13. James, M.; Nelson, A.; Brule, A.; Schulz, J.C. Platypus: a time-of-flight neutron reflectometer at Australia's new research reactor, *Journal of Neutron Research* **2006**, *14*, 91-108.

CHAPTER 5: DELIVERY OF COLISTIN USING GOLD NANOPARTICLES

This chapter is an article which will be submitted for publication and is entitled 'Delivery of Colistin using Gold Nanoparticles'. It is authored by **Melanie Fuller**, Harriet Whiley and Ingo Köper. It explored the formation of Colistin coated gold nanoparticles and their antibiotic properties, then subsequently compared the antibiotic activity of the nanoparticles to using Colistin alone.

This research was based on the findings of Chapter 4 as it was shown that the pre-treatment using cationic gold nanoparticles led to more damage in the membrane than for Colistin alone. Colistin was electrostatically attached to the surface of both cationic and anionic gold nanoparticles. These complexes were then tested for antibiotic activity. It was expected that the Colistin coated nanoparticles would have greater antibiotic action than Colistin alone based on previous reports in literature for other antibiotics. This has been discussed further within the chapter.

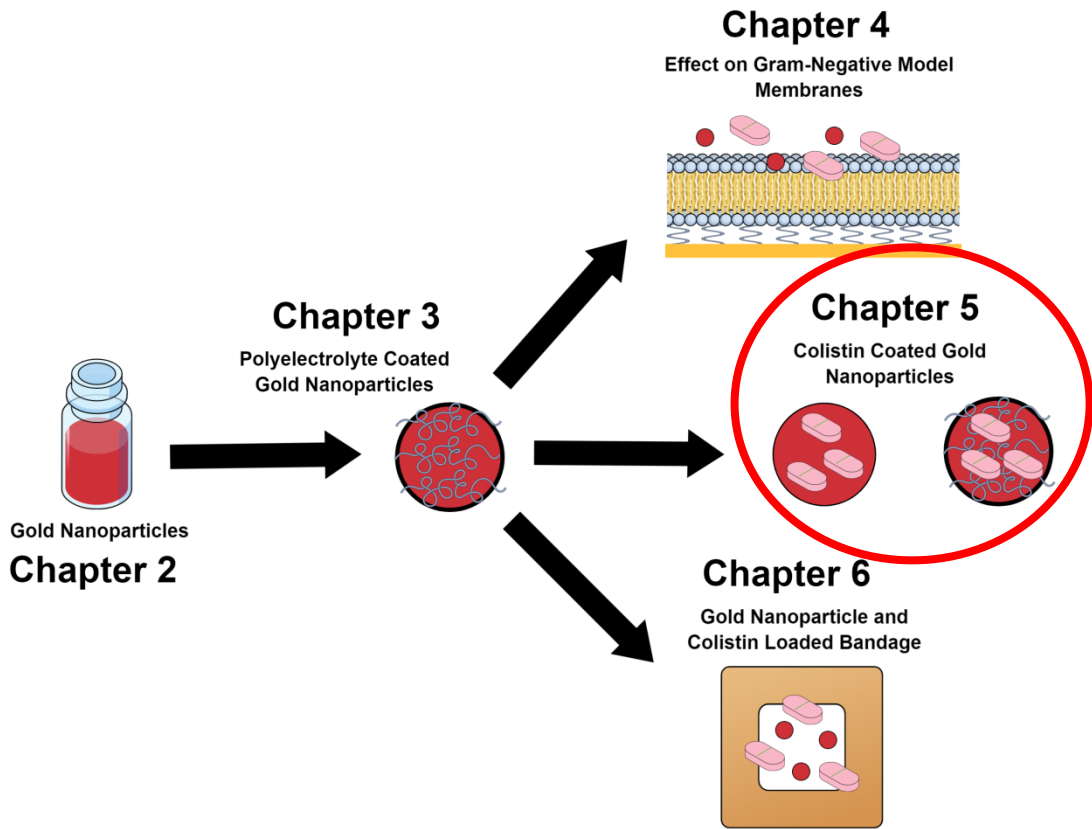


Figure 21: Diagram of the overall thesis, indicating Chapter 5 and how it fits into the larger body of work.

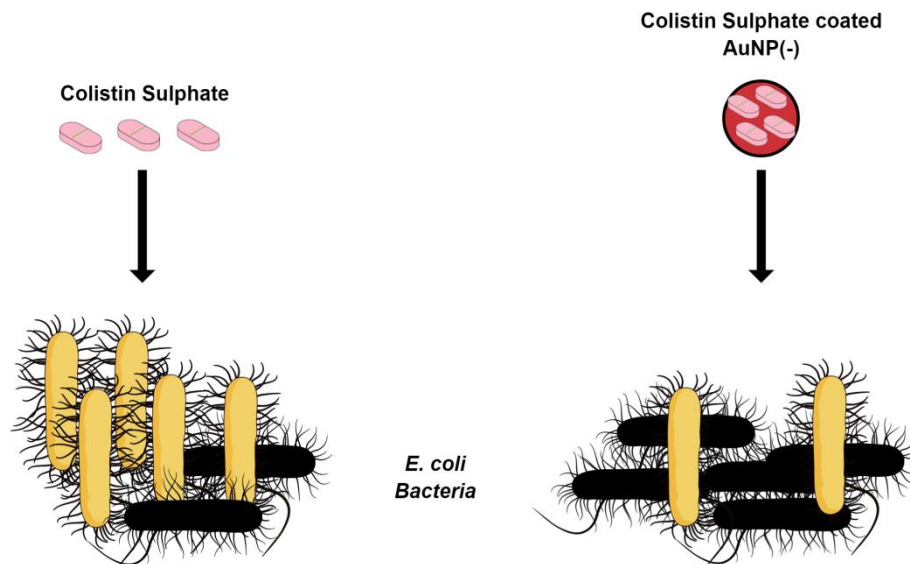


Figure 22: Graphical abstract from the Chapter 5 'Delivery of Colistin using Gold Nanoparticles'.

Abstract:

Antibiotic resistance is set to become one of the greatest threats to human existence and new treatments or more effective ways of treating infections have to be developed. Colistin is considered a last-line of defence antibiotic which has decreased usage due to undesirable side effects and thus has reduced resistance. Due to the rise of pathogens that are resistant to all common antibacterial drugs, Colistin is once again being considered as a treatment option. As Colistin's side effects are dose dependent; it is therefore desirable to be able to treat infections using Colistin with the same therapeutic effect but at a lower dosage. Gold nanoparticles have been used as a vehicle for Colistin delivery, with a Colistin coating on both negatively charged and positively charged gold nanoparticles. This study demonstrated that by delivering Colistin on an anionic gold nanoparticle, the minimum inhibitory concentration of *E. coli* was reduced 6 fold compared to antibiotic alone. The addition of Colistin coated gold nanoparticles (both positive and negatively charged) significantly reduced the growth of *E. coli* in nutrient broth over a 24 h period, with 10,000 times lower CFU per mL at 8 h compared to the control. It has also been shown that both anionic and cationic 5 nm diameter gold nanoparticles are not inherently antibacterial and do not affect bacterial growth. The anionic Colistin coated gold nanoparticles therefore show great promise for delivery of Colistin at a lower dosage with improved efficacy.

1.0 Introduction:

The prevalence of antibiotic resistance is quickly becoming one of the world's greatest health challenges with predictions of over 10 million deaths worldwide by 2050.¹ Due to the global over-prescription and misuse of antibiotics, bacteria are increasingly developing resistance to common antibiotics.² When bacteria become resistant to multiple antibiotics, they are labelled as multi- drug resistant and infections from these bacteria are difficult and expensive to treat. Currently, these resistant bacterial infections are treated with last-line antibiotics. These antibiotics are less commonly prescribed and often have higher toxicities or side

effects. One of these last-line drugs is Polymyxin E, better known as Colistin Sulfate. Colistin's clinical use began in the 1950s; however, its use was phased out in the 1970s due to its nephrotoxic and neurotoxic side effects.^{3,4} A growing increase in the number of Gram-negative pathogens that are resistant to all common antibacterial drugs has led to the reconsideration of Colistin, which, due to a lack of clinical use, is for the most part still effective at killing bacteria compared to other more common antibiotics.^{5,6} Colistin interacts with the outer membrane of Gram-negative bacteria, primarily displacing calcium and magnesium ions. This increases the permeability of the membrane and therefore decreases its stability significantly, leading to the leakage of cell contents and eventual cell death.^{3,4,7}

As the side effects of Colistin are dose-dependent, it would be beneficial for the patient if a lower dose could be administered whilst still providing the same therapeutic effect.⁸ It has previously been shown, that the addition of antibiotics with metal nanoparticles can lower the susceptibility of bacteria and improve the efficacy of the antibiotic.^{9,10} Therefore it is hypothesised that Colistin can be attached onto gold nanoparticles (AuNPs) and these particles can provide the same antibacterial effects at a lower Colistin dosage. Thus, this work focuses on developing a stable Colistin coated gold nanoparticle system to lower the dosage of Colistin required to inhibit bacterial growth.

Due to the low cytotoxicity, ease of functionalisation and high surface to volume ratio, AuNPs have been successfully used as drug delivery vehicles.¹¹⁻¹⁵ Drug-conjugated AuNPs have been investigated widely^{16,17}, however antibiotic conjugation has been explored only recently. Amoxicillin coated and Kanamycin conjugated gold nanoparticles have both shown an increase in antibacterial activity compared to the antibiotic alone, suggesting the conjugation to gold nanoparticles plays a role in the mechanism of action.^{9,10} Likewise two Carbapenem antibiotics (Imipenem and Meropenem) have been conjugated through thiol bonds to AuNPs and this attachment reduced bacterial resistance compared to the free drug whilst also improving the therapeutic activity.¹⁸

Here, a simple electrostatic self-assembly has been utilised to attach Colistin onto citrate capped gold nanoparticles. Colistin is a cationic antibiotic, which can attach by electrostatic attraction to the negatively charged citrate capped AuNPs. With Colistin being administered in its sulfate salt form, it has the potential to destabilise the AuNP causing aggregation. Therefore, Colistin coated citrate capped gold nanoparticles (ColAu(-)) have been compared to polyelectrolyte and Colistin coated AuNPs. Due to its biocompatibility and the ability to increase stability of nanoparticle systems, Poly(diallyldimethylammonium chloride (PDADMAC) has been used as the polyelectrolyte coating.¹⁹ PDADMAC was mixed with Colistin to fabricate PDADMAC Colistin coated gold nanoparticles (ColAu(+)) (Fig. 23).

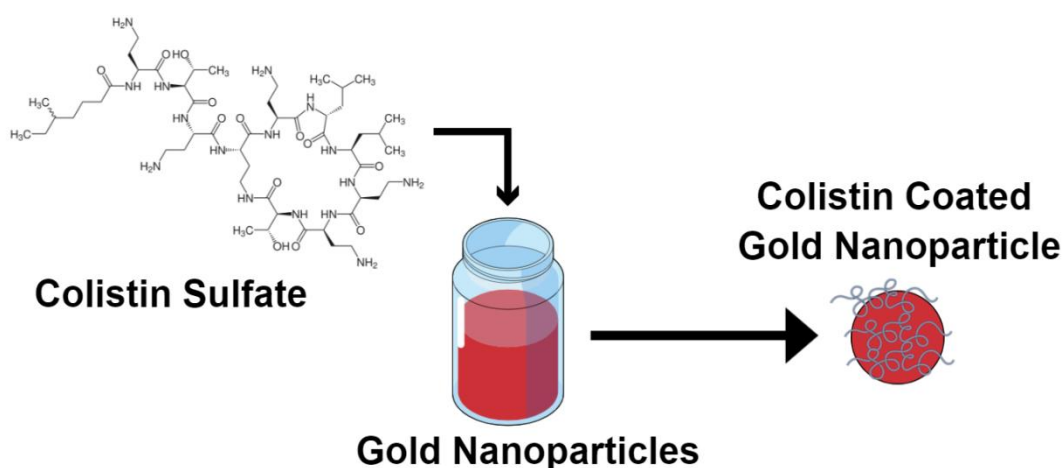


Figure 23: Schematic of the electrostatic attachment of Colistin onto the AuNP surface.

The resultant coated gold nanoparticles (both ColAu(+) and ColAu(-)) have been characterised by UV-Vis spectroscopy and zeta potential measurements. Microbiological studies including the minimum inhibitory concentration (MIC), cell growth and cell viability assays were conducted to analyse the difference of delivering Colistin with and without gold nanoparticles.

2.0 Materials and Methods:

2.1 Fabrication of Colistin and PDADMAC coated gold nanoparticles:

3 mL of 5 mg/mL PDADMAC (<100,000 Mw) (Sigma-Aldrich, Castle Hill, Australia) in 1 mM NaCl was mixed with 200 μ L of 20 mg/mL Colistin Sulfate Salt (Sigma-Aldrich, Castle Hill, Australia) and stirred for 1 h. 2 mL 5 nm diameter citrate capped gold nanoparticles (Nanocomposix, San Diego, USA) were added and mixed for a further hour. The sample was then centrifuged at 14500 rpm for 40 minutes and the supernatant was removed. 1 mL of ultrapure water was added and the sample sonicated for 10 minutes before being washed twice more.

2.2 Fabrication of Colistin coated gold nanoparticles:

200 μ L of 20 mg/mL Colistin Sulfate Salt (Sigma-Aldrich, Castle Hill, Australia) was added dropwise to 2 mL of 5 nm citrate capped gold nanoparticles (Nanocomposix, San Diego, USA) and the AuNP/Colistin mixture was mixed for 1 h. The solution was centrifuged at 14500 rpm for 40 minutes and the supernatant was removed. 1 mL of ultrapure water was added and the solution was sonicated for 10 minutes before being washed twice more.

2.3 Characterisation of Col-PDADMAC-AuNP and Col-AuNP:

The size and charge of the coated gold nanoparticles was determined by UV-Vis spectroscopy (Cary-50 Spectrophotometer, Australia) and Zeta potential measurements (Malvern Zetasizer Nano). The concentration of the Colistin present on the nanoparticles was determined by UV-Vis spectroscopy at a wavelength of 219 nm.

2.4 Minimum inhibitory concentration:

Minimum inhibitory concentrations were determined using 96 well microplate assay. The bacterial inoculum was prepared by incubating a single colony of *Escherichia coli* American Type Culture Collection (ATCC) 700891 in nutrient broth (Sigma Aldrich, Australia) at 37°C for 6 h with constant shaking. The cells were then centrifuged, washed and resuspended in sterile ultrapure water. The

concentration was adjusted by diluting in sterile ultrapure water to an OD600 to 0.1 au. This equated to a *E. coli* concentration 10^3 CFU/mL, which was confirmed by serially diluting and drop plating 10 μ l onto nutrient agar. Total CFU were counted after being incubated at 37°C for 24 hr.

The 96 well microplate assay was prepared with 50 μ l of nutrient broth. 50 μ l of 50 μ l/mL Colistin was added to the first well and then a serial 1:10 dilution was made in each subsequent well. Similarly, 50 μ l of the ColAu(-) and ColAu(+) were used in subsequent rows in well 1 (Table S5). In each row, well 1 contained 50 μ l of Colistin or either ColAu(+) or ColAu(-), 50 μ l of nutrient broth and 50 μ l of bacteria at 10^3 CFU. Bacteria was not included in the negative controls. The 96 well microplates were incubated at 37°C, overnight with constant shaking. Growth was then assessed by measuring the turbidity at OD600 using the Nanodrop Spectrophotometer (Thermo Fisher Scientific, Australia) and also by drop plating 10 μ L onto nutrient agar plates (Sigma Aldrich, Australia) which were incubated overnight at 37°C. *E. coli* with no antibiotics was used as the positive control as well as the addition of AuNPs (both PDADMAC coated and citrate capped) to ensure they are not inherently antibacterial. Nutrient broth on its own was used as a negative control. All MICs were conducted in triplicate.

2.5 Effect on *E. coli* growth curve:

To determine the effect of ColAu(-) or ColAu(+) on the growth curve of *E. coli* 9 mL of nutrient broth, 1 mL ColAu(+) and ColAu(-) was added with a single colony of *E. coli* (ATCC 700891). The samples were incubated at 37°C with shaking. The growth of *E. coli* was measured every two hours by monitoring changes in turbidity (OD600) (Nanodrop Spectrophotometer, Thermo Fisher Scientific, Australia). *E. coli* in nutrient broth was used as a positive control while Colistin in nutrient broth with *E. coli* as well as nutrient broth alone were used as a negative controls. This was conducted in triplicate.

2.6 Effect on *E. coli* viability:

To investigate the effect of the ColAu(-) or ColAu(+) on *E. coli* viability, single colonies of *E. coli* (ATCC 700891) were incubated in 9 mL nutrient broth at 37°C with 1 mL of ColAu(-) or ColAu(+) for 8 h with constant shaking. This was conducted in triplicate with the following controls; nutrient broth with only *E. coli*, nutrient broth with no *E. coli*, nutrient broth with *E. coli* and a high concentration of Colistin (10 mg/mL) and nutrient broth with *E. coli* and citrate capped and PDADMAC coated AuNP. Growth was measured after 4 h and 8 h of incubation by serially diluting and drop plating 10 μ L onto nutrient agar plates (Sigma Aldrich, Australia). Agar plates were incubated overnight at 37°C and total colonies were counted. The comparison between *E. coli* concentration with the addition of ColAuNPs compared to the controls determined the effect Col coated NPs have on growth of *E. coli*.

3.0 Results and Discussion:

3.1 Confirming the attachment of Colistin:

As Colistin is cationic, the molecule will attach to the negatively charged citrate capped nanoparticles through electrostatic interactions. Similarly, when Colistin is mixed with PDADMAC, they interact mainly through electrostatic interactions, however other interactions might also be present. All samples showed similar amounts of Colistin loading on the surface of the nanoparticles after three wash cycles. The ColAu(-) sample had an average of 108 ± 18 μ g/mL while the ColAu(+) sample had 87.6 ± 17 μ g/mL of Colistin (Table 10).

The presence of Colistin on the surface of the nanoparticles can be observed through UV-Vis spectroscopy. The peak at 219 nm in a spectrum of Colistin coated AuNPs is indicative of Colistin Sulfate (Fig. S7). The concentration of Colistin was determined using a calibration curve (Fig. S8). After three wash cycles, any excess Colistin that is not attached to the nanoparticles, is removed in the wash steps.

The addition of Colistin at the nanoparticle surface was also confirmed through the changes in zeta potential. The citrate capped gold nanoparticles had a zeta potential of -9.6 ± 8.9 mV whereas both the ColAu(+) and ColAu(-) had positively charged zeta potentials (Table 10). The change in charge indicates the attachment of cationic ligands on the particle's surface.

3.2 Stability of the nanoparticles after attachment:

For a drug-delivery application, the stability of the functionalised nanoparticles is important. The ColAu(-) nanoparticle solution aggregated relatively quickly, while the ColAu(+) solutions showed a higher colloidal stability, in good agreement with previous results showing increased stability of PDADMAC-coated nanoparticles.¹⁹ The difference in stability is evident in both the zeta potential and the UV-Vis red shift. The ColAu(-) nanoparticles had a close to zero zeta potential and red-shifted an additional 25 nm compared to the ColAu(+) sample, suggesting the formation of larger aggregates (Table 10).

Table 10: Comparison of the amount of Colistin concentration, zeta potential and AuNP absorbance peak of ColAu(-) and ColAu(+).

	Zeta Potential (mV) (pH 5.9±0.1)	Colistin Concentration (µg/mL)	AuNP Peak (nm)
AuNP(-)	-9.6 ± 8.9	0	513
ColAu(-)	6.5 ± 3.7	108 ± 18	555
ColAu(+)	35 ± 15	87.6 ± 17	530
PDADMAC-AuNP(+)	35 ± 8.9	0	539

The antibacterial effect of the ColAu(+) and ColAu(-) nanoparticles were tested by incubating *E. coli* with the nanoparticles. The bacterial growth curve as well as minimum inhibitory concentrations were investigated.

3.3 Antimicrobial efficacy of ColAuNPs:

MICs were conducted to ascertain the effectiveness of the ColAuNPs against *E. coli*. The MIC decreased 6.8 fold between Colistin on its own and ColAu(-). There was however, no significant difference between the MIC of Colistin and ColAu(+).

Table 11: Minimum Inhibitory Concentration of Colistin, ColAu(+) and ColAu(-) against *E. coli* (ATCC 700891).

	MIC* ($\mu\text{g/mL}$)
Colistin	1.56 ± 0.26
ColAu(+)	1.18 ± 0.17
ColAu(-)	0.23 ± 0.03

*MIC is representative of the concentration of Colistin on the NPs.

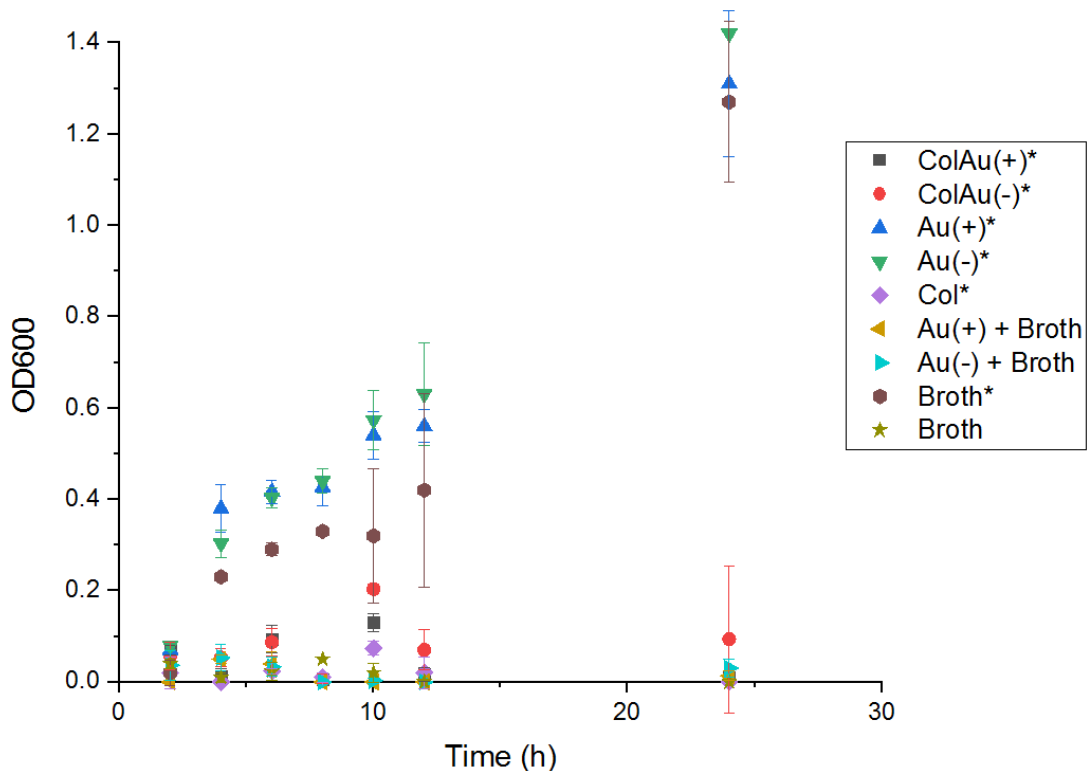


Figure 24: Effect of ColAu(+), ColAu(-) and Colistin on the growth curve of *E. coli* (ATCC 700891) in nutrient broth measured by changes in turbidity (OD600). *Indicates *E. coli* was present in the sample.

E. coli growth was monitored over a 24 h period using OD600 measurements. *E. coli* exposed to both ColAu(+) and ColAu(-) did not show any significant bacterial growth over the 24 h period, similar to the control sample that was exposed to a significantly higher concentration of Colistin as an additional negative control (Fig. 24). The addition of Au(+) and Au(-) without the drug did not affect the growth of the bacteria, thus showing no inherent antimicrobial properties.

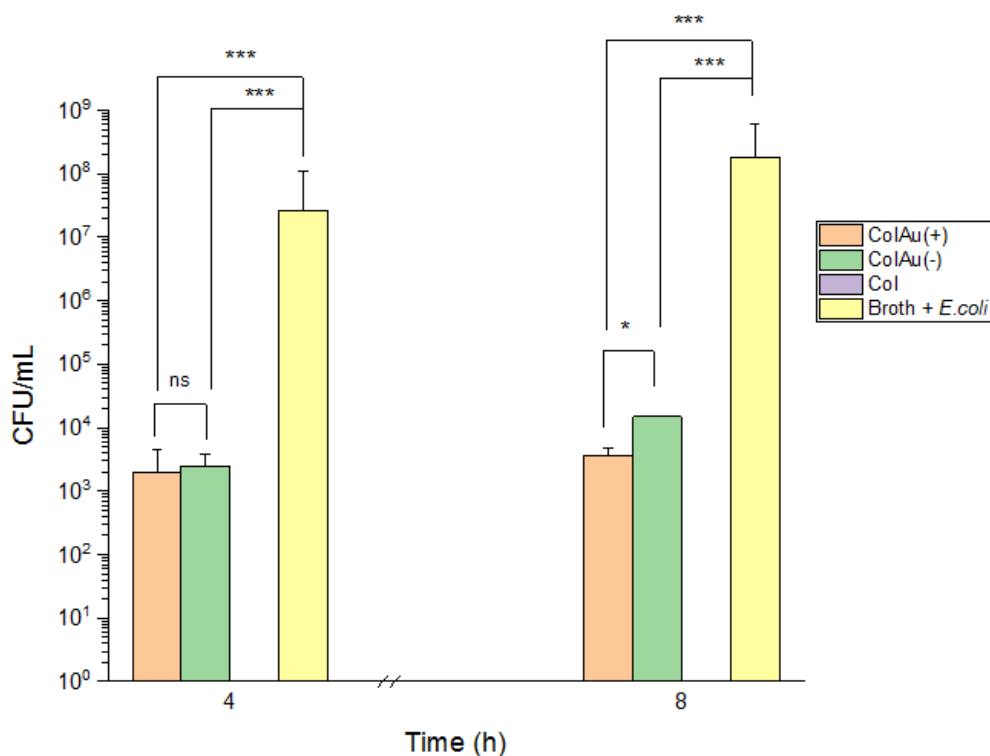


Figure 25: Concentration of *E. coli* (CFU/mL) after 4 and 8 hrs of growth (at 37°C) in nutrient broth containing ColAu(+), ColAu(-) and Colistin compared to the positive control (*E. coli* and nutrient broth). *P<0.05, ***P<0.0005, ns P>0.05 using one way ANOVA.

While the growth curve experiments demonstrated that ColAu(+) and ColAu(-) limited the growth of *E. coli*, the cell viability assay demonstrated that the *E. coli* was still viable. The difference in concentration of *E. coli* observed in the viability assay between the Colistin coated nanoparticles and the positive control was statistically significant; suggesting that a higher Colistin concentration on the surface of the nanoparticles might be needed for complete growth inhibition. The Colistin sample on its own which was used as a negative control, contained a much greater concentration of Colistin and no bacteria was detected on drop plates over the 8 h. Thus the ColAuNPs both were effective in significantly reducing the growth of *E. coli* compared to no treatment however it does suggest that increasing the amount of Colistin within the NP would be required to prevent all growth.

The delivery of Colistin via a less stable coating, lowered the MIC of *E. coli* compared to the more stable CoIAu(+) system. Thus it could be suggested that larger aggregates of Colistin coated AuNP, are more toxic to *E. coli* compared with smaller, stable particles. This behaviour has been observed in other antibiotic-gold nanoparticle systems, where Ampicillin, Streptomycin and Kanamycin conjugated AuNPs, which all showed evidence of aggregation, had lower MICs than the respective antibiotics alone.²⁰ Thus delivering Colistin as a coating on anionic gold nanoparticles is more effective at inhibiting bacterial growth compared to Colistin alone.

4.0 Conclusion:

This work has shown that Colistin can be easily used to coat gold nanoparticles for potential use in antibiotic delivery. The method uses a simple layer-by-layer attachment based primarily on electrostatic interactions between the negatively charged gold nanoparticles and the positively charged antibiotic, Colistin. The stability of the Colistin coated NP was improved when the cationic polymer, PDADMAC was used in the coating process. The concentration of Colistin on the surface was similar in both CoIAu(+) and CoIAu(-) samples and therefore the addition of PDADMAC does not considerably influence the drug-carrying load of the nanoparticles. Delivering Colistin via AuNPs showed a decrease in the MIC against *E. coli* with a 6.7 fold decrease observed for CoIAu(-) compared to Colistin on its own. Therefore, a smaller dosage could be given for the same bacterial effect. AuNP on their own were shown not to affect bacterial growth and therefore are not inherently antibacterial. In addition, CoIAu(+) and CoIAu(-) inhibited *E. coli* growth over an 8 h time period with a 10^4 CFU per mL reduction in total growth compared to *E. coli* without the presence of an antibiotic. Overall, Colistin can be delivered via anionic AuNP with improved efficacy than Colistin in its current form, which shows potential for developing a more efficient delivery method at a lower antibiotic dosage.

Acknowledgements:

M. F. acknowledges the support from the Australian Institute of Nuclear Science and Engineering (AINSE) for the PGRA top-up scholarship and the Australian Government for the Research Training Scholarship.

References:

1. Khurana, C.; Chudasama, B. Nanoantibiotics: strategic assets in the fight against drug-resistant superbugs, *International journal of nanomedicine* **2018**, *13*, 3-6.
2. Goossens, H., Ferech, Matus., Vander Stichele, Robert., Elseviers, Monique. Outpatient antibiotic use in Europe and association with resistance: a cross-national database study, *The Lancet* **2005**, *365*, 579-587.
3. Justo, J.A.; Bosso, J.A. Adverse reactions associated with systemic polymyxin therapy, *Pharmacotherapy* **2015**, *35*, 28-33.
4. Sans-Serramitjana, E.; Fusté, E.; Martínez-Garriga, B.; Merlos, A.; Pastor, M.; Pedraz, J.L.; Esquisabel, A.; Bachiller, D.; Vinuesa, T.; Viñas, M. Killing effect of nanoencapsulated colistin sulfate on *Pseudomonas aeruginosa* from cystic fibrosis patients, *Journal of Cystic Fibrosis* **2016**, *15*, 611-618.
5. Sahbudak Bal, Z.; Kamit Can, F.; Yazici, P.; Berna Anil, A.; Duyu, M.; Yilmaz Ciftdogan, D.; Nisel Yilmaz, O.; Cilli, F.; Karapinar, B. The evaluation of safety and efficacy of colistin use in pediatric intensive care unit: Results from two reference hospitals and review of literature, *Journal of infection and chemotherapy : official journal of the Japan Society of Chemotherapy* **2018**, *24*, 370-375.
6. Bialvaei, A.Z.; Samadi Kafil, H. Colistin, mechanisms and prevalence of resistance, *Current Medical Research and Opinion* **2015**, *31*, 707-721.
7. Andersson, J.; Fuller, M.A.; Wood, K.; Holt, S.A.; Köper, I. A tethered bilayer lipid membrane that mimics microbial membranes, *Physical Chemistry Chemical Physics* **2018**, *20*, 12958-12969.

8. Ordooei Javan, A.; Shokouhi, S.; Sahraei, Z. A review on colistin nephrotoxicity, *European Journal of Clinical Pharmacology* **2015**, *71*, 801-810.
9. Demurtas, M.; Perry, C.C. Facile one-pot synthesis of amoxicillin-coated gold nanoparticles and their antimicrobial activity, *Gold Bulletin* **2014**, *47*, 103-107.
10. Payne, J.N.; Waghvani, H.K.; Connor, M.G.; Hamilton, W.; Tockstein, S.; Moolani, H.; Chavda, F.; Badwaik, V.; Lawrenz, M.B.; Dakshinamurthy, R. Novel Synthesis of Kanamycin Conjugated Gold Nanoparticles with Potent Antibacterial Activity, *Frontiers in Microbiology* **2016**, *7*.
11. Reum, N.; Fink-Straube, C.; Klein, T.; Hartmann, R.W.; Lehr, C.-M.; Schneider, M. Multilayer Coating of Gold Nanoparticles with Drug-Polymer Coadsorbates, *Langmuir* **2010**, *26*, 16901-16908.
12. Labala, S.; Mandapalli, P.K.; Kurumaddali, A.; Venuganti, V.V.K. Layer-by-Layer Polymer Coated Gold Nanoparticles for Topical Delivery of Imatinib Mesylate To Treat Melanoma, *Molecular Pharmaceutics* **2015**, *12*, 878-888.
13. Song, S.; Hao, Y.; Yang, X.; Patra, P.; Chen, J. Using Gold Nanoparticles as Delivery Vehicles for Targeted Delivery of Chemotherapy Drug Fludarabine Phosphate to Treat Hematological Cancers, *Journal of nanoscience and nanotechnology* **2016**, *16*, 2582-2586.
14. Boisselier, E.; Astruc, D. Gold nanoparticles in nanomedicine: preparations, imaging, diagnostics, therapies and toxicity, *Chemical Society Reviews* **2009**, *38*, 1759-1782.
15. Cobley, C.M.; Chen, J.; Cho, E.C.; Wang, L.V.; Xia, Y. Gold nanostructures: a class of multifunctional materials for biomedical applications, *Chemical Society Reviews* **2011**, *40*, 44-56.
16. Kalimuthu, K.; Lubin, B.-C.; Bazylevich, A.; Gellerman, G.; Shpilberg, O.; Luboshits, G.; Firer, M.A. Gold nanoparticles stabilize peptide-drug-conjugates for sustained targeted drug delivery to cancer cells, *Journal of nanobiotechnology* **2018**, *16*, 34-34.

17. Kim, C.K.; Ghosh, P.; Pagliuca, C.; Zhu, Z.-J.; Menichetti, S.; Rotello, V.M. Entrapment of Hydrophobic Drugs in Nanoparticle Monolayers with Efficient Release into Cancer Cells, *Journal of the American Chemical Society* **2009**, *131*, 1360-1361.
18. Shaker, M.A.; Shaaban, M.I. Formulation of carbapenems loaded gold nanoparticles to combat multi-antibiotic bacterial resistance: In vitro antibacterial study, *International Journal of Pharmaceutics* **2017**, *525*, 71-84.
19. Fuller, M.; Köper, I. Polyelectrolyte-Coated Gold Nanoparticles: The Effect of Salt and Polyelectrolyte Concentration on Colloidal Stability, *Polymers (Basel)* **2018**, *10*, 1336.
20. Saha, B.; Bhattacharya, J.; Mukherjee, A.; Ghosh, A.; Santra, C.; Dasgupta, A.K.; Karmakar, P. In Vitro Structural and Functional Evaluation of Gold Nanoparticles Conjugated Antibiotics, *Nanoscale Research Letters* **2007**, *2*, 614.

CHAPTER 6: NANOPARTICLES IN AN ANTIBIOTIC-LOADED NANOMESH FOR DRUG DELIVERY

This chapter is published in RSC Advances and is entitled 'Nanoparticles in an Antibiotic-Loaded Nanomesh for Drug Delivery'. It is authored by **Melanie Fuller**, Ashley Carey, Harriet Whiley, Rio Kurimoto, Mitsuhiro Ebara and Ingo Köper. It is a research article which explores the use of electrospun polymer nanomesh for use in antibiotic drug delivery. This chapter uses knowledge gained through Chapters 2, 3 and 4 to develop a proof-of-concept bandage that is able to release antibiotics over an extended 14-day timeframe at a dosage sufficient to kill *E. coli*. The cationic gold nanoparticles fabricated in Chapter 3 as well as anionic citrate capped gold nanoparticles were added to the mesh during fabrication as it was expected they would increase bacterial susceptibility, as observed in Chapter 4.

The research presented in this chapter has brought all the aspects of the thesis together, to provide a delivery mechanism for Colistin that incorporates gold nanoparticles (Fig. 26). Although this is only preliminary work, it suggests that the addition of the gold nanoparticles plays a significant role in the release of antibiotic from the mesh.

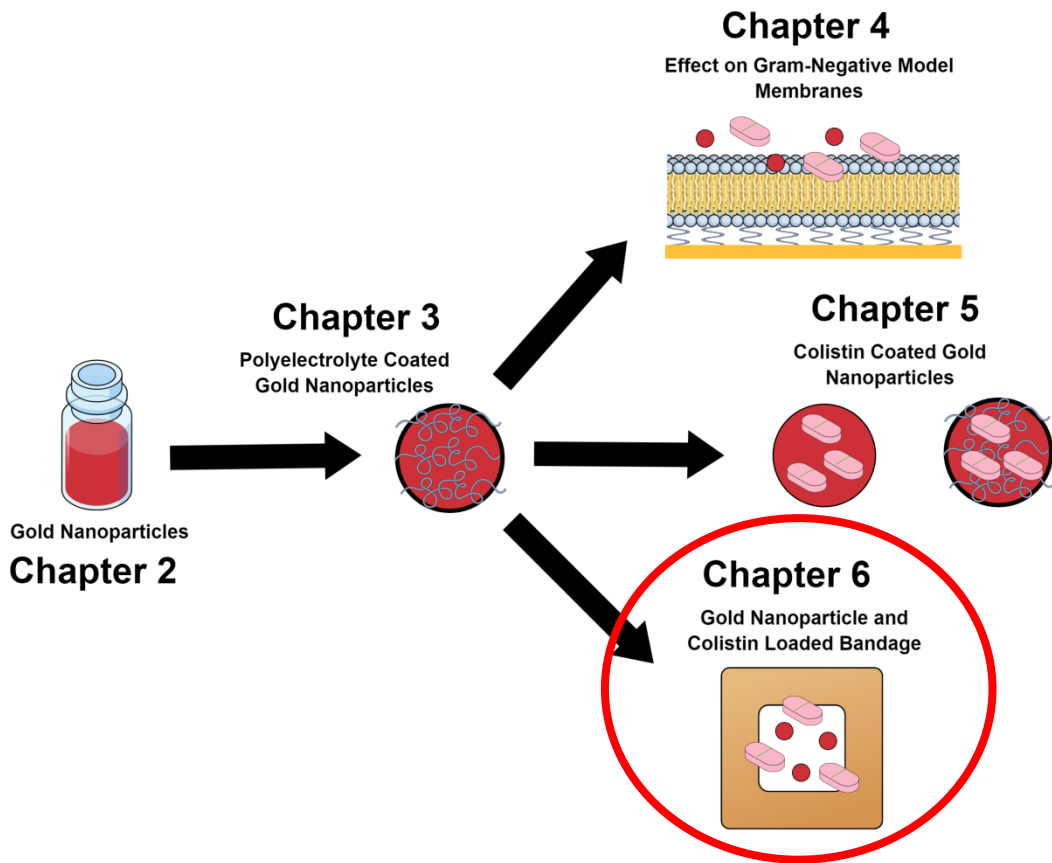


Figure 26: Diagram of the overall thesis, indicating Chapter 6 and how it fits into the larger body of work.

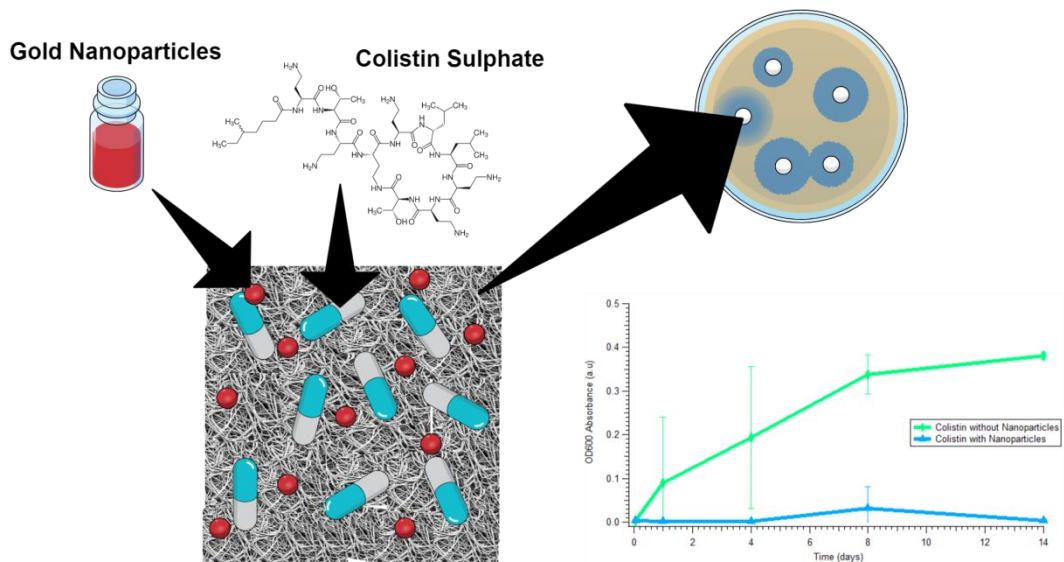


Figure 27: Graphical abstract from the publication 'Nanoparticles in an Antibiotic-Loaded Nanomesh for Drug Delivery'.

Abstract:

Antibiotic loaded nanomeshes were fabricated by electrospinning polycaprolactone, a biocompatible polymer, with 12.5% w/w Colistin, 1.4% w/w Vancomycin and either cationic or anionic gold nanoparticles in varying combinations. The resulting nanomeshes had different antibiotic release profiles, with citrate capped gold nanoparticles combined with Colistin having the highest sustained release over 14 days for a 4 mg, 1.5 cm² nanomesh. The electrospinning parameters were optimised to ensure the spinning of a homogenous mesh and the addition of antibiotics were confirmed through ¹H NMR and ATR-FTIR. This research, as a proof of concept, suggests an opportunity for fabricating nanomesh which contain gold nanoparticles as a drug release mechanism for antibiotics.

1.0 Introduction:

With the over-prescription of antibiotics worldwide, bacterial resistance is becoming a significant threat to public health.¹ When bacteria are resistant to three or more types of antibiotic classes, they are labelled as multi-drug resistant and there is a limited number of antibiotics available to be used in a final attempt to treat the infection.^{2,3} Two examples of these last-line drugs are the polypeptide antibiotics, Colistin and Vancomycin.⁴ Colistin, which has previously been limited in its use due to the incidence of adverse effects including nephrotoxicity and neurotoxicity, is resurfacing more frequently for treatment.^{5,6} It is often used to treat multi-resistant Gram-negative bacteria, where other antibiotics are no longer effective. Colistin's mechanism relies on the electrostatic interaction between the negatively charged phosphate groups of the Lipopolysaccharide (LPS) bacterial outer cell membrane and the positively charged amino groups of Colistin.^{7,8} When the positively charged Colistin comes into contact with the bacterial cell membrane, it causes defects in the membrane, leading to leakage of the cell contents and ultimately cell death.⁹ It also binds and neutralizes the Lipid A portion of the LPS, which is the endotoxin of Gram-negative bacteria.⁸ Often, multiple antibiotics are used in combination to treat resistant bacteria, and Vancomycin is one of the more popular choices to treat Gram-positive Methicillin-

Resistant *Staphylococcus Aureus* (MRSA) infections.^{10,11} Vancomycin's antibacterial action is different from that of Colistin, where it inhibits the cell wall synthesis of susceptible organisms.¹² It does this by inhibiting the peptidoglycan synthesis in late stage bacterial cell wall formation.¹³

Delivering the antibiotics directly to the infection site rather than via an oral dosage is beneficial as the oral ingested dosage is distributed not only at the infection site but also non-specifically around the body. The non-specificity means a high dosage needs to be given to ensure the concentration at the site of infection is significant enough to effectively treat it. The dosage can be lowered if delivered to the infection site directly, which can reduce side effects and complications. Although the dosage is 'reduced' compared to the oral dosage, the concentration of antibiotics delivered to the infection site can still be higher, ensuring the bacteria cannot survive and cause resistance.

In order to deliver the antibiotics to a specific site, the antibiotics need to be mobilised on a scaffold, and in this case they have been embedded into a fibrous mesh produced using a technique called electrospinning. Electrospinning has gained considerable interest in the biomedical community as it offers promise in many applications¹⁴ including wound management¹⁵, drug delivery¹⁶ and antibiotic coatings.¹⁷ Other emerging applications for electrospun meshes include air filtration¹⁸⁻²² and oil-water emulsion separation.^{23,24} In electrospinning, a syringe is loaded with a polymer that has been dissolved in a volatile solvent. A high voltage is then applied between the needle connected to the syringe, and the collector plate (Fig. 28). The voltage causes the polymer solution to form a Taylor cone as it leaves the syringe, at which point the electrostatic forces induce a jet of liquid, as it overcomes the surface tension.^{25,26}

Electrospinning can produce controlled micro or nano-sized fibres that are deposited onto a substrate. The properties of the fibres can be adjusted by varying parameters such as the viscosity of the polymer solution, choice of solvent, the voltage supplied, needle gauge as well as the needle to collector plate distance.^{27,28}

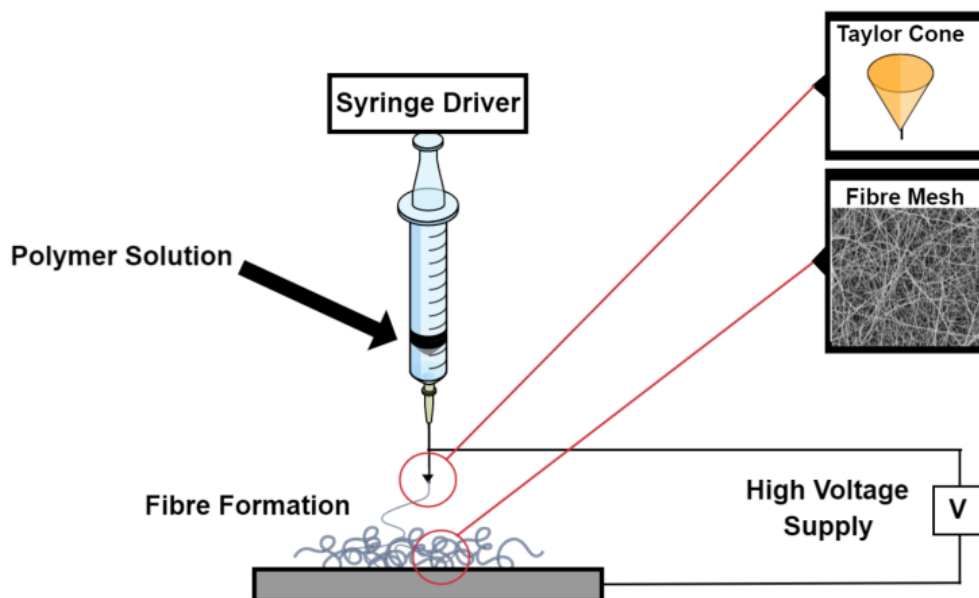


Figure 28: Schematic of the electrospinning instrument showing the Taylor cone and mesh formation.

The production process allows for various additives to be included into the fibres, as long as they can be mixed with the original polymer solution. Here, two antibiotics, Colistin (Col) and Vancomycin (Van) were added. Additionally, 5 nm diameter gold nanoparticles with either a negatively charged citrate capping Au(-) or a positively charged Polydiallyldimethylammonium chloride (PDADMAC) coating Au(+), were added to determine if small, charged particles within the polymer matrix affect the antibiotic release.

Gold nanoparticles were chosen in addition to the antibiotics as positively charged nanoparticles have shown in literature to cause damage to the bacterial membranes.^{29,30} In a recent study, a strong correlation was found between poor bacterial viability and the attachment of positively charged gold nanoparticles on Gram-negative bacteria.³¹ Thus both anionic and cationic gold nanoparticles were included in the mesh to determine if they have any effect when paired with antibiotics within the nanomesh.

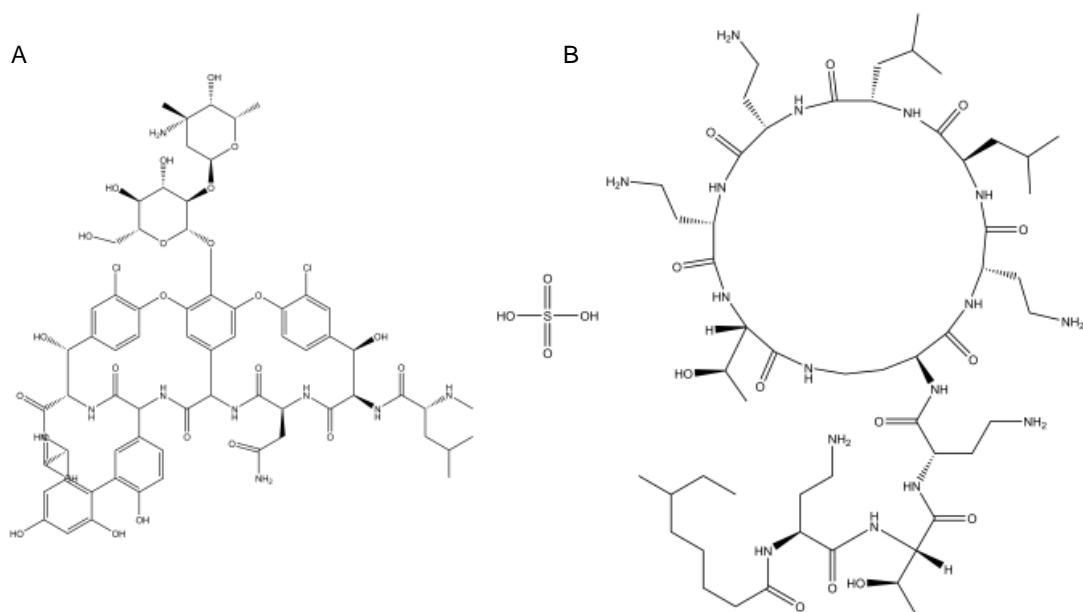


Figure 29: The chemical structure of (A) Vancomycin and (B) Colistin.

2.0 Materials and Methods:

2.1 Mesh Formation:

4, 7, 8, 9 and 10% w/w ϵ -polycaprolactone (PCL) solutions were prepared by dissolving PCL (Average Mn 80,000) (Sigma Aldrich, Kaohsiung, Taiwan) in 1,1,1,3,3,3-hexafluoroisopropanol (HFIP) (Sigma Aldrich, Kaohsiung, Taiwan) and left overnight at $\sim 40^{\circ}\text{C}$. The PCL/HFIP solution was then loaded into a 5 mL syringe with a 22-gauge needle and electrospun with an applied voltage of 20 kV (Nanon-01A, MECC Co. Ltd, Fukuoka, Japan), with a 20 cm working distance and 20 cm horizontal needle movement for 3 h at flow rates of 0.5 mL/h and 1 mL/h. The fibres were spun directly onto aluminium foil on a stationary collector plate. The fibre mesh was removed from the aluminium foil prior to further investigation. After spinning was completed, the mesh was dried in a vacuum to remove any excess HFIP and stored at -20°C until its use.

2.2 Mesh imaging:

A 0.5 cm² piece of nanomesh was sputter coated with a thin layer of gold before being imaged via SEM (NEO-Scope JCM-5000 table top SEM, JEOL, Japan) at an accelerating voltage of 10 kV. The software ImageJ was used to analyse the diameter of the fibres, where the mean diameter of a minimum 50 fibres was used to determine fibre thickness.

2.3 Antibiotic Addition to Nanomesh:

60 mg of Colistin Sulfate Salt ($\geq 15,000$ U/mg) (Sigma Aldrich, Castle Hill, Australia) was dissolved in 1 mL HFIP (for a total 12.5 w/w loading of Colistin) before being vortexed with 7% w/w PCL just prior to electrospinning. All meshes were electrospun with the same spinning parameters as described in the PCL mesh formation, except for the flow rate which was kept constant at 1 mL/h. For the addition of Vancomycin, 100 μ l of 50 mg/mL Vancomycin Hydrochloride in DMSO (Sigma Aldrich, Tokyo, Japan) was mixed with 0.5 mL HFIP and then vortexed before being added to 7% w/w PCL in HFIP for a total w/w Vancomycin loading of 1.4%. In the case of the meshes containing both antibiotics, the antibiotics were prepared as above and mixed together prior to being added to the PCL solution. For the addition of the negatively charged gold nanoparticles, 500 μ l of 5 nm diameter citrate capped gold nanoparticles (10^{13} particles/mL) (Nanocomposix, San Diego, USA) were added to the drug solution prior to addition to the PCL solution. For the addition of positively charged gold nanoparticles, 5 nm diameter PDADMAC coated gold nanoparticles were fabricated using a previously published method.³² 500 μ l of the fabricated nanoparticles (10^{13} particles/mL) were then added as per the citrate capped gold nanoparticle method.

2.4 Characterisation of antibiotic addition into the mesh:

A 1 cm² piece of mesh was cut and placed on the crystal of an Attenuated Total Reflection Fourier Transform Infra-Red (ATR-FTIR) spectrophotometer (FTIR-8400S; Shimadzu Co., Ltd, Kyoto, Japan) and was used to confirm Vancomycin

was present in the mesh. To confirm the addition of Colistin, experiments were performed using ^1H NMR (Bruker 600 MHz Avance III, Australia) where 10 mg of mesh was dissolved in a mix of 95% DMSO- d_6 and 5% D_2O . A 5 mm BBFO probe was used and excitation sculpting was conducted to remove the D_2O peak. The parameters used for the ^1H NMR experiments were an acquisition time of 1.36 s, a relaxation delay of 1 s and line broadening of 0.3.

2.5 *In vitro* antibiotic release:

Drug release studies were conducted by cutting 1.5 cm^2 pieces of mesh, weighing them and placing them in vials with 2 mL Dulbecco's Phosphate Buffered Saline (D-PBS) (Sigma Aldrich, Tokyo, Japan). The mesh pieces were then placed in a water bath with shaking at 37° C to mimic physiological conditions. At different time points the 2 mL DPBS was removed and replaced under sink conditions. After being removed, the aliquot was immediately frozen and stored at -20°C until ready to be measured, to prevent loss of antibiotic action. Removal of the aliquot at the various time points was completed in triplicate for all meshes measured. The concentration of the two antibiotics were determined by UV-Vis spectroscopy (JASCO V-650 Spectrophotometer, Japan) at a wavelength of 214 nm for Colistin and 280 nm for Vancomycin using a Quartz cuvette. The data was normalised to 4 mg mesh weights for consistency. The cumulative percentage release was calculated using equation 1.³¹

$$\text{Cumulative release (\%)} = \frac{M_t}{M_\infty} \times 100 \quad (1)$$

Where M_t is the amount of antibiotic released at time t and M_∞ is the initial loading amount of antibiotic into the nanomesh.

2.6 Broth Dilution Assay:

1 mL of DH5 α Escherichia coli (*E. coli*) bacteria (Invitrogen, Japan) was added to 1 mL of Lysogeny broth (LB) medium (Sigma Aldrich, Japan) and incubated for 18 h at 37°C. After 18 h, 1 mL of the bacteria was added to each of the 2 mL aliquots taken from the in-vitro drug release study and then incubated at 37°C for 24 h. Turbidity was used as an indicator of cell growth in the presence of

antibiotics released from *in vitro* studies. The absorbance was measured using UV-Vis Spectroscopy (JASCO V-650 spectrophotometer, Japan) at 600 nm optical density. Experiments were conducted in triplicate and the average absorbance was determined. Vancomycin mesh release was used as a positive control.

2.7 Zone of Inhibition (ZOI) Assay:

E. coli American Type Culture Collection (ATCC) 700891 bacterial lawns were grown on nutrient agar plates (Sigma-Aldrich, Australia) for 24 h at 37°C. 8 mm diameter disks were cut from various meshes and placed under UV-light to sterilise for 20 minutes. The disks were then transferred onto the agar plates and incubated for 48 h at 37°C. After 48 h, the diameter of the zone of inhibition was recorded. Each mesh type was tested in triplicate. PCL with no antibiotics was used as a negative control and the Vancomycin only mesh was used as a positive control.

3.0 Results and Discussion:

3.1 Optimisation of Parameters for Mesh Formation:

Meshes were produced with various flow rates and % w/w of PCL, while the working distance, voltage, deposition time and needle size were kept constant. An ideal mesh for drug release would have homogenous fibres with no visible defects.³³ In order to develop an ideal mesh, the concentrations of PCL as well as the flow rates were altered and the meshes were then imaged to determine their homogeneity and fibre thickness (Fig. 30). 4% w/w PCL led to significant beading defects regardless of the flow rate. Beading leads to inhomogeneous fibres and can result from two different processes. The low viscosity of the solution can cause the solution to fall through the syringe too quickly, leading to a droplet. If the droplet falls, a new Taylor cone needs to be formed which leads to distinct and separated beads. The second reason for beading being observed is when the polymer solution is too viscous, as the solution will take too long to fall through the syringe which causes breaks in the electrospinning.³⁴ Again, a new

Taylor cone will need to be formed causing beading defects. The 1 mL/h was observed to have a greater number of defects and this may be due to the faster flow rate, where the low viscosity means the polymer solution is falling through as well as being pushed faster than the 0.5 mL/h. To remove the beading, a higher polymer weight was used.

Polymer percentages of 7, 8, 9 and 10% w/w resulted in meshes with various fibre diameters. For 7% w/w PCL, the fibres had a diameter of 246 ± 76 nm with homogenous fibre diameters and no apparent beading defects. The 8% and 9% w/w PCL had no observable difference between the flow rates, however minor defects and various fibre diameters can be observed. These defects are different from the beading in the 4% w/w PCL as they are elongated within the fibre, causing differences in thicknesses along the length of the fibre. This is likely due to the viscosity being too high, leading to elongated beading within the fibre itself. Finally, the 10% w/w PCL mesh showed a variety of fibre diameters, which is not ideal in a drug delivery application (Table S6). Thus for the electrospinning conditions used, the optimal polymeric solution concentration was determined to be 7% w/w as it produced the thinnest, most homogenous fibres compared to the other percentages tested. 7% w/w PCL was used in the formation of all the meshes to assess the addition of antibiotics and nanoparticles for drug delivery.

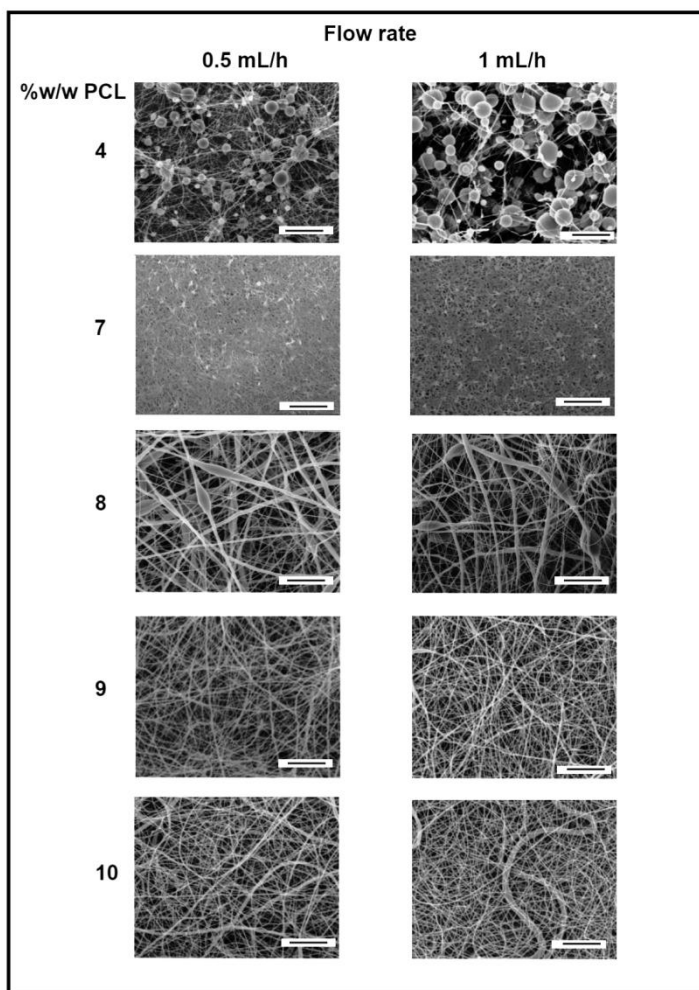


Figure 30: SEM images of different %w/w of PCL in HFIP showing the changes in morphology at a flow rate of 0.5 mL/hr and 1 mL/hr. All scale bars are 10 μm .

3.2 Addition of Antibiotics into the Nanomesh:

Confirmation of the addition of Colistin and Vancomycin was achieved through a series of characterisation techniques. For NMR, peaks corresponding to the introduction of Colistin occurred at approximately 4.5, 2.9 and 1.85 ppm and were not observed in the PCL sample (Fig. 31).

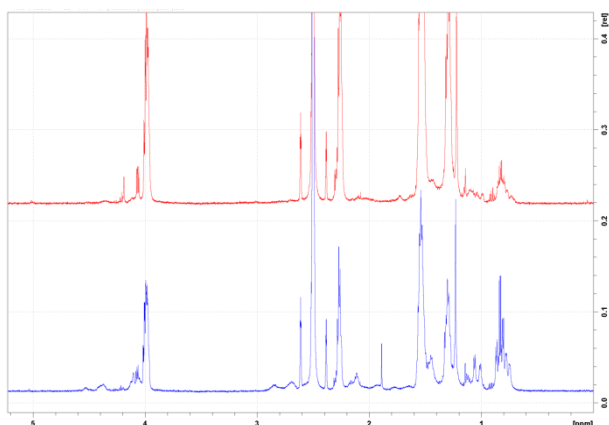


Figure 31: (Top) ^1H NMR of 10 mg PCL in 95% DMSO, 5% D_2O . (Bottom) ^1H NMR of 10 mg PCL with Colistin in 95% DMSO, 5% D_2O .

ATR-FTIR confirmed the addition of Vancomycin into the nanomesh. The chemical structures of both antibiotics (Fig. 29) have many of the same functional groups, with the exception of an ether. The FTIR spectrum showed a characteristic ether peak at $\sim 1030\text{ cm}^{-1}$ which was only present in the sample containing Vancomycin. (Fig. 32) Similarly, both antibiotics contain an amine group within their structure whereas PCL does not. The signal at $\sim 3300\text{ cm}^{-1}$ corresponding to the amine group further indicates the presence of both Colistin and Vancomycin in the mesh.

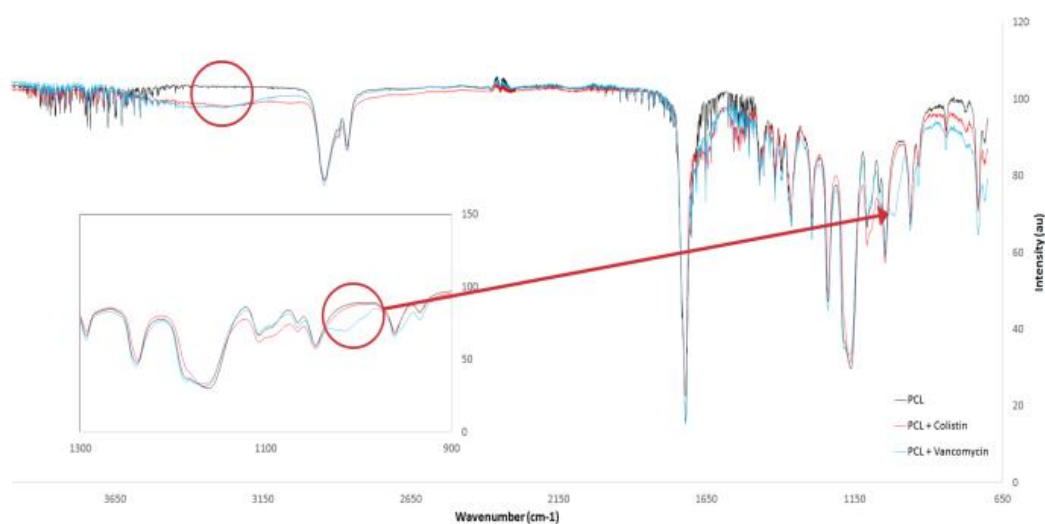


Figure 32: ATR-FTIR of PCL, PCL + Colistin and PCL + Vancomycin nanomesh confirming the addition of the antibiotics with an ether peak for Vancomycin at $\sim 1030\text{ cm}^{-1}$ (see inset) and amine groups at 3300 cm^{-1} for both antibiotics.

3.3 Zone of Inhibition Assay:

Zone of inhibition assays were used to test the antibiotic activity of Colistin released from the mesh (Fig. 33). *E. coli* lawns were grown on nutrient agar and small circular pieces of mesh were cut out and placed on the bacterial lawns. As *E. coli* is Gram negative, only Colistin meshes were tested as *E. coli* is not susceptible to Vancomycin. All meshes containing Colistin produced a ZOI with varying diameters. The control meshes of PCL and PCL with both cationic and anionic nanoparticles showed no inhibition of the bacteria. The ZOI assay was used as a qualitative method only to test for antibiotic action as Colistin is known to diffuse slowly and poorly through agar and often leads to unreliable and inaccurate diameters.³⁵

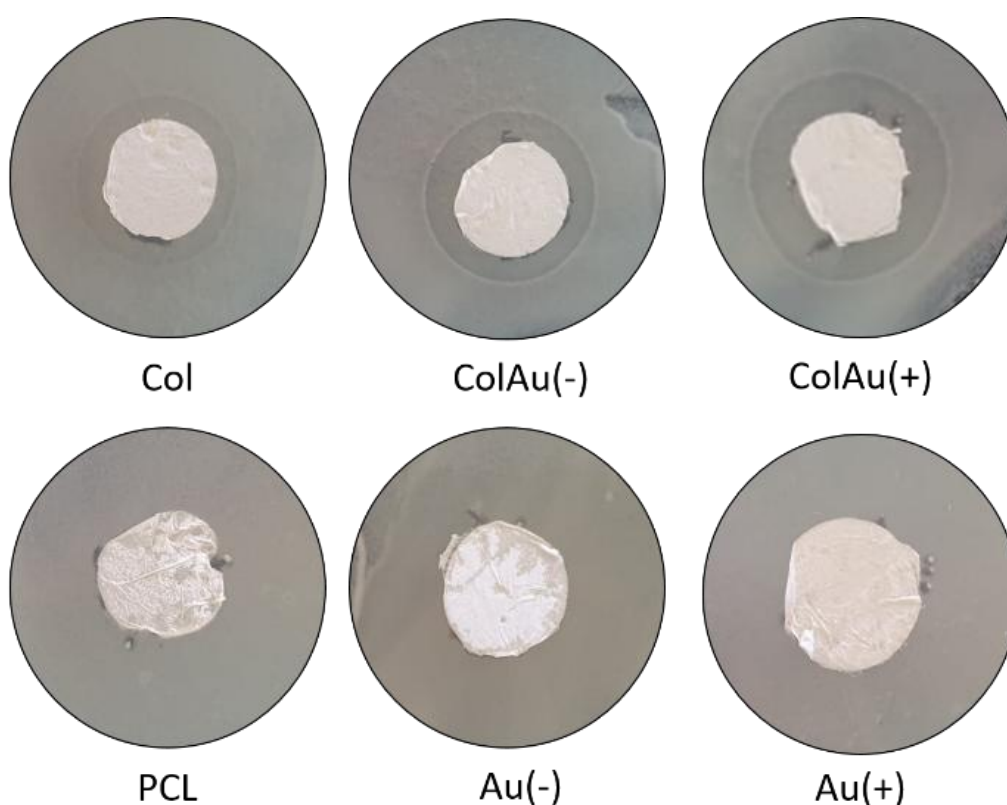


Figure 33: Zone of Inhibition assays after 48 h for meshes tested on *E. coli* lawns with 8 mm mesh disks.

3.4 Drug Release Studies:

With confirmation of antibiotic loading through FTIR and ^1H NMR, a drug release study was conducted to determine the amount of antibiotic being released from the mesh over time (Fig. 34). Drug concentrations were determined by UV/Vis spectroscopy.

The drug release behaviour for 7% w/w PCL with varying antibiotic and gold nanoparticle combinations was monitored to determine the most efficient drug release profile. All samples exhibited a burst release in the first few hours before reaching a plateau around day 5. This burst release is due to diffusion, where the drug diffuses out from the mesh within the first few hours of being submerged in DPBS.^{36,37}

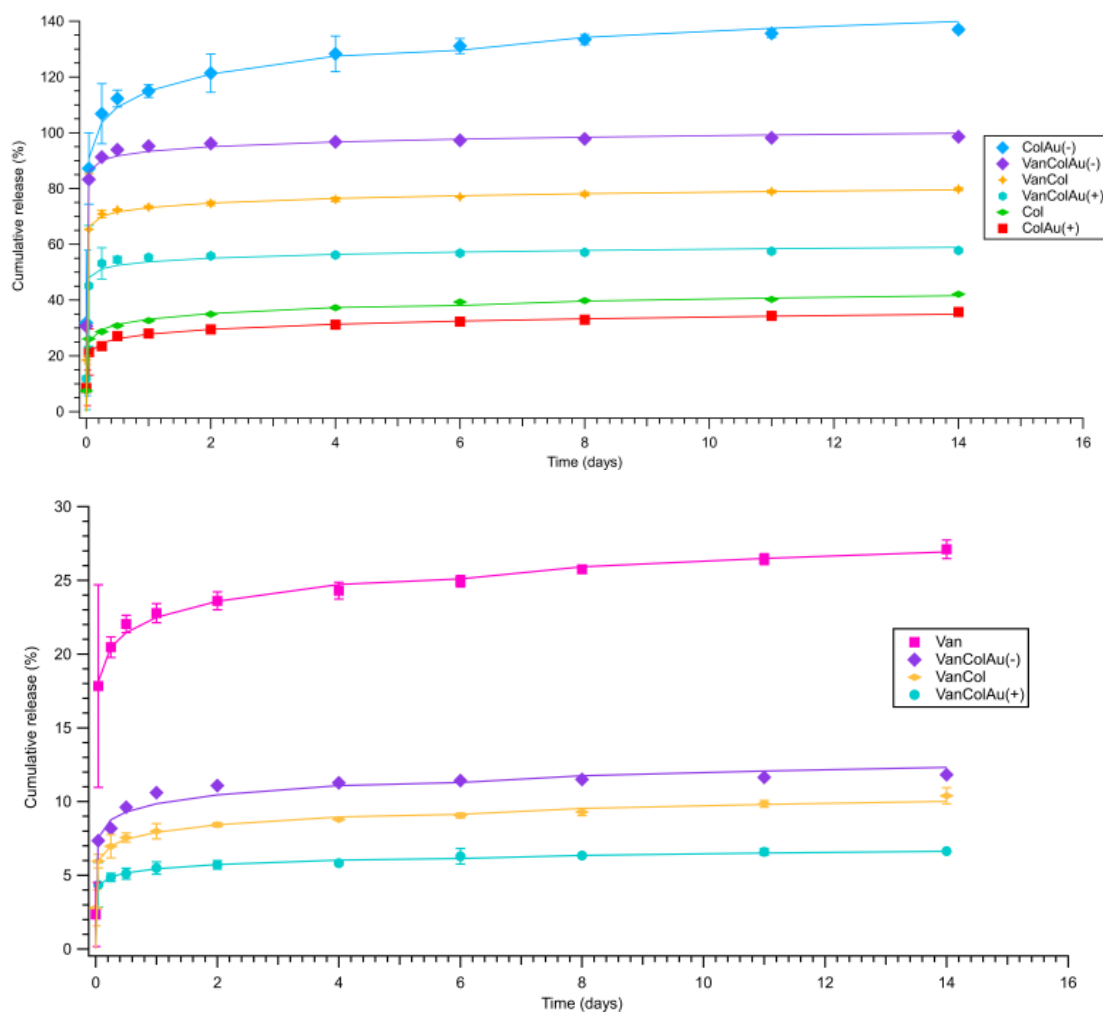


Figure 34: Top: Colistin cumulative release, Bottom: Vancomycin cumulative release. Both show Korsmeyer-Peppas fitting models.

The total amount of drug released varied significantly between different drug combinations. As all the mesh combinations had the same amount of Colistin added during the formation of the mesh, the differences observed are most likely due to different release mechanisms. It is noted the cumulative percentage is above 100% however this is due to the theoretical maximum amount of Colistin being calculated for the total weight of the mesh and then divided by the average 1.5 cm² piece of mesh weight.

The ColAu(-) sample had the greatest release of Colistin compared to the other combinations (Fig. 34). The addition of positively charged gold nanoparticles saw a similar release to the Colistin mesh alone. This suggests that nanoparticles of the opposite charge to the drug can increase the release from the fibres. This altered release has been previously documented for changes in fibre texture, the pH differences of core and shell fibres and fibre shell thickness however to the author's knowledge, changes to release rates due to charged nanoparticles within the mesh has not been previously observed.^{38,39} However, it has been shown that in core-shell electrospinning, positively charged drugs are found to migrate to the surface of the fibres compared to neutral drugs which remain in the core.⁴⁰ This is due to the charge generation of the surface of the polymer during electrospinning. The positively charged drugs are repelled from the inner needle surface and are drawn toward the grounded collector plate.⁴¹ Although in this case there is no core-shell, the negatively charged nanoparticles are likely interacting with the Colistin, in effect neutralising its cationic charge and encapsulating it further into the fibre. Whereas for the meshes with positively charged nanoparticles the particles and drug repel each other with minimal interaction, allowing the highly cationic Colistin (+5 net charge) to migrate to the fibre surface.⁴² Thus, the addition of anions when using a cationic drug should increase the release time of the drug from fibres.

For the Vancomycin release, when on its own, Vancomycin releases approximately 25% of the initial loading which is relatively low compared to the release of Colistin. This is due to the differences in their solubility in the electrospinning solvent HFIP. However, in comparison to the other combinations of the Vancomycin meshes, the Vancomycin only mesh release is high, with the

VanCol, VanColAu(+) and VanColAu(-) only releasing between 6-12%. The addition of the positively charged nanoparticles to the Vancomycin mesh had no significant effect, which mirrored what was observed in the Colistin mesh. The addition of the negatively charged nanoparticles also had no significant effect which is expected as Vancomycin is amphoteric with only a slight positive charge when dissolved within HFIP.⁴³ This further supports the idea that the charge of a drug and the addition of charged particles within a nanomesh system affects the drug positioning within a fibre, which ultimately determines the release profile.

To analyse the release kinetics, all meshes containing Colistin were fitted to zero-order, first-order, Higuchi, Hixson-Crowell and Korsmeyer-Peppas models (Table S7). The fitting was evaluated by the correlation coefficient (R^2). These models were chosen as they model different release mechanisms including diffusion and erosion.

The kinetics did not correlate with zero order, which compares the cumulative amount of drug released versus time. The plots shows a curvilinear profile for all meshes and the regression values were low indicating the release is not zero-order. The first order model, which compares the log of cumulative percentage of drug remaining versus time had a similar profile to zero order, where the data shows to be curvilinear. Again, the regression value was smaller than other models for all meshes tested.

The Korsmeyer-Peppas model (log cumulative percentage of drug released compared to log time) had the best fit for the release of Colistin for all the meshes, characterised by the highest R^2 values (Table S7). The analysis of the Korsmeyer-peppas model provides insight into the mechanisms of drug release, being both erosion and diffusion based.⁴⁴ This is determined by the values of the drug release exponent, n , which in this case is the slope of the Korsmeyer-Peppas model plot (Table S7). When n is equal to or less than 0.45, it is an indication that the release mechanism is Fickian diffusion.⁴⁵ Fickian diffusion occurs when the polymer's relative relaxation time is considerably shorter than the diffusion time of water transport, which is controlled by the concentration gradient. If the n value is between 0.45 and 0.89 it indicates non-Fickian diffusion also known as analogous transport.⁴⁶ This type of transport has both erosion and

diffusion as part of the release mechanism. When n is equal to or greater than 0.89 it indicates Class II Transport where the mechanism is erosion based.⁴⁷ In all meshes, n is less than 0.45 for Colistin release which is an indication of Fickian diffusion.

In order to examine how the release would affect bacteria over a 14 day time period, an *in vitro* bacterial study was conducted where *E. coli* was added to the aliquots of DPBS that was removed at various time points during the Colistin release study. The absorbance was then used to determine bacterial growth over time. The *In vitro* study confirmed the initial results showing that ColAu(-) produced the most efficient nanomesh. For the ColAu(-) nanomesh, the bacterial growth was severely hindered over 14 days whereas all other meshes had bacterial growth observed through their absorbance at 600 nm (Fig. 35). This data was in agreement with the results from the cumulative Colistin release, showing that the addition of small charged particles can alter the release profile.

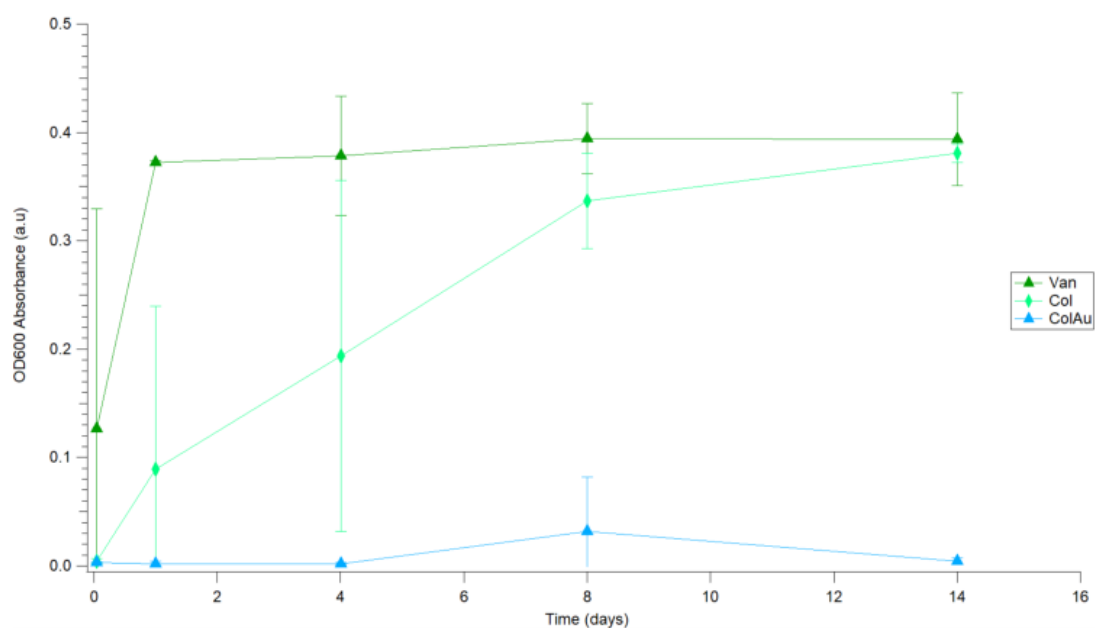


Figure 35: Absorbance at OD600 monitoring increased turbidity representing *E. coli* growth in aliquots removed during the Colistin release study of Van, Col, and ColAu(-) nanomesh samples in DPBS over various time points.

4.0 Conclusion:

This research described the fabrication of Colistin and Vancomycin loaded PCL nanomesh utilising an electrospinning approach for sustained drug release. Homogenous fibres were formed through optimisation of the electrospinning process, with 7% w/w PCL at 1 mL/hr producing the most uniform nanomesh. 12.5% w/w of Colistin and 1.4% w/w of Vancomycin were introduced into the polymer matrix prior to spinning. Both Colistin and Vancomycin were released from the nanomesh over a 14-day period, with Colistin releasing at a higher cumulative percentage than Vancomycin. The addition of small charged nanoparticles altered the release of the antibiotics from the nanomesh. The addition of citrate capped gold nanoparticles likely neutralised Colistin's charge, causing the antibiotic to migrate toward the centre of the fibre, prolonging its release profile. However, the addition of positively charged gold nanoparticles did not significantly alter the release of Colistin from the mesh compared to Colistin alone. Further investigation is needed to determine if other small charged particles affect the release of drugs from single spun fibres and how it affects the release over time. This bandage has a number of potential uses, ranging from remote wound treatment to burns dressings. However, as it is a pharmaceutical application, the stability of the mesh under different storage conditions as well as the toxicological properties also need to be evaluated.

Acknowledgements:

The authors would like to thank the Australian Institute of Nuclear Science and Engineering (AINSE Ltd) (Award –PGRA) for the top-up scholarship, the National Institute for Materials Science (NIMS) for the internship and the Australian Government Research Training Program for providing financial assistance. The authors would also like to acknowledge the assistance of Martin Johnston from Flinders University for his assistance with running the ^1H NMR.

References:

1. Llor, C.; Bjerrum, L. Antimicrobial resistance: risk associated with antibiotic overuse and initiatives to reduce the problem, *Ther Adv Drug Saf.* **2014**, *5*, 229-241.
2. Sweeney, M.T.; Lubbers, B.V.; Schwarz, S.; Watts, J.L. Applying definitions for multidrug resistance, extensive drug resistance and pandrug resistance to clinically significant livestock and companion animal bacterial pathogens, *J Antimicrob Chemother.* **2018**, *73*, 1460-1463.
3. Li, J.; Rayner, C.R.; Nation, R.L.; Owen, R.J.; Spelman, D.; Tan, K.E.; Liolios, L. Heteroresistance to Colistin in Multidrug-Resistant *Acinetobacter baumannii*, *Antimicrob Agents Chemother.* **2006**, *50*, 2946-2950.
4. Garbis, H.; van Tonningen, M.R.; Reuvers, M. 2.6 - Anti-infective agents. In *Drugs During Pregnancy and Lactation (Second Edition)*, Schaefer, C., Peters, P., Miller, R.K., Eds. Academic Press: Oxford, 2007; pp. 123-177.
5. Markou, N.; Apostolakos, H.; Koumoudiou, C.; Athanasiou, M.; Koutsoukou, A.; Alamanos, I.; Gregorakos, L. Intravenous colistin in the treatment of sepsis from multiresistant Gram-negative bacilli in critically ill patients, *Crit Care.* **2003**, *7*, R78-R83.
6. Edrees, N.E.; Galal, A.A.A.; Abdel Monaem, A.R.; Beheiry, R.R.; Metwally, M.M.M. Curcumin alleviates colistin-induced nephrotoxicity and neurotoxicity in rats via attenuation of oxidative stress, inflammation and apoptosis, *Chem Biol Interact.* **2018**, *294*, 56-64.
7. Gurjar, M. Colistin for lung infection: an update, *J Intensive care* **2015**, *3*, 3.
8. Bialvaei, A.Z.; Samadi Kafil, H. Colistin, mechanisms and prevalence of resistance, *Curr Med Res Opin.* **2015**, *31*, 707-721.
9. Martis, N.; Leroy, S.; Blanc, V. Colistin in multi-drug resistant *Pseudomonas aeruginosa* blood-stream infections: A narrative review for the clinician, *J Infect.* **2014**, *69*, 1-12.

10. Hassoun, A.; Linden, P.K.; Friedman, B. Incidence, prevalence, and management of MRSA bacteremia across patient populations-a review of recent developments in MRSA management and treatment, *Crit care*. **2017**, *21*, 211-211.
11. Holland, T.L.; Arnold, C.; Fowler, V.G., Jr. Clinical management of Staphylococcus aureus bacteremia: a review, *JAMA* **2014**, *312*, 1330-1341.
12. Watanakunakorn, C. Mode of action and in-vitro activity of vancomycin, *J Antimicrob Chemother* **1984**, *14*, 7-18.
13. Reynolds, P.E. Structure, biochemistry and mechanism of action of glycopeptide antibiotics, *Eur J Clin Microbiol Infect Dis*. **1989**, *8*, 943-950.
14. Agarwal, S.; Wendorff, J.H.; Greiner, A. Use of electrospinning technique for biomedical applications, *Polymer* **2008**, *49*, 5603-5621.
15. Gizaw, M.; Thompson, J.; Faglie, A.; Lee, S.-Y.; Neuenschwander, P.; Chou, S.-F. Electrospun Fibers as a Dressing Material for Drug and Biological Agent Delivery in Wound Healing Applications, *Bioengineering (Basel)* **2018**, *5*, 9.
16. Torres-Martinez, E.J.; Cornejo Bravo, J.M.; Serrano Medina, A.; Pérez González, G.L.; Villarreal Gómez, L.J. A Summary of Electrospun Nanofibers as Drug Delivery System: Drugs Loaded and Biopolymers Used as Matrices, *Curr Drug Deliv* **2018**, *15*, 1360-1374.
17. Castro-Mayorga, J.L.; Fabra, M.J.; Cabedo, L.; Lagaron, J.M. On the Use of the Electrospinning Coating Technique to Produce Antimicrobial Polyhydroxyalkanoate Materials Containing In Situ-Stabilized Silver Nanoparticles, *Nanomaterials (Basel)* **2016**, *7*, 4.
18. Lv, D.; Wang, R.; Tang, G.; Mou, Z.; Lei, J.; Han, J.; De Smedt, S.; Xiong, R.; Huang, C. Ecofriendly Electrospun Membranes Loaded with Visible-Light-Responding Nanoparticles for Multifunctional Usages: Highly Efficient Air Filtration, Dye Scavenging, and Bactericidal Activity, *ACS Applied Materials & Interfaces* **2019**, *11*, 12880-12889.

19. Zhu, M.; Han, J.; Wang, F.; Shao, W.; Xiong, R.; Zhang, Q.; Pan, H.; Yang, Y.; Samal, S.K.; Zhang, F., et al. Electrospun Nanofibers Membranes for Effective Air Filtration, *Macromolecular Materials and Engineering* **2017**, *302*, 1600353.
20. Lv, D.; Zhu, M.; Jiang, Z.; Jiang, S.; Zhang, Q.; Xiong, R.; Huang, C. Green Electrospun Nanofibers and Their Application in Air Filtration, *Macromolecular Materials and Engineering* **2018**, *303*, 1800336.
21. Zhu, M.; Xiong, R.; Huang, C. Bio-based and photocrosslinked electrospun antibacterial nanofibrous membranes for air filtration, *Carbohydrate Polymers* **2019**, *205*, 55-62.
22. Zhu, M.; Hua, D.; Zhong, M.; Zhang, L.; Wang, F.; Gao, B.; Xiong, R.; Huang, C. Antibacterial and Effective Air Filtration Membranes by “Green” Electrospinning and Citric Acid Crosslinking, *Colloid and Interface Science Communications* **2018**, *23*, 52-58.
23. Ma, W.; Zhang, M.; Liu, Z.; Huang, C.; Fu, G. Nature-inspired creation of a robust free-standing electrospun nanofibrous membrane for efficient oil–water separation, *Environmental Science: Nano* **2018**, *5*, 2909-2920.
24. Ma, W.; Zhao, J.; Oderinde, O.; Han, J.; Liu, Z.; Gao, B.; Xiong, R.; Zhang, Q.; Jiang, S.; Huang, C. Durable superhydrophobic and superoleophilic electrospun nanofibrous membrane for oil-water emulsion separation, *J Colloid Interface Sci* **2018**, *532*, 12-23.
25. Kurtz, I.; Schiffman, J. Current and Emerging Approaches to Engineer Antibacterial and Antifouling Electrospun Nanofibers, *Materials* **2018**, *11*, 1059.
26. Lee, J.K.Y.; Chen, N.; Peng, S.; Li, L.; Tian, L.; Thakor, N.; Ramakrishna, S. Polymer-based composites by electrospinning: Preparation & functionalization with nanocarbons, *Prog Polym Sci.* **2018**, *86*, 40-84.
27. Li, D.; Xia, Y. Electrospinning of Nanofibers: Reinventing the Wheel?, *Adv Mater.* **2004**, *16*, 1151-1170.

28. Mirjalili, M.; Zohoori, S. Review for application of electrospinning and electrospun nanofibers technology in textile industry, *J Nanostruct Chem.* **2016**, *6*, 207-213.
29. Li, X.; Robinson, S.M.; Gupta, A.; Saha, K.; Jiang, Z.; Moyano, D.F.; Sahar, A.; Riley, M.A.; Rotello, V.M. Functional Gold Nanoparticles as Potent Antimicrobial Agents against Multi-Drug-Resistant Bacteria, *ACS Nano* **2014**, *8*, 10682-10686.
30. Zhou, Y.; Kong, Y.; Kundu, S.; Cirillo, J.D.; Liang, H. Antibacterial activities of gold and silver nanoparticles against Escherichia coli and bacillus Calmette-Guérin, *J Nanobiotechnology* **2012**, *10*, 19.
31. Feng, Z.V.; Gunsolus, I.L.; Qiu, T.A.; Hurley, K.R.; Nyberg, L.H.; Frew, H.; Johnson, K.P.; Vartanian, A.M.; Jacob, L.M.; Lohse, S.E., et al. Impacts of gold nanoparticle charge and ligand type on surface binding and toxicity to Gram-negative and Gram-positive bacteria, *Chem Sci.* **2015**, *6*, 5186-5196.
32. Fuller, M.; Köper, I. Polyelectrolyte-Coated Gold Nanoparticles: The Effect of Salt and Polyelectrolyte Concentration on Colloidal Stability, *Polymers (Basel)* **2018**, *10*, 1336.
33. Bala Balakrishnan, P.; Gardella, L.; Forouharshad, M.; Pellegrino, T.; Monticelli, O. Star poly(ϵ -caprolactone)-based electrospun fibers as biocompatible scaffold for doxorubicin with prolonged drug release activity, *Colloids Surf B.* **2018**, *161*, 488-496.
34. Haider, A.; Haider, S.; Kang, I.-K. A comprehensive review summarizing the effect of electrospinning parameters and potential applications of nanofibers in biomedical and biotechnology, *Arab J Chem.* **2015**.
35. Poirel, L.; Jayol, A.; Nordmann, P. Polymyxins: Antibacterial Activity, Susceptibility Testing, and Resistance Mechanisms Encoded by Plasmids or Chromosomes, *Clin Microbiol Rev.* **2017**, *30*, 557-596.

36. Misra, S.; Pandey, H.; Patil, S.; Ramteke, P.; Pandey, A. Tolnaftate-Loaded Polyacrylate Electrospun Nanofibers for an Impressive Regimen on Dermatophytosis, *Fibers* **2017**, *5*, 41.
37. Lin, W.-C.; Yeh, I.-T.; Niyama, E.; Huang, W.-R.; Ebara, M.; Wu, C.-S. Electrospun Poly(ϵ -caprolactone) Nanofibrous Mesh for Imiquimod Delivery in Melanoma Therapy, *Polymers* **2018**, *10*, 231.
38. Ding, Y.; Li, W.; Zhang, F.; Liu, Z.; Zanjanzadeh Ezazi, N.; Liu, D.; Santos, H.A. Electrospun Fibrous Architectures for Drug Delivery, Tissue Engineering and Cancer Therapy, *Adv Funct Mater.* **2019**, *29*, 1802852.
39. Shalumon, K.T.; Lai, G.-J.; Chen, C.-H.; Chen, J.-P. Modulation of Bone-Specific Tissue Regeneration by Incorporating Bone Morphogenetic Protein and Controlling the Shell Thickness of Silk Fibroin/Chitosan/Nanohydroxyapatite Core–Shell Nanofibrous Membranes, *ACS Appl Mater Interfaces.* **2015**, *7*, 21170-21181.
40. Angkawinitwong, U.; Awwad, S.; Khaw, P.T.; Brocchini, S.; Williams, G.R. Electrospun formulations of bevacizumab for sustained release in the eye, *Acta Biomater.* **2017**, *64*, 126-136.
41. Alexander L. Yarin, B.P., Seeram Ramakrishna. *Fundamentals and Applications of Micro- and Nanofibres*, 1st ed.; Cambridge University Press: Cambridge 2014.
42. Bergen, P.J.; Li, J.; Rayner, C.R.; Nation, R.L. Colistin methanesulfonate is an inactive prodrug of colistin against *Pseudomonas aeruginosa*, *Antimicrob Agents Chemother* **2006**, *50*, 1953-1958.
43. Jamzad, S.; Fassihi, R. Role of surfactant and pH on dissolution properties of fenofibrate and glipizide--a technical note, *AAPS PharmSciTech* **2006**, *7*, E33-E33.
44. Kumar, P.; Ganure, A.L.; Subudhi, B.B.; Shukla, S. Design and Comparative Evaluation of In-vitro Drug Release, Pharmacokinetics and Gamma Scintigraphic Analysis of Controlled Release Tablets Using Novel pH Sensitive

Starch and Modified Starch- acrylate Graft Copolymer Matrices, *IJPR* **2015**, *14*, 677-691.

45. Cabañas, M.V.; Peña, J.; Román, J.; Vallet-Regí, M. Tailoring vancomycin release from β -TCP/agarose scaffolds, *Eur J Pharm Sci.* **2009**, *37*, 249-256.

46. Hayashi, T.; Kanbe, H.; Okada, M.; Suzuki, M.; Ikeda, Y.; Onuki, Y.; Kaneko, T.; Sonobe, T. Formulation study and drug release mechanism of a new theophylline sustained-release preparation, *Int J Pharm.* **2005**, *304*, 91-101.

47. Amit, N.; Bibek, L.; Kalyan, S. Development of hydroxyapatite-ciprofloxacin bone-implants using »Quality by design«, *Acta Pharm.* **2011**, *61*, 25-36.

CHAPTER 7: CONCLUSIONS AND FUTURE DIRECTIONS

The research presented in this thesis has highlighted the potential for the use of gold nanoparticles in antibiotic delivery. This has been shown through delivery of Colistin as a nanoparticle coating as well as through an electrospun proof-of-concept antibiotic loaded bandage. Delivery via these means opens up new possibilities for treatment with antibiotics, especially in the age of antibiotic resistance. Delivering Colistin in a more efficient manner, where susceptibility is increased while dosage is reduced, could assist in limiting side-effects and preventing bacterial survival which otherwise can foster resistance.

As shown in Chapter 2, the far-reaching medical applications of polyelectrolyte coated gold nanoparticles are immense and it is important that we understand how to coat nanoparticles using polyelectrolytes effectively. Providing the optimum coating conditions allows for stable particles which is imperative for consistency in medical applications. Experiments conducted in Chapter 3 demonstrate the optimum coating parameters to be a concentration of 5 mg/mL PDADMAC in 1 mM NaCl for 5 nm diameter citrate capped gold nanoparticles. This research has formed the basis for stable polyelectrolyte coated gold nanoparticles which have been used throughout the proceeding chapters.

The effect of cationic PDADMAC coated gold nanoparticles on Gram-negative bacterial model membranes was explored to determine if they play a role in the disruption of the membrane. This is of importance as disruption could lead to improved antibiotic delivery - especially for membrane targeting antibiotics. It was found that smaller concentrations (3.6×10^{11} particles/mL) of nanoparticles do not affect the membrane significantly, nor is binding observed. However, at higher concentrations (3.6×10^{12} particles/mL) the membrane undergoes significant disruption which includes particles binding to the outer membrane. Although disruption is not apparent at the lower nanoparticle concentration, by pre-treating the membrane with nanoparticles, damage to the membrane is more significant after Colistin addition than if Colistin is added alone. It was also found that adding nanoparticles and Colistin simultaneously did not differ significantly in membrane damage compared with adding Colistin alone. Therefore, the finding that the pre-

treatment of nanoparticles causes a greater effect in membrane disruption is important for understanding how to increase the susceptibility of bacteria to antibiotics.

With this new finding, and recent successes of others in coating gold nanoparticles with antibiotics, the next step in this research area was to coat gold nanoparticles with Colistin. By coating the anionic particles in Colistin, the minimum inhibitory concentration of *E. coli* was decreased 6.8-fold compared to Colistin alone. It was also shown that gold nanoparticles (both cationic and anionic) at an approximate concentration of 3.6×10^{11} particles/mL have no effect on the growth of bacteria. This was in agreement with findings from neutron scattering for the same nanoparticle concentration. By coating anionic nanoparticles in Colistin, the concentration of antibiotic can be reduced compared to Colistin on its own to achieve the same therapeutic effect.

With a greater understanding of the use of gold nanoparticles in increasing susceptibility, the next step was being able to use this knowledge in a real-world application. Keeping within an antibiotic theme, a proof-of-concept bandage was developed that could release sufficient amounts of Colistin over a 14 day period. The amount of Colistin released was altered by the inclusion of anionic gold nanoparticles within the electrospun fibre mesh matrix. Comparatively, the addition of cationic gold nanoparticles, as used in the previous chapters within this thesis, did not significantly alter the release of Colistin from the mesh compared to Colistin in the mesh alone. The mesh release itself is complex and further in-depth analysis of the nanofiber mesh's mechanical properties as well as the effects of the nanoparticles on release need to be explored further.

Although the mechanical properties of PCL mesh are well documented in literature, additives such as nanoparticles and antibiotics alter those properties. Understanding the effects that these additives have would be beneficial, especially for medical applications as the properties of the mesh can be fine-tuned to the application itself. As there are several release possibilities, future studies should focus on diffusion and degradation for Colistin and gold nanoparticle release. This is because these were identified as the main mechanisms determined for the specific mesh in Chapter 6. The difference

between these mechanisms of release can be seen in Figure 36. There are three important characteristics of the mesh that should be monitored when the additives of Colistin and nanoparticles are incorporated. These are the change in tensile strength, hydrophobicity (including wettability) and degradation.

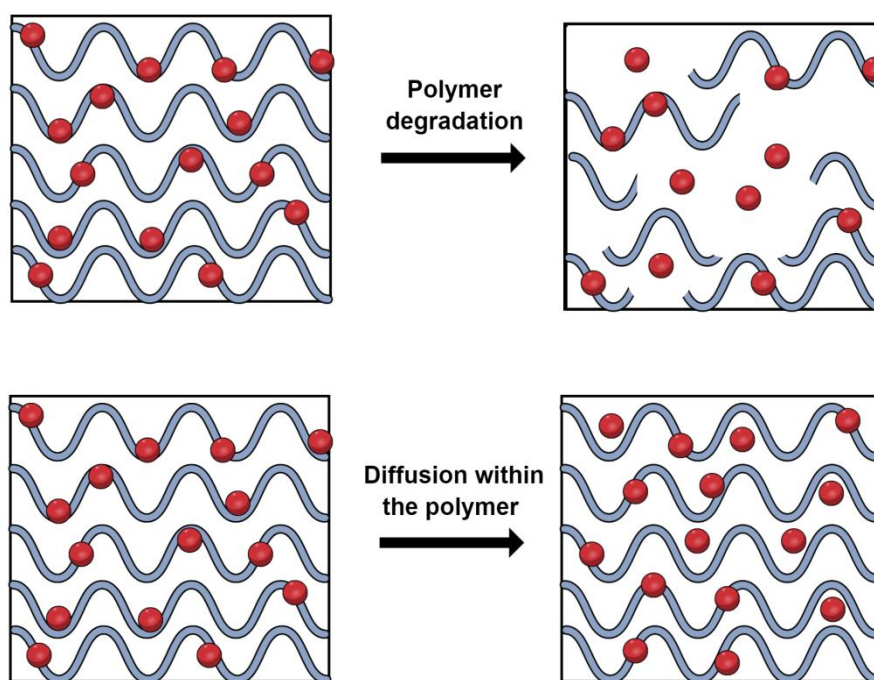


Figure 36: Schematic of mechanisms for release of the additives Colistin and gold nanoparticles from a PCL nanomesh.

The tensile strength of the mesh is generally measured using uniaxial testing and is represented by a stress-strain curve. Measuring the tensile strength is important in understanding the mechanical abilities of the material. This is especially pertinent in biomedicine to ensure the material can withstand the forces used during surgery and for tissue regeneration and growth.^{1,2} Compared to other common biopolymers, PCL in general has excellent mechanical properties which is advantageous for use in a variety of applications.³ The tensile strength, strain at break and Young's modulus has shown to vary significantly depending on fibre diameter. These values can vary from 7.6-30.6 MPa for Young's modulus, 0.9-6.3 MPa for the ultimate tensile strength and 49-442% for strain at break for fibres between 100 - 3400 nm in diameter.³ A general trend has been found in the strength where decreasing the fibre diameter leads to increasing stiffness and tensile strength whilst the breaking strain decreases

significantly.^{4,5} This trend however changes depending on the additives and polymer composition of the nanomesh. As an example, in a PCL/PLGA mesh containing the hepatitis B drug Tenofovir, the tensile strength and Young's modulus increased only infinitesimally whilst the addition of Chitosan in a PCL mesh has a significant increase in Young's modulus.^{6,7} The effects of the addition of Colistin can also be measured through the tensile strength. The addition of small molecular drugs have shown to lower the crystallinity of semi-crystalline polyether electrospun materials, altering the tensile strength.⁸ It is difficult to predict how the addition of either gold nanoparticles or Colistin will affect the mechanical strength of the mesh and hence this will need to be explored in future work.

Similar to the tensile strength, the degradation of PCL over time is also important as it plays a role in drug release as observed in the release kinetics in Chapter 6. The degradation *in vivo* of PCL is slow and research suggests it can take more than two years to degrade.⁹ However, additives such as nanoclay have proven to completely degrade PCL nanofibres in as little as 96 h.¹⁰ The complete degradation in this case refers to a total loss of structural integrity. The current theory behind the accelerated degradation is due to a lower hydrophobicity than PCL alone. The ability of the additives to absorb water within the mesh structure leads to hydrolytic degradation and an increase in media throughout the mesh scaffold.^{10,11} As Colistin is hydrophilic theoretically this would lower the hydrophobicity of the PCL nanomesh and hence it would be expected that degradation would be accelerated compared to PCL on its own. In order to measure the degradation, a number of techniques should be used. The first is atomic force microscopy (AFM) which has recently gained traction in understanding biomaterials as it can characterise the surface topography of the mesh as well as the physical, chemical and mechanical properties.¹² An example of determining degradation can be seen in figure 37, where submersing the mesh in various mediums can alter the surface roughness which is an indicator of degradation.

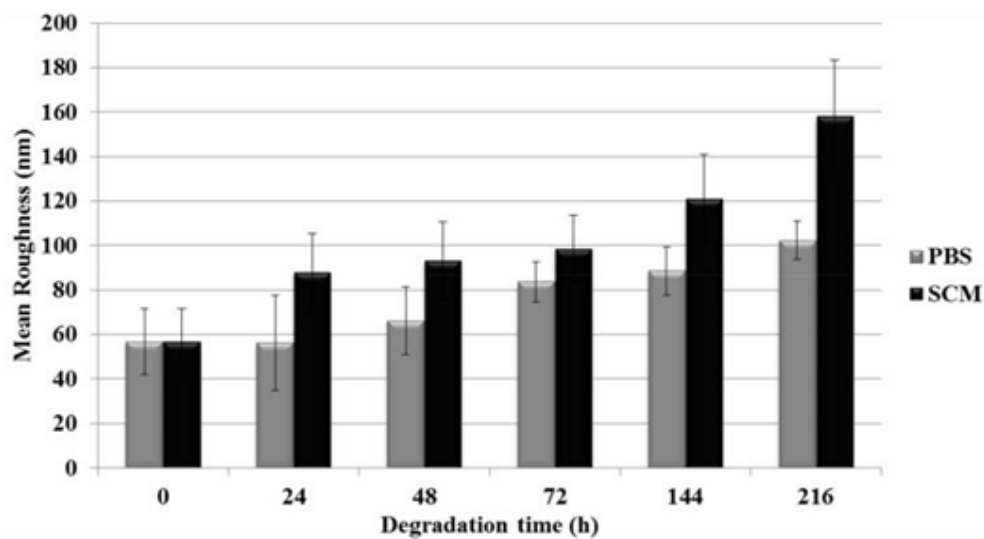


Figure 37: Mean roughness of a PCL/gelatin electrospun nanomesh with increasing degradation time in either phosphate buffered saline (PBS) or simulated culture medium (SCM) measured using quantitative AFM analysis.¹²

SEM is also another important tool in monitoring degradation as changes in the fibre structure including the breakage of fibres, decrease in diameter and changes in porosity can be observed (Fig. 38).¹³ Although often a qualitative method, it is still important in monitoring and confirming the degradation over time.

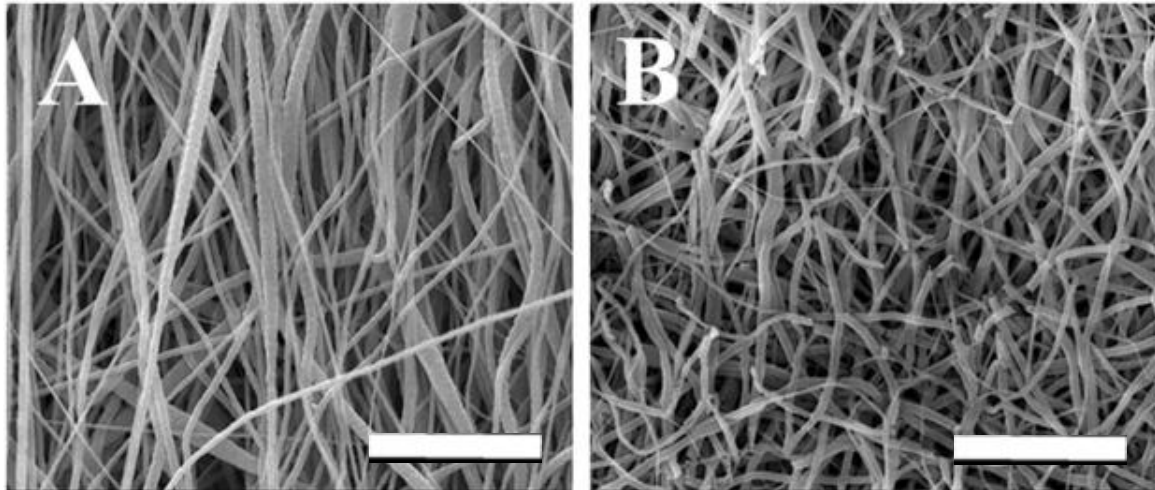


Figure 38: Example of degradation of PCL fibres before (A) and after (B) implantation for 18 months. as a vascular implant in rats.¹⁴ Scale bar is 20 μm . Reprinted with permission from John Wiley and Sons.

Lastly, a more common way to measure degradation is through weight loss over time. It is known that the mass lost increases (and hence degradation increases) as crystallinity of the mesh decreases.¹⁵ This is due to amorphous regions being more sensitive to hydrolysis.^{15,16} The addition of Colistin and gold nanoparticles would be expected to lower the crystallinity of the mesh, meaning the mass loss would be greater than for PCL alone. Changes in crystallinity as Colistin or nanoparticles are added to PCL could be measured through wide angle X-ray diffraction (XRD) analysis.¹⁷

The change in hydrophobicity and wettability of the mesh upon addition of hydrophilic substances such as Colistin could also be monitored through the use of contact angle measurements. It has been previously reported by others that using additives such as collagen or gelatin greatly increases the hydrophilicity, with contact angles dropping to 0° in some cases.^{18,19}

Once the mesh has been characterised sufficiently, the next step is determining how effective it would be as a wound dressing. It has already been tested against planktonic bacteria in Chapter 6, however it would be unlikely for planktonic bacteria to occur in an *in vivo* scenario. A more realistic scenario to test its antibiotic capabilities would include testing on biofilms and known resistant bacteria. Biofilms consist of one or more types of microorganisms that are

associated with a surface. Approximately 90% of the biofilm mass is its extracellular polymeric substances (EPS), which includes DNA and proteins. The EPS forms a matrix which surround and embeds the cells, hence the EPS is one of the reasons biofilms are so difficult to remove and eradicate.^{20,21} Biofilms are incredibly tolerant to changes in their environment and show greater resistance to antibiotics compared to their planktonic counterpart.²² Attempts have already been made to target biofilms in PCL nanomesh with some promising results. In a recent study, the antibiotic tetracycline was impregnated in a mixture of PCL, poly(LD-lactide) (PLA) and gelatin electrospun fibres. The mesh was able to successfully inhibit the formation of biofilms related to dental implants and thus holds great promise as an antibacterial dental implant coating.²³ In another study, Vancomycin was incorporated into a PLGA mesh and was able to be released in high concentrations into the brain tissue of rats suffering cerebral infections. The mesh or antibiotic release did not cause any adverse effects on the brain.²⁴ In this case, the mesh was inserted into the brain tissue rather than used topically. In general, the area of antibiotic loaded nanomesh for wound dressing applications is fairly new and thus has significant areas for growth.

In order to test the topical bandage on biofilms there are several experimental assays which could be used. These include a microtitre biofilm inhibition assay and a Biofilm Ring Test.^{25,26} The microtitre biofilm inhibition assay works by growing bacteria in a 96-well plate and then staining with crystal violet (CV).²⁷ Differences in growth of the biofilm will change the measured absorbance of the CV. Similarly, the Biofilm Ring Test is a quick method to determine if a biofilm has formed, and works by growing bacteria in the presence of magnetic beads in a 96 well plate. After a period of time, the plate is placed on a magnet which attracts the beads into the centre of the wells.²⁸ If a biofilm forms, it will prevent the beads moving into the centre which can be quantified using a specific plate reader.²⁵ These assays could be used by placing the mesh in media, collecting the released contents of the mesh and putting the collected solution into the assays. This will determine if the amount of Colistin released is sufficient to prevent the biofilm growth.

A potential extension of the topical nanomesh application would be to anneal the mesh to the surface of medical implants. Sepsis from biofilms is most commonly associated with implantable medical devices such as orthopaedic implants and intravascular catheters.²⁹⁻³¹ Patients who undergo a medical implant and suffer serious infections are likely to require the implant be removed or replaced which impacts on the length of hospital stay, recovery time and also increased mortality rates.³² It is estimated that on average, 2-5% of medical implants are contaminated and the cost of treating an infection from an implant is estimated to be approximately 100,000 USD.^{33,34} With this in mind, being able to reduce the instances of device related infections would be beneficial for the patient as well as the economy. In literature there are few examples of annealed electrospun coatings containing antibiotics for prevention of biofilm formation. However one study of interest is the addition of Vancomycin, Rifampin (Rif), Linezolid (Lin) and Daptomycin (Dap) in various combinations, annealed to orthopaedic implants via PLGA/PCL nanomesh.³⁵ The combinations of Van/Rif, Lin/Lin + Rif and Dap/Dap + Rif showed no biofilm growth over 14 days *in vivo* whilst preventing infection-induced bone changes in mice.³⁵

There are therefore many additional experiments which need to take place in order to fully understand the capabilities and limitations of this mesh. I hope that this work highlights the possibilities and potential of this mesh system to eventually reach a clinical application as a controlled release antibiotic wound dressing.

References:

1. Cipitria, A.; Skelton, A.; Dargaville, T.R.; Dalton, P.D.; Hutmacher, D.W. Design, fabrication and characterization of PCL electrospun scaffolds—a review, *Journal of Materials Chemistry* **2011**, *21*, 9419-9453.
2. Mochane, M.J.; Motsoeneng, T.S.; Sadiku, E.R.; Mokhena, T.C.; Sefadi, J.S. Morphology and Properties of Electrospun PCL and Its Composites for Medical Applications: A Mini Review, *Applied Sciences* **2019**, *9*, 2205.

3. Kim, H.H.; Kim, M.J.; Ryu, S.J.; Ki, C.S.; Park, Y.H. Effect of fiber diameter on surface morphology, mechanical property, and cell behavior of electrospun poly(ϵ -caprolactone) mat, *Fibers and Polymers* **2016**, *17*, 1033-1042.
4. Lim, C.T.; Tan, E.P.S.; Ng, S.Y. Effects of crystalline morphology on the tensile properties of electrospun polymer nanofibers, *Applied Physics Letters* **2008**, *92*, 141908.
5. Wu, X.-F.; Dzenis, Y.A. Size effect in polymer nanofibers under tension, *Journal of Applied Physics* **2007**, *102*, 044306.
6. Chou, S.-F.; Woodrow, K.A. Relationships between mechanical properties and drug release from electrospun fibers of PCL and PLGA blends, *Journal of the Mechanical Behavior of Biomedical Materials* **2017**, *65*, 724-733.
7. Dumitriu, R.P.; Mitchell, G.R.; Davis, F.J.; Vasile, C. Functionalized Coatings by Electrospinning for Anti-oxidant Food Packaging, *Procedia Manufacturing* **2017**, *12*, 59-65.
8. Yakub, G.; Toncheva, A.; Manolova, N.; Rashkov, I.; Kussovski, V.; Danchev, D. Curcumin-loaded poly(L-lactide-co-D,L-lactide) electrospun fibers: Preparation and antioxidant, anticoagulant, and antibacterial properties, *Journal of Bioactive and Compatible Polymers* **2014**, *29*, 607-627.
9. Gaharaw, A., K; Schexnailder, P., J.; Schmidt, G. Nanocomposite Polymer Biomaterials for Tissue Repair of Bone and Cartilage: A Material Science Perspective, *Nanobiomaterials Handbook*. New York: CRC Press, Taylor & Francis Group **2011**, 24.
10. Gaharwar, A., K., Mukundan, S., Karaca, Elif., Dolatshahi-Pirouz, Alireza., Patel, Alpesh., Ranharanjan, Kaushik., Mihaila, Silvia, M., Iviglia, G., Zhnag, Hongbin. & Khademhosseini, Ali. Nanoclay-Enriched Poly(ϵ -caprolactone) Electrospun Scaffolds for Osteogenic Differentiation of Human Mesenchymal Stem Cells, *Tissue Engineering: Part A* **2014**, *20*, 2088-2101.
11. Lam, C.X.; Savalani, M.M.; Teoh, S.H.; Hutmacher, D.W. Dynamics of in vitro polymer degradation of polycaprolactone-based scaffolds: accelerated

versus simulated physiological conditions, *Biomedical materials (Bristol, England)* **2008**, 3, 034108.

12. Marrese, M.; Guarino, V.; Ambrosio, L. Atomic Force Microscopy: A Powerful Tool to Address Scaffold Design in Tissue Engineering, *Journal of functional biomaterials* **2017**, 8.

13. Munj, H.R.; Lannutti, J.J.; Tomasko, D.L. Understanding drug release from PCL/gelatin electrospun blends, *Journal of Biomaterials Applications* **2017**, 31, 933-949.

14. Li, W.; Chen, J.; Xu, P.; Zhu, M.; Wu, Y.; Wang, Z.; Zhao, T.; Cheng, Q.; Wang, K.; Fan, G., et al. Long-term evaluation of vascular grafts with circumferentially aligned microfibers in a rat abdominal aorta replacement model, *Journal of Biomedical Materials Research Part B: Applied Biomaterials* **2018**, 106, 2596-2604.

15. Höglund, A.; Hakkarainen, M.; Albertsson, A.C. Degradation Profile of Poly(ϵ -caprolactone)–the Influence of Macroscopic and Macromolecular Biomaterial Design, *Journal of Macromolecular Science, Part A* **2007**, 44, 1041-1046.

16. Sisson, A.L.; Ekinci, D.; Lendlein, A. The contemporary role of ϵ -caprolactone chemistry to create advanced polymer architectures, *Polymer* **2013**, 54, 4333-4350.

17. Rather, H.A.; Thakore, R.; Singh, R.; Jhala, D.; Singh, S.; Vasita, R. Antioxidative study of Cerium Oxide nanoparticle functionalised PCL-Gelatin electrospun fibers for wound healing application, *Bioactive Materials* **2018**, 3, 201-211.

18. Chen, Z.C.C.; Ekaputra, A.K.; Gauthaman, K.; Adaikan, P.G.; Yu, H.; Hutmacher, D.W. In vitro and in vivo analysis of co-electrospun scaffolds made of medical grade poly(ϵ -caprolactone) and porcine collagen, *Journal of Biomaterials Science, Polymer Edition* **2008**, 19, 693-707.

19. Gupta, D.; Venugopal, J.; Prabhakaran, M.P.; Dev, V.R.G.; Low, S.; Choon, A.T.; Ramakrishna, S. Aligned and random nanofibrous substrate for the in vitro culture of Schwann cells for neural tissue engineering, *Acta Biomaterialia* **2009**, *5*, 2560-2569.
20. Algburi, A.; Comito, N.; Kashtanov, D.; Dicks, L.M.T.; Chikindas, M.L. Control of Biofilm Formation: Antibiotics and Beyond, *Applied and Environmental Microbiology* **2017**, *83*, e02508-02516.
21. Kerr, C.J.; Osborn, K.S.; Rickard, A.H.; Robson, G.D.; Handley, P.S. 41 - Biofilms in water distribution systems. In *Handbook of Water and Wastewater Microbiology*, Mara, D., Horan, N., Eds. Academic Press: London, 2003; pp. 757-775.
22. Percival, S.L.; Hill, K.E.; Williams, D.W.; Hooper, S.J.; Thomas, D.W.; Costerton, J.W. A review of the scientific evidence for biofilms in wounds, *Wound Repair and Regeneration* **2012**, *20*, 647-657.
23. Shahi, R.G.; Albuquerque, M.T.P.; Münchow, E.A.; Blanchard, S.B.; Gregory, R.L.; Bottino, M.C. Novel bioactive tetracycline-containing electrospun polymer fibers as a potential antibacterial dental implant coating, *Odontology* **2017**, *105*, 354-363.
24. Tseng, Y.-Y.; Kao, Y.-C.; Liao, J.-Y.; Chen, W.-A.; Liu, S.-J. Biodegradable drug-eluting poly[lactic-co-glycol acid] nanofibers for the sustainable delivery of vancomycin to brain tissue: in vitro and in vivo studies, *ACS Chem Neurosci* **2013**, *4*, 1314-1321.
25. Haney, E.F.; Trimble, M.J.; Cheng, J.T.; Vallé, Q.; Hancock, R.E.W. Critical Assessment of Methods to Quantify Biofilm Growth and Evaluate Antibiofilm Activity of Host Defence Peptides, *Biomolecules* **2018**, *8*, 29.
26. Olivares, E.; Badel-Berchoux, S.; Provot, C.; Jaulhac, B.; Prévost, G.; Bernardi, T.; Jehl, F. The BioFilm Ring Test: a Rapid Method for Routine Analysis of *Pseudomonas aeruginosa* Biofilm Formation Kinetics, *Journal of Clinical Microbiology* **2016**, *54*, 657-661.

27. Martínez Díaz, Y.; Vanegas Laverde, G.; Reina Gamba, L.; Mayorga Wandurraga, H.; Arévalo-Ferro, C.; Ramos Rodríguez, F.; Duque Beltrán, C.; Castellanos Hernández, L. Biofilm inhibition activity of compounds isolated from two *Eunicea* species collected at the Caribbean Sea, *Revista Brasileira de Farmacognosia* **2015**, *25*, 605-611.
28. Chavant, P.; Gaillard-Martinie, B.; Talon, R.; Hebraud, M.; Bernardi, T. A new device for rapid evaluation of biofilm formation potential by bacteria, *Journal of microbiological methods* **2007**, *68*, 605-612.
29. Costerton, J.W.; Montanaro, L.; Arciola, C.R. Biofilm in implant infections: its production and regulation, *The International journal of artificial organs* **2005**, *28*, 1062-1068.
30. Khardori, N.; Yassien, M. Biofilms in device-related infections, *Journal of industrial microbiology* **1995**, *15*, 141-147.
31. Kennedy, P.; Brammah, S.; Wills, E. Burns, biofilm and a new appraisal of burn wound sepsis, *Burns* **2010**, *36*, 49-56.
32. Khatoon, Z.; McTiernan, C.D.; Suuronen, E.J.; Mah, T.-F.; Alarcon, E.I. Bacterial biofilm formation on implantable devices and approaches to its treatment and prevention, *Heliyon* **2018**, *4*, e01067-e01067.
33. Darouiche, R. Treatment of Infections Associated with Surgical Implants, *The New England Journal of Medicine* **2004**, *350*, 1422-1429.
34. Wang, M.; Tang, T. Surface treatment strategies to combat implant-related infection from the beginning, *Journal of Orthopaedic Translation* **2019**, *17*, 42-54.
35. Ashbaugh, A.G.; Jiang, X.; Zheng, J.; Tsai, A.S.; Kim, W.S.; Thompson, J.M.; Miller, R.J.; Shahbazian, J.H.; Wang, Y.; Dillen, C.A., et al. Polymeric nanofiber coating with tunable combinatorial antibiotic delivery prevents biofilm-associated infection in vivo, *Proceedings of the National Academy of Sciences of the United States of America* **2016**, *113*, E6919-e6928.

APPENDICES

A Supplementary Information for the publication: **Fuller, M.** & Köper, I. Polyelectrolyte-coated Gold Nanoparticles: the Effect of Salt and Polyelectrolyte Concentration on colloidal stability, *Polymers*, 2018. DOI: 10.3390/polym10121336.

B Supplementary Information for Chapter 4: Increasing Antibiotic Susceptibility - The use of Cationic Gold Nanoparticles in Gram-Negative Bacterial Membrane Models.

C Supplementary Information for Chapter 5: Delivery of Colistin using Gold Nanoparticles.

D Supplementary Information for the publication: **Fuller, M.**, Carey, A., Whiley, H., Kurimoto, R., Ebara, M. & Köper, I. Nanoparticles in an Antibiotic-Loaded Nanomesh for Drug Delivery, 2019. DOI: 10.1039/C9RA06398F.

E Journal formatted manuscript for the publication: **Fuller, M.** & Köper, I. Biomedical Applications of Polyelectrolyte Coated Spherical Gold Nanoparticles, *Nano Convergence*, 2019. DOI: 10.1186/s40580-019-0183-4

F Journal formatted manuscript for the publication: **Fuller, M.** & Köper, I. Polyelectrolyte-coated Gold Nanoparticles: the Effect of Salt and Polyelectrolyte Concentration on colloidal stability, *Polymers*, 2018. DOI: 10.3390/polym10121336.

G Journal formatted manuscript for the publication: **Fuller, M.**, Carey, A., Whiley, H., Kurimoto, R., Ebara, M. & Köper, I. Nanoparticles in an Antibiotic-Loaded Nanomesh for Drug Delivery, 2019. DOI: 10.1039/C9RA06398F.

Appendix A:

Supplementary Information from the publication 'Polyelectrolyte-coated Gold Nanoparticles: the Effect of Salt and Polyelectrolyte Concentration on colloidal stability'.

Table S1: Difference in SPR peak and absorbance for citrate capped AuNP and PDADMAC coated AuNP in Ethanol, Tween20 and PBS.

	Δ SPR Peak between NPs in MilliQ and NPs in varying solvents (nm)		
Samples	Ethanol	Tween 20	PBS
Citrate Capped AuNP	23 ± 0.38	6 ± 0.31	*
PDADMAC Coated AuNP	6 ± 0.94	2 ± 0.47	*
	Absorbance (a.u.)		
Citrate Capped AuNP	0.149 ± 0.08	0.08 ± 0.008	*
PDADMAC Coated AuNP	0.173 ± 0.001	0.130 ± 0.0009	*

*All samples in PBS irreversibly aggregated and were unable to be removed from the centrifuge tubes with a concentration of AuNP suitable for UV-Vis.

Appendix B:

Supplementary Information for Chapter 4; Increasing Antibiotic Susceptibility -
The use of Cationic Gold Nanoparticles in Gram-Negative Bacterial Membrane
Models.

Table S2: Sparsely tethered bilayer with the addition of 100 μL cationic AuNP and the addition of 10 mg/mL Colistin sulfate. The thickness and roughness are given in \AA , hydration is given in volume % and SLD is given in 10^{-6}\AA^{-2} .

Wafer 1	80% DPhyTL, 94% RcLPS		
	Bilayer	Bilayer + 100 μL AuNP(+)	Bilayer + 100 μL AuNP(+) + 10mg/mL Colistin
Scale factor	0.98 ± 0.01	0.97 ± 0.01	1.02 ± 0.01
Fronting SLD	2.07	2.07	2.07
Backing SLD	6.21 ± 0.01	6.21 ± 0.01	6.19 ± 0.01
Backing roughness	7.28 ± 0.20	6.99 ± 0.71	5.86 ± 0.67
SiO ₂ thickness	4.36 ± 0.17	4.17 ± 0.12	4.15 ± 0.12
SiO ₂ SLD	3.47	3.47	3.47
SiO ₂ hydration	0.00	0.00	0.00
SiO ₂ roughness	4.59 ± 0.19	4.01 ± 0.00	4.67 ± 0.17
Cr thickness	18.2 ± 0.12	18.2 ± 0.14	18.3 ± 0.16
Cr SLD	3.02 ± 0.00	3.02 ± 0.00	3.02 ± 0.00
Cr hydration	0.00	0.00	0.00
Cr roughness	9.10 ± 0.46	9.40 ± 0.36	9.75 ± 0.17
Au thickness	191 ± 0.06	191 ± 0.02	191 ± 0.21
Au SLD	4.49 ± 0.00	4.49 ± 0.00	4.49 ± 0.01
Au hydration	0.00	0.00	0.00
Au roughness	4.44 ± 0.21	4.00 ± 0.00	4.20 ± 0.16
Tether thickness	6.19 ± 0.13	6.01 ± 0.00	6.00 ± 0.00
Tether SLD	1.47 ± 0.00	1.46 ± 0.00	1.45 ± 0.02
Tether hydration	16.6 ± 1.72	10.9 ± 0.12	8.12 ± 0.09
Tether roughness	4.39 ± 0.18	4.00 ± 0.00	9.23 ± 0.48
Inner HG thickness	6.44 ± 0.20	6.00 ± 0.00	6.39 ± 0.11
Inner HG SLD	0.94 ± 0.02	0.78 ± 0.12	1.92 ± 0.04
Inner HG hydration	18.9 ± 0.73	19.6 ± 0.00	18.6 ± 0.38
Inner HG roughness	4.62 ± 0.23	4.44 ± 0.16	9.41 ± 0.23
Inner HC thickness	11.2 ± 0.15	11.0 ± 0.00	9.75 ± 0.35
Inner HC SLD	-0.6 ± 0.08	-0.39 ± 0.00	-0.36 ± 0.03
Inner HC hydration	4.16 ± 0.73	4.95 ± 0.02	4.94 ± 0.00
Inner HC roughness	4.62 ± 0.23	4.17 ± 0.16	4.49 ± 0.29
Outer HC thickness	11.3 ± 0.14	11.1 ± 0.10	14.8 ± 0.34
Outer HC SLD	-0.39 ± 0.00	-0.35 ± 0.03	-0.36 ± 0.02
Outer HC hydration	4.22 ± 0.18	6.36 ± 0.21	1.28 ± 0.15
Outer HC roughness	7.32 ± 0.29	8.06 ± 0.75	11.6 ± 0.2
Outer HG thickness	10.7 ± 0.35	12.0 ± 0.01	12.0 ± 0.01
Outer HG SLD	2.56 ± 0.02	2.83 ± 0.01	2.73 ± 0.02
Outer HG hydration	67.9 ± 0.01	63.8 ± 0.88	11.1 ± 0.72
Outer HG roughness	7.28 ± 0.20	7.66 ± 0.02	5.30 ± 0.21

Table S3: Sparsely tethered bilayer compared to the same bilayer with 100 μL cationic AuNP added simultaneously with 10 mg/mL Colistin sulfate. The thickness and roughness are given in \AA , hydration is given in volume-% and SLD is given in 10^{-6}\AA^{-2} .

Wafer 2	80% DPhyTL, 94% RcLPS	
	Bilayer	Bilayer + 100 μL AuNP(+) + 10 mg/mL Colistin
Scale factor	0.93 \pm 0.01	0.96 \pm 0.01
Fronting SLD	2.07	2.07
Backing SLD	5.98 \pm 0.01	5.99 \pm 0.01
Backing roughness	5.64 \pm 2.05	5.00 \pm 0.00
SiO ₂ thickness	18.5 \pm 0.30	19.0 \pm 0.39
SiO ₂ SLD	3.47	3.47
SiO ₂ hydration	0.00	0.00
SiO ₂ roughness	4.99 \pm 0.36	4.53 \pm 0.73
Cr thickness	12.6 \pm 0.31	12.6 \pm 0.20
Cr SLD	3.02 \pm 0.05	3.02 \pm 0.00
Cr hydration	0.00	0.00
Cr roughness	9.19 \pm 0.41	8.67 \pm 0.25
Au thickness	180 \pm 0.37	184 \pm 0.44
Au SLD	4.22 \pm 0.02	4.25 \pm 0.01
Au hydration	0.00	0.00
Au roughness	8.57 \pm 0.35	9.31 \pm 0.33
Tether thickness	8.30 \pm 0.21	8.25 \pm 0.18
Tether SLD	1.81 \pm 0.09	1.28 \pm 0.12
Tether hydration	8.47 \pm 0.80	8.12 \pm 0.01
Tether roughness	5.28 \pm 0.34	5.41 \pm 0.40
Inner HG thickness	5.18 \pm 0.13	6.08 \pm 0.45
Inner HG SLD	1.42 \pm 0.05	1.67 \pm 0.08
Inner HG hydration	32.9 \pm 3.09	38.3 \pm 1.76
Inner HG roughness	5.28 \pm 0.34	8.66 \pm 1.25
Inner HC thickness	10.3 \pm 0.21	10.3 \pm 0.25
Inner HC SLD	-0.08 \pm 0.04	-0.28 \pm 0.08
Inner HC hydration	5.63 \pm 0.02	4.91 \pm 0.01
Inner HC roughness	5.28 \pm 0.34	8.87 \pm 0.345
Outer HC thickness	10.3 \pm 0.21	10.3 \pm 0.18
Outer HC SLD	-0.08 \pm 0.04	-0.11 \pm 0.04
Outer HC hydration	5.95 \pm 0.01	5.72 \pm 0.01
Outer HC roughness	5.28 \pm 0.34	14.2 \pm 0.09
Outer HG thickness	18.5 \pm 0.67	16.2 \pm 0.83
Outer HG SLD	4.33 \pm 0.07	4.38 \pm 0.08
Outer HG hydration	65.6 \pm 1.86	44.4 \pm 0.02
Outer HG roughness	9.27 \pm 0.18	7.35 \pm 0.32

Table S4: Sparsely tethered bilayer compared to the same bilayer with 1 mL cationic AuNP added and then addition of 10 mg/mL Colistin sulfate. The thickness and roughness are given in Å, hydration is given in volume-% and SLD is given in 10^{-6} \AA^{-2} .

Wafer 3	80% DPhyTL, 94% RcLPS		
	Bilayer	Bilayer + 1 mL AuNP(+)	Bilayer + 1 mL AuNP(+) + 10 mg/mL Colistin
Scale factor	0.97 ± 0.01	1.03 ± 0.01	1.00 ± 0.01
Fronting SLD	2.07	2.07	2.07
Backing SLD	6.11 ± 0.01	6.37 ± 0.01	6.07 ± 0.01
Backing roughness	3.28 ± 0.70	2.53 ± 0.22	6.61 ± 0.97
SiO ₂ thickness	10.2 ± 0.21	10.8 ± 0.14	10.8 ± 0.36
SiO ₂ SLD	3.47	3.47	3.47
SiO ₂ hydration	0.00	0.00	0
SiO ₂ roughness	2.35 ± 0.16	2.24 ± 0.16	4.18 ± 0.55
Cr thickness	10.3 ± 0.28	10.3 ± 0.16	10.4 ± 0.29
Cr SLD	3.02 ± 0.00	3.02 ± 0.00	3.02 ± 0.00
Cr hydration	0.00	0.00	0.00
Cr roughness	9.60 ± 0.47	9.60 ± 0.18	9.25 ± 0.43
Au thickness	200 ± 0.29	202 ± 0.22	203 ± 0.44
Au SLD	4.30 ± 0.02	4.12 ± 0.01	4.42 ± 0.01
Au hydration	0.00	0.00	0.00
Au roughness	6.52 ± 0.58	4.57 ± 0.12	5.43 ± 0.63
Tether thickness	6.28 ± 0.26	6.49 ± 0.18	6.78 ± 0.44
Tether SLD	0.61 ± 0.61	0.68 ± 0.02	0.66 ± 0.07
Tether hydration	11.6 ± 0.80	14.7 ± 0.15	13.5 ± 1.08
Tether roughness	6.52 ± 0.58	4.99 ± 0.04	4.15 ± 0.33
Inner HG thickness	5.98 ± 0.58	7.23 ± 0.33	7.06 ± 0.48
Inner HG SLD	0.84 ± 0.25	1.12 ± 0.07	0.89 ± 0.04
Inner HG hydration	11.1 ± 0.00	17.2 ± 2.47	14.6 ± 2.34
Inner HG roughness	4.92 ± 0.26	4.00 ± 0.01	3.68 ± 0.36
Inner HC thickness	13.8 ± 0.65	13.5 ± 0.19	13.9 ± 0.64
Inner HC SLD	-0.33 ± 0.06	-0.43 ± 0.01	-0.32 ± 0.05
Inner HC hydration	3.59 ± 0.35	3.63 ± 0.57	2.71 ± 0.19
Inner HC roughness	3.90 ± 0.09	4.95 ± 0.00	3.83 ± 0.41
Outer HC thickness	12.1 ± 0.64	12.6 ± 0.29	13.1 ± 0.45
Outer HC SLD	-0.14 ± 0.07	-0.17 ± 0.01	-0.36 ± 0.62
Outer HC hydration	2.46 ± 0.2	3.11 ± 0.00	3.37 ± 0.23
Outer HC roughness	8.24 ± 1.01	16.5 ± 1.19	9.70 ± 0.42
Outer HG thickness	12.6 ± 1.56	9.82 ± 0.13	13.4 ± 0.49
Outer HG SLD	3.75 ± 0.28	2.62 ± 0.08	2.65 ± 0.07
Outer HG hydration	71.6 ± 0.02	11.9 ± 0.94	46.1 ± 0.02
Outer HG roughness	4.01 ± 0.32	6.61 ± 0.13	3.56 ± 0.32

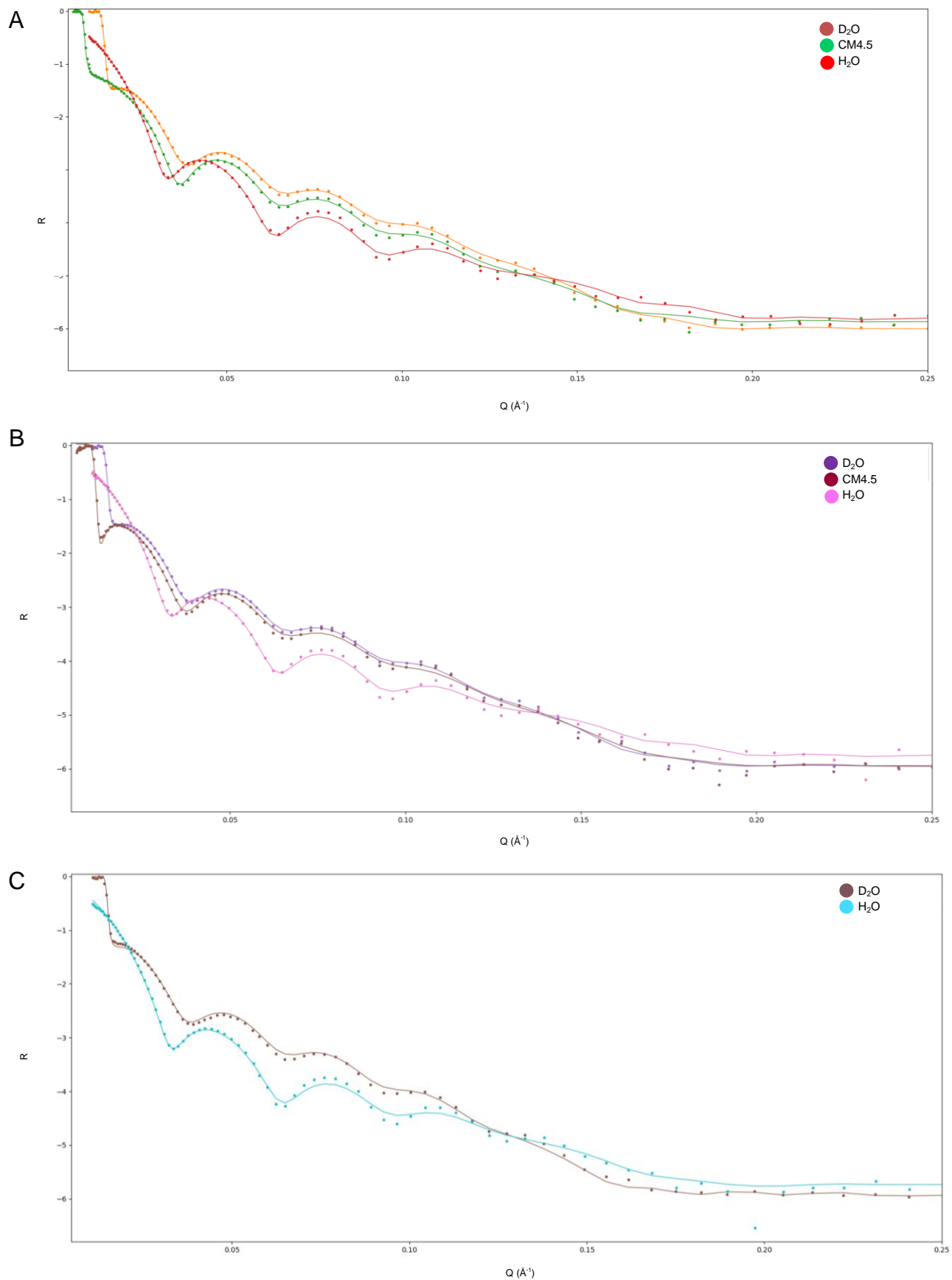


Figure S1: Reflectivity plot of LPS bilayer (A), bilayer after exposure to 100 μL cationic gold nanoparticles (B) and bilayer after exposure to 10 mg/mL Colistin sulfate (C).

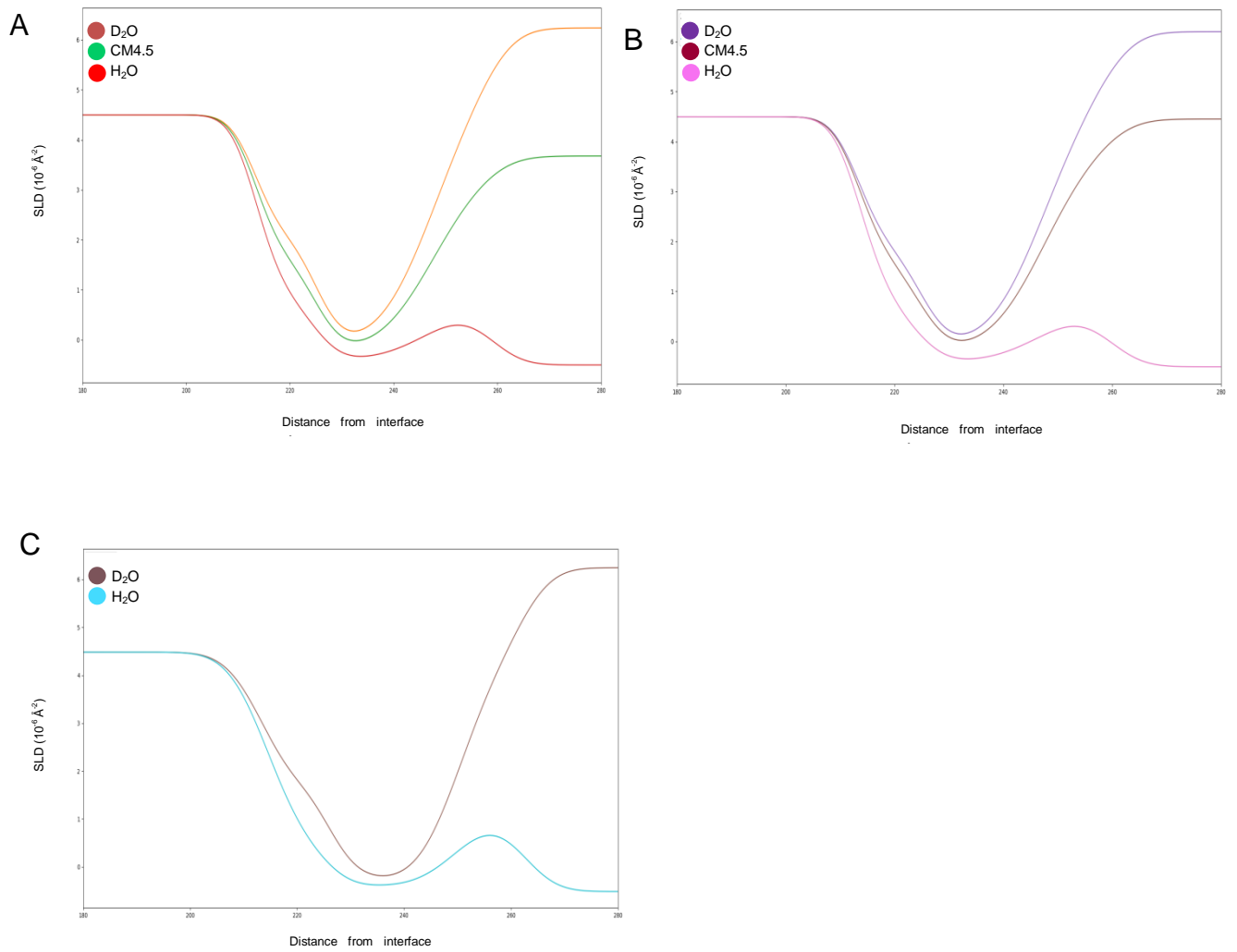


Figure S2: SLD plot of LPS bilayer (A), bilayer after exposure to 100 μL cationic gold nanoparticles (B) and bilayer after exposure to 10 mg/mL Colistin sulfate (C).

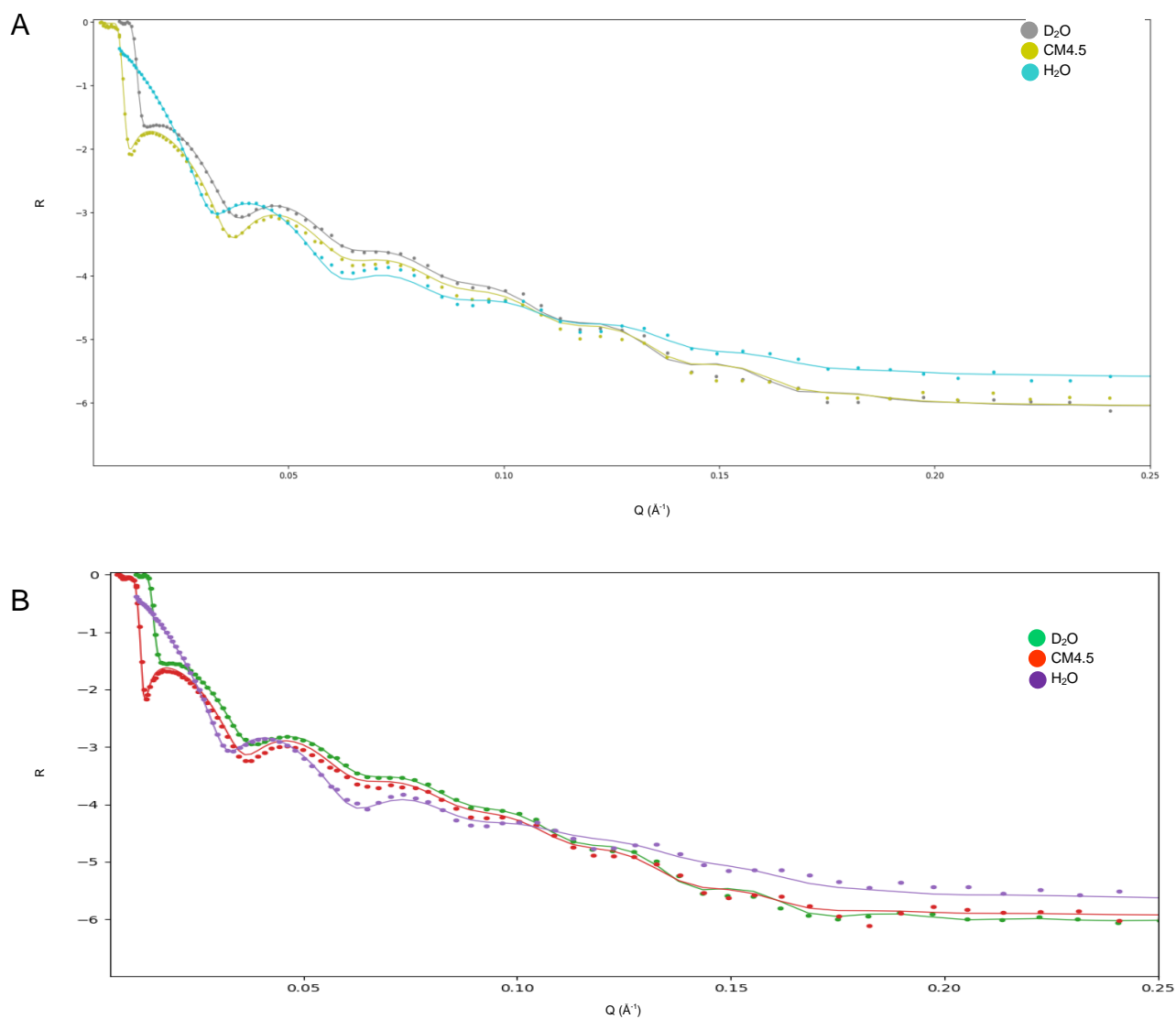


Figure S3: Reflectivity plot of LPS bilayer (A), bilayer after exposure to 100 μL cationic gold nanoparticles and 10 mg/mL Colistin sulfate simultaneously (B).

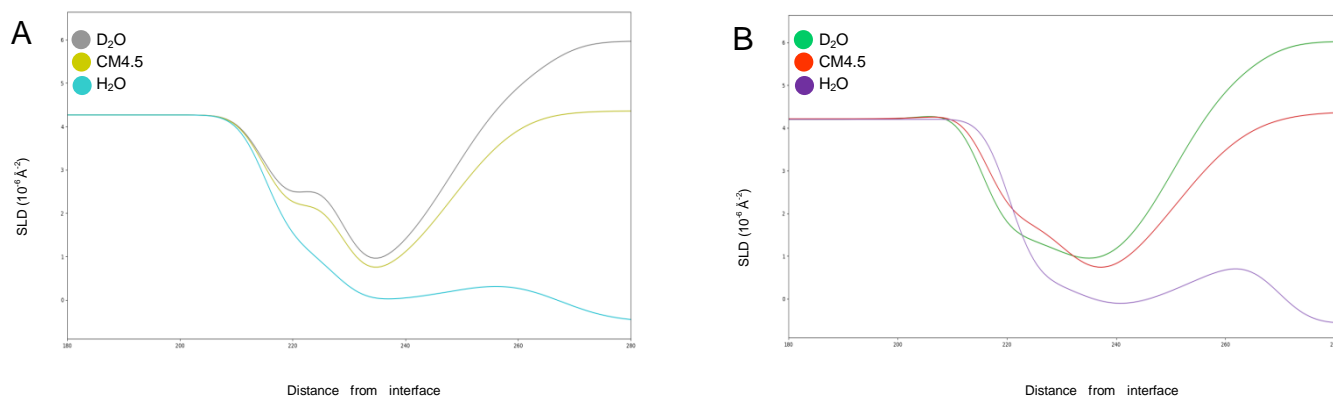


Figure S4: SLD plot of LPS bilayer (A), bilayer after exposure to 100 μL cationic gold nanoparticles and 10 mg/mL Colistin sulfate simultaneously (B).

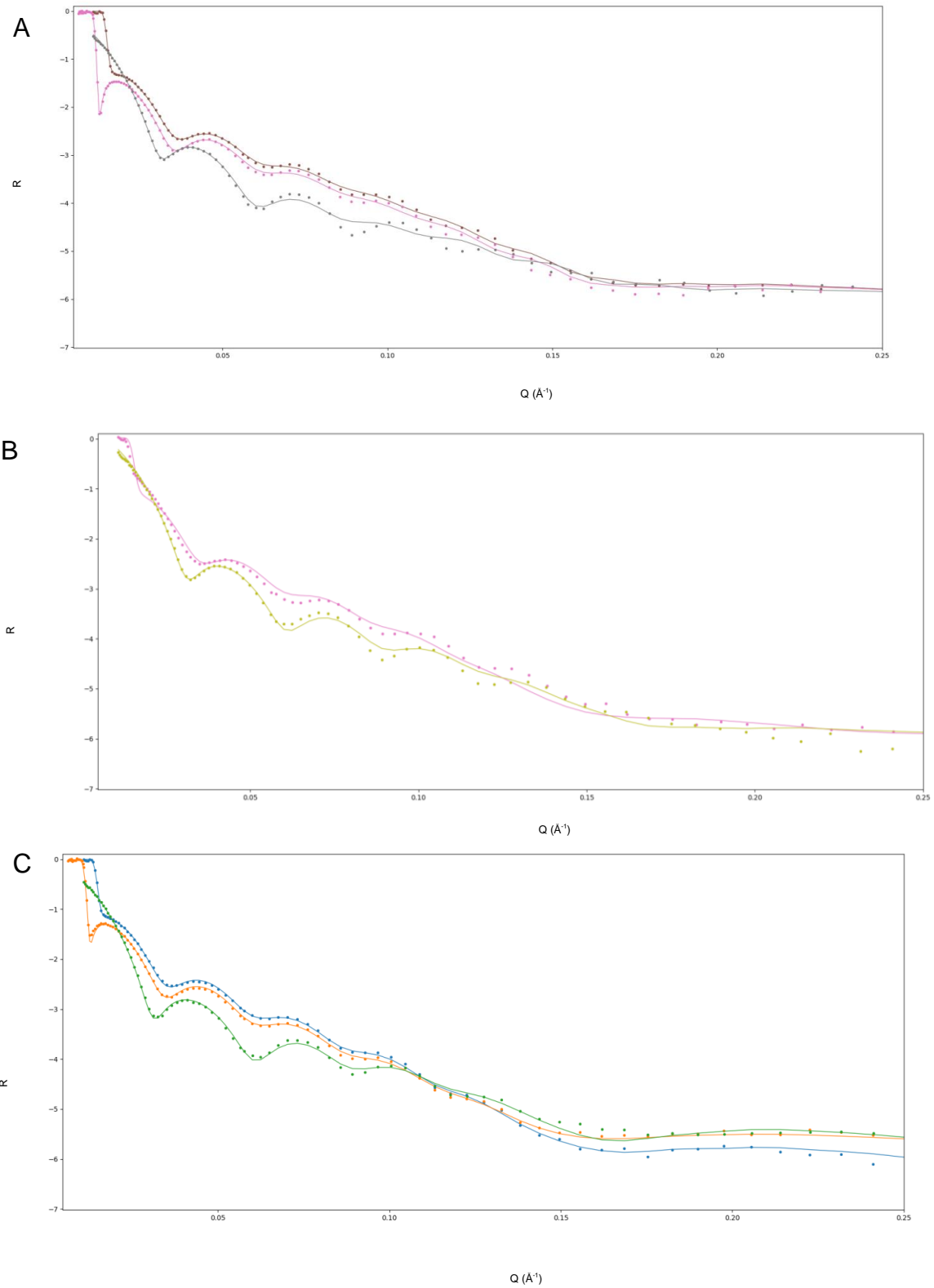


Figure S5: Reflectivity plot of LPS bilayer (A), bilayer after exposure to 1 mL cationic gold nanoparticles (B) and bilayer after exposure to 10 mg/mL Colistin sulfate (C)

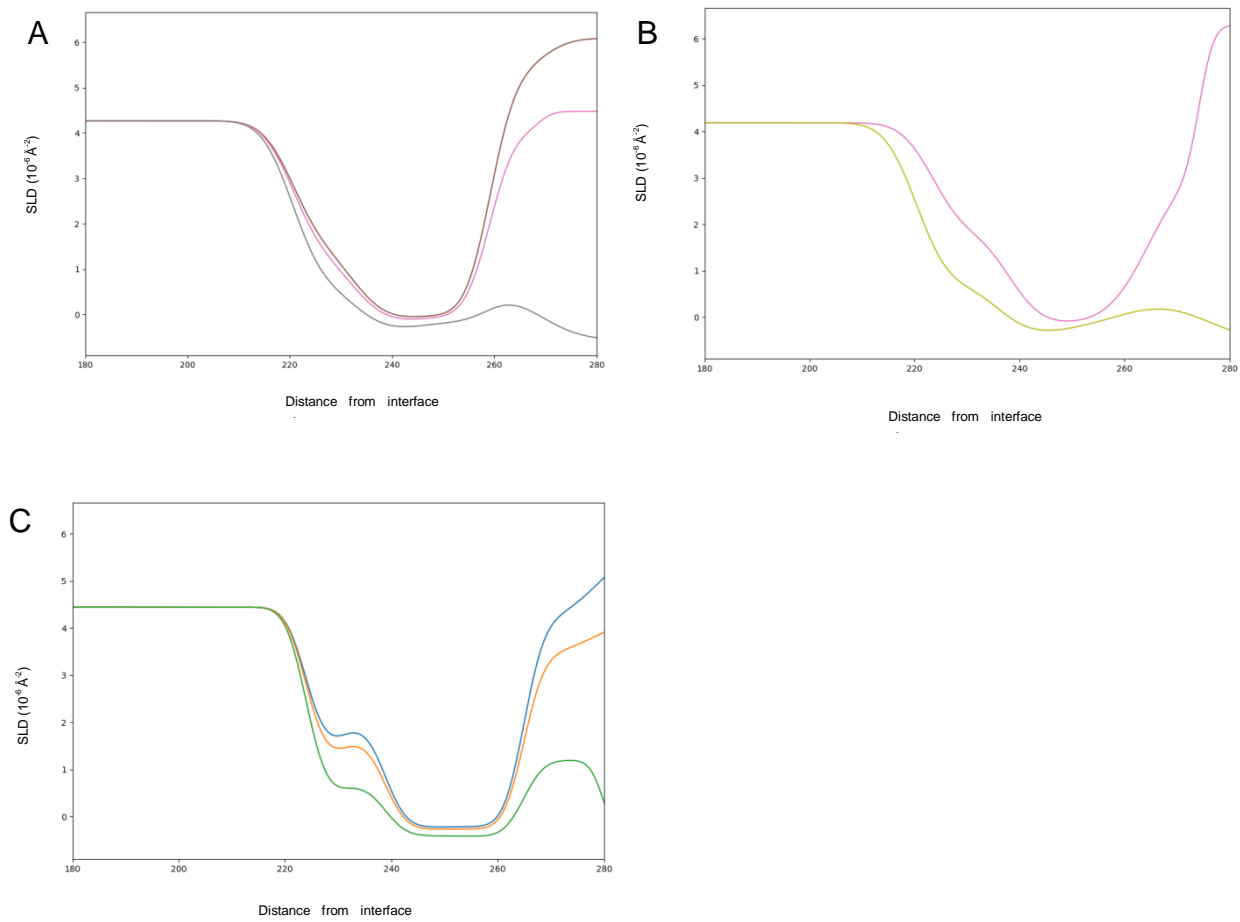


Figure S6: SLD plot of LPS bilayer (A), bilayer after exposure to 1 mL cationic gold nanoparticles (B) and bilayer after exposure to 10 mg/mL Colistin sulfate (C).

Appendix C:

Supplementary Information from Chapter 5; 'Delivery of Colistin using Gold Nanoparticles'.

Table S5: MIC experimental set-up showing constituents in well 1. Broth and bacteria indicate 50 μL nutrient broth and 50 μL of 10^3 CFU *E. coli* respectively. Concentrations of ColAuNP and Colistin are halved for each subsequent well prior to the addition of *E. coli*.

Plate 1	Well 1
A	50 μL ColAu(-) Broth Bacteria
B	50 μL ColAu(-) Broth Bacteria
C	50 μL ColAu(-) Broth Bacteria
D	50 μL ColAu(+) Broth Bacteria
E	50 μL ColAu(+) Broth Bacteria
F	50 μL ColAu(+) Broth Bacteria
G	Broth Bacteria
H	Broth

Plate 2	Well 1
A	50 μL Col Broth Bacteria
B	50 μL Col Broth Bacteria
C	50 μL Col Broth Bacteria
D	Blank
E	50 μL Au(-) Broth
F	50 μL Au(+) Broth
G	50 μL ColAu(+) Broth
H	50 μL ColAu(+) Broth

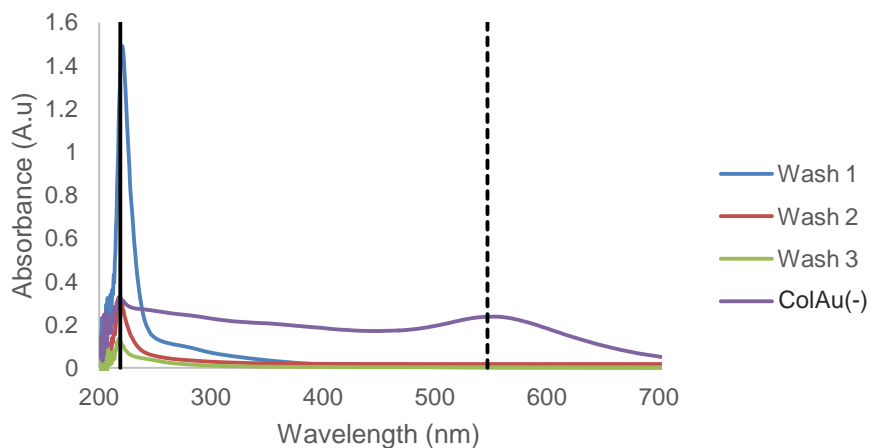


Figure S7: A: UV-Vis spectra of the ColAu(-) with three washes. The solid line shows the maximum peak of Colistin at 219 nm and the dotted line is the surface plasmon resonance peak of the gold nanoparticles at 555 nm.

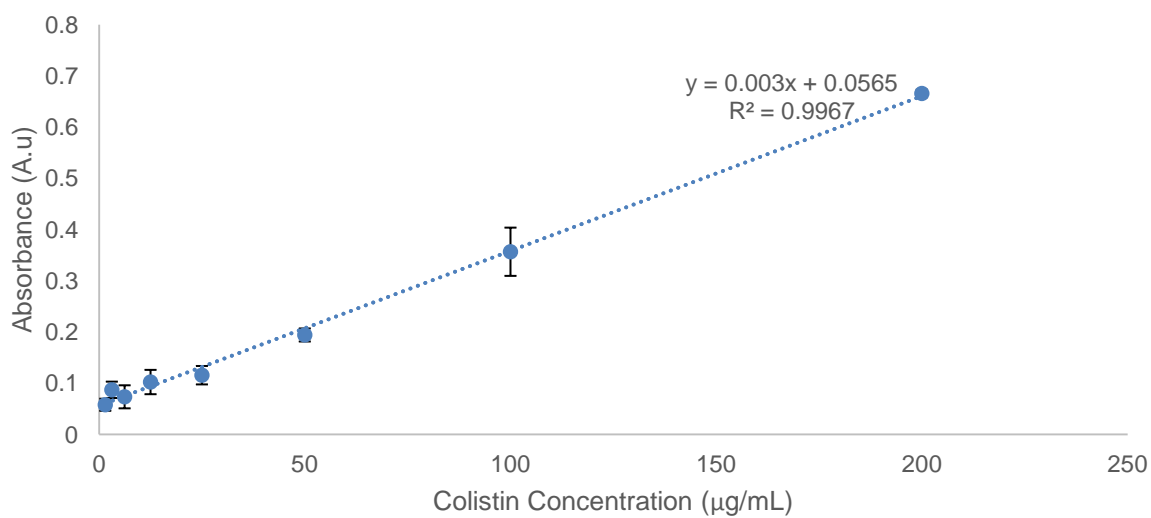


Figure S8: Calibration curve of Colistin Sulfate at a wavelength of 219 nm.

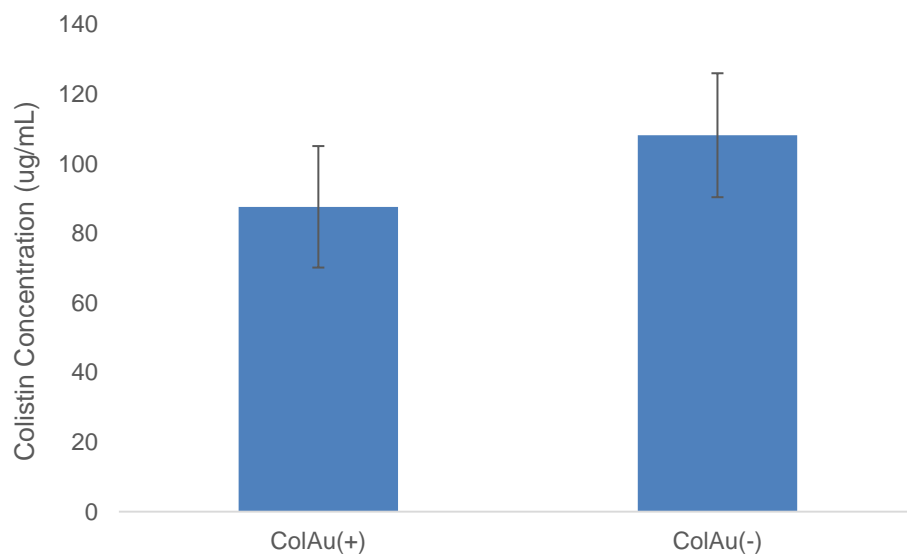


Figure S9: The concentration of Colistin present in ColAu(+) compared to the ColAu(-).

Appendix D:

Supplementary Information from the publication 'Nanoparticles in an Antibiotic-Loaded Nanomesh for Drug Delivery'.

Table S6: ImageJ analysis of fibre diameters for various PCL% w/w at 0.5 mg/mL and 1 mg/mL flow rates.

Sample PCL (%)	Fibre diameter at 0.5 mg/h (nm)	Fibre diameter at 1 mg/h (nm)
4	277 ± 72.0	312 ± 85.0
7	246 ± 76.0	293 ± 83.0
8	551 ± 313	549 ± 315
9	462 ± 184	418 ± 146
10	464 ± 204	465 ± 330

Table S7: Drug release kinetics of Colistin from various electrospun mesh samples.

Mesh Sample	Zero Order		First Order		Higuchi Model		Korsmeyer-Peppas Model		Hixson Model	
	R ²	K ₀	R ²	K ₁	R ²	K _H	R ²	n	R ²	K _C
Col	0.766	0.9696	0.789	-0.0065	0.9266	4.269	0.9849	0.0857	0.7814	0.0201
ColAu(-)	0.6403	2.565	0.1051	-0.0253	0.8274	11.674	0.9771	0.0744	0.2833	0.1844
ColAu(+)	0.7798	0.5346	0.8037	-0.0052	0.9193	3.612	0.9829	0.0878	0.7958	0.0163
ColVan	0.7014	0.7391	0.7763	-0.0127	0.8572	3.2567	0.9852	0.0316	0.7522	0.0286
ColVanAu(-)	0.4384	0.6214	0.7715	-0.0582	0.6206	2.9471	0.8842	0.0255	0.6583	0.0714
ColVanAu(+)	0.3886	0.4718	0.4221	-0.0044	0.555	2.2471	0.816	0.0351	0.4108	0.0122

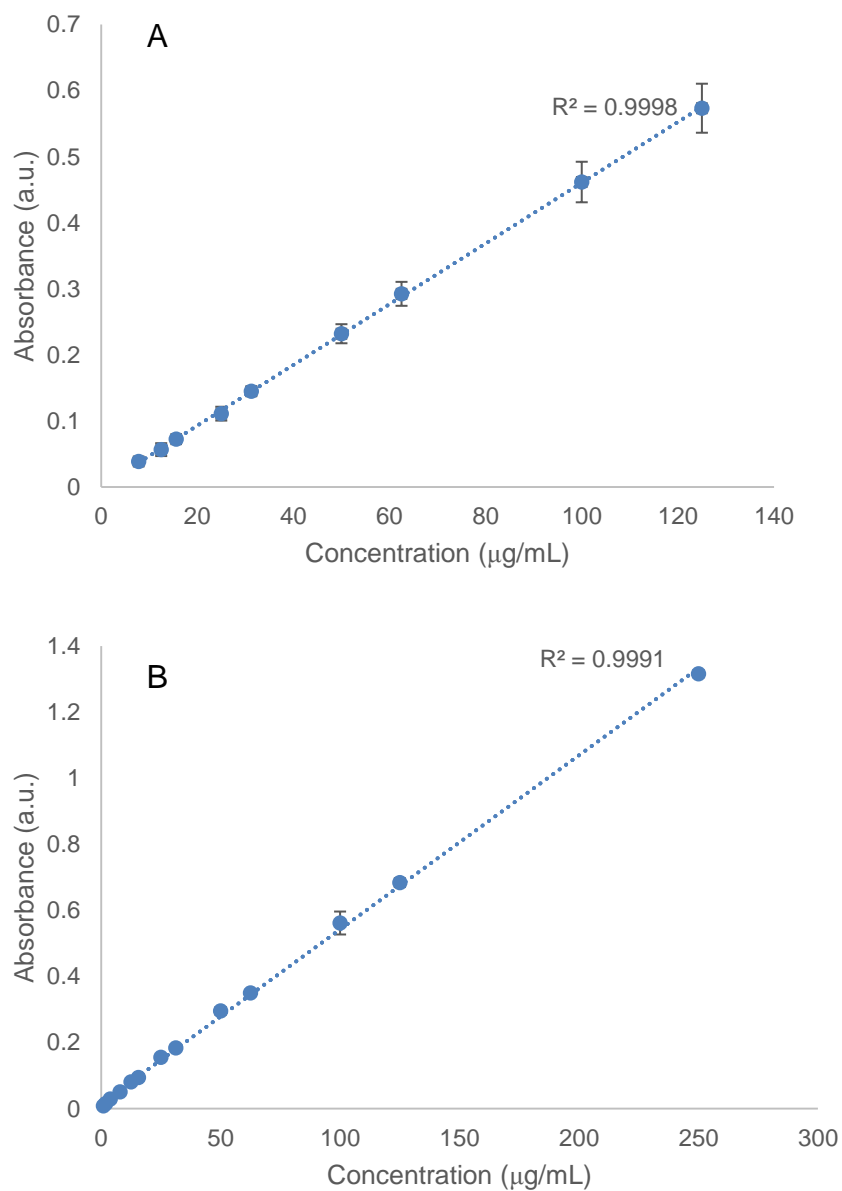



Figure S10: Calibration curves of (A) Colistin and (B) Vancomycin in DPBS using UV-Vis Spectroscopy at 214 nm and 290 nm respectively.

REVIEW

Open Access



Biomedical applications of polyelectrolyte coated spherical gold nanoparticles

Melanie A. Fuller and Ingo Köper^{*} 

Abstract

Surface modified gold nanoparticles are becoming more and more popular for use in biomaterials due to the possibility for specific targeting and increased biocompatibility. This review provides a summary of the recent literature surrounding polyelectrolyte coatings on spherical gold nanoparticles and their potential biomedical applications. The synthesis and layer-by-layer coating approach are briefly discussed together with common characterisation methods. The potential applications and recent developments in drug delivery, gene therapy, photothermal therapy and imaging are summarized as well as the effects on cellular uptake and toxicity. Finally, the future outlook for polyelectrolyte coated gold nanoparticles is explored, focusing on their use in biomedicine.

Keywords: Polyelectrolyte, Gold nanoparticles, Nanoparticles, Gold, Biomedical

1 Introduction

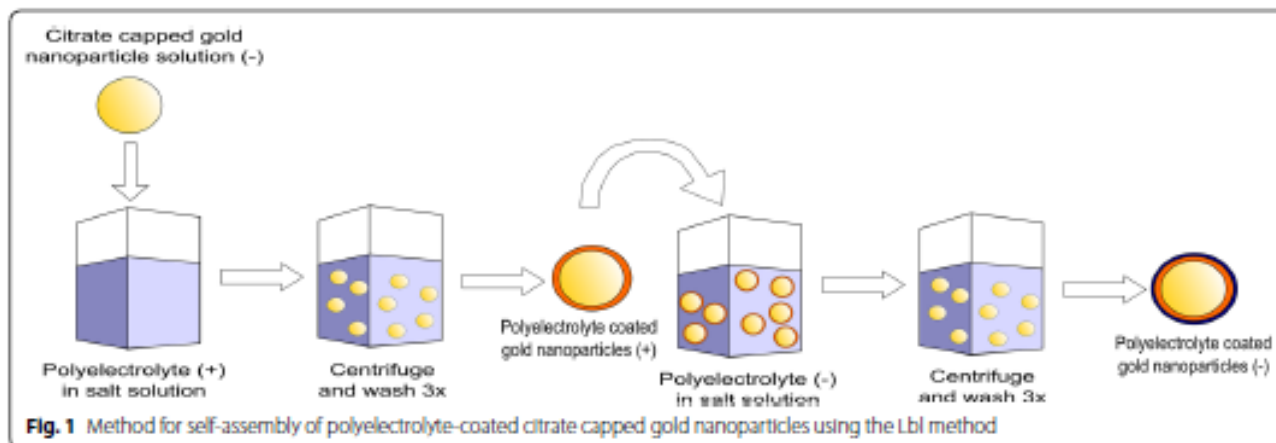
Gold nanoparticles (AuNPs) can be described as solid gold particles with a diameter between 1 and 100 nm, and have the potential to be used in a range of biomedical applications due to their unique physical and optical properties [1–4]. Examples of these unique properties include the surface plasmon resonance (SPR) effect, which can give information about the local particle environment as well as the physical dimensions of the particles. Furthermore, by employing the Surface Enhanced Raman Scattering (SERS), AuNPs can be used as probes to enhance Raman scattering applications [5–8]. After a typical synthesis, AuNPs are coated with an organic material or capping agent which provides stability to the particles. One of the advantages of AuNPs is that they can be easily functionalized with a range of different materials including antibodies, proteins, ligands, DNA, polymers and polyelectrolytes [9–11]. This ease of functionality is useful in many of the biomedical applications which are discussed here.

Polyelectrolytes (PEs) are polymers of repeating units which contain an ionizable group [12]. These charged polymers can be used to coat surfaces and particles in a

number of ways including covalent attachment, hydrogen bonding and electrostatic interactions between layers [13, 14]. While there are many ways PEs can be attached to nanoparticles (NPs), this review will focus on the electrostatic attachment of PE coatings as they are easy to produce and have a range of applications from microfluidics to water membrane filtration systems [14, 15]. Specifically, the Layer-by-layer (LbL) approach will be reviewed, where PEs can be attached to a surface in a single or multilayer deposition. Essentially the LbL electrostatic approach uses two solutions of opposite charge. A substrate can be dipped into a solution or a particle solution can be mixed with PEs to coat a surface (Fig. 1) [16, 17]. Once a coating of the polyelectrolyte has been added, the charge on the substrate or particle is inverted, and hence a subsequent polymer layer of opposite charge can be applied. The number of layers applied determines the total thickness of the polymer coating [13]. Due to the ease of deposition, LbL polyelectrolyte coatings have been initially investigated on flat substrates for a wide range of applications, but now the coating of 3-dimensional objects is also being explored [15, 18, 19]. These objects, such as spherical nanoparticles, offer larger surface area to volume ratios and larger reactive surface areas, which is essential in drug delivery and catalysis [20, 21].

The coating efficiency of the PEs on NPs is influenced by the shape of the nanoparticle, the type, length and

*Correspondence: ingo.koepfer@flinders.edu.au
Flinders Institute for NanoScale Science and Technology, Flinders University, Bedford Park, SA 5042, Australia



concentration of the polymer, as well as the total salt concentration in the solution used [22, 23]. Gold nanorods (GNRs) have been the most widely studied 3D particle shape for PE coatings, as their structure allows for relatively homogeneous coatings. Additionally, they have been extensively used in sensing applications, as their surface plasmon is particularly sensitive to changes in the local environment [20, 24–27]. This review however is focused on exploring spherical AuNPs, and comprehensive reviews of AuNRs can be found elsewhere [28, 29]. The curved surface of small (< 50 nm) NPs makes it difficult to form complete and homogeneous coatings, in part due to the lack of flexibility of the polymer chains, resulting in poor coverage on the nanoparticle surface and a decrease in stability of the coating [30]. In general, incomplete coatings can cause particle aggregation [23, 31, 32]. To avoid incomplete coatings, the polymer which is coating the NP needs to be in excess to ensure complete coverage on the surface [23]. Similarly the addition of salt in the coating solution typically allows for more flexibility in the PE chains, which can lead to an improved coverage of the particles [22, 33–35].

2 Synthesis of polyelectrolyte coated nanoparticles

There are many different approaches to synthesizing AuNPs, each aiming to control nanoparticle size, shape and surface functionality [36–38]. In the Turkevich

method, hydrogen tetrachloroaurate (HAuCl_4) is treated with citric acid in boiling water, with the citrate acting both as a reducing and stabilizing agent [39, 40]. This method produces NPs with diameters in the range of 10–20 nm, with the particle size being controlled by the gold to citrate ratio [41]. Alkanethiol-stabilized AuNPs, which are soluble in organic solvents, can be formed using tetraoctylammonium bromide (TOAB) as the capping agent and sodium borohydride (NaBH_4) as the reducing agent [42]. Depending on the gold-to-thiol ratio, temperature and reduction rate, NPs between 1.5 and 5 nm in diameter can be produced [42]. Other synthesis methods resulting in size and particle uniformity distributions use different reducing agents such as sucrose, ethylenediaminetetraacetic acid, fruit extracts and amines [43–47].

The capping agent used in the NP synthesis influences which PE can be used for the initial coating. The Lbl technique is based on the attraction of oppositely charged layers and is the main interaction employed in coating AuNPs with PEs. Commonly used PE polymers are shown in Table 1. The charge of the PE is important as the polymer will electrostatically attach to a particle only if the capping agent is of opposite charge [14]. For example, after the Turkevich method which caps the particles in negatively charged citrate, only positively charged PEs will attach.

Table 1 Commonly used polyelectrolytes showing their charge at pH 7 and their current applications

Abbreviation	Name	Charge at neutral pH	Application	References
PEI	Polyethylenimine	Positive	Gene therapy, drug delivery	[48, 49]
PAH	Polyallylamine hydrochloride	Positive	Drug delivery, gene therapy	[50, 51]
PSS	Polystyrene sulfonate	Negative	Drug delivery	[52, 53]
PLL	Poly-L-lysine	Positive	Gene therapy	[54]

3 Characterising the attachment of polyelectrolytes onto gold nanoparticles

Typically, the attachment of PE coatings on AuNPs is characterized using Surface Plasmon Resonance (SPR), Dynamic Light Scattering (DLS) and zeta potential. Other methods such as Transmission Electron Microscopy (TEM) and Nuclear Magnetic Resonance (NMR) are commonly used but will not be discussed here.

3.1 Surface plasmon resonance

A surface plasmon is a charge-density oscillation phenomenon, which exists at the interface of two media with dielectric constants of opposite signs [55]. Noble metals have a negative dielectric constant and are therefore ideal materials for surface plasmon detection. When light of a specific wavelength interacts with a AuNP, it causes a collective oscillation of the free electrons in the metal [56]. When the incoming electromagnetic wave has the same wavevector as the oscillating conduction electrons, resonance occurs (Fig. 2) and the incoming energy is absorbed into the plasmon wave. Typically, SPR is observed by measuring the absorbance of the NP-containing solution as a function of wavelength. The resulting signal depends on the shape, size, surface ligand, solvent, temperature and proximity of other NPs in the solution [57, 58]. For example, spherical AuNPs exhibit size dependent absorption peaks (surface plasmon band) from 500 to 550 nm [11, 59].

Aggregation of NPs can be observed by a red-shifting and broadening of the SPR peak, and the colour of the NP solution changes from a red to blue due to interparticle plasmon coupling [60]. The addition of a polymer layer onto the surface of the AuNP results in a change in the dielectric properties at the nanoparticle surface which shifts the SPR peak (Fig. 3a, b) [30]. As each polymer layer is added, the peak's wavelength increases as the dielectric property changes. Due to this, the Lbl addition

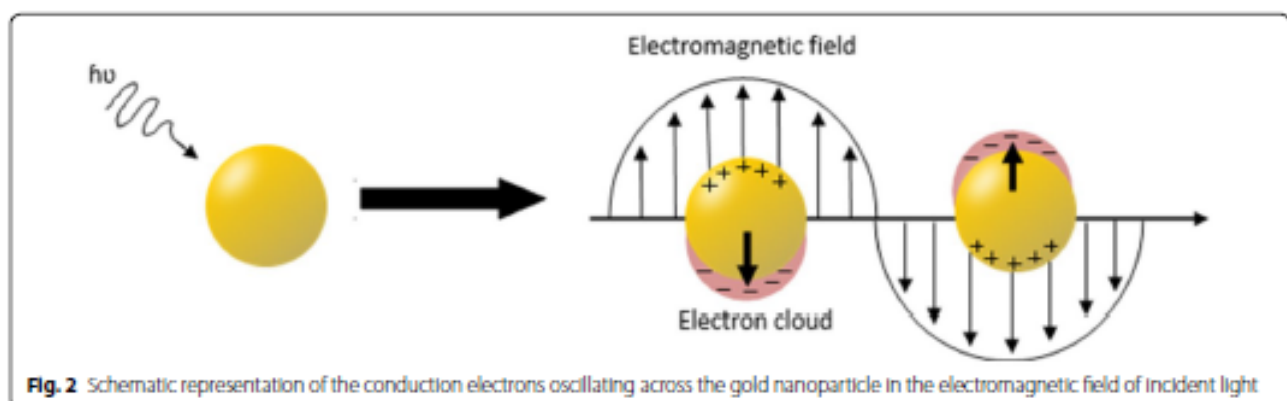
of PE multilayer architectures can be monitored through changes in the NPs SPR peak (Fig. 3a).

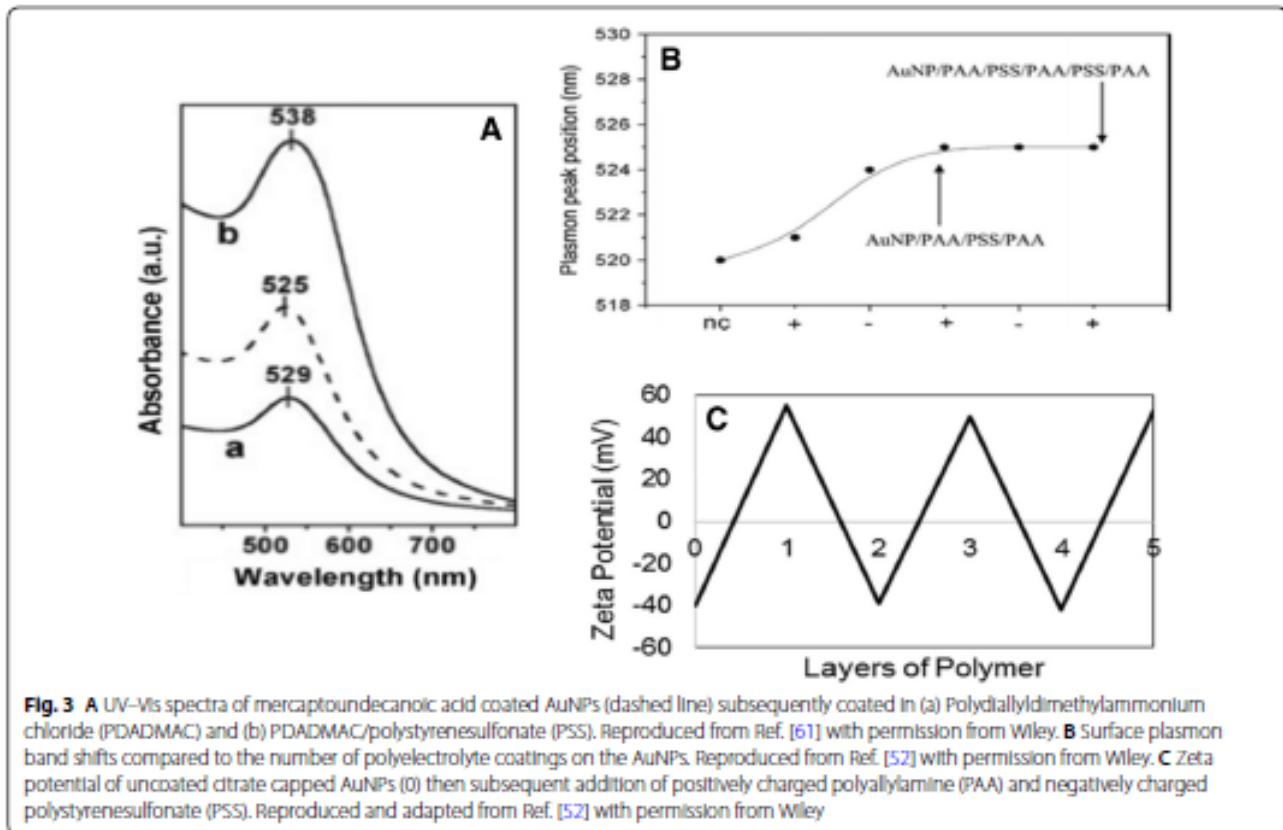
3.2 Zeta potential

Measuring the zeta potential of AuNPs is a quick and efficient way to determine the charge of the particles and the stability of the colloidal system [62]. The zeta potential can be described as the potential at the shear plane of a solid particle moving under an electric field, where the shear plane is the boundary at the solid–liquid interface, between the stationary and diffuse layers [63, 64]. At neutral pH, citrate capped AuNPs have a resulting negative charge, which attracts positively charged electrolyte ions. These ions then form an electrical layer at the surface of the particle, known as the Stern layer. A secondary layer called the diffuse layer also forms, which consists of both positive and negative ions with a high counter-ion charge. Together these two layers make up an electrical double layer. The zeta potential of the particle corresponds to the amount of energy required to shear a particle and associated double layer from the bulk solution. In order to calculate the zeta potential, the electrophoretic mobility of a particle is measured in a direct current electric field [62]. Stable colloidal solutions typically have zeta potentials smaller than -30 mV or larger than $+30$ mV. Values between these potentials indicate unstable solutions, as the particles do not carry enough charge to repel each other, which can lead to aggregation [65]. In the case of PE-coated NPs, the charge of the coated particles alternates between a positive and negative charge, depending on the polymers used (Fig. 3c). This process is often used to show attachment of the polyelectrolyte layer, as well as to confirm the colloidal stability of the system.

4 Uptake and interaction with cells

Biocompatibility is essential in any biomedical application as well as the ability for the uptake of NPs into cells, especially for applications such as drug delivery.





The interactions of the particle with the cell membrane is ultimately what determines cellular uptake, as it is the key to the regulation of the uptake process [66]. Cellular interactions and cellular uptake is a large and complex topic area and hence, this section will only discuss the main considerations with select examples. More in-depth explanations in this area can be found in other review articles [67, 68]. The cellular uptake of AuNPs is dependent on the size, charge and surface properties of the NP [69]. Other biological factors include the type of cell, cellular recognition and the temperature [70]. These biological factors also affect the protein corona, which is a protein layer attached to the AuNP, brought about by the proteins found in the body (in vivo) and in serum (in vitro) which attach to the NPs surface [70].

There are five ways in which mammalian cells can internalize nanoparticles: phagocytosis, macropinocytosis, clatherin-mediated, caveolin-mediated and clatherin/caveolin-independent endocytosis [71–74]. Of these pathways, clatherin and caveolin mediated endocytosis are often widely grouped as receptor mediated endocytosis [66, 75–77]. It has been proposed that receptor mediated endocytosis is the primary mechanism for cellular entry of AuNPs less than 100 nm in diameter into mammalian cells [67, 78]. In receptor mediated endocytosis,

NPs which have ligands on their surface that target specific receptors, attach to the cells by receptor–ligand binding. The membrane of the cell then wraps around the NP, internalizing it into the cell. The kinetics of this process depend on the size of the NP, with generally a faster uptake for larger NPs [70, 78]. However, the size and uptake will change depending on the protein corona and its composition when it forms around the particle. The addition of serum to in vitro assays provides a more realistic biological environment, as the proteins in the serum can attach to the NP forming the protein corona. This corona prevents the NP from having direct contact with the cell membrane, hence altering the uptake. The uptake rate is determined by the receptor diffusion kinetics and the thermodynamic driving force for the membrane wrapping [78]. This rate was shown to be dependent on the cell type, particle size and the composition of the protein corona.

Fastest cell uptake has been shown for NPs with diameters of around 55 nm. The chemical energy released by the receptor–ligand interaction produces enough free energy (thermodynamic driving force) to drive the NP into the cell [78–80]. For NPs smaller than 40 nm in diameter, the receptor–ligand interactions cannot provide enough energy to ‘wrap’ the NP on the cell’s surface

as there are fewer ligands that can interact with receptors, and not enough chemical energy is produced to overcome the more unfavorable deformation of the cell membrane [80]. In order for smaller NPs to be taken into the cell, clusters of NPs are required to overcome the energy barrier to internalization [78]. However, when taking into account the protein corona, for 50 nm diameter AuNP in serum, the presence of the corona decreased the uptake efficiency significantly, with a 70% decrease in RAW 264.7 cells (model mouse macrophage cells) and a 40% decrease in Hep G2 cells (human liver cancer cells). For 20 nm and 5 nm AuNP, it was found the inhibitory effect of the corona on cellular uptake becomes negligible for both types of cells [70]. Even with a considerably lower uptake efficiency, the uptake was still higher in larger (50 nm) AuNP, suggesting for biomedical applications, ≥ 50 nm AuNPs should be used [70].

The influence of the surface charge on cellular uptake is relatively well understood, but also dependant on a number of experimental factors. These experimental factors, including particle size, surface functionalisation, NP shape and cell type are often observed to interplay with each other, making identifying differences of one variable a complex endeavour. Typically, positively charged NPs are more easily taken up by the cell, probably due to being attracted by the negatively charged cell membrane [81–83]. However, proteins from the growth serum of cells can absorb to both cationic and anionic particles, forming a protein corona which has the potential to alter their charge and thus minimizes attractive forces [84, 85]. The effect of proteins adsorbing onto AuNPs has been observed through numerous studies including absorption on curcumin-functionalized AuNP where the uptake in human prostate cancer cells was decreased when curcumin-AuNP were in the presence of serum containing media compared to serum-free media [86].

The localization of the NP inside the cells is important for biomedical applications but once again the intracellular distribution of AuNPs depends on a number of factors including size, concentration, and serum/media type. NPs with no specific surface functionalisation and a diameter of less than 6 nm have been shown to enter the nucleus of various cells [87–89]. Similarly, other studies have observed that diameters of greater than 6 nm do not enter the nucleus but often enter cells inside vesicles [78, 90–92]. Knowing the size range of NPs which reach the nucleus is important for inducing apoptosis in cells when treating conditions such as cancer and therefore, needs to be taken into consideration depending on the application.

The biodistribution of AuNP when injected into mice, was observed to change depending on the charge of a 2 nm core AuNP [93]. Although the research did not use

PEs to alter the charge, similar results would be expected when using PEs. It was found that positively charged NPs accumulate in the filtering regions of the spleen and liver, indicating they filter from the bloodstream at a faster rate than anionic or neutral NPs. The neutral NPs were shown to accumulate in the arteries and negatively charged NPs were found homogenously distributed within the kidney. Another key difference was the neutral NPs which were shown to interact with the immune system. This interaction however, may be due to the type of proteins which make up the corona surrounding the particle [93].

In terms of PE coated AuNP, there was very little research found surrounding the uptake and cellular interactions. Thus, the majority of uptake and interaction research has come from studies on AuNP with a large variety of coatings. When comparing experiments for AuNPs, despite it being such a large research area, it is difficult to form conclusions for *in vitro* studies, as there are many complex parameters which dictate the cellular response. The cell type, serum used, AuNP size, concentration and charge among others can alter the outcome significantly. Similarly another difficulty is being able to predict the biodistribution as the protein corona which forms when the NPs enter the body, (*i.e.* blood, lung etc.) changes as the NP is transported through different regions such as the bloodstream [93]. Overall the uptake and distribution is a complex interplay between different experimental factors which makes drawing direct comparisons difficult.

5 Applications

The unique optical and physical properties of AuNPs and the increased biocompatibility of PE-coated nanoparticles has led to a range of potential biomedical applications, including drug delivery, gene therapy and cancer therapy (Table 1) [50, 52, 53, 69, 94]. The type of PE used has a significant influence on the usage of particles and the interaction of particles with tissues and cells. A fundamental understanding of the influence of the PEs on interactions with biological material is hence crucial to optimize their use. There are two main delivery methods for drug delivery: targeted and non-targeted. In targeted delivery, a ligand, generally an antibody or peptide, is attached to the NP and will target a receptor on a specific cell [95, 96]. Non-targeted delivery is the delivery without targeting specific cells, where the drug will be released to both healthy and diseased cells. The type of delivery is extremely important in applications such as gene therapy and photothermal therapy, where treatment needs to be given into a specific area of the body. siRNA delivery for example will target a specific cell's cytoplasm to achieve down-regulation (80–90% decrease) of an overproduced protein [97]. Similarly in photothermal therapy, ensuring

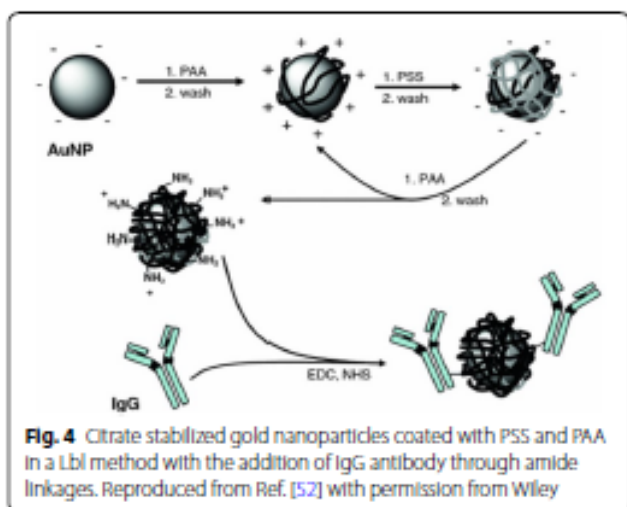
the AuNPs reaches the diseased cells to cause cell death rather than healthy cells is vital to reduce collateral damage [98].

5.1 Drug delivery

Targeted drug delivery allows for an increased concentration of drug to be given to a specific cell type compared to conventional untargeted delivery. In many cases this higher concentration increases the efficacy and decreases unwanted side effects, especially useful for drugs that can have debilitating side effects such those used in chemotherapy. Attaching ligands such as antibodies to the surface of a drug carrier allows drug release into specific cells which have the correct receptors.

For targeted drug delivery, PE coatings can be used as anchoring points for antibodies. This was shown in a proof of concept study, where IgG monoclonal antibodies, which target proteins overexpressed in cancer cells, were anchored to the surface of polyallylamine (PAA) and PSS coated AuNPs (Fig. 4) [52]. Conceptually, this could have great implications for the cancer treatments, as drugs could be loaded inside the AuNP or within the PE layers and then be targeted to cancer cells by the antibody attached on its surface. This would mean a lower dose of chemotherapy could be given with less systemic exposure, lessening the side effects and increasing the survival rate. Issues, however, with this type of antibody targeting is the administration into the body, where unlike an *in vitro* test there are many proteins which attach themselves to foreign bodies like NPs, making the receptor to antibody attachment problematic.

One of the advantages of the PE systems is that water insoluble drugs, which previously have been difficult to deliver, now have an easier pathway [99]. This is shown to be possible through the use of multilayer based drug

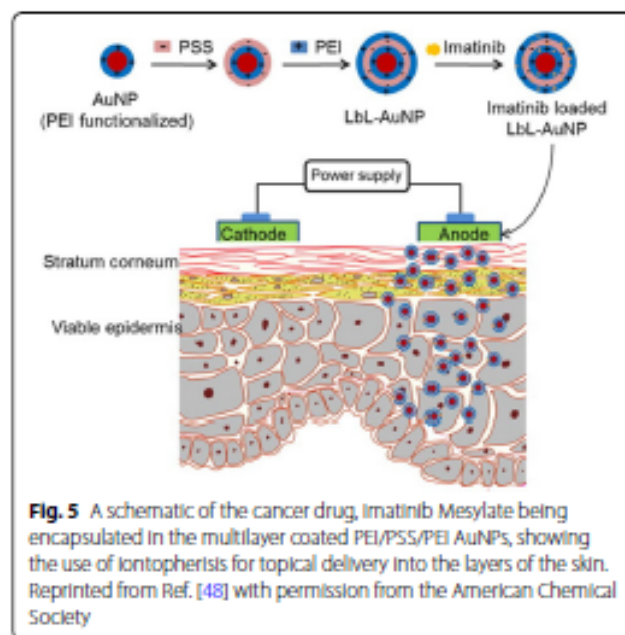


carrier systems, where a vehicle such as a NPs can have water-insoluble drugs encapsulated within its PE chains. In a proof of concept study, three polymer layers with one containing a water-insoluble drug, were absorbed onto a NP carrier and this carrier was able to increase the drug deposition efficiency by a factor of 100 [53]. In order to trap the drug, citrate coated AuNPs were used, then subsequently coated with polyallylamine hydrochloride (PAH) before the complexed drug was mixed with PSS and electrostatically attached to the PAH coating.

A more recent proof of concept study has found that the drug, Imatinib Mesylate (IM), used for cancer treatment could be encapsulated into PSS/PEI multilayer functionalized gold nanoparticles (Fig. 5). This IM-PSS/PEI-AuNP system was tested in several ways with uptake into B16F10 murine melanoma cells measured as well as an *in vitro* skin penetration study [48]. At a gold concentration greater than 50 μM and IM concentrations above 31 μM , the IM-PSS/PEI-AuNP had a significantly higher growth inhibition of cancer cells compared to IM alone. The *in vitro* skin penetration studies conducted using pig ear skin, showed the use of iontophoresis (voltage gradient on the skin) enhanced the skin penetration of the IM-PSS/PEI-AuNPs. Thus a topical treatment of IM-PSS/PEI-AuNPs with iontophoresis shows potential for enhanced melanoma treatment compared to IM alone.

5.2 Gene therapy

Small interfering RNA (siRNA) delivery has the potential to be used in therapeutics to temporarily silence genes which could have significant effects on genetic diseases,



however siRNA are notoriously difficult to deliver due to instability [100]. PE coated AuNPs have been shown to be better delivery vehicles than commonly used polymer vehicles [49]. Other delivery platforms such as cationic lipids and polymers have shown promise however instability is often the biggest issue, leading to decreases in efficacy [69]. In a proof of concept study, siRNA has been attached onto a PE coated AuNP system and delivered into CHO-K1 cells (hamster ovary cells) which express enhanced green fluorescent protein (EGFP) [69]. The siRNA successfully reduced the EGFP expression and the cells remained viable after the addition of the AuNPs.

The current gold standard for non-viral gene transfection is using PEI or Lipofectamine. PEI is a polyelectrolyte in its own right, however, in this case, it is used to form a polyplex with DNA, rather than as a coating. This gold standard has been recently challenged in a study which synthesized PEI (25 kDa) coated AuNP as DNA nanocarriers which found that these nanoparticles were more efficient gene vectors than both Lipofectamine and un-modified PEI [49]. PEI coated nanoparticles also showed low cell cytotoxicity and were fabricated in a simple one-pot method. Thus PE coated gold nanoparticles show great promise for gene transfection in the future, as they can out-perform the current gold standard.

One of the challenges with using PEs is that the strong interaction of oppositely charged polymers often leads to retardation of the payload release. Changing the pH of the PE system can be a way to overcome this problem by allowing for a charge reversal of the PE in acidic conditions, leading to release of the siRNA. Using the charge reversal method, a study which used PEI/PAH-Cit/PEI/MUA-AuNPs to release siRNA into cancer cells was able to knock-down 80% of Lamin A/C protein expression in acidic conditions, whereas the siRNA remained attached at a neutral or basic pH [94]. Interestingly, the siRNA was released with 14% more efficiency than what is commercially available for this knockdown.

5.3 Photothermal therapy

Hyperthermia is a cancer treatment that has been used since the early 1990s [101]. When heat, typically just above the physiological temperature, is generated in a region of the body, it can lead to damage and destruction of cells [101]. In Photothermal therapy, the heating is more intense and is applied to a specific area though the use of NPs, resulting in fewer unwanted side effects compared to the hyperthermic treatment [102]. AuNPs can be targeted to a site in the body (i.e. a tumor) by manual injection or through targeted delivery. An external laser with a wavelength between 650 and 1350 nm is then aimed at the specific site where the NPs absorb or scatter that light [103]. This wavelength range is important

as it can deeply penetrate through healthy tissue to reach the AuNPs. The absorbed light causes resonance and is converted into heat, which is released to the surrounding tissue causing cellular death. Although this concept has been shown in several examples, so far PE coated AuNPs have not been used. However, PE-coated GNRs have been shown to be effective in killing cancer cells in mice and cell lines through photothermal therapy [104–107]. Compared to GNR, there is little research surrounding spherical AuNPs for use in Photothermal therapy, likely due to the potentially limited applications, as this therapy seeks to penetrate and heat the deeper tissue with near infrared (NIR) light. As spherical nanoparticles tend to have absorbance between 500 and 550 nm, this does not target the NIR region and thus will not penetrate deep tissue in the same way as other shapes such as nanorods would [108]. Recent studies using AuNP have overcome this by using aggregated or clustered nanoparticles, as this shifts the absorbance peak to higher wavelengths, allowing the wavelength of absorption to be within the therapeutic window [109, 110].

5.4 Imaging

Imaging in medicine is an important tool for a number of procedures including the localization and diagnosis of cancers. The optical properties of gold make it very attractive for use as a contrast agent in imaging. So far, PE coated GNRs have been used for imaging applications rather than spherical AuNPs. A comprehensive review on PE GNRs and their imaging capabilities can be found by Pissuwan and Niidome and is not within the scope of this review [29].

Photoacoustic (PA) imaging and computed tomography (CT) are also useful tools in clinical practice for imaging. PA imaging is based on the PA effect, where pulsed laser light is utilized as probing energy which produces acoustic waves by thermal expansion. These waves are then detected at the surface of the tissue by ultrasound and are re-constructed to form an image [111]. A study in which PEG-b-poly(ϵ -caprolactone) was tethered to AuNPs showed a strong plasmon coupling effect where NIR absorption induced plasmon coupling causing an increase in PA signal with high conversion efficiency [112]. Similarly AuNP have also shown promise as CT contrast agents due to their favourable properties. CT images are produced by a combination of X-ray images taken at different angles by rotation around an object, to form a cross-sectional 3D image known as a CT scan. Depending on what is being imaged, contrast agents can be used to highlight specific areas such as blood vessels or the tissue structure of organs by attenuating the X-rays to improve image quality [113]. Gold nanoparticles are being explored for their use as a contrast agent

in CT due to gold having a high atomic number and electron density, meaning it has good X-ray attenuation ability. In an experiment using a range of sizes of PEGylated AuNP as a contrast agent for CT scans, it was found NPs with a size of 13.2 nm and sizes greater than 34.8 nm performed ~20% better in attenuation intensity than Idohexal, a common CT contrast agent [114]. Thus the area of imaging is extremely promising for PE coated AuNP and AuNPs in general.

6 Toxicity

The cytotoxicity of AuNPs is extremely important, especially if they are being used in the biomedical field. The cytotoxicity is dependent on the size, shape, functionalisation, surface charge and aggregation of the NPs as well as biological factors including the type of cell and the uptake mechanisms into the cell [115–119]. PE coatings on AuNPs appear to be relatively non-toxic to cells, however other factors including the type of coating and the NP size need to be considered. For example, PAH coated 18 nm diameter AuNP were compared with CTAB, citrate and poly(acrylic acid) (PAA) coated AuNPs. They were exposed to SH-SY5Y (human neuroblastoma) cells for 24 h and after incubation all coatings except the CTAB coating showed >95% cell viability. Interestingly, when 40 nm PAA coated AuNP were used, cell viability dropped considerably to only 10% using the same gold concentration [120]. Another study has a similar result, where 10 nm diameter PEI coated AuNP showed to be biocompatible through *in vitro* cytotoxicity studies, where in gold concentrations of up to 400 μM they were shown to be non-toxic to three different cancer cell lines (HCT116 colorectal carcinoma, MCF7 breast adenocarcinoma and PC3 prostate adenocarcinoma) [121]. Whereas, the 23 nm diameter PEI coated AuNP showed a moderate level of cytotoxicity to the same three cancer cell lines, with IC_{50} results below 80 μM [121]. In both experiments the larger nanoparticles proved to be more cytotoxic than their smaller counterparts. In contrast to this, a recent study has found that *in vitro* toxicity of PEG coated AuNPs is dependent upon size of the particles and the dose, with smaller size and higher concentration leading to increased cytotoxicity [2]. Similarly in another study, 1.4 nm AuNPs were found to be 100 times more toxic than 15 nm AuNPs using the same coating [122]. Thus there are discrepancies found about size and toxicity throughout the literature which further emphasizes the complexity of experimental design, especially when testing *in vitro*.

With many discrepancies found, drawing conclusions from the collective body of evidence is difficult as results vary depending on a number of experimental factors. The toxicity seems to be dependent on the size, surface

functionalisation, concentration and surface charge of the AuNP as well as cell type, serum used, incubation time etc. Although there are many studies on AuNP toxicity, there are very few studies on the toxicity of PE coated AuNP. In order to understand the role PEs play in the toxicity space, standardized protocols for both *in vivo* and *in vitro* studies including appropriate cell types, assays and dosages would be beneficial to directly compare different coatings to determine the toxicity in a range of cell types.

7 Conclusions and future outlook

The available literature on PE coated spherical AuNPs is limited compared to AuNP with other coatings or its PE coated GNR counterpart. The interaction of AuNP with cells as well as their uptake is dictated by a range of parameters and despite a large body of research, drawing conclusions is difficult as there are many inconsistencies and complexities to consider. Variables such as the cell type, the medium used, AuNP size, concentration and charge, among others, can significantly alter the outcome and hence care needs to be taken when comparing results from literature.

In this review it was found that typically, ≥ 50 nm diameter AuNP have the highest uptake efficiency compared to smaller AuNPs. In terms of biomedical applications, PE coated AuNPs have shown great potential in areas such as siRNA delivery, imaging and drug delivery. PE coated AuNPs have shown to be very effective as siRNA carriers—even more so than the current gold standard of gene transfection. In addition, proof-of-concept studies have indicated they can be used as effective drug delivery vehicles. Also the use of AuNP in imaging techniques such as photoacoustic imaging and computed tomography have shown great promise in initial studies, with PEGylated AuNPs out-performing Idohexal, a common CT contrast agent.

There is however, a large gap of knowledge and more research is required to determine how various experimental parameters (size of the PE, salt concentration of PE mixture, strength of the attached anion on the AuNPs surface and pH) play a role in the deposition of PEs onto the AuNPs. Other challenges include how the addition of the PE coatings on AuNPs affects the cellular uptake and interactions with cells both *in vitro* and *in vivo*. A standardized protocol for both *in vivo* and *in vitro* studies would be beneficial to directly compare different coatings and to determine the toxicity in a range of cell types. The future outlook for the use of PE coated AuNPs is positive, and this review has shown several of the possible uses in biomedicine. There is still much research to be conducted to better understand these systems and how each individual parameter impacts how they interact with cells

but the initial literature in this area shows promise that PE coated AuNPs could reach their potential in the biomedical field.

Authors' contributions

MF conducted the literature review and drafted the paper. IK supervised and assisted in editing the manuscript. Both authors read and approved the final manuscript.

Acknowledgements

The authors would like to thank the Australian Institute of Nuclear Science and Engineering (AINSE Ltd) (Award-PGRA) for the top-up scholarship and the Australian Government Research Training Program for providing financial assistance.

Competing interests

The authors declare that they have no competing interests.

Availability of data and materials

Not applicable.

Funding

Not applicable.

Publisher's Note

Springer Nature remains neutral with regard to jurisdictional claims in published maps and institutional affiliations.

Received: 17 January 2019 Accepted: 20 March 2019

Published online: 24 April 2019

References

- N. Elahi, M. Kamali, M.H. Baghersad, *Talanta* **184**, 537–556 (2018)
- X. Li, Z. Hu, J. Ma, X. Wang, Y. Zhang, W. Wang, Z. Yuan, *Colloids Surf. B* **167**, 260–266 (2018)
- B.K. Nanjwade, A.B. Sarkat, T. Srichana, in *Characterization and biology of nanomaterials for drug delivery*, ed. by S.S. Mohapatra, S. Ranjan, N. Dasgupta, R.K. Mishra, S. Thomas (Elsevier, Amsterdam, 2019), pp. 337–350
- J. Piella, N.G. Bastús, V. Puntes, *Biocorjugate Chem.* **28**(1), 88–97 (2017)
- M.A. Kerr, F. Yan, *J. Spectrosc.* **2016**, 8 (2016)
- Y.C. Cao, R. Jin, C.A. Mirkin, *Science* **297**(5586), 1536–1540 (2002)
- M.J. Ashley, M.R. Bourgeois, R.R. Murthy, C.R. Laramy, M.B. Ross, R.R. Naik, G.C. Schatz, C.A. Mirkin, *J. Phys. Chem. C* **122**(4), 2307–2314 (2018)
- L.A. Lane, X. Qian, S. Nie, *Chem. Rev.* **115**(19), 10489–10529 (2015)
- L. Fratoddi, I. Venditti, C. Carretti, M.V. Russo, *Nano Res.* **8**(6), 1771–1799 (2015)
- F.-Y. Kong, J.-W. Zhang, R.-F. Li, Z.-X. Wang, W.-J. Wang, W. Wang, *Molecules* **22**(9), 1445 (2017)
- Y.-C. Yeh, B. Cseran, V.M. Rotello, *Nanoscale* **4**(6), 1871–1880 (2012)
- C. Qu, B. Jing, S. Wang, Y. Zhu, *J. Phys. Chem. B* **121**(37), 8829–8837 (2017)
- G. Decher, *Science* **277**(5330), 1232 (1997)
- E. Guzmán, A. Mateos-Maroto, M. Ruano, F. Ortega, R.G. Rubio, *Adv. Colloid Interface Sci.* **249**, 290–307 (2017)
- A. Figoli, J. Hoinikis, S.A. Altinkaya, J. Bundschuh, *Application of nanotechnology in membranes for water treatment* (CRC Press, Boca Raton, 2017)
- F. Caruso, *Adv. Mater.* **13**(1), 11–22 (2001)
- P.S. Brown, B. Bhushan, *Sci. Rep.* **5**, 8701 (2015)
- C. Elouas, D. Lopez-Torres, M. Hernaez, I.R. Matias, F.J. Arregui, *Nanoscale Res. Lett.* **8**(1), 539 (2013)
- R.R. Costa, M. Alatorre-Medza, J.F. Mano, *Biotechnol. Adv.* **33**(6, Part 3), 1310–1326 (2015)
- A. Yu, Z. Liang, J. Cho, F. Caruso, *Nano Lett.* **3**(9), 1203–1207 (2003)
- V. Shah, C. Malardier-Jugroot, M. Jugroot, *Mater. Chem. Phys.* **196**, 92–102 (2017)
- D.J. Gittins, F. Caruso, *J. Phys. Chem. B* **105**(29), 6846–6852 (2001)
- M. Fuller, I. Köper, *Polymers* **10**(12), 1336 (2018)
- N. Thi Nhat Hang, N. Thi Le Trinh, L. Thi Thanh Tuyen, N. Canh Minh Thang, N. Thi Phuong Phong, *Adv. Nat. Sci-Nanosci.* **7**(1), 015006 (2016)
- K.S. Lee, M.A. El-Sayed, *J. Phys. Chem. B* **110**(39), 19220–19225 (2006)
- C. Yu, J. Irudayaraj, *Anal. Chem.* **79**(2), 572–579 (2007)
- J.R. Matthews, C.M. Payne, J.H. Hafner, *Langmuir* **31**(36), 9893–9900 (2015)
- L. An, Y. Wang, Q. Tian, S. Yang, *Materials* **10**(12), 1372 (2017)
- D. Pissuwan, T. Niidome, *Nanoscale* **7**(1), 59–65 (2015)
- A. Dorris, S. Rucareanu, L. Reven, C.J. Barrett, R.B. Lennox, *Langmuir* **24**(6), 2532–2538 (2008)
- L. Nayef, R. Castiello, M. Tabrizian, *Macromol. Biosci.* **17**(6), 1600535 (2017)
- T.L. Pugh, W. Heller, *J. Polym. Sci.* **47**(149), 219–227 (1960)
- S. Ahmed, M.A. Sheraz, U.I. Rehman, *AAPS PharmSciTech* **14**(2), 870–879 (2013)
- S. Maiti, S. Jana, B. Laha, *Design and development of new nanocarriers* (William Andrew Publishing, Norwich, 2018), pp. 223–256
- R.R. Netz, J.-F. Joanny, *Macromolecules* **32**(26), 9013–9025 (1999)
- R. Sardar, J.S. Shumaker-Parry, *J. Am. Chem. Soc.* **133**(21), 8179–8190 (2011)
- J. Piella, N.G. Bastús, V. Puntes, *Chem. Mater.* **28**(4), 1066–1075 (2016)
- H. Xia, Y. Xiahou, P. Zhang, W. Ding, D. Wang, *Langmuir* **32**(23), 5870–5880 (2016)
- J. Turkevich, P.C. Stevenson, J. Hillier, *Discuss. Faraday Soc.* **11**, 55–75 (1951)
- Z. Xiang, K. Wang, W. Zhang, S.W. Teh, A. Peli, P.L. Mok, A. Higuchi, S. Suresh Kumar, *J. Cluster Sci.* **29**(1), 1–7 (2018)
- G. Frens, *Nat. Phys. Sci.* **241**, 20–22 (1973)
- M. Brust, M. Walker, D. Bethell, D.J. Schiffrin, R. Whyman, *J. Chem. Soc. Chem. Commun.* **7**, 801–802 (1994)
- J.D.S. Newman, G.J. Blanchard, *Langmuir* **22**(13), 5882–5887 (2006)
- H. Dozol, G. Mériguet, B. Ancian, V. Cabuil, H. Xu, D. Wang, A. Abou-Hassan, *J. Phys. Chem. C* **117**(40), 20958–20966 (2013)
- S. Arghya, G. Manoj, S. Pragna, D. Manab, B. Utpal, *Adv. Nat. Sci-Nanosci.* **7**(2), 025005 (2016)
- Y. Jang, N. Lee, J. Kim, Y. Park, Y. Piao, *Nanomaterials* **8**(4), 252 (2018)
- V. Gopinath, S. Priyadarshini, D. MubarakAli, M.F. Loke, N. Thajudhin, N.S. Alharbi, T. Yadavalli, M. Alagiri, J. Vadivelu, *Arab. J. Chem.* **10**, 1107–1117 (2017)
- S. Labala, P.K. Mandapalli, A. Kurumadali, V.V.K. Venuganti, *Mol. Pharm.* **12**(3), 878–888 (2015)
- M. Ortega-Munoz, M.D. Giron-Gonzalez, R. Salto-Gonzalez, A.B. Jodar-Reyes, S.E. De Jesus, F.J. Lopez-Jaramillo, F. Hernandez-Mateo, F. Santoyo-Gonzalez, *Chem. Asian J.* **11**(23), 3365–3375 (2016)
- E.C. Drexler, A.M. Alkhalay, X. Huang, C.J. Murphy, M.A. El-Sayed, *Chem. Soc. Rev.* **41**(7), 2740–2779 (2012)
- X. Xie, S. Xu, P. Pi, J. Cheng, X. Wen, X. Liu, S. Wang, *AIChE J.* **64**(3), 810–821 (2018)
- B. Masereel, M. Dinguidi, C. Bouzin, N. Moniotte, O. Feron, B. Gallez, T. Vander Borgh, C. Michiels, S. Lucas, *J. Nanopart. Res.* **13**(4), 1573–1580 (2011)
- N. Reum, C. Fink-Straube, T. Klein, R.W. Hartmann, C.-M. Lehr, M. Schneider, *Langmuir* **26**(22), 16901–16908 (2010)
- Y. Lee, S.H. Lee, J.S. Kim, A. Maruyama, X. Chen, T.G. Park, *J. Controlled Release* **155**(1), 3–10 (2011)
- J. Homola, S.S. Yee, G. Gauglitz, *Sens. Actuators B Chem.* **54**(1), 3–15 (1999)
- A. Vincenzo, P. Roberto, F. Marco, M.M. Onofrio, I. Maria Antonia, *J. Phys.: Condens. Matter* **29**(20), 203002 (2017)
- T. Felicia, B. Monica, B. Lucian, A. Simion, *Nanotechnology* **18**(25), 255702 (2007)
- H.-H. Chang, C.J. Murphy, *Chem. Mater.* **30**(4), 1427–1435 (2018)
- G. Mie, *Ann. Phys.* **330**(3), 377–445 (1908)
- H. Aldewachi, T. Chalet, M.N. Woodroffe, N. Bricklebank, B. Sharrack, P. Gardiner, *Nanoscale* **10**(1), 18–33 (2018)
- K.S. Mayya, B. Schoeler, F. Caruso, *Adv. Funct. Mater.* **13**(3), 183–188 (2003)
- S. Pollastri, A.F. Gualtieri, M.L. Gualtieri, M. Hanuskova, A. Cavallo, G. Gaudino, *J. Hazard. Mater.* **276**, 469–479 (2014)

63. S. Spriano, V. Sarath Chandra, A. Cochis, F. Uberti, L. Rimondini, E. Bertone, A. Vitale, C. Scolari, M. Ferrari, F. Cirisano, G. Gautier di Confiengo, S. Ferraris, *Mater. Sci. Eng. C* **74**, 542–555 (2017)
64. T. Luxbacher, (Anton Paar GmbH, Austria, 2014)
65. J.A.A. Junior, J.B. Baldo, *New J. Glass Ceramics* **04**(02), 9 (2014)
66. S. Behzadi, V. Serpooshan, W. Tao, M.A. Hamaly, M.Y. Alkawareek, E.C. Dreaden, D. Brown, A.M. Alkhalay, O.C. Farokhzad, M. Mahmoudi, *Chem. Soc. Rev.* **46**(14), 4218–4244 (2017)
67. X. Cheng, X. Tian, A. Wu, J. Li, J. Tian, Y. Chong, Z. Chai, Y. Zhao, C. Chen, C. Ge, *ACS Appl. Mater. Interfaces* **7**(37), 20568–20575 (2015)
68. C. Corbo, R. Molinaro, A. Parodi, N.E.T. Furman, F. Salvatore, E. Tasciotti, *Nanomedicine* **11**(1), 81–100 (2016)
69. A. Elbakry, A. Zaky, R. Liebl, R. Rachel, A. Goepferich, M. Breunig, *Nano Lett.* **9**(5), 2059–2064 (2009)
70. F. Charbgo, M. Nejabat, K. Abnous, F. Soltani, S.M. Taghdisi, M. Aliboland, W. Thomas Shier, T.W.J. Steele, M. Ramezani, *J. Controlled Release* **272**, 39–53 (2018)
71. J.M. Blander, R. Medzhitov, *Nat. Immunol.* **7**(10), 1029–1035 (2006)
72. M.A. Dobrowska, S.E. McNeil, *Nat. Nano* **2**(8), 469–478 (2007)
73. S.D. Conner, S.L. Schmid, *Nature* **422**(6927), 37–44 (2003)
74. A.U. Aderem, *Annu. Rev. Immunol.* **17**(1), 593–623 (1999)
75. N. Oh, J.-H. Park, *Int. J. Nanomed.* **9**(Suppl 1), 51–63 (2014)
76. S.D. Xiang, A. Scholzen, G. Minigo, C. David, V. Apostolopoulos, P.L. Mottram, M. Plebanski, *Methods* **40**(1), 1–9 (2006)
77. F. Fekri, R.C. Delos Santos, R. Karshafian, C.N. Antonescu, *PLoS ONE* **11**(6), e0156754 (2016)
78. B.D. Chithrani, W.C.W. Chan, *Nano Lett.* **7**(6), 1542–1550 (2007)
79. H. Gao, W. Shi, L.B. Freund, *Proc. Natl. Acad. Sci. U. S. A.* **102**(27), 9469–9474 (2005)
80. V.P. Torchilin, *Smart pharmaceutical nanocarriers* (Imperial College Press, New Jersey, 2015)
81. L. Shang, K. Nienhaus, G.U. Nienhaus, *J. Nanobiotechnology* **12**(1), 5 (2014)
82. A.C. Wong, D.W. Wright, *Small* **12**(40), 5592–5600 (2016)
83. C.C. Fleischer, C.K. Payne, *Acc. Chem. Res.* **47**(8), 2651–2659 (2014)
84. A.M. Alkhalay, P.K. Nagaria, C.R. Hexel, T.J. Shaw, C.J. Murphy, M.D. Wyatt, *Small* **5**(6), 701–708 (2009)
85. C.M. Goodman, C.D. McCusker, T. Yilmaz, V.M. Rotello, *Bioconjugate Chem.* **15**(4), 897–900 (2004)
86. S. Nambiar, E. Osei, A. Fleck, J. Darko, A.J. Mutsaers, S. Wettig, *Appl. Nanoscience* **8**(3), 347–357 (2018)
87. S. Huo, S. Jin, X. Ma, X. Xue, K. Yang, A. Kumar, P.C. Wang, J. Zhang, Z. Hu, X.-J. Liang, *ACS Nano* **8**(6), 5852–5862 (2014)
88. J.A. Ryan, K.W. Overton, M.E. Speight, C.N. Oldenburg, L. Loo, W. Robarge, S. Franzen, D.L. Feldheim, *Anal. Chem.* **79**(23), 9150–9159 (2007)
89. M. Kodha, Y.M. Wang, E. Hutter, D. Maysinger, U. Stochaj, *Theranostics* **5**(4), 357–370 (2015)
90. R. Shukla, V. Barisal, M. Chaudhary, A. Basu, R.R. Bhorde, M. Sastry, *Langmuir* **21**(23), 10644–10654 (2005)
91. N. Pernodet, X. Fang, Y. Sun, A. Bakhtina, A. Ramakrishnan, J. Sokolov, A. Ulman, M. Rafailovich, *Small* **2**(6), 766–773 (2006)
92. G. Han, P. Ghosh, V.M. Rotello, *Nanomedicine (Lond)* **2**(1), 113–123 (2007)
93. S.G. Elici, Y. Jiang, B. Yan, S.T. Kim, K. Saha, D.F. Moyano, G. Yesilbag Tonga, L.C. Jackson, V.M. Rotello, R.W. Vachet, *ACS Nano* **10**(5), 5536–5542 (2016)
94. S. Guo, Y. Huang, Q. Jiang, Y. Sun, L. Deng, Z. Liang, Q. Du, J. Xing, Y. Zhao, P.C. Wang, A. Dong, X.-J. Liang, *ACS Nano* **4**(9), 5505–5511 (2010)
95. A. Lamprecht, N. Ubrich, H. Yamamoto, U. Schafer, H. Takeuchi, P. Maincent, Y. Kawashima, C.M. Lehr, *J. Pharmacol. Exp. Ther.* **299**(2), 775–781 (2001)
96. R. Singh, J.W. Lillard, *Exp. Mol. Pathol.* **86**(3), 215–223 (2009)
97. T.S. Zatssepin, Y.V. Kotelevtsev, V. Koteliansky, *Int. J. Nanomed.* **11**, 3077–3086 (2016)
98. M. Singh, D.C.C. Harris-Birtill, S.R. Markar, G.B. Hanna, D.S. Elson, *Nanomed. Nanotechnol.* **11**(8), 2083–2098 (2015)
99. Y.N. Konar, R. Gurry, E. Allemann, *J. Photochem. Photobiol. B* **66**(2), 89–106 (2002)
100. R. Kanasty, J.R. Dorkin, A. Vegas, D. Anderson, *Nat. Mater.* **12**(11), 967–977 (2013)
101. N.S. Abadeer, C.J. Murphy, *J. Phys. Chem. C* **120**(9), 4691–4716 (2016)
102. E.S. Day, J.G. Morton, J.L. West, *J. Biomech. Eng.* **131**(7), 074001 (2009)
103. E. S. D. Rache S. Riley, *Wiley Interdiscip. Rev. Nanomed. Nanobiotechnol.* **9**(4) (2017)
104. X. Huang, I.H. El-Sayed, W. Qian, M.A. El-Sayed, *J. Am. Chem. Soc.* **128**(6), 2115–2120 (2006)
105. D.K. Kirui, S. Krishnan, A.D. Strickland, C.A. Batt, *Macromol. Biosci.* **11**(6), 779–788 (2011)
106. B. Wang, J.-H. Wang, Q. Liu, H. Huang, M. Chen, K. Li, C. Li, X.-F. Yu, P.K. Chu, *Biomaterials* **35**(6), 1954–1966 (2014)
107. J. Wang, B. Dong, B. Chen, Z. Jiang, H. Song, *Dalton Trans.* **41**(36), 11134–11144 (2012)
108. Z. Bao, X. Liu, Y. Liu, H. Liu, K. Zhao, *Asian. J. Pharm. Sci.* **11**(3), 349–364 (2016)
109. X. Cheng, R. Sun, L. Yin, Z. Chai, H. Shi, M. Gao, *Adv. Mater.* **29**(6), 1604894 (2017)
110. T. Curry, R. Kopelman, M. Shilo, R. Popovtzer, *Contrast Media Mol. Imaging* **9**(1), 53–61 (2014)
111. S. Mallidi, S. Kim, A. Karpouk, P.P. Joshi, K. Sokolov, S. Emelianov, *Photoacoustics* **3**(1), 26–34 (2015)
112. P. Huang, J. Lin, W. Li, P. Rong, Z. Wang, S. Wang, X. Wang, X. Sun, M. Aronova, G. Niu, R.D. Leapman, Z. Nie, X. Chen, *Angew. Chem. Int. Ed.* **52**(52), 13958–13964 (2013)
113. H. Lusic, M.W. Grinstaff, *Chem. Rev.* (2013). <https://doi.org/10.1021/cr200358s>
114. Y. Dou, Y. Guo, X. Li, X. Li, S. Wang, L. Wang, G. Lv, X. Zhang, H. Wang, X. Gong, J. Chang, *ACS Nano* **10**(2), 2536–2548 (2016)
115. A.M. Alkhalay, C.J. Murphy, *J. Nanopart. Res.* **12**(7), 2313–2333 (2010)
116. M. Sathishkumar, S. Pavagadhi, A. Mahadevan, R. Balasubramanian, *Ecotoxicol. Environ. Saf.* **114**, 232–240 (2015)
117. Y. Zhang, D. Xu, W. Li, J. Yu, Y. Chen, *J. Nanomater.* **2012**, 7 (2012)
118. S. Vial, R.L. Reis, J.M. Oliveira, *Curr. Opin. Solid State Mater. Sci.* **21**(2), 92–112 (2017)
119. A. Wozniak, A. Malankowska, G. Nowaczyk, B.F. Grzeskowiak, K. Tuśnio, R. Słomski, A. Zaleska-Medynska, S. Jurga, *J. Mater. Sci. Mater. Med.* **28**(6), 92 (2017)
120. K.A. Moore, K.M. Pate, D.D. Soto-Ortega, S. Lohse, N. van der Munnik, M. Lim, K.S. Jackson, V.D. Lyles, L. Jones, N. Glassgow, V.M. Napumeheno, S. Mobley, M.J. Uline, R. Mahtab, C.J. Murphy, M.A. Moss, *J. Biol. Eng.* **11**(1), 5 (2017)
121. M. Bouché, S. Fournel, A. Kichler, T. Selvam, J.-L. Gallani, S. Bellemín-Laponnaz, *Eur. J. Inorg. Chem.* **2018**(25), 2972–2975 (2018)
122. Y. Pan, A. Leifert, D. Ruau, S. Neuss, J. Bornemann, G. Schmid, W. Brandau, U. Simon, W. Jahnen-Dechent, *Small* **5**(18), 2067–2076 (2009)

Submit your manuscript to a SpringerOpen® journal and benefit from:

- Convenient online submission
- Rigorous peer review
- Open access: articles freely available online
- High visibility within the field
- Retaining the copyright to your article

Submit your next manuscript at ► springeropen.com

Article

Polyelectrolyte-Coated Gold Nanoparticles: The Effect of Salt and Polyelectrolyte Concentration on Colloidal Stability

Melanie Fuller  and Ingo Köper 

Flinders Institute for Nanoscale Science and Technology, College for Science and Engineering, Flinders University, Bedford Park 5042, South Australia; melanie.fuller@flinders.edu.au

* Correspondence: ingo.koepfer@flinders.edu.au

Received: 8 November 2018; Accepted: 29 November 2018; Published: 3 December 2018



Abstract: Gold nanoparticles are widely used in biomedical applications. Their ease of surface modification, biocompatibility and the presence of surface plasmons makes them ideal tools for a variety of investigations. Polyelectrolyte-coated gold nanoparticles are employed in areas such as imaging, drug delivery and gene therapy; however, it is not well understood how different factors such as the polyelectrolyte and salt concentration affect the coating on the nanoparticles and hence their performance. Here, these parameters were systematically varied and their effect on the stability of the colloidal nanoparticle suspension was monitored. An increase in the polyelectrolyte concentration from 0 to 30 mg/mL led to a red shift of the surface plasmon peak and an increase in the zeta potential. Concentrations between 5 mg/mL and 30 mg/mL resulted in the most stable systems, with 1 mg/mL being the most unstable. Stable nanoparticle suspensions were formed in salt concentrations below 50 mM, while higher concentrations caused colloidal instability and irreversible aggregation.

Keywords: polyelectrolyte; stability; gold nanoparticles; gold; biomedical

1. Introduction

Surface modified gold nanoparticles (AuNPs) are becoming more frequently used in biomedical applications and thus being able to understand the effects various surface coatings have on these NPs is becoming more important [1,2]. AuNPs are being utilised because they are biocompatible and their optical and physical properties make them suitable for sensing purposes. The presence of surface plasmons allows changes in the local environment of the particle to be determined, and the ability to functionalise the surface easily with a range of moieties including polymers, proteins, DNA and polyelectrolytes makes AuNPs suitable for various applications.

The layer-by-layer (LbL) method of coating NPs and planar substrates using polyelectrolytes (PEs) is well established [3–5]. LbL coatings with PEs have distinct advantages over other surface modification methods, specifically the ease of assembly on a wide range of substrates. The LbL method allows the sequential addition of oppositely charged PEs onto a substrate through primarily electrostatic interactions (Figure 1) [6]. Polyanions and polycations can be used alternatively to build up multilayer systems which can be used in applications ranging from water treatment to protein immobilisation [7,8]. The ease of deposition of PEs onto NP surfaces is a result of the simple electrostatic interactions that govern the LbL attachment process. These interactions depend on the type, length and concentration of the PE, as well as the concentration and type of salt used during the assembly process [9]. These variables need to be optimised, especially when depositing PEs onto NPs, as the colloidal stability of the system can be easily affected. According to the DLVO theory, a colloidal solution requires repulsive forces

such as electrostatic or steric stabilisation to prevent aggregation from occurring [10]. Electrostatically stabilised systems have an electric double layer, which is due to the surface charge and solvated ions in solution. This double layer results in inter-particle Coulomb repulsion forces which decay exponentially with the particle to particle distance [11]. The thickness of the double layer (Debye length) can be affected by the salt concentration. Increasing salt concentration leads to an increase in the effective screening of these charges, which causes a decrease in the Debye length and hence in the effective distance of the Coulombic interactions [12]. Steric stabilisation can also occur from the absorption of larger molecules such as PEs onto the particle's surface [11]. These larger molecules can provide a protective layer around the particle, which can also prevent aggregation. As PE-coated NPs can potentially be used in biomedical applications, the colloidal stability is extremely important, as aggregation can alter their in vitro behaviour such as NP uptake and cytotoxicity as well as in vivo fate including biodistribution [13].

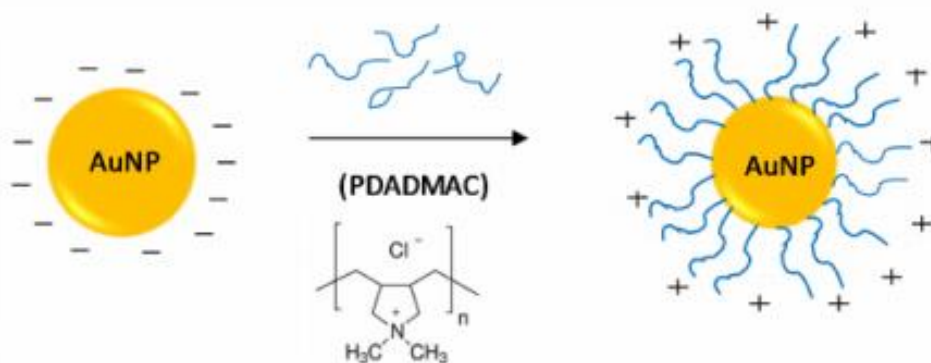


Figure 1. Layer-by-layer (LbL) attachment of polydiallyldimethylammonium chloride (PDADMAC) onto citrate-capped gold nanoparticles.

The assembly mechanisms as well as the effect of salt, PE concentration and temperature on the formation of planar PE-films are well understood [14]. However, the coating of highly curved surfaces such as the surface of small NPs has not been as thoroughly researched. This is partially due to the added difficulty of coating a highly curved surface and potential aggregation issues with altering the surface coating of NPs. Nevertheless, understanding how salt and concentration affects PE coatings on NP could allow for their use in a wider range of applications.

Here, the effects of both PE concentration and the salt concentration during layer formation has been explored to determine how they affect the formation of a PE-coating on AuNPs. PE concentrations which are too low can lead to incomplete particle coverage and subsequent aggregation. Concentrations that are too high will lead to particle bridging, especially when higher molecular weight polymers are used. Bridging occurs when the polymers absorb simultaneously on more than one particle, 'grouping' the particles together causing aggregation [15]. When salt concentrations are too high, it can lead to screening of interparticle electrostatic repulsions, which are needed to prevent aggregation [16,17]. However, it has been proposed that concentrations that are too low can lead to inflexibility of the PE chains, which wrap around the NP resulting in an inadequate or incomplete coating, similar to low PE concentrations [9].

The coating of nanoparticles with PEs can be described by three different scenarios [16]: (1) an excess of particles leads to partial and 'patchy' coatings on the nanoparticles, which often results in an increase in particle-particle attractions and subsequent aggregation; (2) equal charge proportions of colloids and PEs yields coated NPs with an overall charge near the isoelectric point of the PE. This in effect neutralises the charge causing the particles to move closer together and aggregate; (3) an excess of PE results in stable solutions of NPs that are saturated by the PE. This final scenario can be expressed as a ratio of polyelectrolyte chains to nanoparticles (PC/NP) and can be calculated by taking

the mass of polymer used and dividing by the polymer mass per chain (polymer M_w /Avogadro's number) [18]. That number is then divided the number of nanoparticles to give PC/NP. Previously, ratios of 200–4000PC/NP provided the most stability, with the least aggregation [16].

Here, the adsorption of polydiallyldimethylammonium chloride (PDADMAC) of differing concentrations onto AuNPs has been explored using ultraviolet-visible (UV-vis) spectroscopy and zeta-potential measurements. The PE concentration in which the NPs are most stable has then been used to investigate how the salt concentration affects the electrostatic attachment and colloidal stability. By determining the optimum concentrations for the PE and salt, the PE-AuNP system could be better adapted for use in biomedical applications. The optimised salt and PE concentrations were then used to determine if PDADMAC-coated AuNP are more stable than citrate capped AuNP. This was tested through a variety of solvents including ethanol, 10% Tween20 and PBS.

2. Materials and Methods

2.1. Polyelectrolyte (PE) Concentration

5 nm diameter AuNPs at a concentration of 8.4×10^{13} particles/mL were purchased from NanoComposix (San Diego, CA, USA). 2 mL of this particle solution were then mixed with 3 mL of PDADMAC (Sigma Aldrich, Castle Hill, Australia), average $M_w < 100,000$) solution with concentrations of 0, 0.1, 1, 5, 10 or 30 mg/mL. The AuNP/PDADMAC mixtures were stirred overnight before centrifuging at 14500 rpm for 40 min. The supernatant was removed and the pellet resuspended in 1 mL of 1 mM NaCl. This washing was repeated three times to remove any excess PDADMAC. The pH of the nanoparticle solution was adjusted to pH = 6 using 1 M HCl and measured using the Mettler Toledo pH Meter. The attachment of the PEs onto the NPs and the subsequent stability of the NPs was determined through the use of UV-vis spectroscopy (Cary 50) in 1 mM NaCl with the wavelength range of 400–800 nm. Zeta potential (Malvern Zetasizer Nano, Malvern Instruments Ltd, Malvern, UK) was measured using flow cells with 1 mM NaCl. All experiments were conducted in triplicate.

2.2. Salt Concentration

PDADMAC (average $M_w < 100,000$) in solution, was diluted to a concentration of 5 mg/mL using differing NaCl concentrations of 0, 0.1, 1, 5, 10 and 30 mg/mL. 3 mL of the PDADMAC solution was added to 2 mL of AuNPs and the AuNP/PDADMAC mixture was stirred overnight before centrifuging at 14,500 rpm for 40 min. The supernatant was removed and the pellet resuspended in 1 mL of the same salt concentration. This washing was repeated three times to remove any excess PDADMAC. The pH was adjusted to pH = 6 as per the polyelectrolyte concentration method above. The attachment and stability was also measured as per the PDADMAC concentration protocol; however, during the zeta potential measurements, the samples were measured in their respective salt concentrations. All experiments were conducted in triplicate.

2.3. Solvent Stability

Three mL of 5 mg/mL PDADMAC (average $M_w < 100,000$) in 1 mM NaCl were stirred for 3 h with 2 mL of 5 nm AuNP solution. After 3 h, the sample was centrifuged at 14,500 rpm for 40 min. The supernatant was removed and the pellet resuspended in 1 mM NaCl. This washing was repeated three times to remove any excess PDADMAC. On the final centrifugation step, 50 μ L of the pellet was resuspended in 1 mL of 100% ethanol, 10% Tween20 or PBS in triplicate. Similarly, 50 μ L of citrate capped 5 nm AuNP (NanoComposix, San Diego, CA, USA) were added to 1 mL of the same three solvents in triplicate. All solutions were then left for 36 h at ambient temperature before surface plasmon resonance (SPR) peak changes were measured by UV-vis spectroscopy (Cary 50) in their respective solvents. In each case, the UV-vis spectrophotometer was blanked with the solvent being used to ensure the solvent itself did not contribute to changes in the SPR peak.

3. Results and Discussion

PDADMAC was chosen to coat the NP as it is a strong, highly charged polyelectrolyte, with one cationic charge group per monomer [19]. The type and length of polyelectrolyte remained unchanged for the duration of the experiment and the ionic strength of the medium was controlled to probe the effect of different PE concentrations on the coating of the AuNPs. The specific Mw of PDADMAC was chosen as the longer chains can more effectively wrap around the AuNP, providing better surface coverage.

3.1. Effect of PE Concentration

In order to investigate the effect of PE concentration on the stability of the colloidal solution, five different concentrations of PDADMAC were used to coat the AuNPs, and the SPR absorbance peaks were measured using UV-vis spectroscopy (Figure 2). Changes in the local nanoparticle environment influence the position of the peak as well as its amplitude. Particle aggregation causes a red-shift in the UV-vis absorption spectrum due to a decrease in interparticle distance [20]. Thus the stability can be monitored through the peak position.

At very low PE concentrations (0.1 mg/mL), the AuNPs fully aggregated after 24 h (Table 1). This concentration corresponds to a PC/NP ratio of 21.5, most likely falling into scenario 2 of near equal charges. This was confirmed through zeta potential measurements, where the cationic PE neutralised the negative charge on the AuNP (Figure 2B). Concentrations below 5 mg/mL have unsaturated layers of PE on the NPs, leading to lower and unstable zeta potentials, as the attractive Van der Waals forces become dominant. Charge neutralisation causes the nanoparticles to move closer together, which results in an unstable suspension and particle aggregation [21]. This is also likely to be the cause for the near zero zeta potential reading in the 1 mg/mL sample, indicating its instability.

Higher concentrations above 5 mg/mL, corresponding to scenario 3 with an excess of PE, led to stable solutions. The PE coatings resulted in shifts in the SPR peak and significantly positive zeta potentials. Above 5 mg/mL, the zeta potential remained relatively stable and this can be attributed to the complete PE coatings on the NPs (Figure 2B). Prior to the plateau in zeta potential, the absorption of PE onto the NP is quantitative, where there would be in effect no free PE still in solution [22].

Table 1. Concentrations of PDADMAC showing polyelectrolyte chains to nanoparticles (PC/NP) ratio, compared to their average surface plasmon resonance (SPR) peak position and zeta potentials at pH 6.0 \pm 0.3.

PDADMAC Concentration (mg/mL)	PC/NP Ratio	SPR Maximum Absorbance Peak (nm)	Absorbance (a.u.)	Zeta Potential (mV)
0	0	513 \pm 0.3	0.48 \pm 0.2	-9.6 \pm 8.9
0.1	21.5	-*	-*	0.3 \pm 3.7
1.0	215	537 \pm 1.5	0.10 \pm 0.09	5.7 \pm 14
5.0	1075	539 \pm 0.47	0.58 \pm 0.04	35 \pm 8.9
10	2150	540 \pm 2.5	0.45 \pm 0.07	39 \pm 9.1
30	6450	542 \pm 0.94	0.51 \pm 0.08	48 \pm 7.9

* Fully aggregated and was unable to be removed from the centrifuge tubes with a concentration of AuNP suitable for ultraviolet-visible (UV-Vis) spectroscopy.

The absorbance values varied for the different PE concentrations. In principle, the absorbance should be independent of the coating concentration, however particles can be lost through repeated centrifugation wash steps, resulting in lower absorbance values. The lowest absorbance values were observed for 1 mg/mL, where most of the particles aggregated and precipitated out of solution.

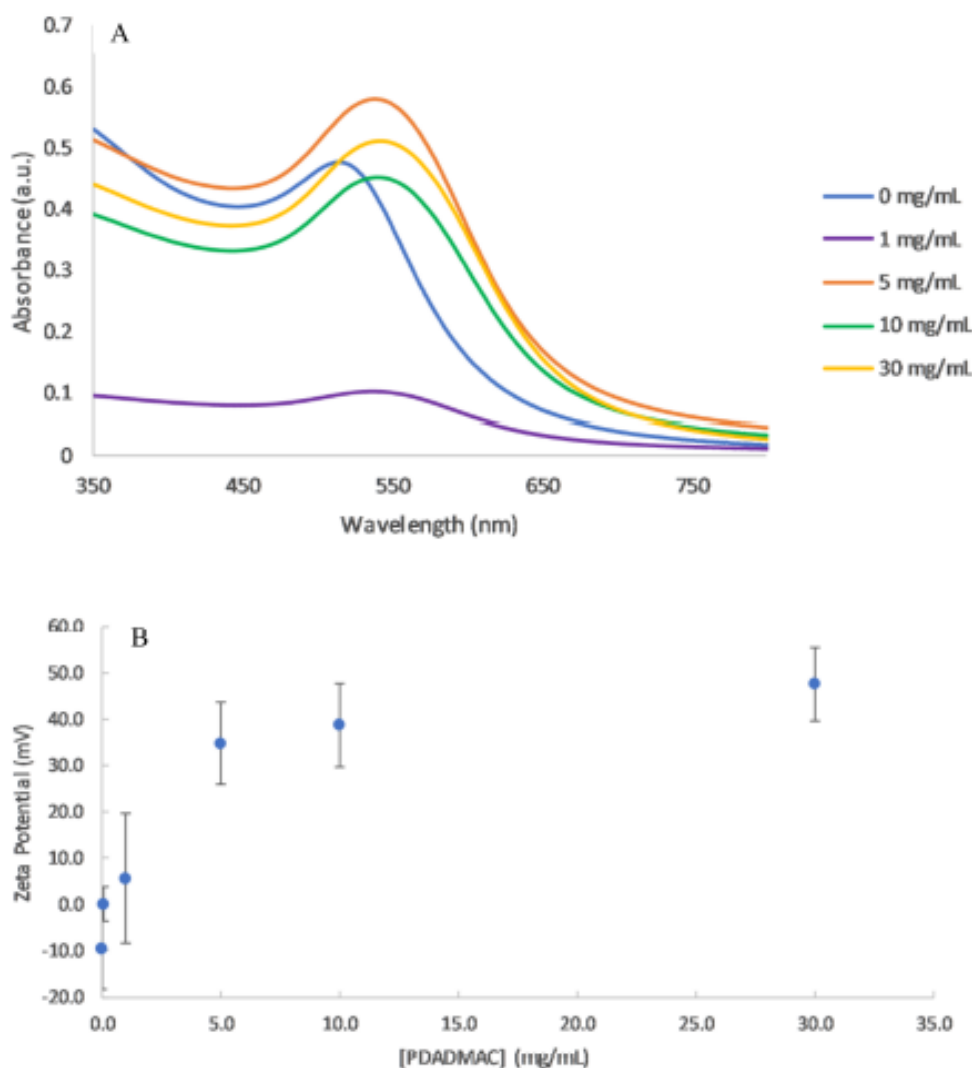


Figure 2. (A) UV-vis spectra of PDADMAC coated AuNP at concentrations of 0–30 mg/mL PDADMAC in 1 mM NaCl. (B) Zeta potential measurements as a function of PDADMAC concentration at pH 6.0.

The addition of a PDADMAC layer to the AuNP changed the overall dielectric constant of the particles, which resulted in a red shift of the SPR peak. A small change in the SPR peak may also be due to the size of NPs increasing with an additional layer, although this will be minor compared to the change in dielectric constant. The shift was dependent on the PE concentration. For 1 mg/mL PDADMAC, the SPR shifted by 24 nm (Figure 2A). This shift was much larger than values of 1.5–2 nm reported in other studies [16]. However, both the type and molecular weight of the PE were different in each study which may explain the larger SPR shift. With increasing amounts of the polymer, the SPR peak wavelength increased slowly as not only is the dielectric material surrounding the particle changing, but also the particles are becoming slightly larger with the absorption of the polymer onto the surface [23].

The data collected is in agreement with past studies on PC/NP ratios, where the greatest stability of PE-coated NPs was apparent for PC/NP ratios between 1000–4000 [16]. However, is likely dependent on the structure and Mw of the PE.

3.2. Effect of Salt Concentration

As the likelihood of inter-particle bridging and hence aggregation increases with increasing PE concentration, the lowest stable polymer concentration (5 mg/mL) was used for subsequent salt effect studies. On planar substrates, the maximum coverage of PDADMAC typically increases with increasing ionic strength [24]. For spherical nanoparticles, the absorbance should, thus, increase with increasing salt concentration. However, colloidal stability becomes a greater issue in coating NPs as increasing the salt concentration can increase the Debye screening length. This increased Debye screening length decreases the repulsive electrostatic interactions and hence Van der Waal's forces dominate causing NP aggregation. Experimentally, an increase in salt concentration caused the NPs to become less stable and at concentrations above 0.05 M, the NPs irreversibly attached to the centrifugation tubes (Table 2). For 0.1 M and 0.5 M NaCl, samples fully aggregated and precipitated. For concentrations of 0.05 M and below, there was no significant difference in peak wavelength (Figure 3) however; the peak absorbance was much lower indicating the nanoparticles have likely started to attach to the centrifuge tubes.

Table 2. The average SPR peak and absorbance as determined by UV-vis spectroscopy for 5 mg/mL PDADAMAC-coated AuNP.

Salt Concentration (M)	Average SPR Peak (nm)	Average Absorbance (a.u.)
0	543 ± 1.2	0.69 ± 0.04
0.001	539 ± 0.47	0.58 ± 0.04
0.05	540 ± 3.7	0.17 ± 0.05
0.1	*	*
0.5	*	*

* At 0.1 M and 0.5 M, the sample irreversibly aggregated and was unable to be removed from the centrifuge tubes with a concentration of AuNP suitable for UV-vis spectroscopy.

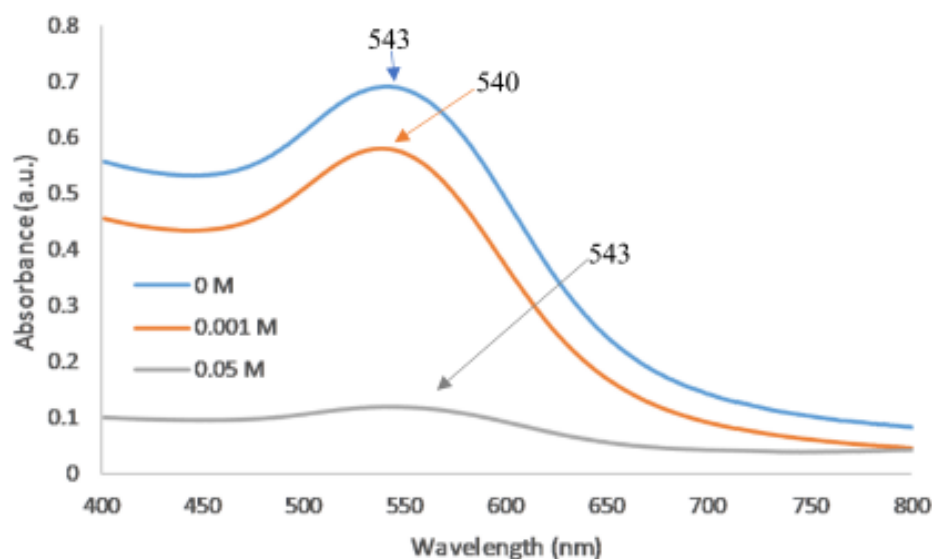


Figure 3. UV-vis spectra of varying salt concentrations of 5 mg/mL PDADMAC on 5 nm AuNPs.

3.3. Effect of Solvent

It has been observed that the addition of a PE layer to Au nanorods can increase the stability of NPs in a range of solvents where they otherwise would aggregate [25]. Due to this, the optimised conditions for PDADMAC attachment were used to test the stability of the coated AuNPs in three different solvents: ethanol, Tween20 and phosphate-buffered saline (PBS) to determine if the addition

of the PE coating enhanced the NPs stability. The changes were monitored as Δ SPR, which is the difference between the SPR peak in water and the solvent being tested. The larger the shift observed the more likely the NPs are aggregating.

In ethanol, there was a significant shift in the SPR peak, especially for citrate capped AuNPs with Δ SPR = 23 nm, indicating aggregation of the nanoparticles (See supporting information). In comparison, Δ SPR for PDADMAC coated particles was only 6 nm, suggesting a protective effect of the polyelectrolyte coating that reduces the tendency for particle aggregation in ethanol.

Tween 20 had been reported to be a stabilising agent for citrate-capped AuNPs [26,27]. In good agreement with these results, there was no significant difference observed for both citrate-capped and PDADMAC-coated AuNP when exposed to the surfactant.

Finally, PBS was used as it is often used in cell culture studies [28,29]. PBS has a relatively high NaCl concentration (~0.1 M). Similar to the results above, both citrate capped and PDADMAC AuNPs aggregated and attached to the centrifugation tubing, hence no peak could be measured using UV-vis spectroscopy.

4. Conclusions

The optimised conditions for polyelectrolyte coatings of 5 nm diameter citrate capped AuNPs were determined to be 5 mg/mL of PDADMAC in 1 mM NaCl. These conditions resulted in the most stable solutions as shown by zeta potential and UV-vis spectroscopy measurements. Additionally, a PC/NP ratio between 1000–4000 resulted in the most stable solutions, in good agreement with the literature. High salt concentrations led to aggregation to the nanoparticles. Finally, when the nanoparticles were suspended in ethanol, the PDADMAC-coated AuNPs showed little aggregation compared to the citrate-coated AuNPs. Further stability testing is required to understand how PDADMAC coatings can prevent aggregation, especially in freeze-thaw experiments. Different polyelectrolytes and nanoparticles will have different influences on the optimised conditions; however, it would be expected that like-sized nanoparticles coated in strong polyelectrolytes would behave in a similar way and, thus, optimisation conditions would be comparable.

Supplementary Materials: The following are available online at <http://www.mdpi.com/2073-4360/10/12/1336/s1>, Table S1: Difference in SPR peak and absorbance for citrate capped AuNP and PDADMAC coated AuNP in Ethanol, Tween20 and PBS.

Author Contributions: Data curation, M.E.; Investigation, L.K.; Supervision, L.K.; Writing—original draft, M.E.; Writing—review & editing, L.K.

Funding: The authors would like to thank the Australian Institute of Nuclear Science and Engineering (AINSE Limited) for providing financial assistance (Award-PGRA) and the Australian Government for the Research Training Program Scholarship.

Conflicts of Interest: The authors declare no conflicts of interest.

References

1. Siafaka, P.; Üstündağ Okur, N.; Karavas, E.; Bikiaris, D. Surface Modified Multifunctional and Stimuli Responsive Nanoparticles for Drug Targeting: Current Status and Uses. *Int. J. Mol. Sci.* **2016**, *17*, 1440. [CrossRef] [PubMed]
2. Khan, M.S.; Vishakante, G.D.; Siddaramaiah, H. Gold nanoparticles: A paradigm shift in biomedical applications. *Adv. Colloid Interface Sci.* **2013**, *199–200*, 44–58. [CrossRef] [PubMed]
3. Santos, A.C.; Caldas, M.; Pattekari, P.; Fontes Ribeiro, C.; Ribeiro, A.J.; Lvov, Y.; Veiga, F. Chapter 16-Layer-by-Layer coated drug-core nanoparticles as versatile delivery platforms A2-Grumezescu, Alexandru Mihai. In *Design and Development of New Nanocarriers*; William Andrew Publishing: New York, NY, USA, 2018; pp. 595–635. [CrossRef]
4. Richardson, J.J.; Björmalm, M.; Caruso, F. Technology-driven layer-by-layer assembly of nanofilms. *Science* **2015**, *348*. [CrossRef]

5. Harris, C.M.; Miller, S.G.; Andresen, K.; Thompson, L.B. Quantitative measurement of sodium polystyrene sulfonate adsorption onto CTAB capped gold nanoparticles reveals hard and soft coronas. *J. Colloid Interface Sci.* **2018**, *510*, 39–44. [[CrossRef](#)] [[PubMed](#)]
6. Hirsjärvi, S.; Peltonen, L.; Hirvonen, J. Layer-by-layer polyelectrolyte coating of low molecular weight poly(lactic acid) nanoparticles. *Colloids Surf. B Biointerfaces* **2006**, *49*, 93–99. [[CrossRef](#)] [[PubMed](#)]
7. Wang, S.; Chen, K.; Xu, Y.; Yu, X.; Wang, W.; Li, L.; Guo, X. Protein immobilization and separation using anionic/cationic spherical polyelectrolyte brushes based on charge anisotropy. *Soft Matter* **2013**, *9*, 11276–11287. [[CrossRef](#)]
8. Wandrey, C.; Hernández-Barajas, J.; Hunkeler, D. Diallyldimethylammonium Chloride and its Polymers. In *Radical Polymerisation Polyelectrolytes*; Capek, I., Hernández-Barajas, J., Hunkeler, D., Reddinger, J.L., Reynolds, J.R., Wandrey, C., Eds.; Springer: Berlin/Heidelberg, Germany, 1999; pp. 123–183. [[CrossRef](#)]
9. Gittins, D.I.; Caruso, F. Tailoring the Polyelectrolyte Coating of Metal Nanoparticles. *J. Phys. Chem. B* **2001**, *105*, 6846–6852. [[CrossRef](#)]
10. Hierrezuelo, J.; Sadeghpour, A.; Szilágyi, L.; Vaccaro, A.; Borkovec, M. Electrostatic Stabilization of Charged Colloidal Particles with Adsorbed Polyelectrolytes of Opposite Charge. *Langmuir ACS J. Surf. Colloids* **2010**, *26*, 15109–15111. [[CrossRef](#)]
11. Polte, J. Fundamental growth principles of colloidal metal nanoparticles—A new perspective. *CrystEngComm* **2015**, *17*, 6809–6830. [[CrossRef](#)]
12. Egger, C.C.; Anderson, M.W.; Tiddy, G.J.T.; Casci, J.L. In situ NMR and XRD studies of the growth mechanism of SBA-1. *Phys. Chem. Chem. Phys.* **2005**, *7*, 1845–1855. [[CrossRef](#)]
13. Moore, T.L.; Rodriguez-Lorenzo, L.; Hirsch, V.; Balog, S.; Urban, D.; Jud, C.; Rothen-Rutishauser, B.; Lattuada, M.; Petri-Fink, A. Nanoparticle colloidal stability in cell culture media and impact on cellular interactions. *Chem. Soc. Rev.* **2015**, *44*, 6287–6305. [[CrossRef](#)] [[PubMed](#)]
14. Tang, K.; Besseling, N.A.M. Formation of polyelectrolyte multilayers: Ionic strengths and growth regimes. *Soft Matter* **2016**, *12*, 1032–1040. [[CrossRef](#)] [[PubMed](#)]
15. Huang, H.; Ruckenstein, E. The Bridging Force between Colloidal Particles in a Polyelectrolyte Solution. *Langmuir ACS J. Surf. Colloids* **2012**, *28*, 16300–16305. [[CrossRef](#)] [[PubMed](#)]
16. Schneider, G.; Decher, G. Functional Core/Shell Nanoparticles via Layer-by-Layer Assembly. Investigation of the Experimental Parameters for Controlling Particle Aggregation and for Enhancing Dispersion Stability. *Langmuir ACS J. Surf. Colloids* **2008**, *24*, 1778–1789. [[CrossRef](#)] [[PubMed](#)]
17. Bizmark, N.; Ioannidis, M.A. Effects of Ionic Strength on the Colloidal Stability and Interfacial Assembly of Hydrophobic Ethyl Cellulose Nanoparticles. *Langmuir ACS J. Surf. Colloids* **2015**, *31*, 9282–9289. [[CrossRef](#)] [[PubMed](#)]
18. Benoit, D.N.; Zhu, H.; Lillierose, M.H.; Verm, R.A.; Ali, N.; Morrison, A.N.; Fortner, J.D.; Avendano, C.; Colvin, V.L. Measuring the Grafting Density of Nanoparticles in Solution by Analytical Ultracentrifugation and Total Organic Carbon Analysis. *Anal. Chem.* **2012**, *84*, 9238–9245. [[CrossRef](#)] [[PubMed](#)]
19. Notley, S.M.; Norgren, M. Adsorption of a strong polyelectrolyte to model lignin surfaces. *Biomacromolecules* **2008**, *9*, 2081–2086. [[CrossRef](#)] [[PubMed](#)]
20. Cho, K.; Lee, Y.; Lee, C.-H.; Lee, K.; Kim, Y.; Choi, H.; Ryu, P.-D.; Lee, S.Y.; Joo, S.-W. Selective Aggregation Mechanism of Unmodified Gold Nanoparticles in Detection of Single Nucleotide Polymorphism. *J. Phys. Chem. C* **2008**, *112*, 8629–8633. [[CrossRef](#)]
21. Mengarelli, V.; Auvray, L.; Pastré, D.; Zeghal, M. Charge inversion, condensation and decondensation of DNA and polystyrene sulfonate by polyethylenimine. *Eur. Phys. J. E* **2011**, *34*, 127. [[CrossRef](#)] [[PubMed](#)]
22. Kleimann, J.; Gehin-Delval, C.; Auweter, H.; Borkovec, M. Super-stoichiometric charge neutralization in particle-polyelectrolyte systems. *Langmuir ACS J. Surf. Colloids* **2005**, *21*, 3688–3698. [[CrossRef](#)] [[PubMed](#)]
23. Quinsaat, J.E.Q.; Nuesch, E.A.; Hofmann, H.; Opris, D.M. Dielectric properties of silver nanoparticles coated with silica shells of different thicknesses. *RSC Adv.* **2013**, *3*, 6964–6971. [[CrossRef](#)]
24. Schwarz, S.; Buchhammer, H.M.; Lunkwitz, K.; Jacobasch, H.J. Polyelectrolyte adsorption on charged surfaces: Study by electrokinetic measurements. *Colloids Surf. A Physicochem. Eng. Asp.* **1998**, *140*, 377–384. [[CrossRef](#)]
25. Alkilany, A.M.; Thompson, L.B.; Murphy, C.J. Polyelectrolyte Coating Provides a Facile Route to Suspend Gold Nanorods in Polar Organic Solvents and Hydrophobic Polymers. *ACS Appl. Mater. Interfaces* **2010**, *2*, 3417–3421. [[CrossRef](#)] [[PubMed](#)]

26. Shih, Y.-C.; Ke, C.-Y.; Yu, C.-J.; Lu, C.-Y.; Tseng, W.-L. Combined Tween 20-Stabilized Gold Nanoparticles and Reduced Graphite Oxide–Fe₃O₄ Nanoparticle Composites for Rapid and Efficient Removal of Mercury Species from a Complex Matrix. *ACS Appl. Mater. Interfaces* **2014**, *6*, 17437–17445. [[CrossRef](#)] [[PubMed](#)]
27. Lin, C.-Y.; Yu, C.-J.; Lin, Y.-H.; Tseng, W.-L. Colorimetric Sensing of Silver(I) and Mercury(II) Ions Based on an Assembly of Tween 20-Stabilized Gold Nanoparticles. *Anal. Chem.* **2010**, *82*, 6830–6837. [[CrossRef](#)] [[PubMed](#)]
28. McCarthy, K.D.; de Vellis, J. Preparation of separate astroglial and oligodendroglial cell cultures from rat cerebral tissue. *J. Cell Biol.* **1980**, *85*, 890–902. [[CrossRef](#)] [[PubMed](#)]
29. Tuomola, E.M.; Salminen, S.J. Adhesion of some probiotic and dairy Lactobacillus strains to Caco-2 cell cultures. *Int. J. Food Microbiol.* **1998**, *41*, 45–51. [[CrossRef](#)]



© 2018 by the authors. Licensee MDPI, Basel, Switzerland. This article is an open access article distributed under the terms and conditions of the Creative Commons Attribution (CC BY) license (<http://creativecommons.org/licenses/by/4.0/>).



Nanoparticles in an antibiotic-loaded nanomesh for drug delivery†

Cite this: *RSC Adv.*, 2019, 9, 30064Melanie A. Fuller,^{abc} Ashley Carey,^a Harriet Whiley,^b Rio Kurimoto,^c Mitsuhiro Ebara^{id}^c and Ingo Köper^{id}^{*a}

Antibiotic loaded nanomeshes were fabricated by electrospinning polycaprolactone, a biocompatible polymer, with 12.5% w/w Colistin, 1.4% w/w Vancomycin and either cationic or anionic gold nanoparticles in varying combinations. The resulting nanomeshes had different antibiotic release profiles, with citrate capped gold nanoparticles combined with Colistin having the highest sustained release over 14 days for a 4 mg, 1.5 cm² nanomesh. The electrospinning parameters were optimised to ensure the spinning of a homogenous mesh and the addition of antibiotics was confirmed through ¹H NMR and ATR-FTIR. This research, as a proof of concept, suggests an opportunity for fabricating nanomeshes which contain gold nanoparticles as a drug release mechanism for antibiotics.

Received 16th August 2019
Accepted 16th September 2019

DOI: 10.1039/c9ra06398f

rsc.li/rsc-advances

1 Introduction

With the over-prescription of antibiotics worldwide, bacterial resistance is becoming a significant threat to public health.¹ When bacteria are resistant to three or more types of antibiotic classes, they are labelled as multi-drug resistant and there is a limited number of antibiotics available to be used in a final attempt to treat the infection.^{2,3} Two examples of these last line drugs are the polypeptide antibiotics, Colistin and Vancomycin.⁴ Colistin, which has previously been limited in its use due to the incidence of adverse effects including nephrotoxicity and neurotoxicity, is resurfacing more frequently for treatment.^{5,6} It is often used to treat multi-resistant Gram-negative bacteria, where other antibiotics are no longer effective. Colistin's mechanism relies on the electrostatic interaction between the negatively charged phosphate groups of the lipopolysaccharide (LPS) bacterial outer cell membrane and the positively charged amino groups of Colistin.^{7,8} When the positively charged Colistin comes into contact with the bacterial cell membrane, it causes defects in the membrane, leading to leakage of the cell contents and ultimately cell death.⁹ It also binds and neutralizes the lipid A portion of the LPS, which is the endotoxin of Gram-negative bacteria.⁸ Often, multiple antibiotics are used in combination to treat resistant bacteria, and Vancomycin is one of the more popular choices to treat Gram-positive Methicillin-

Resistant *Staphylococcus aureus* (MRSA) infections.^{10,11} Vancomycin's antibacterial action is different from that of Colistin, where it inhibits the cell wall synthesis of susceptible organisms.¹² It does this by inhibiting the peptidoglycan synthesis in late stage bacterial cell wall formation.¹³

Delivering the antibiotics directly to the infection site rather than *via* an oral dosage is beneficial as the oral ingested dosage is distributed not only at the infection site but also non-specifically around the body. The non-specificity means a high dosage needs to be given to ensure the concentration at the site of infection is significant enough to effectively treat it. The dosage can be lowered if delivered to the infection site directly, which can reduce side effects and complications. Although the dosage is 'reduced' compared to the oral dosage, the concentration of antibiotics delivered to the infection site can still be higher, ensuring the bacteria cannot survive and cause resistance.

In order to deliver the antibiotics to a specific site, the antibiotics need to be immobilised on a scaffold, and in this case they have been embedded into a fibrous mesh produced using a technique called electrospinning. Electrospinning has gained considerable interest in the biomedical community as it offers promise in many applications,¹⁴ including wound management,¹⁵ drug delivery¹⁶ and antibiotic coatings.¹⁷ Other emerging applications for electrospun meshes include air filtration^{18–22} and oil-water emulsion separation.^{23,24} In electrospinning, a syringe is loaded with a polymer that has been dissolved in a volatile solvent. A high voltage is then applied between the needle connected to the syringe, and the collector plate (Fig. 1). The voltage causes the polymer solution to form a Taylor cone as it leaves the syringe, at which point the electrostatic forces induce a jet of liquid, as it overcomes the surface tension.^{25,26}

^aInstitute for NanoScale Science and Technology, Flinders University, Bedford Park, South Australia, 5042, Australia. E-mail: Ingo.koepfer@flinders.edu.au

^bCollege of Science and Engineering, Flinders University, Bedford Park, South Australia, 5042, Australia

^cInternational Center for Materials Nanoarchitectonics, National Institute for Materials Science, Tsukuba, Ibaraki, 305-0047, Japan

† Electronic supplementary information (ESI) available. See DOI: 10.1039/c9ra06398f

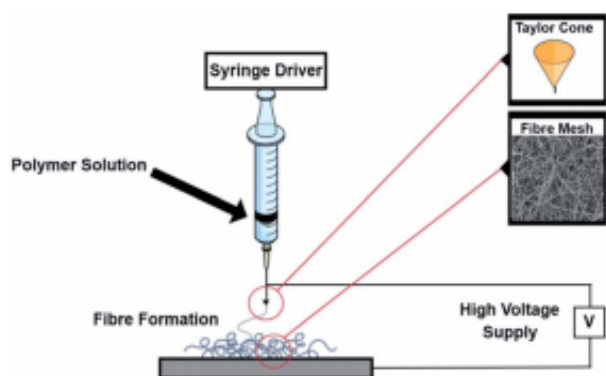


Fig. 1 Schematic of the electrospinning instrument showing the Taylor cone and mesh formation.

Electrospinning can produce controlled micro or nano-sized fibres that are deposited onto a substrate. The properties of the fibres can be adjusted by varying parameters such as the viscosity of the polymer solution, choice of solvent, the voltage supplied, needle gauge as well as the needle to collector plate distance.^{27,28}

The production process allows for various additives to be included into the fibres, as long as they can be mixed with the original polymer solution. Here, two antibiotics, Colistin (Col) and Vancomycin (Van) were added. Additionally, 5 nm diameter gold nanoparticles with either a negatively charged citrate capping Au(−) or a positively charged polydiallyldimethylammonium chloride (PDADMAC) coating Au(+), were added to determine if small, charged particles within the polymer matrix affect the antibiotic release.

Gold nanoparticles were chosen in addition to the antibiotics as positively charged nanoparticles have shown in literature to cause damage to the bacterial membranes.^{29,30} In a recent study, a strong correlation was found between poor bacterial viability and the attachment of positively charged gold nanoparticles on Gram-negative bacteria.³¹ Thus both anionic and cationic gold nanoparticles were included in the mesh to determine if they have any effect when paired with antibiotics within the nanomesh.

2 Materials and methods

2.1 Mesh formation

4, 7, 8, 9 and 10% w/w ϵ -polycaprolactone (PCL) solutions were prepared by dissolving PCL (average M_n 80 000) (Sigma Aldrich, Kaohsiung, Taiwan) in 1,1,1,3,3,3-hexafluoroisopropanol (HFIP) (Sigma Aldrich, Kaohsiung, Taiwan) and left overnight at ~ 40 °C. The PCL/HFIP solution was then loaded into a 5 mL syringe with a 22-gauge needle and electrospun with an applied voltage of 20 kV (Nanon-01A, MECC Co. Ltd, Fukuoka, Japan), with a 20 cm working distance and 20 cm horizontal needle movement for 3 h at flow rates of 0.5 mL h^{-1} and 1 mL h^{-1} . The fibres were spun directly onto aluminium foil on a stationary collector plate. The fibre mesh was removed from the aluminium foil prior to further investigation. After spinning

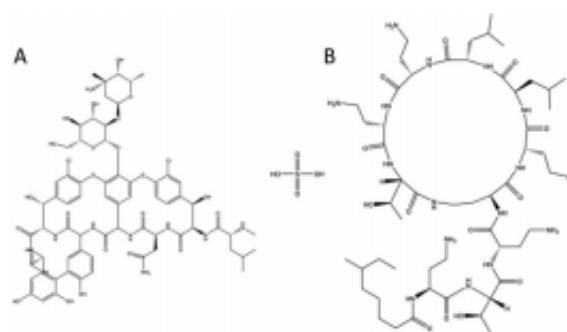


Fig. 2 The chemical structure of (A) Vancomycin and (B) Colistin.

was completed, the mesh was dried in a vacuum to remove any excess HFIP and stored at -20 °C until its use.

2.2 Mesh imaging

A 0.5 cm^2 piece of nanomesh was sputter coated with a thin layer of gold before being imaged *via* SEM (NEO-Scope JCM-5000 table top SEM, JEOL, Japan) at an accelerating voltage of 10 kV. The software ImageJ was used to analyse the diameter of the fibres, where the mean diameter of a minimum 50 fibres was used to determine fibre thickness.

2.3 Antibiotic addition to nanomesh

60 mg of Colistin sulphate salt ($\geq 15\,000 \text{ U mg}^{-1}$) (Sigma Aldrich, Castle Hill, Australia) was dissolved in 1 mL HFIP (for a total 12.5 w/w loading of Colistin) before being vortexed with 7% w/w PCL just prior to electrospinning. All meshes were electrospun with the same spinning parameters as described in the PCL mesh formation, except for the flow rate which was kept constant at 1 mL h^{-1} . For the addition of Vancomycin, 100 μL of 50 mg mL^{-1} Vancomycin hydrochloride in DMSO (Sigma Aldrich, Tokyo, Japan) was mixed with 0.5 mL HFIP and then vortexed before being added to 7% w/w PCL in HFIP for a total w/w Vancomycin loading of 1.4%. In the case of the meshes containing both antibiotics, the antibiotics were prepared as above and mixed together prior to being added to the PCL solution. For the addition of the negatively charged gold nanoparticles, 500 μL of 5 nm diameter citrate capped gold nanoparticles (10^{13} particles per mL) (Nanocomposix, San Diego, USA) were added to the drug solution prior to addition to the PCL solution. For the addition of positively charged gold nanoparticles, 5 nm diameter PDADMAC coated gold nanoparticles were fabricated using a previously published method.²² 500 μL of the fabricated nanoparticles (10^{13} particles per mL) were then added as per the citrate capped gold nanoparticle method.

2.4 Characterisation of antibiotic addition into the mesh

A 1 cm^2 piece of mesh was cut and placed on the crystal of an Attenuated Total Reflection Fourier Transform Infra-Red (ATR-FTIR) spectrophotometer (FTIR-8400S; Shimadzu Co., Ltd, Kyoto, Japan) and was used to confirm Vancomycin was present

in the mesh. To confirm the addition of Colistin, experiments were performed using ^1H NMR (Bruker 600 MHz Avance III, Australia) where 10 mg of mesh was dissolved in a mix of 95% DMSO- d_6 and 5% D_2O . A 5 mm BBFO probe was used and excitation sculpting was conducted to remove the D_2O peak. The parameters used for the ^1H NMR experiments were an acquisition time of 1.36 s, a relaxation delay of 1 s and line broadening of 0.3.

2.5 *In vitro* antibiotic release

Drug release studies were conducted by cutting 1.5 cm^2 pieces of mesh, weighing them and placing them in vials with 2 mL Dulbecco's Phosphate Buffered Saline (D-PBS) (Sigma Aldrich, Tokyo, Japan). The mesh pieces were then placed in a water bath with shaking at 37 $^\circ\text{C}$ to mimic physiological conditions. At different time points the 2 mL DPBS was removed and replaced under sink conditions. After being removed, the aliquot was immediately frozen and stored at -20 $^\circ\text{C}$ until ready to be measured, to prevent loss of antibiotic action. Removal of the aliquot at the various time points was completed in triplicate for all meshes measured. The concentration of the two antibiotics were determined by UV-vis spectrophotometry (JASCO V-650 Spectrophotometer, Japan) at a wavelength of 214 nm for Colistin and 280 nm for Vancomycin using a quartz cuvette. The data was normalised to 4 mg mesh weights for consistency. The cumulative percentage release was calculated using eqn (1).²¹

$$\text{Cumulative release (\%)} = \frac{M_t}{M_\infty} \times 100 \quad (1)$$

where M_t is the amount of antibiotic released at time t and M_∞ is the initial loading amount of antibiotic into the nanomesh.

2.6 Broth dilution assay

1 mL of DH5 α *Escherichia coli* (*E. coli*) bacteria (Invitrogen, Japan) was added to 1 mL of lysogeny broth (LB) medium (Sigma Aldrich, Japan) and incubated for 18 h at 37 $^\circ\text{C}$. After 18 h, 1 mL of the bacteria was added to each of the 2 mL aliquots taken from the *in vitro* drug release study and then incubated at 37 $^\circ\text{C}$ for 24 h. Turbidity was used as an indicator of cell growth in the presence of antibiotics released from *in vitro* studies. The absorbance was measured using UV-vis Spectrophotometry (JASCO V-650 spectrophotometer, Japan) at 600 nm optical density. Experiments were conducted in triplicate and the average absorbance was determined. Vancomycin mesh release was used as a positive control.

2.7 Zone of inhibition (ZOI) assay

E. coli American Type Culture Collection (ATCC) 700891 bacterial lawns were grown on nutrient agar plates (Sigma-Aldrich, Australia) for 24 h at 37 $^\circ\text{C}$. 8 mm diameter disks were cut from various meshes and placed under UV-light to sterilise for 20 minutes. The disks were then transferred onto the agar plates and incubated for 48 h at 37 $^\circ\text{C}$. After 48 h, the diameter of the zone of inhibition was recorded. Each mesh type was tested in triplicate. PCL with no antibiotics was used as

a negative control and the Vancomycin only mesh was used as a positive control.

3 Results and discussion

3.1 Optimisation of parameters for mesh formation

Meshes were produced with various flow rates and % w/w of PCL, while the working distance, voltage, deposition time and needle size were kept constant. An ideal mesh for drug release would have homogenous fibres with no visible defects.²² In order to develop an ideal mesh, the concentrations of PCL as well as the flow rates were altered and the meshes were then imaged to determine their homogeneity and fibre thickness (Fig. 3). 4% w/w PCL led to significant beading defects regardless of the flow rate. Beading leads to inhomogeneous fibres and can result from two different processes. The low viscosity of the solution can cause the solution to fall through the syringe too quickly, leading to a droplet. If the droplet falls, a new Taylor cone needs to be formed which leads to distinct and separated beads. The second reason for beading being observed is when the polymer solution is too viscous, as the solution will take too long to fall through the syringe which causes breaks in the

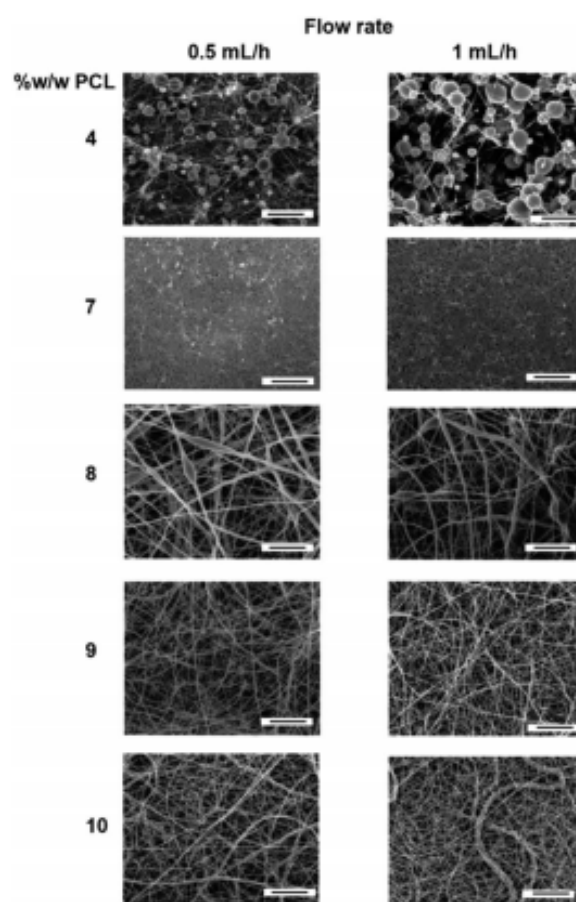


Fig. 3 SEM images of different %w/w of PCL in HFIP showing the changes in morphology at a flow rate of 0.5 mL h^{-1} and 1 mL h^{-1} . All scale bars are 10 μm .

electrospinning.³⁴ Again, a new Taylor cone will need to be formed causing beading defects. The 1 mL h^{-1} was observed to have a greater number of defects and this may be due to the faster flow rate, where the low viscosity means the polymer solution is falling through as well as being pushed faster than the 0.5 mL h^{-1} . To remove the beading, a higher polymer weight was used.

Polymer percentages of 7, 8, 9 and 10% w/w resulted in meshes with various fibre diameters. For 7% w/w PCL, the fibres had a diameter of $246 \pm 76 \text{ nm}$ with homogenous fibre diameters and no apparent beading defects. The 8% and 9% w/w PCL had no observable difference between the flow rates, however minor defects and various fibre diameters can be observed. These defects are different from the beading in the 4% w/w PCL as they are elongated within the fibre, causing differences in thicknesses along the length of the fibre. This is likely due to the viscosity being too high, leading to elongated beading within the fibre itself. Finally, the 10% w/w PCL mesh showed a variety of fibre diameters, which is not ideal in a drug delivery application (Table S1†). Thus for the electrospinning conditions used, the optimal polymeric solution concentration was determined to be 7% w/w as it produced the thinnest, most homogenous fibres compared to the other percentages tested. 7% w/w PCL was used in the formation of all the meshes to assess the addition of antibiotics and nanoparticles for drug delivery.

3.2 Addition of antibiotics into the nanomesh

Confirmation of the addition of Colistin and Vancomycin was achieved through a series of characterisation techniques. For NMR, peaks corresponding to the introduction of Colistin occurred at approximately 4.5, 2.9 and 1.85 ppm and were not observed in the PCL sample (Fig. 4).

ATR-FTIR confirmed the addition of Vancomycin into the nanomesh. The chemical structures of both antibiotics (Fig. 2) have many of the same functional groups, with the exception of an ether. The FTIR spectrum showed a characteristic ether peak at $\sim 1030 \text{ cm}^{-1}$ which was only present in the sample containing Vancomycin (Fig. 5). Similarly, both antibiotics contain an amine

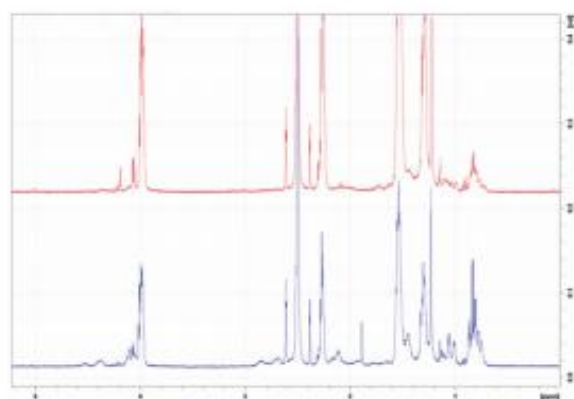


Fig. 4 (Top) ^1H NMR of 10 mg PCL in 95% DMSO, 5% D_2O . (Bottom) ^1H NMR of 10 mg PCL with Colistin in 95% DMSO, 5% D_2O .

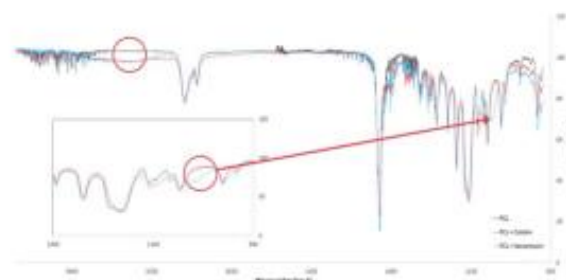


Fig. 5 ATR-FTIR of PCL, PCL + Colistin and PCL + Vancomycin nanomesh confirming the addition of the antibiotics with an ether peak for Vancomycin at $\sim 1030 \text{ cm}^{-1}$ (see inset) and amine groups at 3300 cm^{-1} for both antibiotics.

group within their structure whereas PCL does not. The signal at $\sim 3300 \text{ cm}^{-1}$ corresponding to the amine group further indicates the presence of both Colistin and Vancomycin in the mesh.

3.3 Zone of inhibition assay

Zone of inhibition assays were used to test the antibiotic activity of Colistin released from the mesh (Fig. 6). *E. coli* lawns were grown on nutrient agar and small circular pieces of mesh were cut out and placed on the bacterial lawns. As *E. coli* is Gram-negative, only Colistin meshes were tested as *E. coli* is not susceptible to Vancomycin. All meshes containing Colistin produced a ZOI with varying diameters. The control meshes of PCL and PCL with both cationic and anionic nanoparticles showed no inhibition of the bacteria. The ZOI assay was used as a qualitative method only to test for antibiotic action as Colistin is known to diffuse slowly and poorly through agar and often leads to unreliable and inaccurate diameters.³⁵

3.4 Drug release studies

With confirmation of antibiotic loading through FTIR and ^1H NMR, a drug release study was conducted to determine the

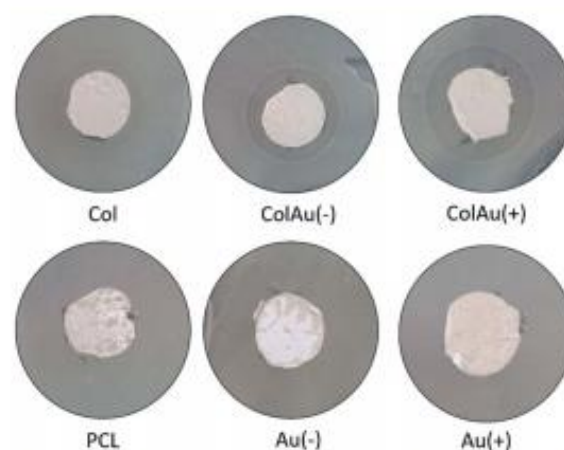


Fig. 6 Zone of inhibition assays after 48 h for meshes tested on *E. coli* lawns with 8 mm mesh disks.

amount of antibiotic being released from the mesh over time (Fig. 7). Drug concentrations were determined by UV/vis spectroscopy.

The drug release behaviour for 7% w/w PCL with varying antibiotic and gold nanoparticle combinations was monitored to determine the most efficient drug release profile. All samples exhibited a burst release in the first few hours before reaching a plateau around day 5. This burst release is due to diffusion, where the drug diffuses out from the mesh within the first few hours of being submerged in DPBS.^{36,37}

The total amount of drug released varied significantly between different drug combinations. As all the mesh combinations had the same amount of Colistin added during the formation of the mesh, the differences observed are most likely due to different release mechanisms. It is noted the cumulative percentage is above 100% however this is due to the theoretical maximum amount of Colistin being calculated for the total weight of the mesh and then divided by the average 1.5 cm² piece of mesh weight.

The ColAu(-) sample had the greatest release of Colistin compared to the other combinations (Fig. 7). The addition of positively charged gold nanoparticles saw a similar release to the Colistin mesh alone. This suggests that nanoparticles of the opposite charge to the drug can increase the release from the fibres. This altered release has been previously documented for changes in fibre texture, the pH differences of core and shell fibres and fibre shell thickness however to the author's knowledge, changes to release rates due to charged nanoparticles within the mesh has not been previously observed.^{38,39} However, it has been shown that in core-shell electrospinning, positively charged drugs are found to migrate to the surface of the fibres compared to neutral drugs which remain in the core.⁴⁰ This is due to the charge generation of the surface of the polymer during electrospinning. The positively charged drugs are

repelled from the inner needle surface and are drawn toward the grounded collector plate.⁴¹ Although in this case there is no core-shell, the negatively charged nanoparticles are likely interacting with the Colistin, in effect neutralising its cationic charge and encapsulating it further into the fibre. Whereas for the meshes with positively charged nanoparticles the particles and drug repel each other with minimal interaction, allowing the highly cationic Colistin (+5 net charge) to migrate to the fibre surface.⁴² Thus, the addition of anions when using a cationic drug should increase the release time of the drug from fibres.

For the Vancomycin release, when on its own, Vancomycin releases approximately 25% of the initial loading which is relatively low compared to the release of Colistin. This is due to the differences in their solubility in the electrospinning solvent HFIP. However, in comparison to the other combinations of the Vancomycin meshes, the Vancomycin only mesh release is high, with the VanCol, VanColAu(+) and VanColAu(-) only releasing between 6–12%. The addition of the positively charged nanoparticles to the Vancomycin mesh had no significant effect, which mirrored what was observed in the Colistin mesh. The addition of the negatively charged nanoparticles also had no significant effect which is expected as Vancomycin is amphoteric with only a slight positive charge when dissolved within HFIP.⁴³ This further supports the idea that the charge of a drug and the addition of charged particles within a nanomesh system affects the drug positioning within a fibre, which ultimately determines the release profile.

To analyse the release kinetics, all meshes containing Colistin were fitted to zero-order, first-order, Higuchi, Hixson-Crowell and Korsmeyer-Peppas models (Table S2†). The fitting was evaluated by the correlation coefficient (R^2). These models were chosen as they model different release mechanisms including diffusion and erosion.

The kinetics did not correlate with zero order, which compares the cumulative amount of drug released *versus* time. The plots shows a curvilinear profile for all meshes and the regression values were low indicating the release is not zero-order. The first order model, which compares the log of cumulative percentage of drug remaining *versus* time had a similar profile to zero order, where the data shows to be curvilinear. Again, the regression value was smaller than other models for all meshes tested.

The Korsmeyer-Peppas model (log cumulative percentage of drug released compared to log time) had the best fit for the release of Colistin for all the meshes, characterised by the highest R^2 values (Table S2†). The analysis of the Korsmeyer-Peppas model provides insight into the mechanisms of drug release, being both erosion and diffusion based.⁴⁴ This is determined by the values of the drug release exponent, n , which in this case is the slope of the Korsmeyer-Peppas model plot (Table S2†). When n is equal to or less than 0.45, it is an indication that the release mechanism is Fickian diffusion.⁴⁵ Fickian diffusion occurs when the polymer's relative relaxation time is considerably shorter than the diffusion time of water transport, which is controlled by the concentration gradient. If the n value is between 0.45 and 0.89 it indicates non-Fickian diffusion

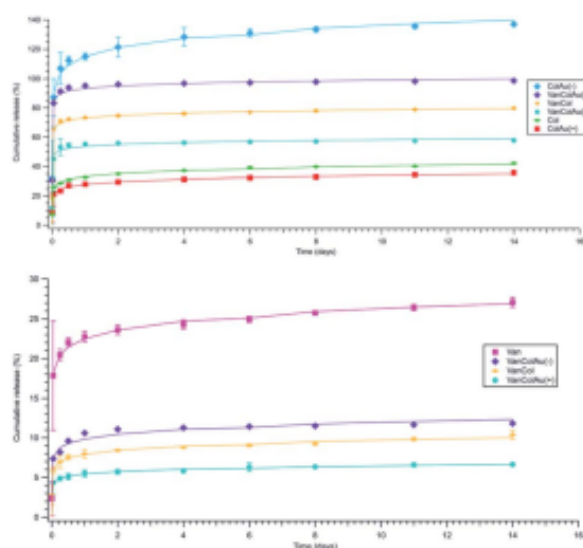


Fig. 7 (Top) Colistin cumulative release, (Bottom) Vancomycin cumulative release. Both show Korsmeyer-Peppas fitting models.

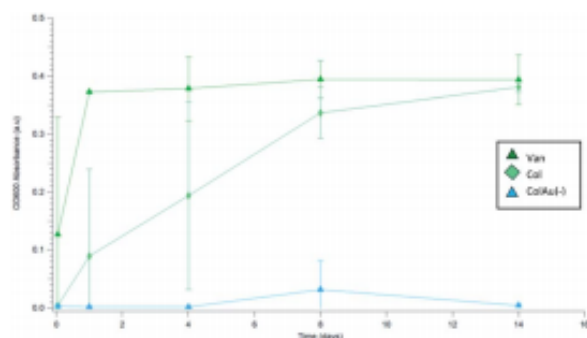


Fig. 8 Absorbance at OD₆₀₀ monitoring increased turbidity representing *E. coli* growth in aliquots removed during the Colistin release study of Van, Col, and ColAu(-) nanomesh samples in DPBS over various time points.

also known as analogous transport.⁴⁶ This type of transport has both erosion and diffusion as part of the release mechanism. When n is equal to or greater than 0.89 it indicates class II transport where the mechanism is erosion based.⁴⁷ In all meshes, n is less than 0.45 for Colistin release which is an indication of Fickian diffusion.

In order to examine how the release would affect bacteria over a 14 day time period, an *in vitro* bacterial study was conducted where *E. coli* was added to the aliquots of DPBS that was removed at various time points during the Colistin release study. The absorbance was then used to determine bacterial growth over time. The *in vitro* study confirmed the initial results showing that ColAu(-) produced the most efficient nanomesh. For the ColAu(-) nanomesh, the bacterial growth was severely hindered over 14 days whereas all other meshes had bacterial growth observed through their absorbance at 600 nm (Fig. 8). This data was in agreement with the results from the cumulative Colistin release, showing that the addition of small charged particles can alter the release profile.

4 Conclusion

This research described the fabrication of Colistin and Vancomycin loaded PCL nanomesh utilising an electrospinning approach for sustained drug release. Homogenous fibres were formed through optimisation of the electrospinning process, with 7% w/w PCL at 1 mL h⁻¹ producing the most uniform nanomesh. 12.5% w/w of Colistin and 1.4% w/w of Vancomycin were introduced into the polymer matrix prior to spinning. Both Colistin and Vancomycin were released from the nanomesh over a 14 day period, with Colistin releasing at a higher cumulative percentage than Vancomycin. The addition of small charged nanoparticles altered the release of the antibiotics from the nanomesh. The addition of citrate capped gold nanoparticles likely neutralised Colistin's charge, causing the antibiotic to migrate toward the centre of the fibre, prolonging its release profile. However, the addition of positively charged gold nanoparticles did not significantly alter the release of Colistin from the mesh compared to Colistin alone. Further

investigation is needed to determine if other small charged particles affect the release of drugs from single spun fibres and how it affects the release over time. As it is a pharmaceutical application, the stability of the mesh under different storage conditions as well as the toxicological properties also need to be evaluated.

Conflicts of interest

There are no conflicts to declare.

Acknowledgements

The authors would like to thank the Australian Institute of Nuclear Science and Engineering (AINSE Ltd) (Award - PGRA) for the top-up scholarship, the National Institute for Materials Science (NIMS) for the internship and the Australian Government Research Training Program for providing financial assistance. The authors would also like to acknowledge the assistance of Martin Johnston from Flinders University for his assistance with running the ¹H NMR.

Notes and references

- C. Llor and L. Bjerrum, *Ther. Adv. Drug Saf.*, 2014, 5, 229–241.
- M. T. Sweeney, B. V. Lubbers, S. Schwarz and J. L. Watts, *J. Antimicrob. Chemother.*, 2018, 73, 1460–1463.
- J. Li, C. R. Rayner, R. L. Nation, R. J. Owen, D. Spelman, K. E. Tan and L. Liolios, *Antimicrob. Agents Chemother.*, 2006, 50, 2946–2950.
- H. Garbis, M. R. van Tonningen and M. Reuvers, in *Drugs During Pregnancy and Lactation*, ed. C. Schaefer, P. Peters and R. K. Miller, Academic Press, Oxford, 2nd edn, 2007, pp. 123–177.
- N. Markou, H. Apostolakis, C. Koumoudiou, M. Athanasiou, A. Koutsoukou, I. Alamanos and L. Gregorakos, *Crit. Care*, 2003, 7, R78–R83.
- N. E. Edrees, A. A. A. Galal, A. R. Abdel Monaem, R. R. Beheiry and M. M. M. Metwally, *Chem. Biol. Interact.*, 2018, 294, 56–64.
- M. Gurjar, *J. Intensive Care Med.*, 2015, 3, 3.
- A. Z. Bialvaei and H. Samadi Kafil, *Curr. Med. Res. Opin.*, 2015, 31, 707–721.
- N. Martis, S. Leroy and V. Blanc, *J. Infect.*, 2014, 69, 1–12.
- A. Hassoun, P. K. Linden and B. Friedman, *Crit. Care*, 2017, 21, 211.
- T. L. Holland, C. Arnold and V. G. Fowler, *J. Am. Med. Assoc.*, 2014, 312, 1330–1341.
- C. Watanakunakorn, *J. Antimicrob. Chemother.*, 1984, 14, 7–18.
- P. E. Reynolds, *Eur. J. Clin. Microbiol. Infect. Dis.*, 1989, 8, 943–950.
- S. Agarwal, J. H. Wendorff and A. Greiner, *Polymer*, 2008, 49, 5603–5621.
- M. Gizaw, J. Thompson, A. Faglie, S.-Y. Lee, P. Neuenschwander and S.-F. Chou, *Bioengineering*, 2018, 5, 9.

- 16 E. J. Torres-Martinez, J. M. Cornejo Bravo, A. Serrano Medina, G. L. Pérez González and L. J. Villarreal Gómez, *Curr. Drug Delivery*, 2018, **15**, 1360–1374.
- 17 J. L. Castro-Mayorga, M. J. Fabra, L. Cabedo and J. M. Lagaron, *Nanomaterials*, 2016, **7**, 4.
- 18 D. Lv, R. Wang, G. Tang, Z. Mou, J. Lei, J. Han, S. De Smedt, R. Xiong and C. Huang, *ACS Appl. Mater. Interfaces*, 2019, **11**, 12880–12889.
- 19 M. Zhu, J. Han, F. Wang, W. Shao, R. Xiong, Q. Zhang, H. Pan, Y. Yang, S. K. Samal, F. Zhang and C. Huang, *Macromol. Mater. Eng.*, 2017, **302**, 1600353.
- 20 D. Lv, M. Zhu, Z. Jiang, S. Jiang, Q. Zhang, R. Xiong and C. Huang, *Macromol. Mater. Eng.*, 2018, **303**, 1800336.
- 21 M. Zhu, R. Xiong and C. Huang, *Carbohydr. Polym.*, 2019, **205**, 55–62.
- 22 M. Zhu, D. Hua, M. Zhong, L. Zhang, F. Wang, B. Gao, R. Xiong and C. Huang, *Colloid Interface Sci. Commun.*, 2018, **23**, 52–58.
- 23 W. Ma, M. Zhang, Z. Liu, C. Huang and G. Fu, *Environ. Sci.: Nano*, 2018, **5**, 2909–2920.
- 24 W. Ma, J. Zhao, O. Oderinde, J. Han, Z. Liu, B. Gao, R. Xiong, Q. Zhang, S. Jiang and C. Huang, *J. Colloid Interface Sci.*, 2018, **532**, 12–23.
- 25 I. Kurtz and J. Schiffman, *Materials*, 2018, **11**, 1059.
- 26 J. K. Y. Lee, N. Chen, S. Peng, L. Li, L. Tian, N. Thakor and S. Ramakrishna, *Prog. Polym. Sci.*, 2018, **86**, 40–84.
- 27 D. Li and Y. Xia, *Adv. Mater.*, 2004, **16**, 1151–1170.
- 28 M. Mirjalili and S. Zohoori, *J. Nanostruct. Chem.*, 2016, **6**, 207–213.
- 29 X. Li, S. M. Robinson, A. Gupta, K. Saha, Z. Jiang, D. F. Moyano, A. Sahar, M. A. Riley and V. M. Rotello, *ACS Nano*, 2014, **8**, 10682–10686.
- 30 Y. Zhou, Y. Kong, S. Kundu, J. D. Cirillo and H. Liang, *J. Nanobiotechnol.*, 2012, **10**, 19.
- 31 Z. V. Feng, I. L. Gunsolus, T. A. Qiu, K. R. Hurley, L. H. Nyberg, H. Frew, K. P. Johnson, A. M. Vartanian, L. M. Jacob, S. E. Lohse, M. D. Torelli, R. J. Hamers, C. J. Murphy and C. L. Haynes, *Chem. Sci.*, 2015, **6**, 5186–5196.
- 32 M. Fuller and I. Köper, *Polymers*, 2018, **10**, 1336.
- 33 P. Bala Balakrishnan, L. Gardella, M. Forouharshad, T. Pellegrino and O. Monticelli, *Colloids Surf., B*, 2018, **161**, 488–496.
- 34 A. Haider, S. Haider and I.-K. Kang, *Arabian J. Chem.*, 2015, 1165–1188.
- 35 L. Poirel, A. Jayol and P. Nordmann, *Clin. Microbiol. Rev.*, 2017, **30**, 557–596.
- 36 S. Misra, H. Pandey, S. Patil, P. Ramteke and A. Pandey, *Fibers*, 2017, **5**, 41.
- 37 W.-C. Lin, I.-T. Yeh, E. Niyama, W.-R. Huang, M. Ebara and C.-S. Wu, *Polymers*, 2018, **10**, 231.
- 38 Y. Ding, W. Li, F. Zhang, Z. Liu, N. Zanzanizadeh Ezazi, D. Liu and H. A. Santos, *Adv. Funct. Mater.*, 2019, **29**, 1802852.
- 39 K. T. Shalumon, G.-J. Lai, C.-H. Chen and J.-P. Chen, *ACS Appl. Mater. Interfaces*, 2015, **7**, 21170–21181.
- 40 U. Angkawitwong, S. Awwad, P. T. Khaw, S. Brocchini and G. R. Williams, *Acta Biomater.*, 2017, **64**, 126–136.
- 41 B. Pourdeyhimi, A. L. Yarin and S. Ramakrishna, *Fundamentals and Applications of Micro- and Nanofibres*, Cambridge University Press, Cambridge, 1st edn, 2014.
- 42 P. J. Bergen, J. Li, C. R. Rayner and R. L. Nation, *Antimicrob. Agents Chemother.*, 2006, **50**, 1953–1958.
- 43 S. Jamzad and R. Fassihi, *AAPS PharmSciTech*, 2006, **7**, E33.
- 44 P. Kumar, A. L. Ganure, B. B. Subudhi and S. Shukla, *Int. J. Pharm. Res.*, 2015, **14**, 677–691.
- 45 M. V. Cabañas, J. Peña, J. Román and M. Vallet-Regí, *Eur. J. Pharm. Sci.*, 2009, **37**, 249–256.
- 46 T. Hayashi, H. Kanbe, M. Okada, M. Suzuki, Y. Ikeda, Y. Onuki, T. Kaneko and T. Sonobe, *Int. J. Pharm.*, 2005, **304**, 91–101.
- 47 N. Amit, L. Bibek and S. Kalyan, *Acta Pharm.*, 2011, **61**, 25–36.